DISSERTATION

Submitted to the
Combined Faculties of Natural Sciences and Mathematics
of the Ruperto Carola University Heidelberg, Germany
for the degree of
Doctor of Natural Sciences

Presented by
M.Sc. Jan Hendrik Rieger
born in: Brilon, Germany
Oral examination: 07.11.2019

Targets of tumor-infiltrating lymphocyte reactivity in pancreatic cancer

Referees:
Prof. Dr. Rienk Offringa
Prof. Dr. Viktor Umansky

The applicant, Jan Hendrik Rieger, declares that he is the sole author of the submitted dissertation and no other sources or help from those specifically referred to have been used. Additionally, the applicant declares that he has not applied for permission to enter an examination procedure at any other institution and that this dissertation has not been presented to any other faculty and has not been used in its current or in any other form in another examination.

Location and Date

Name and Signature

F.E.A.R.

- Papa Roach, 2014

Acknowledgements

First and foremost I would like to thank my doctoral advisor, **Prof. Dr. Rienk Offringa**, for taking me up as his PhD student and giving me the opportunity to work on this project. I appreciate your continuous help and the discussions over the past years. During the time in your lab I had the opportunity to take part in great scientific discussions and could learn several valuable lessons.

Furthermore, I would like to thank **Dr. Isabel Poschke** for her great support as experimental supervisor of my PhD project and the scientific discussions over the past years.

I would like to thank **Dr. Michael Volkmar** for his great support, discussions and scientific advice on any molecular biological or bioinformatical question arising over the cause of this project.

In addition, I would like to thank **Prof. Dr. Viktor Umansky** for being my second referee and thesis advisory committee member. I really appreciated your the scientific input during the TAC meetings.

Moreover, I would like to thank **Prof. Dr. Gerald Willimsky** and **Prof. Dr. Magnus von Knebel-Doeberitz** for being my additional thesis advisory committee members.

A great thanks to **Johanna Lehmann**, **Jennifer Hermes** and **Aaron Rodriguez Ehrenfried** for their great support during this work. Your constant help took a lot of stress off of me over the past years.

Furthermore, I would like to thank **Janina Rebmann** and **Claudia Lauenstein** for their great support during the molecular biological experiments. Your technical experience in molecular biological experimentation helped me save a lot of time.

Thanks to **Daniel Baumann**, **Julian Mochayedi**, **Tanja Hägele** for the great discussions, coffee breaks and fun times over the past years. It was a great pleasure meeting and working with you guys.

In addition, I would like to thank the rest of the **G180 Team** for the great time in the lab and for withstanding the at times exquisite choice of music in the cell culture.

I would also like to thank **PD Dr. Dr. Angelika Riemer**, **Dr. Mogjib Salek** and **Dr. Renata Blatnik** for their support and the scientific discussions on the mass spectrometry part of this thesis.

Moreover, I would like to thank **Sabrina Purr**, **Dr. Florian Wessel**, **Dr. Hans-Henning Böhm** and **Dr. Rafael Carretero** for their support on S2 experimentation and frequent spontaneous help whenever I ran out of supplies in the S2 lab.

A great thanks to **Dr. Timo Kehl** for his great support and the discussions on all S2 related work that was carried out during this thesis.

In addition, thanks to **Dr. Julia Wolanski** for her scientific/ experimental advise, numerous discussions and great support during difficult times.

A great thanks to **Dr. Eva Klein**, **Dr. Julia Wolanski**, **Soumya Mohapatra** and **Dr. Isabel Poschke** for spell-checking and counter reading my dissertation. The great effort you put into this meant a lot to me.

Thanks to **Manuel Reitberger** for the constant supply of special cell media.

Last, but not least, I would like to thank my **family** and **friends** for their constant support and advice at any time of my PhD. Your support made it possible for me to keep on going, no matter how difficult things appeared to become.

Summary

With little to no progress in the treatment of pancreatic cancer over the past decades, novel approaches to cover the high unmet medical need are long overdue. However, the long lasting notion of PDAC being a 'non-immunogenic' neoplasm lacking uniform infiltration of effector lymphocytes and holding an immunosuppressive microenvironment has so far precluded the use of adoptive T cell therapy in this malignancy. Furthermore, the overall low mutational burden of pancreatic cancer led to the assumption of decreased frequencies in immunogenic neoepitopes targeted by T cells. Nevertheless, the recent identification of frequently occurring effector T cells recognizing their autologous tumor in pancreatic cancer indicates a potential use of PDAC derived TILs against the malignancy. In addition, exome analyses of larger patient cohorts indicated that formation of immunogenic, mutation derived epitopes in PDAC might be more frequent than previously expected. Nevertheless, to date functional analyses identifying and characterizing the epitopes recognized by pancreatic cancer TIL are yet to be carried out.
Thus, we set out to develop screening approaches to reliably identify mutation derived epitopes within pancreatic cancer patients. This development was approached with two complementary strategies, first by looking into the antigens recognized by PDAC TILs and second by directly identifying the epitopes presented on the surface of the PDAC derived tumor cells.
We addressed the antigen recognition by developing a novel expression based screening system. Since PDAC is frequently infiltrated by $CD4^+$ and $CD8^+$ T cells (both of which populations potentially mount anti tumor immune responses), combined with a low number of tumor mutations, we needed an approach able to screen for both, MHC-I and MHC-II restricted antigens. Therefore, we designed a system based on shuttling antigens into both, the major histocompatibility complex (MHC)-I and -II antigen presentation pathways, in order to define the reactivity of PDAC TILs in a completely unbiased fashion (i.e. not depending on MHC restriction and/or epitope prediction algorithms). Furthermore, we validated the use of a targeted mass spectrometry based approach to directly identify epitopes presented on the surface of PDAC derived cells lines. In addition, the application of both approaches in a small patient cohort was used to draw initial conclusions on the feasibility of both approaches for an extension to larger patient cohorts.
Taken together, the presented study describes the development and validation of screening methodologies capable of identifying antigens in the context of low mutational burden malignancies such as pancreatic cancer. These methodologies lay the foundation for the functional proof of concept studies of antigen reactive T cells infiltrating pancreatic cancer, opening new ways for the application of adoptive T cell transfer in this fatal disease.

Zusammenfassung

Angesichts der geringen Fortschritte bei der Behandlung von Bauchspeicheldrüsenkreb in den letzten Jahrzehnten sind neue Ansätze zur Deckung des hohen Behandlungsbedarfs längst überfällig. Aufgrund der Annahme, dass ductale Adenokarzinome des Pankreas (PDAC) „nicht immunogene“ Neoplasien seien, welche nicht von Effektorlymphozyten infiltriert sind und über ein immunsuppressives Mikromilieu verfügen, wurde eine adoptive T-Zell Therapie für diese Erkrankung bisher ausgeschlossen. Darüber hinaus führte die geringe Mutationslast von Bauchspeicheldrüsenkrebs zu der Annahme, dass die von T Zellen erkannten, immunogenen Neoepitope seltener vorhanden sind. Dennoch deutet die kürzlich gezeigte Häufung von Effektor-T-Zellen (TILs), die ihren autologen Tumor erkennen, auf eine mögliche Verwendung von PDAC TILs gegen den Tumor hin. Darüber hinaus zeigten Exomanalysen größerer Patientenkohorten, dass die Bildung immunogener, von Mutationen abgeleiteter Epitope in PDAC häufiger auftreten als bislang erwartet. Jedoch fehlen bislang funktionelle Analysen zur Identifizierung und Charakterisierung der von PDAC TIL erkannten Epitope.

In der vorliegenden Arbeit haben wir verschiedene Screening Abläufe entwickelt, um mutationsbedingte Epitope bei Pankreaskrebspatienten zuverlässig zu identifizieren. Die Entwicklung dieser Ansätze wurde mit zwei komplementären Strategien verfolgt. Zum Einen durch die Untersuchung der von PDAC TILs erkannten Antigene und zum Anderen durch direkte Identifizierung der auf der Oberfläche der von PDAC abgeleiteten Tumorzellen präsentierten Epitope.

Im Zusammenhang der Antigenerkennung durch PDAC TIL haben wir ein neues expressionsbasiertes Screening System entwickelt. Da PDAC häufig von $CD4^+$- und $CD8^+$-T-Zellen infiltriert wird (von denen beide Populationen potenzielle anti tumor Immunantworten aufweisen), benötigten wir einen Ansatz, der gleichzeitig MHC-I und MHC-II restringierte Antigene identifiziert. Aus diesem Grund haben wir ein System entwickelt, das darauf basiert Antigene in den Haupthistokompatibilitätskomplex (MHC)-I- und -II Präsentationspfad zu leiten, um die Reaktivität von PDAC TILs völlig unvoreingenommen zu bestimmen (d.h. unabhängig von der MHC-Restriktion und von Epitopvorhersagealgorithmen). Darüber hinaus validierten wir die Verwendung eines zielgerichteten massenspektrometrischen Ansatzes zur direkten Identifizierung von Epitopen, die auf der Oberfläche von PDAC-abgeleiteten Zelllinien präsentiert werden. Zudem wurden aus der Anwendung beider Ansätze in einer kleinen Patientenkohorte erste Rückschlüsse auf die Durchführbarkeit beider Ansätze für eine Ausweitung auf größere Patientenkohorten gezogen.

Zusammengefasst beschreibt die vorgestellte Studie die Entwicklung und Validierung von Screening Methoden, mit denen Antigene im Zusammenhang von malignen Erkrankungen mit geringer Mutationsbelastung (z.B. Bauchspeicheldrüsenkreb) identifiziert werden können. Die vorgestellten Methoden bilden die Grundlage für funktionelle Studien von antigenreaktiven T-Zellen, die PDAC infiltrieren, und eröffnen neue Möglichkeiten für die Anwendung des adoptiven T-Zelltransfers bei dieser tödlichen Krankheit.

Contents

List of Figures

List of Tables

Abbreviations

%	percent
℃	Degrees Celsius
5-FU	5-fluorouracil
A.D.	Anno Domini
ACK	Ammonium-chloride-potassium
ACVR1B	Activin A Receptor Type 1B
APC	Antigen presenting cell
ARID1A	AT-Rich Interaction Domain 1A
ATF2	Activating Transcription Factor 2
ATM	ATM Serine/Threonine Kinase
ATP	Adenosine Triphosphate
B cell	B Lymphocyte
B.C.	Before Christ
Bcl-2	BCL2 Apoptosis Regulator
BiTE	Bi-specific T cell engager
BRAF	B-Raf Proto-Oncogene, Serine/Threonine Kinase
BRCA	BRCA DNA Repair Associated
BSA	Bovine Serum Albumin
BSL1/ S1	Biosafety level 1
BSL2/ S2	Biosafety level 2
CA19-9	Carbohydrate antigen 19-9
CaCl2	Calcium chloride
cAMP	Cyclic adenosine monophosphate
CaPO4	Calcium phosphate
CAR	Chimeric antigen receptor
CCR	C-C chemokine receptor
CD	Cluster of differentiation
CDKN2A/ p16	Cyclin Dependent Kinase Inhibitor 2A
CEA	Carcinoembryonic antigen
CFSE	Carboxyfluorescein succinimidyl ester
CHAPS	3-[(3-cholamidopropyl)dimethylammonio]-1-propanesulfonate
cm	Centimeter
CO2	Carbondioxide
cTEC	Cortical thymic epithelial cell
CTLA4	Cytotoxic T-lymphocyte-associated protein 4
CTNNB	Catenin Beta 1
CXCR	CXC chemokine receptors
DC	Dendritic cell
DKFZ	German Cancer Research Center
DMSO	Dimethyl sulfoxide
DNA	Deoxyribonucleic acid
dNTP	Deoxyribose nucleoside triphosphate
DTT	Dithiothreitol
EBV	Epstein-Barr virus
EDTA	Ethylenediaminetetraacetic acid
EGF	Epidermal growth factor
EGFR	Epidermal growth factor receptor
ERAD	Endoplasmic-reticulum-associated protein degradation
ERBB2IP	Erbb2 Interacting Protein
FACS	Fluorescence-activated cell sorting/ scanning
FAMMM	Familial atypical multiple mole and melanoma
Fas	Fas Cell Surface Death Receptor

FasL	Fas ligand
FasR	Fas receptor
FCS/ FBS	Fetal calf/ bovine serum
FDA	Food and Drug administration
FGF	Fibroblast growth factor
FOLFIRINOX	Folinic acid, 5-fluorouracil, irinotecan and oxaliplatin
g/L	gram per liter
G1-S	Cell cycle transition phase
GATA6	GATA Binding Protein 6
GM-CSF	Granulocyte-macrophage colony-stimulating factor
GNAS	GNAS Complex Locus
gp100	Glycoprotein 100
GSH	Glutathione
h	hours
H. pylori	Helicobacter pylori
HBS	HEPES buffered saline
HBV	Hepatitis B virus
HEPES	(4-(2-hydroxyethyl)-1-piperazineethanesulfonic acid)
HER-2	Human epidermal growth factor receptor 2
HLA	Human leukocyte antigen
HPV	Human papillomavirus
HSA	Human serum albumin
HY	DEAD-Box Helicase 3 Y-Linked
ICS	Intracellular cytokine staining
IDO	Indoleamine 2,3-Dioxygenase
IFN	Interferon
Ig	Immuneglobulin
IGFR3	Fc Fragment Of IgG Receptor III
IL	Interleukin
InDel	Insertion/ Deletion
iNOS	Inducible Nitric Oxide Synthase
IPMN	Intraductal papillary mucinous neoplasm
KDM6A	Lysine Demethylase 6A
KRAS	KRAS Proto-Oncogene
LAG3	Lymphocyte Activating 3
Lamp1	Lysosomal associated membrane protein 1
LB	Lysogeny broth
M	Molar
MAGE-A1	Melanoma-Associated Antigen 1
MAP2K4	Mitogen-Activated Protein Kinase Kinase 4
MAPK/ ERK	MAPK/ERK pathway
MARK2	Mitogen-Activated Protein Kinase 2
Mart1	Melanoma antigen recognized by T cells 1
MCN	Mucinous cystadenocarcinoma
MDCT	Multi-detector computer tomography
MDSC	Myeloid derived suppressor cell
MHC	Major histocompatibility complex
MIB1	Mindbomb E3 Ubiquitin Protein Ligase 1
min	minutes
MITD	MHC class I trafficking signal
mL	Milliliter
MLL2/3	Histone-Lysine N-Methyltransferase 2/3
mM	Millimolar
MMULV	Moloney Murine Leukemia Virus

MNC	Mucinous noncystic carcinoma
MRI	Magnetic resonance imaging
MS	Mass spectrometry
mTEC	Medullary thymic epithelial cell
mTOR	Mechanistic Target of Rapamycin
MUC-1	Mucin 1
MYCBP2	MYC Binding Protein 2
neg	Negative
NGS	Next generation sequencing
NK cell	Natural killer cell
NKG2D	Killer Cell Lectin Like Receptor K1
NOD	Nucleotide-binding oligomerization domain-containing protein
Notch	Notch receptor
NY-ESO-1	New York esophageal squamous cell carcinoma-1
OT-I	Ovalbumin-specific TCR transgenic murine CD8 T cells
OT-II	Ovalbumin-specific TCR transgenic murine CD4 T cells
PALB2	Partner And Localizer Of BRCA2
PanIN	Pancreatic intraepithelial neoplasia
PAP	Prostatic acid phosphatase
pAPC	Professional antigen presenting cell
PBMC	Peripheral blood mononuclear cell
PBRM1	Polybromo 1
PBS	Phosphate buffered saline
PCR	Polymerase chain reaction
PD1	Programmed cell death protein 1
PDAC	Pancreatic ductal adenocarcinoma
PDL1	Programmed cell death 1 ligand 1
PDX	Patient derived xenograft
Pen/Strep	Penicillin/ Streptomycin
PET	Positron emission tomography
pH	Potential of hydrogen
PHA	Phytohaemagglutinin
PNET	Pancreatic neuroendocrine tumor
pos	Positive
PRR	Pattern recognition receptor
RASGRP3	RAS Guanyl Releasing Protein 3
RBM10	RNA Binding Motif Protein 10
RNA	Ribonucleic acid
RNF43	Ring Finger Protein 43
ROBO/ SLIT	ROBO/ SLIT signaling pathway
ROBO1/2	Roundabout 1/2
ROS	Reactive oxygen species
RT	Room temperature
scFv	Single-chain variable fragment
SDS	Sodium dodecyl sulfate
SETD2	SET Domain Containing 2, Histone Lysine Methyltransferase
SF3B1	Splicing Factor 3b Subunit 1
SLIT2	Slit Guidance Ligand 2
SMAD3/4	SMAD family member 3/4
SMARCA4	ATP-dependent chromatin remodeler SMARCA4
SNV	Small nucleotide variance
SP	Signal Peptide
SPL	Sample processing lab
STAT3	Signal Transducer And Activator Of Transcription 3

SWI/ SNF	SWItch/Sucrose Non-Fermentable
T cell	T lymphocyte
T_{FH}	Follicular helper T cell
T_H	Helper T cell
T_{REG}	Regulatory T cell
T_{cm}	Central memory T cell
TCR	T cell receptor
T_{em}	Effector memory T cell
TEMED	Tetramethylethylendiamin
TGFBR1	Transforming Growth Factor Beta Receptor 1
TGFβ	Transforming growth factor beta
TIL	Tumorinfiltrating lymphocytes
TIM3	T-cell immunoglobulin and mucin-domain containing-3
TLE4	TLE Family Member 4, Transcriptional Corepressor
TLR	Toll-like receptor
TLS	Tertiary lymphoid structures
TMD	Transmembrane domain
TNFα	Tumor necrosis factor alpha
TNM	Tumor node metastatis
TP53/ p53	Tumor Protein p53
TP53BP2	Tumor Protein p53 Binding Protein 2
TRAIL	Tumor Necrosis Factor Related Apoptosis Inducing Ligand
Tris	Tris(hydroxymethyl)-aminomethan
U2AF1	U2 Small Nuclear RNA Auxiliary Factor 1
vs	Versus
Wnt	Proto-oncogene protein Wnt
α	alpha
β	beta
γ	gamma
δ	delta
ε	epsilon
μ	micro
ξ	zeta

Amino acids and nucleotides were abbreviated using the respective standard single letter code.

1 Introduction

1.1 The Pancreas

The organ was first described around 300 B.C. by Herophilus of Chalcedon and later (around 100 A.D.) named by Ruphos of Ephesus as pancreas (greek: παν/pan=all and κρέας/kreas=meat) [1, 2]. The pancreas is approximately 14 - 18 cm large and is located in the anterior pararenal space, posterior to the parietal peritoneum [3]. Macroscopically, the glandular organ is divided into four parts - head, neck, body and tail - and microscopically holds endocrine, as well as exocrine functions [3, 4].
Its endocrine function is rendered by islets of Langerhans, scattered throughout the whole organ in close proximity to blood vessels [5]. First described by Paul Langerhans in 1869 [6], these islets secrete various hormones from specialized cells into the circulation. Islets of Langerhans consist to about 60% of β-cells (producing insulin), 30% α-cells (producing glucagon), <10% δ-cells (producing somatostatin), <5% γ-cells (producing pancreatic polypeptide) and ε-cells (producing ghrelin) [7, 8].
The exocrine portion of a healthy pancreas consists of two major cellular subpopulations: Acinar cells form lobuli in the pancreatic parenchyma and synthesize as well as secrete digestive enzymes (trypsinogen, chymotrypsinogen, amylase, and lipase) into the main pancreatic duct [9]. Epithelial cells line the pancreatic ducts and collect digestive enzymes from the acini [10, 11]. The main pancreatic duct (duct of Wirsung) spans the whole organ and combines with the common bile duct, forming the ampulla of Vater, at the pancreatic head [4]. Penetrating the duodenal wall, both ducts empty into the duodenal lumen via the major duodenal papilla [4].

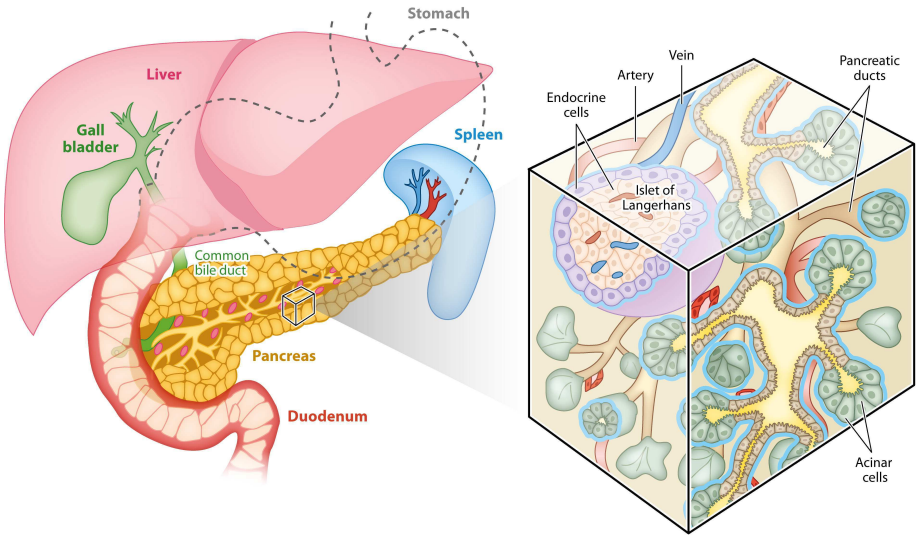

Figure 1 – The healthy adult pancreas. (Left) Location and connectivity of the pancreas in the anterior pararenal space. (Right) Schematic visualization of the cellular composition of the endocrine and exocrine pancreas. Taken from [12]

1.2 Pancreatic Cancer

Over the course of a lifetime, this central digestive and endocrine organ can undergo atypical transformation, giving rise to one of the most life threatening diseases, pancreatic cancer. The majority of cases are diagnosed at a median age of 71 years in both men and women [13]. A diagnosis at an age younger than 40 years is rare [13, 14]. The combination of an initially symptomless progression and early-stage metastasis contribute largely to the overall poor prognosis of pancreatic cancer [15–18]. In most cases patients experience unspecific abdominal discomfort, back pain, weight loss or indigestion prior to diagnosis [19–21].

1.2.1 Subtypes of pancreatic cancer

In accordance with their respective anatomical localization, pancreatic malignancies are subdivided into two categories (i.e. malignancies of the endocrine and the exocrine pancreas):

Malignancies of the endocrine pancreas

Pancreatic Neuroendocrine Tumors (PNET) Due to its anatomical location within the organ this subtype of pancreatic malignancy was previously termed “islet cell tumor” or “pancreatic carcinoid tumor”. In order to arrive at a better consensus, the term neuroendocrine neoplasm was suggested for pancreatic malignancies showing an endocrine phenotype [22–24].
Pancreatic neuroendocrine tumors (PNETs) form a rare subtype of pancreatic malignancies with an overall incidence of 1 - 3% [14, 18, 23–25]. In addition, they grow comparatively slow and are, in most cases, diagnosed at a non-malignant stage, resulting in a better prognosis after surgical treatment compared to tumors of the exocrine portion of the organ [14, 23, 25].
Further sub-classifications of these neuroendocrine neoplasms involve the distinction between tumors with an elevated hormone production (functional; 60 - 70% incidence) and regular levels of hormone production (non-functional; 30 - 40% incidence) [23]. Clinically, non-functional PNETs are often detected at later stages, due to the absence of hormone-related symptoms. In the case of functional PNETs, an earlier diagnosis is mainly possible due to clinical signs of hormone over-expression.
Depending on the respective over-expressed hormone, functional PNETs are further subcategorized into insulinomas (20 - 30%), gastrinomas (15 - 20%), VIPomas (2 - 4%), glucagonomas (1 - 3%) and somatostatinoma ($\approx$1%) [23, 26].

Malignancies of the exocrine pancreas

Approximately 95% of all pancreatic malignancies arise in the exocrine portion of the organ [18, 25]. Based on the cellular subtype and differentiation, these malignancies are further subdivided into the following categories:

Ductal adenocarcinoma With an incidence of approximately 85 - 90% of all cases diagnosed with a pancreatic neoplasm, pancreatic ductal adenocarcinoma represents the most frequent

malignancy of the exocrine pancreas [14, 18]. A detailed description of this subtype is given in section 1.3.

Mucinous Cystadenocarcinoma (MCN) The mucinous cystadenocarcinoma (MCN) is found in approximately 2 - 5% of patients with neoplasms in the exocrine pancreas [18]. MCN should not be mistaken with the mucinous noncystic carcinoma (MNC), a histological variant of the ductal adenocarcinoma [18].
The uni- or multilocular lesions of mucinous cystadenocarcinoma are formed by two distinct cellular subtypes, a luminal epithelial layer and an outer stromal layer which form a frequently calcified capsular structure. These lesions are mostly found in the body and tail of the pancreas [18]. Due to its encapsulated appearance, non-invasive MCN can be resected with an overall good prognosis. In the case of invasive disease, a high degree of invasion is strongly correlated with a poor prognosis [18].

Acinar cell carcinoma The acinar cell carcinoma is comprised of acinar cells, forming small glandular units with an absence of large desmoplastic areas [18]. Diagnosis of this subtype is mostly based on immunohistochemical staining of trypsin and chymotrypsin, as these are highly expressed in about 95% of cases [18]. In total this malignancy represents about 1 - 2% of all pancreatic exocrine neoplasms [14, 18]. The overall prognosis of acinar cell carcinoma is comparable to that of ductal adenocarcinoma with an overall 5-year survival rate of less than 10% [18].

Pancreatoblastoma This special pancreatic neoplasia represents the only form almost exclusively diagnosed in children with a median age of diagnosis of 4 years [18]. With an overall incidence rate of 0.5% of pancreatic malignancies in the whole population, it is one of the least frequent cancers of the pancreas. However, it accounts for 30 - 50% of pancreatic neoplasia diagnosed in children [18]. Macroscopically these lesions present with a defined lobular structure separated by fibrous tissue. Patients with local disease are generally treated by a combination of surgery followed by chemotherapy, leading to an overall very good prognosis. In the case of metastatic disease and in rare occurrences during adulthood treatment remains a challenge [18].

1.3 Pancreatic ductal adenocarcinoma

Pancreatic ductal adenocarcinoma (PDAC) arises from the exocrine portion of the pancreas and can occur throughout the whole organ. Nevertheless, approximately 60 - 70% of presented cases arise within the pancreatic head [18]. Histologically, the microenvironment of PDAC is characterized by a dense desmoplastic network, making up about 80% of the tumor mass, mainly produced by activated pancreatic stellate cells [14, 27, 28]. The main components of this dense stromal architecture are formed by collagen I/ III and fibronectin, creating an overall hypoxic and nutrient deprived microenvironment [14, 29, 30]. Besides this, the origin of the malignant cells (i.e. acinar cell, duct epithelium or ductal progenitor cells), sparsely distributed throughout the tumor stroma, are currently a matter of debate [31–33].

Altogether, PDAC is by far the most prevalent subtype of pancreatic neoplasms with an incidence rate of 85 - 90% of all cases [13, 14, 18]. Yearly, approximately 340.000 new cases (2.5% of all malignancies) of PDAC emerge worldwide, making it the twelfth most frequent cancer in both males and females [18, 34]. However, with overall 5-year survival rates of 25 % for localized, 9.9 % for regionally metastasized and 2.3 % for distantly metastasized disease, it currently forms the fourth leading cause of cancer related deaths (figure 2) [14, 18, 35].

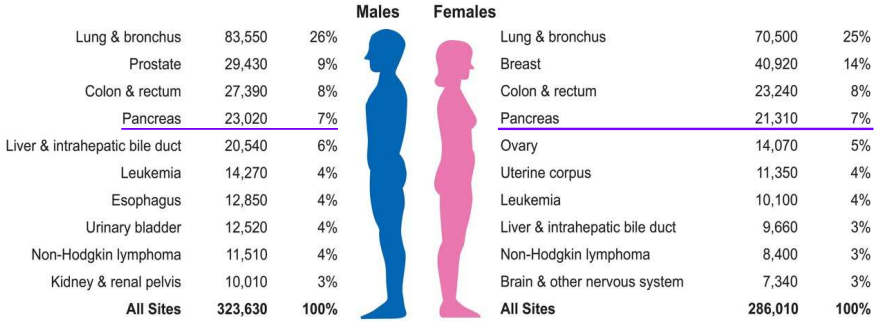

Figure 2 – Annual cancer related death statistics. Indicated are the ten most common causes of cancer related deaths in both male and female patients. The number of annual fatal cases in combination with the respective percentile of all cancer related deaths worldwide are indicated. Adapted from [35]

Given the initially symptomless progression of pancreatic neoplasms, approximately 50 - 60% of patients present at an already unresectable stage of disease with advanced vascular involvement and formation of distant metastases. For these patients there are currently no efficient therapies available (figure 3) [25, 28, 36]. The remainder of patients, presenting with either locally restricted/ primary resectable (15 - 20%) or locally advanced/ borderline resectable (30 - 40% - after neoadjuvant chemotherapy) disease, can currently only undergo extensive surgery followed by chemotherapy [14, 36, 37]. Furthermore, within less than 24 months, approximately 80 - 90% of the patients who undergo surgery and chemotherapy demonstrate fast progressing disease recurrence with an ultimately fatal outcome [38, 39]. Within 5-years post-surgery, almost 95% of patients currently succumb to their disease [18, 38, 39]. Here, the main sites of (metastatic) disease recurrence are either local (pancreatic tissue) or distal (liver, lung and peritoeum; see figure 4) [18, 38, 40].

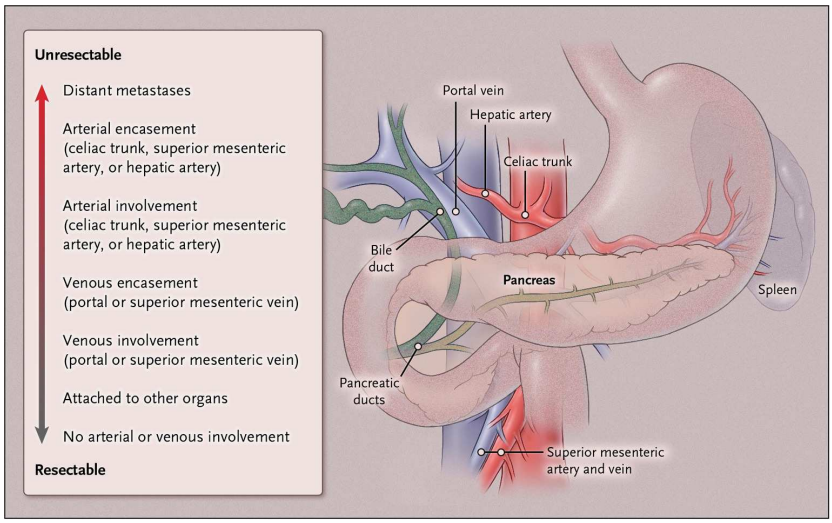

Figure 3 – Surgical resectability of pancreatic cancer. Showing a schematic overview of the anatomical structures leading to PDAC unresectability when involved in tumor progression. Taken from [13]

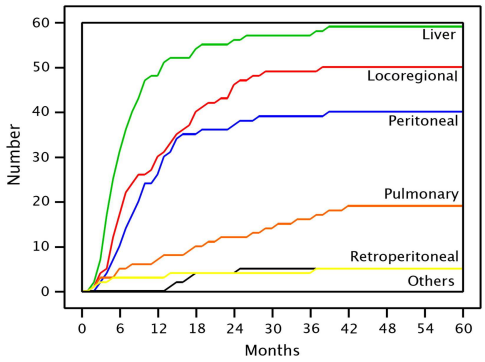

Figure 4 – Patterns of PDAC recurrence following surgery. Indicating the most common site of disease recurrence within 5 years after surgical resection. Taken from [40]

1.3.1 From precursor lesion to invasive malignancy - pathophysiological assessment

Since the transformation process from healthy pancreas to malignant disease can take several decades, multiple stages of premalignant lesions preceding invasive PDAC have been described [13, 18, 41, 42]. Over the course of a lifetime, the number and degree of atypia of premalignant lesions can gradually increase. Nevertheless, it should be noted, that the sole formation of lower grade premalignant lesions does not necessarily lead to full-blown invasive PDAC [43–45]. The following paragraphs show the current consensus of premalignant lesions, associated with PDAC development in more detail:

Pancreatic intraepithelial neoplasia (PanIN) Representing the most common precursor lesion, pancreatic intraepithelial neoplasia (PanIN) is associated with approximately 90% of PDAC cases diagnosed [41]. Depending on the degree of cytologic atypia, PanINs are subdivided into three grades, from minimal (PanIN-1) to high degree atypic deformation (PanIN-3) (see figure 5A) [46]. Upon atypic progression, genetic alterations begin to accumulate within the premalignant cells. Here, activating mutations of *KRAS* already appear in over 95% of early grade PanIN lesions, making it by far the most frequent initiating driver mutation of malignant

cell transformation (see figure 5B) [47, 48]. Additionally, mutational inactivation of *CDKN2A*/ p16, *TP53*/ p53 and *SMAD4* increases in frequency with progression to higher grades of pre-malignant lesions [14, 47].

Intraductal papillary mucinous neoplasm (IPMN) The second most frequent premalignant lesion is represented by intraductal papillary mucinous neoplasms (IPMNs). Here, it needs to be distinguished between the more prevalent non-invasive (60 - 70%) and the infrequent invasive (30 - 40%) lesions [13, 49]. Upon resection, the prognosis for the first is far better, with an overall 5-year survival rate of 70 - 100%. In contrast, the overall 5-year survival for invasive lesions is significantly lower (approximately 30%) [18, 41, 50, 51]. In addition, only approximately 4 - 9% of all PDAC cases are linked to prior formation or presence of IPMN [49, 52, 53].
Histopathologically, these premalignant lesions consist of mucin producing, epithelial papillae associated with the main pancreatic duct or its branches [41] (see figure 5A). With increasing tissue atypia, a growing number of activating mutations in *KRAS* (40 - 60%) and allelic losses (40 - 60%) of *CDKN2A*/ p16 and *TP53*/p53 is detected within these neoplasias [18, 54].

Mucinous noncystic (colloid) carcinoma (MNC or CC) These epithelial neoplasms represent the third most common (2 - 3%) pre-malignant lesion of invasive pancreatic cancer [15, 18, 41, 42]. Overall, these neoplasms mostly manifest as cystic, mucin producing (> 50% of the tumor) nodules in the pancreatic head [55, 56] (see figure 5A). The main recurring mutational alterations found in MNC involve activating mutations in *KRAS* (> 90%), inactivation of *TP53*/ p53 (>40%), as well as *SMAD4* (> 80%), and aberrant methylation of *CDKN2A*/ p16 (>10%) [54, 55, 57–59].

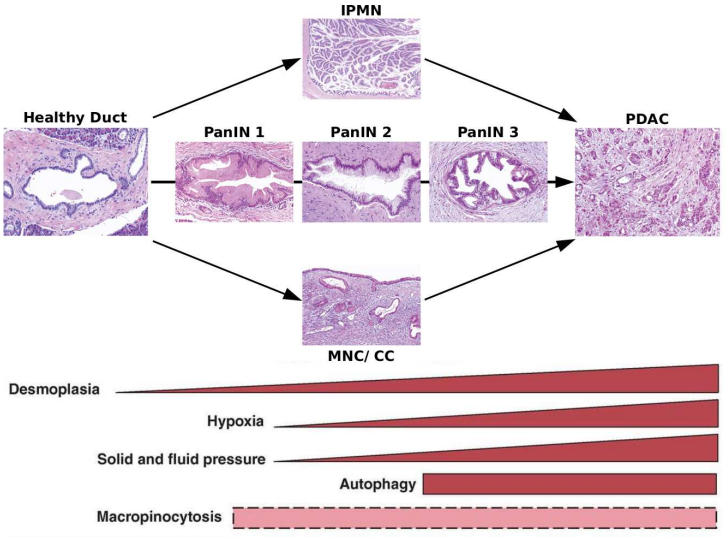

Figure 5 – Development of PDAC from healthy tissue. Schematic overview of the histological progression from healthy pancreas to pancreatic ductal adenocarcinoma through different precursor lesions (top). Increase of molecular and physiological changes taking place with the progression from healthy tissue to PDAC (bottom). Adapted from [48, 60].

1.3.2 Molecular subtypes and mutational landscape of pancreatic ductal adenocarcinoma

The possibility to describe and classify malignancies on a molecular level allowed researchers to further decipher the mutational landscape of pancreatic cancer. Here, two major findings should be highlighted: On the one hand, recurrent mutations together with the involved signaling pathways found in PDAC [61–65] and on the other hand the definition of molecular subtypes of PDAC [64–67]. Both findings might improve patient care in the future. The following paragraphs will briefly summarize the current state of discussions on these topics.

Recurrent Mutations and the involved signaling pathways in PDAC Despite the overall low mutational burden of pancreatic cancer (see figure 6), in-depth whole exome analyses revealed sets of recurring genetic alterations in pancreatic cancer patients [61, 63–65]. With a prevalence of >90%, activating mutations of the proto-oncogene *KRAS* constitute by far the most common recurring mutations found in pancreatic malignancies [64, 65, 68]. Particularly mutations of *KRAS* codon 12 (>40% G12D; >20% G12V; >10% G12R) were found early on during pancreatic cancer development [65]. Due to the central role of *KRAS* in cell signaling, these mutations lead the constitutive activation of the MAPK/ ERK signaling pathway and result in increased cell proliferation rates, as well as apoptosis suppression [61, 69]. Patients displaying *KRAS* wild type variants were recently shown to hold alternative driver mutations in central signaling pathways of cell proliferation*, i.e. BRAF* (MAPK/ ERK pathway), *GNAS* (cAMP-dependent pathway) and *CTNNB1* (Wnt signaling) [65]. Additional hotspots of genetic alteration found in PDAC include inactivating mutations of *CDKN2A* (30 - 40%; G1-S transition regulation), *TP53* (>70%; DNA damage control) and *SMAD4* (>30%; TGFβ signaling) [64, 65, 68]. Furthermore, a small subset of patients (5 - 10%) presents with inherited mutations in DNA damage repair genes (*BRCA1*, *BRCA2*, *ATM* and *PALB2*) [64, 65, 70, 71]. Taken together, these recurring mutations found in PDAC are limited to few signaling pathways involved in cell survival and proliferation (see table 2) [61, 65]. The complexity of communication between these pathways, however, should not be underestimated, as further unraveling of their interplay might help to explain the slow progress in PDAC treatment efficacy and give rise to more effective combination therapies in the future. Besides this, the majority of mutations found in PDAC remain passenger mutations that are typically patient specific (see figure 7).

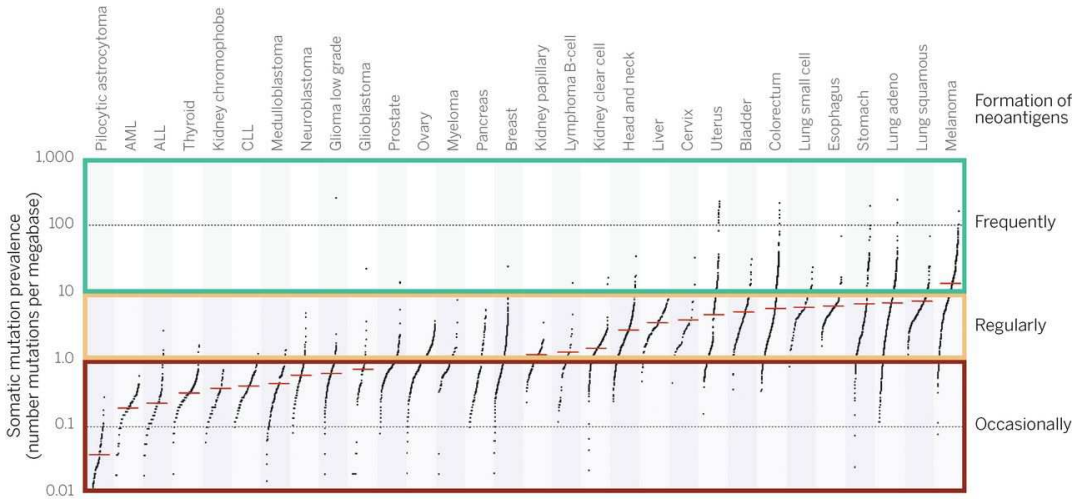

Figure 6 – Tumor associated mutational burden. Shown is the estimated frequency of somatic mutations in combination with frequency of neoantigen forming mutations for malignancies of different anatomical structures. The coloured boxes indicate the range and likelihood of neoantigen formation. Taken from [72].

Table 2 – Core signaling pathways involved in PDAC progression. Indicated are the commonly affected recurring pathways in combination with the fraction of patients affected and the mostly affected genes. Adapted from [61, 64, 65, 73, 74].

Function	Fraction of patients [%]	Commonly affected genes
RAS-MAPK signaling	90 - 95	KRAS, MAP2K4, RASGRP3, BRAF
Cell cycle control	70 - 80	CDKN2A, TP53, TP53BP2
TGFβ signaling	40 - 50	SMAD4, SMAD3, TGFBR1, ACVR1B
Histone modification	20 - 25	KDM6A, SETD2, MLL2, MLL3
RNA processing	16	SF3B1, U2AF1, RBM10
SWI/ SNF complex	10 - 15	ARID1A, PBRM1, SMARCA4
DNA repair	5 - 12	BRCA1, BRCA2, ATM, PALB2, ATF2
ROBO/ SLIT pathway	5 - 15	ROBO1, ROBO2, SLIT2, MYCBP2
Wnt/ Notch signaling	< 10	RNF43, MARK2, MIB1, GATA6, TLE4

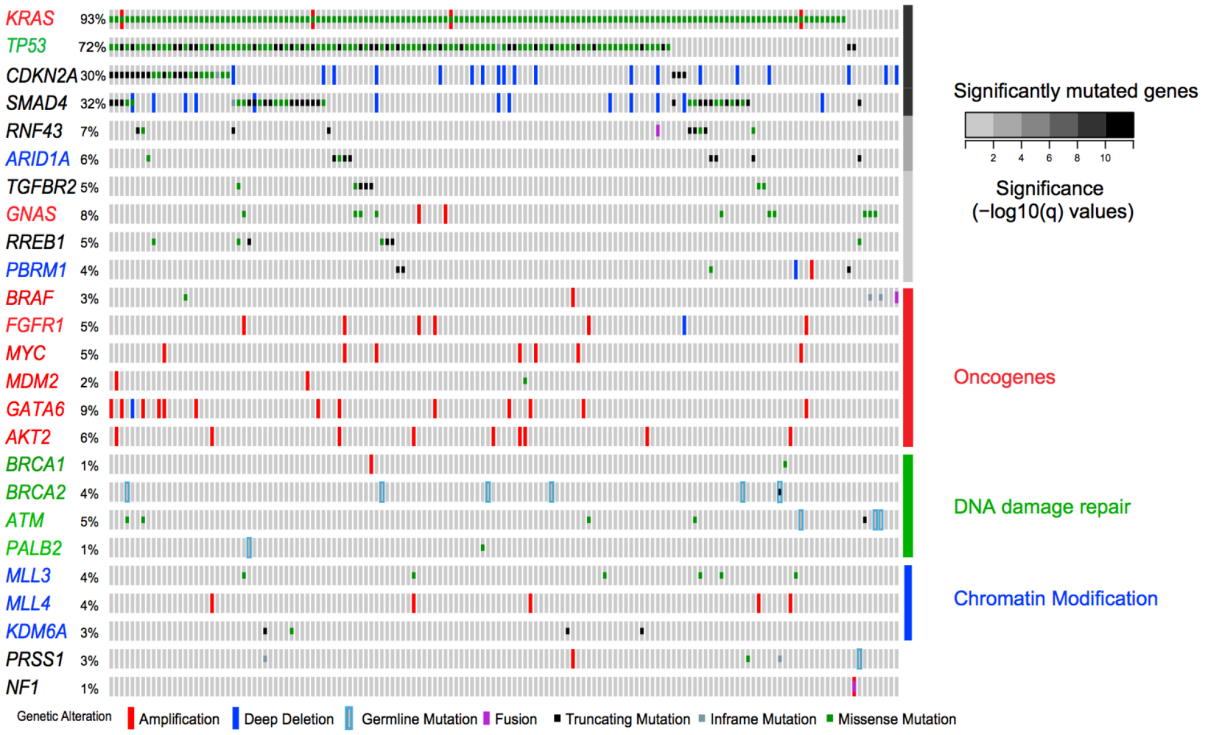

Figure 7 – Mutational landscape of pancreatic ductal adenocarcinoma. Depicted are the most common recurring genomic alterations of 149 PDAC patients. Taken from [65].

Molecular Subtypes of PDAC Over the past years, multiple groups have worked on defining specific molecular subtypes of PDAC, based on gene expression profiling [64–67]. Here, especially the recent work of the "Cancer Genome Atlas Research Network" needs to be mentioned, as they elegantly combined different previous findings on subtype characterization and could confirm parts of these [65]. Splitting their analysis set into high and low purity samples, based on the number on neoplastic cells, they confirmed certain subtype overlaps between previous studies and ruled out other formerly defined subtypes as artifacts of low tumor cell content. Based on this, the currently confirmed molecular subtypes described for pancreatic cancer are divided into the classical/ progenitor [64–67] and the basal-like/ squamous subtype [64, 65, 67]. In the case of the classical/ progenitor subtype a correlation with the expression of genes involving pancreatic cell/ lineage development, fatty acid oxidation, drug metabolism and steroid hormone biosynthesis was found [64]. The basal-like/ squamous subtype on the other hand is characterized by the expression of genes involved in inflammation, hypoxia response, metabolic reprogramming, autophagy and endodermal cell fate abrogation [64]. Although deeper insight into the molecular characteristics of PDAC subtypes is still needed, the recent results show promising future treatment opportunities tailored to recurrent gene expression networks.

1.3.3 Risk factors associated with PDAC

Over the past decades of intensive statistical analyses, certain factors have been associated with an increased risk of developing pancreatic cancer. As expected, factors directly involving the pancreas (chronic inflammation, familial PDAC, diabetes mellitus and obesity) rank among

the most highly increased risks for the development of pancreatic cancer [75–81]. In addition, genetic predispositions with an overall increased risk of unspecific cancer development - Peutz-Jeghers syndrome, familial atypical multiple mole and melanoma (FAMMM) and lynch syndrome - are associated with PDAC [82–86]. A brief summary of the associated risk factors and genetic predispositions is given in table 3.

Table 3 – Risk factors and lifetime risk of inherited syndroms associated with PDAC. FAMMM = Familial atypical multiple mole and melanoma syndrome. Adapted from [13, 14, 18].

Variable	**Associated risk**
Risk factor	*Relative risk [%]*
Chronic pancreatitis[76, 81]	2 - 6
Smoking[87]	2 - 3
Diabetes mellitus[88]	2
Obesity[80]	2
Genetic predisposition (associated genes)	*Lifetime risk [%]*
Hereditary pancreatitis (*PRSS1*, *SPINK1*)[75, 79]	50 - 65
Peutz-Jeghers syndrome (*STK11*)[83]	30 - 40
FAMMM (*CDKN2A*/ p16)[82, 84, 85]	10 - 35
Familial pancreatic cancer (>2 first degree relatives)[65, 77, 78]	5 - 10
Lynch syndrome (*MLH1*, *MSH2*, *MSH6*)[86]	4 - 9
Cystic fibrosis (*CFTR*) [89]	5
Hereditary breast and ovarian cancer (*BRCA1*, *BRCA2*, *PALB2*)[90, 91]	1 - 4

1.3.4 Current standard treatments of pancreatic ductal adenocarcinoma

Seeing the high complexity, diversity and fatality of PDAC, a lot of effort was put into finding a consensus for patient treatment and care. These efforts range from initial diagnosis and staging of the disease up to defining the ideal treatment options for each stage of pancreatic malignancy. The following paragraphs briefly summarize these efforts based on current treatment consensus.

Diagnosis and Staging Due to the short time window available for treatment of PDAC an accurate initial assessment of the disease stage prior to therapy is crucial. Over the past years it was generally agreed to stage PDAC based on the tumor node metastasis (TNM) system [92, 93]. A primary diagnosis of the disease usually appears by chance during routine screenings or medical examinations due to unspecific abdominal discomfort [19–21]. Upon suspicion of PDAC, patients are immediately screened with current state-of-the-art imaging techniques to rule out any kind of misdiagnosis. These techniques involve magnetic resonance imaging (MRI), positron emission tomography (PET), multi-detector computer tomography (MDCT) or endoscopic ultrasonography [13, 14, 94]. Due to arterial and venous phasing techniques [13, 95], MDCT currently forms the most robust and widely available imaging technique for initial staging of the disease [14, 18, 92]. For histological characterization of the tumor stage and potential origin, pathological assessment by endoscopic ultrasonography guided fine needle aspiration is usually applied [14, 96, 97]. Assessing combinations of general serum tumor markers, such as carbohydrate antigen 19-9 (CA19-9), carcinoemryonic antigen (CEA), DUPAN-2 or Span-1, in the context of PDAC is mainly applied as an indicator of metastatic disease

and to monitor disease recurrence [13, 14, 18, 98–102]. Baseline levels of these markers in patients with low stage disease rule out their use as diagnostic markers [14]. Following diagnosis and staging of the disease, surgical resection currently forms the only potentially curative treatment for PDAC [13, 14].

Surgery For patients diagnosed with primary or borderline resectable disease (following neoadjuvant chemotherapy), surgery currently represents the only potentially curative option. Successfully performed for the first time in 1909 by W. Kausch [103], and later optimized amongst others by A. Whipple [104], the pancreaticoduodenectomy (Kausch-Whipple procedure) is the most common surgical intervention for pancreatic malignancies to date [14, 105]. Depending on the disease localization, partial (head), distal (tail) or total (whole organ) pancreaticoduodenectomy is carried out [106, 107] (see figure 8). Due to an increased risk of post surgical complications, total pancreaticoduodenectomy is avoided whenever possible [105]. During early applications of the procedure, post-surgical complications and mortality occurred in approximately 10 - 45% of the patients, depending on the experience of the surgeon. Over the past decades, these complications were counteracted by further improving and refining the procedure, resulting in a post-operation mortality of approximately 2% in highly specialized disease centers today [108–110]. As favorable as improvements of these surgical techniques seemed over the last years, the overall 5-year survival of both, primary and borderline resectable patients, converges to approximately 20 - 25% [36, 111, 112]. This is mainly associated with a fast disease recurrence in almost 90% of the patients receiving surgical resection and follow-up treatments [13, 14].

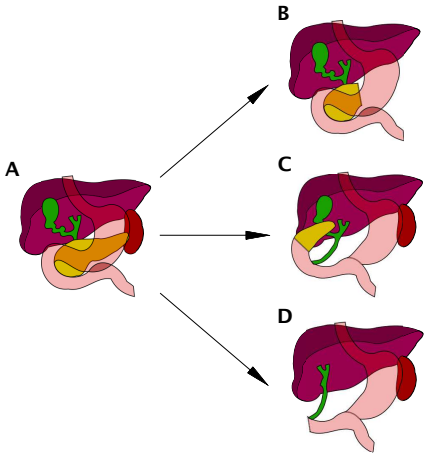

Figure 8 – Schematic representation of different PDAC surgeries. Indicated are the outcomes of the most commonly applied surgical procedures (B - C). In addition, the healthy organ environment surrounding the pancreas is shown in (A). Depending on the organs affected by surgery, the applied procedures include distal pancreatectomy (B), Kausch-Whipple (C) or total pancreatectomy (D).

Neoadjuvant and adjuvant Chemotherapy In the context of pancreatic cancer, chemotherapeutic regimen are applied in either a neoadjuvant or adjuvant setting. In the case of neoadjuvant treatment, the main goal is an overall reduction of tumor mass in patients with borderline resectable disease, allowing for later surgical resection of the remaining tumor tissue. Patients who received surgical resection are later followed up by adjuvant chemotherapy with the aim of

improving disease outcome [13, 14, 18]. Over the past decades, regimen applicable for adjuvant chemotherapy could rarely improve the overall outcome. The major milestones in adjuvant PDAC chemotherapy are summarized below.
Discovered in the context of liver cancer in 1957, 5-fluorouracil (5-FU) later found its way into the early treatment regimen of pancreatic cancer, resulting in an increase in median survival of 9 months compared to surgery alone (20 vs 11 months) [113–116]. Until the late 1990-ies, 5-FU monotherapy was the central therapeutic for advanced pancreatic cancer with no combination therapy giving rise to improved survival [117–120]. In 1997 a randomized trial (CONKO-001) revealed gemcitabine to be the first regimen to modestly improve patients median survival compared to 5-FU in an adjuvant setting (5.7 vs 4.4 months). The improved clinical response (23.8% vs 4.8%) and increased 12-month survival (18% vs 2%) in patients treated with gemcitabine (versus 5-FU) made it the first-line chemotherapeutic regimen for more than the following decade [38, 121]. During this time, the use of targeted therapies against the main signaling pathways involved in PDAC rarely led to a significant improvement of patients overall survival [122, 123]. Here, a combination therapy of Erlotinib, an inhibitor of the epidermal growth factor receptor (EGFR), and gemcitabine formed the first targeted treatment receiving FDA approval in 2005 [124]. Later, Everolismus (mTOR inhibitor) and Sunitinib (receptor tyrosine kinase inhibitor) followed for the treatment of progressive neuroendocrine tumors [125, 126]. In 2011 a phase III clinical trial (PRODIGE 4/ACCORD 11) was the first to show an unequivocal benefit of FOLFIRINOX (folinic acid (leucovorin), 5-fluorouracil, irinotecan and oxaliplatin) compared to gemcitabine monotherapy (11.1 vs 6.8 months median survival) [39]. A less favorable hazard profile later limited the use of FOLFIRINOX to younger and physically fit PDAC patients [39, 127]. Since then, only a few additional studies could show supplementary clinical benefit of gemcitabine combination therapy compared to gemcitabine monotherapy. Especially combinations with nano albumin bound (nab-) paclitaxel (8.5 vs 6.7 months) or capecitabine (10.1 vs 7.4 months) revealed significant survival benefits compared to gemcitabine monotherapy [128, 129]. These results later led to the adaptation of adjuvant therapy of PDAC to a combination regimen of gemcitabine and nab-paclitaxel for patients unable to receive FOLFIRINOX treatment [130].

1.3.5 Disease outcome with current standard of care

However promising recent attempts may seem, even with current standard of care treatments approximately 90 - 95% of patients will ultimately die from their disease within only a few months. All together, the overall 5-year survival currently converges to 25 % for localized, 9.9 % for regionally metastasized and 2.3 % for distantly metastasized disease [14, 18, 35]. Reasons for this poor prognosis include the late diagnosis in most patients, deeming them unresectable, as well as the high rate of disease recurrence in resectable patients after initially successful surgery and chemotherapy [13, 14]. Taken together it becomes obvious, that there is currently no curative option for PDAC available. Treatments applied rather serve palliative care than cure patients, elongating their lives by merely a few months at best.

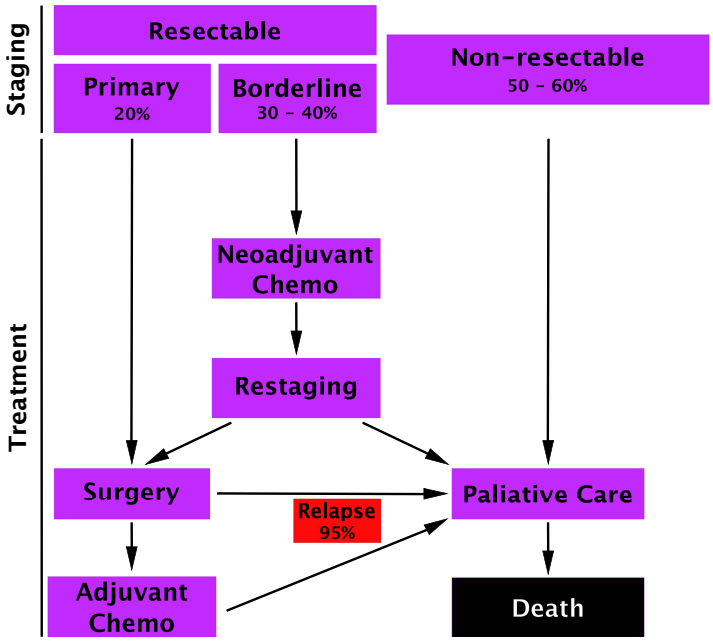

Figure 9 – Current standard of care workflow for the treatment of PDAC. Indicated are the different sections of pancreatic cancer care from disease staging followed by stage dependent treatments to the fatal outcome of the majority of patients.

1.4 Tumor Immunology

Based on Paul Ehrlich's initial assumptions on tumor control by the immune system, back in 1909, a plethora of potential new therapies against one of mankind's most frightening diseases arose [131]. The complex interplay between tumors and the immune system was aptly summarized by H.F. Dvorak as a "wound that does not heal" [132]. The following paragraphs will give a brief overview of the research surrounding tumor immunology, with an emphasis on T cell mediated tumor immunity.

1.4.1 The role of T cells in the anti tumor response

A first indication connecting an immune response to an anti tumor reaction was found when the immunization of mice with irradiated, carcinogen-induced tumor cells led to a subsequent rejection of the non-irradiated cells from the same tumor upon re-challenge [133, 134]. These early results not only indicated that mutation-induced alterations of tumor cells raised an immune response, but also that the immune system was able to create a certain memory against these tumors (after immunization). Nevertheless, these results did not reveal which cell populations were involved in tumor recognition and rejection.
Only later, using immunodeficient, syngeneic mouse strains (e.g. $RAG2^{-/-}$, a strain lacking mature B and T cells [135]and / or $Foxn1^{nu}$, an athymic strain lacking T cells [136]), the influence of certain immune cell populations on specific tumor cells could be studied in detail. During early pre-clinical experiments with these mice, researchers observed an increased susceptibility to carcinogen-induced tumors in immunodeficient mice compared to their wild type counterparts, highlighting the importance of T cells in the protection against carcinogen-induced or spontaneous tumors [137].

The realization of the unequivocal significance of T cells in the anti tumor immune response resulted in the implementation of a first clinical trial which applied tumor infiltrating lymphocytes (TILs) for the treatment of melanoma [138, 139]. The promising results in melanoma therapy were later followed by the use of TILs for the treatment of a variety of malignancies. Results varied from barely measurable responses to durable regressions [140–145]. Further analyses of the target epitopes of these T cells revealed that they consisted of tumor specific mutations or over-expressed self antigens [142, 144, 146], indicating that using T cells was a promising approach for the treatment of malignancies.

1.4.2 Dynamic tumor evolution and neoepitope identification

The most important characteristic of tumor progression is the evolutionary accumulation of genetic alterations during a persons lifetime, leading to selective advantages (e.g. proliferation, survival), as well as disadvantages (e.g. death, senescence), or no influence on the cells overall fate [147–150]. This is especially relevant since each new alteration slowly distinguishes transformed cells from the untransformed surrounding, resulting in their traceability by or protection from the immune system.
The introduction of high throughput sequencing, focussing on the expressed tumor exome, constituted an important milestone in understanding the mutational landscape of tumors on a bigger scale [151–154]. Over the past decades it thus became apparent, that the process of tumor evolution differs greatly between each patient (intertumoural heterogeneity), giving each tumor an individual set of mutational configurations [72, 155]. In addition to these patient variabilities, single lesions were found to already consist of multiple subclonal populations (intratumoural heterogeneity), each with a defined subset of mutations (see figure 10) [156–158]. Thus, genomic instability results in a complex, dynamic set of genetic changes in each malignant cell. In addition, these dynamics could explain the development of therapeutical resistance after initial objective response to a certain treatment [159–162]. Consequently, the use of T cells based therapies against small numbers of mutations might be largely influenced by intratumor heterogeneity and tissue sampling.
The likelihood of exposing malignant cell progression to the immune system by antigen presentation on major histocompatibility complexes (MHC) increases with each additional genetic alteration [163, 164]. These antigens may include over-expressed self-antigens with incomplete T cell tolerance (e.g. by tissue restricted expression), as well as mutation-derived epitopes (neoepitopes) [72]. Over the years, targeting of neoepitopes gained special interest, as the respective T cell pool is not affected by central tolerance and expression is truly tumor-specific [72, 165]. However, their identification was limited by technological hurdles for a long time. Hence, the scope of antitumor T cell immunity remained unclear [155, 166]. Following technological progression and sophisticated experimental execution, it was later shown, that initially nonimmunogenic murine leukemia cells were capable of inducing cytolytic T cell reactivity after chemical mutagenesis [167]. These results reignited the idea of (neo-)antigens involved in the anti tumor T cell response, ultimately resulting in the identification of the first immunogenic, nonmutated self-antigens (MAGE-A1, tyrosinase, Mart-1 and gp100), as well as the realization that mutation derived epitopes are involved in malignancy progression [168–174]. The clinical relevance of neoepitopes was recently further underlined in multiple studies examining T cell

reactivity against certain mutation-derived epitopes [142–144, 146, 175, 176]. Here, the formation, presentation and recognition of neoepitopes resulted in complete disease remission or led to reduced recurrence frequencies [142, 144, 176]. For pancreatic cancer the frequent formation of potentially immunogenic neoepitopes was recently shown bioinformatically (i.e. without functional validation) by patient-based epitope prediction [177, 178].
In addition to the identification of neoepitopes by induction of T cell responses, researchers recently began to explore the tumor HLA ligandome by high-sensitivity mass spectrometry, allowing for direct identification of naturally processed and presented antigens [179–181]. With an expected increase in sensitivity and accessibility in the near future, this approach might become particularly interesting for the identification of true HLA binding epitopes, especially, when taking into account that the current algorithm based epitope prediction methods are far from optimal. To date, predictions for HLA-A02:01 binding epitopes are the most reliable, while other MHC-I alleles and all MHC-II alleles lag behind in prediction accuracy due to smaller training sets for the algorithm's artificial neural networks [182, 183].

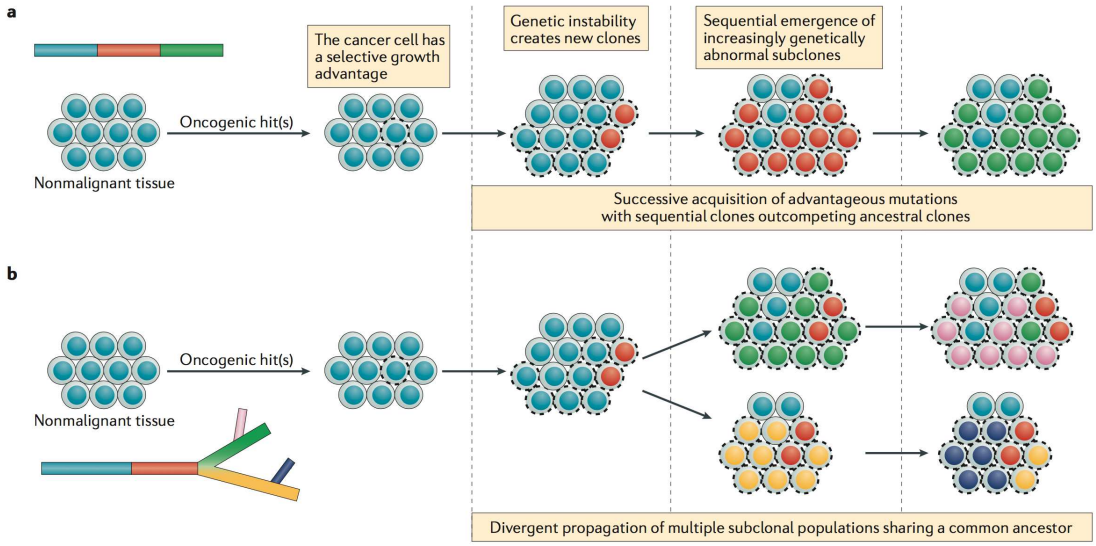

Figure 10 – Models of tumor evolution. Depicted are the two most common pathways of clonal tumor evolution: The linear model of tumor evolution, with surviving dominant clones inheriting the ancestral alterations, leading to a homogenous mutational landscape (Top) and the branched evolution model, leading to the formation of distinct subclonal populations diverging from common ancestral cells (Bottom). Taken from [158].

1.4.3 From immunesurveillance to immunoediting

Technological hurdles hindered the prosecution of Ehrlich's initial ideas, taking another half a century for the field of tumor immunology to slowly start moving ahead. This time by the more precise - yet controversial at the time - assumption of immunosurveillance by Burnet and Thomas, who proposed a sentinel function of the immune system in recognition and elimination of nascent malignancies [184, 185]. Almost another 50 years passed before technologies were advanced enough to collect data supporting their hypothesis and the concept of tumor immune editing was accepted. The current model of immune editing describes a triptych of darwinian selection, from the early onset of atypic transformation over a balanced disease control by the immune system to the fatal outgrowth of the malignancy [186, 187]. During the past decade,

this hypothesis was strengthened by findings in mouse experiments and human clinical trials [144, 153, 188, 189]. The following paragraphs briefly summarize the three stages of this interplay between tumor and immune system.

Elimination This process describes the initial stage of immunoediting, based on the assumptions of immunosurveillance by Burnet and Thomas [186]. During this stage, spontaneous accumulation of transformed cells leads to the initiation of a response cascade mediated by cells of the innate, as well as the adaptive immune system. By upregulation of stress induced markers (e.g. NKG2D, surface calreticulin), transformed cells are initially mainly recognized by natural killer cells (NK cells). NK cell activation in turn leads to the induction of apoptotic tumor cell death (e.g. TRAIL or perforin/ granzyme mediated) and to secretion of pro-inflammatory cytokines (e.g. IFNγ, IL-12). Additionally, macrophages and granulocytes secrete TNFα, IL-1β, IL-12 and reactive oxygen species (ROS), amplifying the inflammatory anti-tumor response. Furthermore, remnants of dying tumor cells are ingested by dendritic cells (DCs), which migrate to the tumor draining lymph nodes, priming $CD4^+$ and $CD8^+$ T cells by processing and presenting tumor derived antigens [190]. In the final stage of malignant cell elimination, tumor specific T cells home to the site of inflammation, inducing antigen specific tumor cell death mediated by Fas and TRAIL receptor pathways.

Equilibrium Due to a constant immune selective pressure and their inherent genetic instability, the remaining malignant cells undergo genetic and epigenetic alterations, ultimately leading to the rise of less immunogenic tumor cell clones. The equilibrium phase of immunoediting is often referred to as a stage of immune mediated tumor dormancy, where anti-tumor (e.g. IFNγ, IL-12) and tumor promoting (e.g. IL-10, IL-23) factors are evened out [187, 191]. It was shown, that specifically T cells, but not innate immune cells, mediate this stage of tumor progression, mainly by antigen specific activation [187, 192–194].

Escape The persistent immune selective pressure against genetically unstable cells ultimately results in the development of clones resistant to immune recognition. The main mechanisms of evasion involve the loss of immune recognition (e.g. loss of MHC-I or tumor antigen expression), increased tumor cell survival by upregulation of antiapoptotic mechanisms (e.g. increased expression the transcription factors STAT3 and Bcl-2), or creation of an immunosuppressive environment (e.g. inhibition of T cell responses by expression of PD-L1 on the tumor cell surface) [144, 195–197]. In addition, an increasing number of immunosuppressive cells - regulatory T cells (T_{reg}), myeloid derived suppressor cells (MDSC) and M2 macrophages - begins to infiltrate the expanding malignant environment [198]. By secretion of regulatory (e.g. iNOS, arginase) and immunesupressive (e.g. TGFβ, IL-10) molecules these cells enhance the inhibition of tumor reactive, effector T cells [191]. All together, the increasingly immunosuppressive environment facilitates disease progression. These mechanisms are summarized in figure 11.

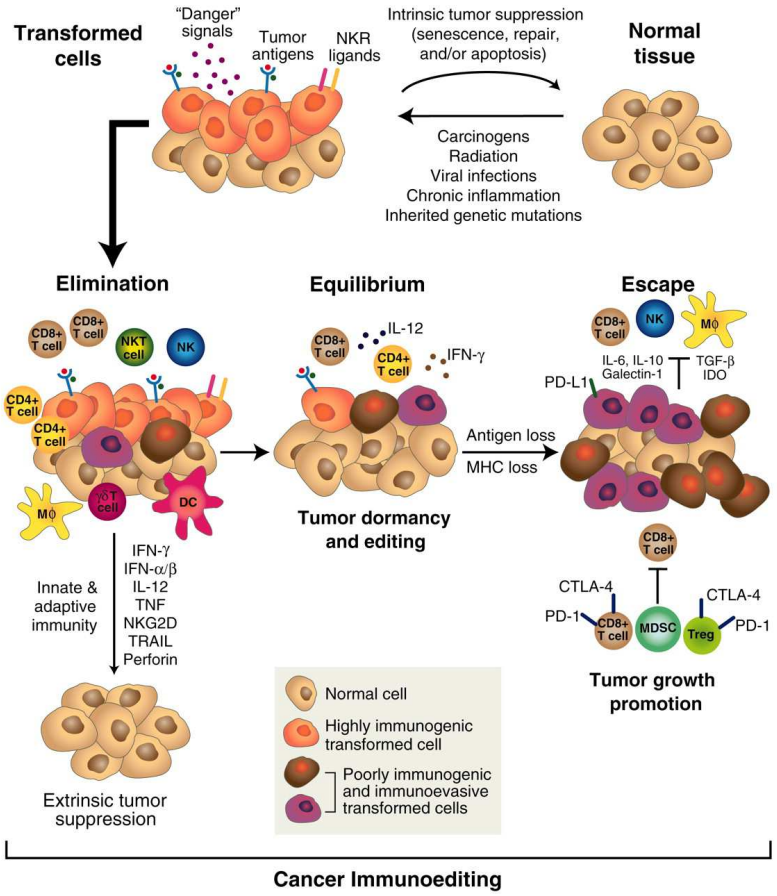

Figure 11 – Schematic representation of the cancer immunoediting concept. Depicted is the transformation from healthy tissue (top right) to tumor suppression (bottom left) or invasive malignant disease under the surveillance of the immune system (middle left to right). Taken from [187]

1.4.4 Cell mediated tumor eradication

It becomes more and more apparent, that the interplay between the tumor and the immune system involves a complex network of cellular interactions. Particularly genome instability, i.e. emerging mutations, is of special interest, as the generated neoepitopes are potentially recognized by immune cells. The following paragraphs will focus on the two major immune cell populations involved in tumor derived antigen presentation and recognition (see figure **??** for a summary of the described processes).

Dendritic cells As professional antigen presenting cells, dendritic cells (DCs) control the initiation and guidance of immune responses. They are phagocytic cells derived from bone marrow haematopoietic progenitor cells ($CD34^+$) and initially differentiate into immature precursors with enhanced antigen uptake and low T cell priming capacity [199–201]. These immature DCs express low levels of MHC and co-stimulatory molecules (e.g. CD80, CD86, CD40) [202]. They reside in the tissue where they screen their surroundings for foreign antigens and molecules, using pattern recognition receptors (PRRs) such as toll-like receptors (TLRs) or NOD-like receptors (NLRs) specialized in the recognition of non-self molecules (e.g. viral nucleic acids or bacterial components) [203, 204]. Once foreign molecules or cellular debris (e.g. from dying tumor cells) are recognized, DCs undergo a maturation process, upregulating the surface expres-

sion of MHC and co-stimulatory molecules, thus increasing their capacity to prime naïve T cells. In addition, this activation leads to an increased uptake of the recognized molecules or cells, combined with enhanced antigen processing and presentation on MHC molecules [205, 206]. Initially, phagocytosed antigens are broken down in the phagosomes and presented on MHC class II molecules. Following an export to the cytosol, combined with proteasomal degradation, antigens may also be cross-presented on MHC class I [203, 204, 207]. Once fully matured, DCs can home to a local lymph node to induce priming of naïve $CD4^+$ and $CD8^+$ T cells. In the context of tumor immunology, the process of dendritic cell maturation upon antigen uptake and presentation can lead to the presentation of mutation derived epitopes, leading to effector T cell responses against the respective neoepitopes.

T cells Originating from haematopoietic stem cells of the bone marrow, this cellular subset matures in the thymus [208]. T cells are carefully selected here in order to avoid self-reactivity. In an initial step, the cells are selected for the capability of their T cell receptor (TCR) to bind either MHC-I or MHC-II on cortical thymic epithelial cells (cTECs) [209–211]. Depending on MHC-TCR interaction, the ensuing maturation of the initially CD4/CD8 double-positive T cells is determined. Increased MHC-I binding leads to $CD8^+$ T cell maturation, whereas MHC-II interaction promotes $CD4^+$ maturation. For the second step of selection, T cells home to the thymic medulla, where they are monitored for self-antigen reactivity [209–211]. Here, T cells binding self-antigens presented by medullary thymic epithelial cells (mTECs) with high affinity receive a death signal and undergo apoptosis. The resulting, naïve T cell pool leaves the thymus and migrates to secondary lymphoid organs awaiting the encounter of target antigens. For proper priming, naïve T cells require presentation of their specific antigen on DCs in order to further differentiate into effector cells. The required signal cascade for this differentiation involves three distinct signals: recognition of the peptide:MHC complex, interaction with costimulatory molecules (such as CD28/B7) expressed by the antigen-presenting cell and the T cell, respectively, and the presence of cytokines secreted by DCs (e.g. IL-12, IL-4, TGFβ) [212, 213]. In the context of $CD4^+$ T cell polarization, the cytokines present during the priming phase determine the later function of the emerging effector cells (see table 4) [213]. Afterwards, resulting effector T cells migrate to the site of inflammation, screening the local tissue for their specific antigen and either initiate destruction of affected cells ($CD8^+$ cytotoxic T cells) or yield support during this reaction ($CD4^+$ helper T cells). Upon recognition of a specific antigen, effector T cells can undergo further differentiation into long-lived memory subsets. They might develop into central memory T cell (T_{cm}), residing in secondary lymphoid organs, or into effector memory cells (T_{em}), mainly circulating in peripheral tissues [214, 215]. These antigen experienced T cells can in turn, unlike naïve T cells, be activated by antigen presenting macrophages and B cells [216, 217]. Prolonged antigen exposure, however, may result in the exhaustion of specific T cell clones. Exhausted T cells are characterized by an upregulated expression of inhibitory receptors (e.g. PD1, LAG-3, TIM-3) and loss of effector cytokine secretion [215, 218, 219].
In the context of tumor control and eradication, primed T cells home from the draining lymph node to the malignant site, searching for their cognate antigen. Arriving in the tumor, $CD4^+$ and $CD8^+$ effector T cells can take over the role of direct tumor killing [220–223]. The main mechanisms involved in this include the expression of Fas ligand (FasL) and, in the case of $CD8^+$ effector cells, TNF-related apoptosis inducing ligand (TRAIL) or secretion of Perforin/

GranzymeB [223, 224]. In addition, $CD4^+$ effector cells can augment an indirect response in $MHC\text{-}II^{neg}$ tumors, via MHC-II restricted antigen recognition on macrophages [222].

Table 4 – Brief overview of T cell subset differentiation. Shown are the different T cell subsets in combination with the cytokines inducing their differentiation from naïve T cells, the surface markers and the effector cytokines characterizing each subset. Adapted from [215].

Subset	Polarization	Induction Factors	Surface marker	Effector Cytokines
$CD8^+$	Cytotoxic T cell	IL-2, IL-12	CD3, CD8	IFNγ, Perforin, Granzyme
$CD4^+$	T_H1	IL-2, IL-12, IFNγ	CXCR3, CCR5	IFNγ
	T_H2	IL-2, IL-4	CCR4, CCR8	IL-4, IL-5, IL-13
	T_H9	IL-2, IL-4, TGFβ	CCR3, CXCR3, CCR6	IL-9
	T_{FH}	IL-6, IL-21	CXCR5, CD40L	IL-21
	T_H17	IL-6, IL-21, IL-23, TGFβ	CCR6	IL-17, IL22
	T_{Reg}	IL-2, TGFβ	PD1, CTLA4	IL-10, TGFβ

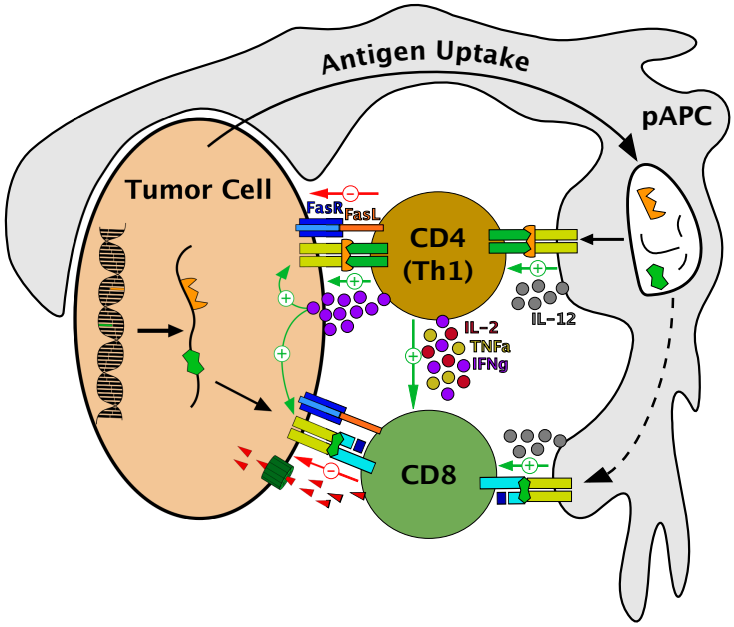

Figure 12 – Schematic overview of T Cell mediated tumor erradication. Shown is the tumor antigen uptake by dendritic cells, subsequent naïve T cell priming and the resulting direct mechanisms involved in the T cell anti tumor response.

1.5 Tumor Immunotherapy

In view of the effective responses our immune system mounts against foreign invaders and its active role in malignancy control, using it to directly target malignancies appears feasible. The following paragraph will give a brief overview of immune therapeutic approaches which have successfully improved our fight against cancer. In light of the aims of the presented thesis, the major focus will be put on adoptive T cell transfer therapies.

1.5.1 Antibody mediated therapy

Monoclonal antibody production and their use in the treatment of haematological malignancies already dates back to the late 1970s. With the approval of Rituximab (anti-CD20) the

first antibody mediated cancer therapy became available in 1997 [225–229]. With the identification and characterization of factors dampening the anti-tumor T cell response (e.g. PD-L1, PD-1, CTLA4) in a broader range of malignancies, especially solid malignancies, a new era in antibody mediated immunotherapy emerged [230–235]. In healthy individuals, these immune-inhibitory molecules are needed to avoid autoimmunity and exacerbated immune reactions [234]. In the course of tumor progression, upregulation of these factors strongly reduces tumor specific T cell immunity, thereby promoting rapid disease progression [234]. As a direct inhibitor of effector T cell function, CTLA4 (a negative regulator of TCR activation) was targeted by the first immune checkpoint inhibitor (Ipilimumab) approved by the FDA in 2011 for patients with advanced melanoma due to its significant impact on tumor regression and patient survival [236–238]. In recent years, more and more immune checkpoint antibodies and their combinations showed clinical efficacy in solid malignancies and received FDA approval (see table 5). Besides the massive success in immune checkpoint inhibition, new therapeutic approaches involve immune stimulatory antibodies (e.g. anti-CD40, anti-CD137, anti-OX40) as well as bi-specific T cell engagers (BiTE antibodies) and are currently being investigated [239–242].

Table 5 – Selected list of currently approved antibody mediated cancer therapies. Based on [243, 244]

Antibody	Target	Type	First FDA Approval	Current indications
Rituximab	CD20	Chimeric IgG1	1997	non-Hodgkin lymphoma
Trastuzumab	HER-2	Humanized IgG1	1998	Breast cancer
Ipilimumab	CTLA4	Human IgG1	2011	Metastatic melanoma
Pembrolizumab	PD-1	Human IgG4	2014	Metastatic melanoma, stomach, lung and bladder cancer
Nivolumab	PD-1	Human IgG4	2014	Metastatic melanoma, lung, liver, kidney and colorectal cancer
Avelumab	PD-L1	Human IgG1	2015	Merkel cell carcinoma
Nivolumab + Ipilimumab	PD-1 + CTLA4	Human IgG4/ IgG1	2015	Metastatic melanoma and renal cell carcinoma
Atezolizumab	PD-L1	Human IgG1	2016	Non-small cell lung and bladder cancer
Durvalumab	PD-L1	Human IgG1/κ	2018	Urothelial carcinoma

1.5.2 Therapeutic vaccination

The efficacy of preventive vaccinations against virus (e.g. by HPV, HBV) and bacteria (e.g. *H. pylori*) induced malignancies has been known for a long time and will, therefore, not be discussed in detail here [245, 246]. Therapeutic vaccines inducing immunity against already established tumors on the other hand gained more attention only recently. Two major approaches are distinguished with regard to their target: Over-expressed self-antigens commonly found in certain types of malignancies, and patient specific, mutation derived epitopes [72, 176, 245, 247, 248]. In the case of vaccination against over-expressed self-antigens (e.g. NY-ESO-1, TP53, MUC-1), central tolerance and autoimmunity are the main hurdles in the induction of tumor restricted, high avidity effector T cells and have dampened the enthusiasm in the past years [246, 249, 250]. With Sipuleucel-T (Provenge), a vaccine consisting of autologous dendritic cells expressing GM-CSF and prostatic acid phosphatase (PAP), a cell based vaccine against prostate cancer received FDA approval in 2010 [251]. A promising approach, focussing on patient specific neoepitopes, became more apparent with an increased access to genome sequencing [154, 176, 248, 252, 253]. Now it was possible to individually tailor multiepitope vaccination approaches to each patient. Even though these formulations do not prevent malignant transformation, they impressively prolonged the patients' progression free survival after surgical resection [176, 248]. These findings indicate that tumor derived candi-

date neoepitopes can induce strong anti tumor T cell immunity.

1.5.3 Adoptive T cell therapy

Considering the influence of T cells on malignancy progression it appears likely that certain T cell subpopulations may counteract disease progression. A major obstacle during the early days was the impossibility of *ex vivo* culture and expansion of T cells [254]. Only with the description and purification of interleukin-2 (IL-2), researchers were able to finally culture and expand T cells *in vitro* [255, 256]. This finding was immediately followed by preclinical studies using *ex vivo* expanded tumor infiltrating lymphocytes (TILs) to treat metastasized murine tumors, revealing the capability of IL-2 and T cells to eradicate established malignancies [139, 257, 258]. Subsequent *in vitro* tests with human melanoma TILs demonstrated their capacity to recognize and specifically lyse their autologous tumor [259]. These results led to the first-in-human transfer of autologous TILs to patients with metastatic melanoma by S. Rosenberg and coworkers [138, 260, 261]. The overall high objective response rates (>30%) in the context of this study were generally promising for future applications across various malignancies [138, 260, 261]. Further optimization of the treatment schedule, including nonmyeolablative lymphodepletion prior to TIL administration, allowed an increase in objective responses of 49% and more in patients with metastatic melanoma [140, 262, 263]. Longterm follow up of these studies showed total remission in approximately 22% of previously relapsed patients, highlighting the curative potential of adoptive TIL transfer [262]. In the following years, adoptive TIL transfer was applied for the treatment of multiple solid malignancies, including colorectal and breast cancer, as well as cholangiocarcinoma achieving disease regression if not complete remission [142, 144, 145, 264]. In addition to these advances, it was shown, that TILs of various entities frequently recognize neoepitopes from the autologous tumor [142–146, 175]. In this regard, two recent trials by E. Tran and coworkers revealed the first clinical evidence of neoepitope derived TIL reactivity in connection with tumor regression and, in one case, immune editing [142, 144]. Their first case showed a direct therapeutic efficacy of a $CD4^+$ TIL infusion product targeting a mutated ERBB2IP epitope in a patient with metastatic cholangiocarcinoma leading to a disease stabilization lasting for 35 months [142]. A second trial showed regression of metastatic colon cancer, followed by immune evasion of a single lesion, upon administration of a HLA-C08:02 restricted, $CD8^+$ TIL product with a single KRAS_G12D specificity [144]. Taken together, the recent results of studies employing adoptive TIL transfer seem promising across multiple solid malignancies. However, it appears to be necessary to administer a combination of $CD4^+$ and $CD8^+$ T cells covering multiple epitope reactivities in order to overcome immune editing and augment cytotoxic reactivity [188, 220, 221, 265]. Focusing on tumor immune infiltrates, researchers could later correlate an increased T cell tumor infiltration to an overall improved patient survival, highlighting the importance of T cell mediated tumor control and eradication [266–269].

An alternative approach to using unmodified TILs is the use of genetically engineered peripheral T cells with known antigen reactivity. Applied for the first time by transferring a TCR with known reactivity (Mart1_27-35) into autologous peripheral T cells of melanoma patients, this approach seemed promising for cases with limited access to autologous TILs [141]. Further improvements in the use of genetically engineered T cells later also allowed the development of

chimeric antigen receptor (CAR) transduced T cells expressing a group of receptors composed of a single-chain variable fragment (scFv) with specific antigen binding (e.g. CD19) and an intracellular signaling domain (e.g. CD3ζ) [270, 271]. With the latest advances in CAR-T cell therapy, the FDA recently approved the first two applications of this approach in patients with B cell acute lymphoblastic leukemia (Kymriah® - αCD19; Novartis) and non-hodgkin lymphoma (Yescarta® - αCD19; Kite Pharma) [272, 273].

1.6 Immunology of PDAC

1.6.1 Immune cell infiltration in PDAC

Pancreatic cancer used to be portrayed as a poorly immunogenic malignancy, with low numbers of TILs being able to engage malignant cells due to the high desmoplastic reaction [274–278]. Recent in-depth analyses of larger patient cohorts revealed frequent antigen experienced effector T cell infiltrates in PDAC, consisting to a slightly larger extent of $CD4^+$ than $CD8^+$ cells [279–281]. The majority of tumor infiltrating $CD4^+$ T cells display a conventional helper T cell phenotype, while only approximately 5 - 15% are T_{reg} cells [279, 282]. Furthermore, increased effector T cell infiltration, both $CD4^+$ and $CD8^+$, was shown to be correlated with an improved patient survival [269, 283, 284]. Moreover, unlike previously assumed, improved imaging techniques suggest that the desmoplastic reaction of PDAC does not hinder the TILs from engaging the tumor cell [269]. The TILs display an effector memory phenotype ($CD45RA^-$, $CCR7^-$, $PD\text{-}1^+$), reflected also in the overall antigen experience [279]. Parts of the T cell infiltrates found in PDAC could additionally be shown to derive from local clonal expansion in tumor resident tertiary lymphoid structures (TLS) [279]. These are formations of immune cells (DCs, B cells, T cells) capable of proper priming of naïve T cells. This process is comparable to lymph node restricted priming and the presence of TLS within PDAC is linked to an improved patient survival [279, 285–287]. Recognition of autologous xenograft tumors and xenograft derived cell lines by *in vitro* expanded TILs additionally highlights the possibility of T cell mediated tumor control in PDAC [279]. Additional co-infiltration of myeloid derived suppressor cells (MDSCs) and M2 macrophages, however, might antagonize the anti tumor efficacy of PDAC infiltrating effector T cells [269, 282, 288, 289].

1.6.2 Cancer immunotherapy in PDAC

Following the major success of cancer immunotherapy in various solid malignancies, researchers aimed at translating these findings into the context of pancreatic cancer [251, 290–292]. The upcoming paragraphs will give a brief overview of the most recent clinical attempts of applying immunotherapy in PDAC.

Antibody mediated therapy The first major arm of immunotherapies applied in pancreatic cancer is formed by the use of immunomodulatory antibodies. Here, especially antibodies targeting the inhibitory molecules CTLA-4 and PD-L1 were tested in patients with advanced stage PDAC, with no effect on patients overall survival or increase in therapy response rates

[293–295]. A main factor for these weak responses is most likely the overall immunosuppressive environment present in PDAC. An approach counteracting this suppressive environment uses an agonist α-CD40 antibody to promote tumor reactive T cells and induce macrophage mediated depletion of tumor stroma [296–298]. The first application of this antibody in PDAC patients led to objective responses in a small subset of 21 patients [239]. Here, the efficacy of the agonist CD40 antibody was highlighted by partial responses in four patients (19%) and disease stabilization in an additional eleven patients (52%) [239].

Vaccination Even though vaccination against already established malignancies appears challenging, a number of studies in PDAC could show promising initial results [299–302]. The most promising of which, the GVAX approach, includes allogeneic GM-CSF secreting tumor cells, fostering immune cell activation and inducing anti tumor immunity [299]. Further enhancements of this approach, using low dose cyclophosphamide for T_{reg} depletion in combination with CRS-207 (mesothelin-expressing *Listeria monocytogenes*), later improved patients overall survival and mounted mesothelin restricted $CD8^+$ T cell immunity [303, 304]. These approaches are still actively investigated and concluding results are yet to be evaluated. Nevertheless, the initial results indicate the possibility of mounting relevant anti-tumor T cell responses within pancreatic cancer upon stimulation.

Adoptive T cell therapy Up to now adoptive T cell transfer in the context of PDAC has rarely been investigated. A first study, using PBMCs, primed *in vitro* with a MUC-1 expressing allogeneic tumor cell line (YPK-1), showed tumor mass reduction upon intravenous injection in patients [305, 306]. A second approach applied mesothelin specific CAR-T cells in an early case report, resulting in 6 months lasting disease stabilization upon CAR-T cell infusion [307]. Even though further investigation of these approaches is necessary, the initial results reveal additional evidence for the possibility of mounting effective anti-tumor T cell responses in pancreatic cancer.

2 Materials

2.1 Consumables

Table 6 – List of consumable materials

Product	Company	Catalog Number
500ml "rapid"-Filtermax 0.2 µm PES	TPP Techno Plastic Products AG, Trasadingen, Switzerland	99500
96 well V-bottom	VWR International GmbH, Darmstadt	CLS3897-100EA
AbC™ capture beads	Life Technologies GmbH, Darmstadt	A10344
ArC™ reactive beads	Life Technologies GmbH, Darmstadt	A10346
BD Discard™ II Sysringe (5 mL)	Becton Dickinson, Franklin Lakes, USA	309050
C-Chip	Biochrom GmbH, Berlin	P DHC-N01
Cell culture dish 100x20 mm Optilux	Corning Inc. New York, USA	353003
Cell culture flasks (T25, T75, T150)	TPP Techno Plastic Products AG, Trasadingen, Switzerland	90026, 90076, 90151
Cell culture plates (6-, 24-, 96-well)	VWR International GmbH, Darmstadt	734-2323, 734-2325, 734-2328
Cell culture plates (non-tissue culture treated)	Corning Inc. New York, USA	CLS3736-100EA
Cell strainer Easystrainer (40, 70, 100 µm)	Greiner Bio-One GmbH, Frickenhausen	542040, 542070, 542000
Centrifuge Tubes (15, 50 mL)	Greiner Bio-One GmbH, Frickenhausen	T1943, T2068
Centrifuge Tubes 225 mL	Becton Dickinson, Franklin Lakes, USA	12556
Cryo vials 2 mL	Simport Ltd., Quebec, Canada	T311-2
Cryo-babies and cryotags	Diversified Biotech, Dedham, MA, USA	RNBW-2200
Disposable Scalpel	Feather Safety Razor Co Ltd., Japan	02.001.30.020
Extra thick blot paoer (7 x 8.4 cm)	Bio-Rad Laboratories GmbH, Munich	170-3966
FACS Tubes	Corning Inc. New York, USA	352008
Falcon™ Disposable Polystyrene Serological Pipets (5, 10, 25, 50 mL)	Corning Inc. New York, USA	7521, 7543, 7551, 7525, 7550
Gene Pulser/MicroPulser Cuvettes, 0.4 cm	Bio-Rad Laboratories GmbH, Munich	165-2088
gentleMACS C tubes	Miltenyi Biotech GmbH, Bergisch Gladbach	130-093-237
Incidin™ Foam	Ecolab Deutschland GmbH, Monheim am Rhein	30 460 10
Incidin™ Pro	Ecolab Deutschland GmbH, Monheim am Rhein	30 765 60
Incuwater-Clean™	AppliChem GmbH, Darmstadt	A5219.0100
InLab® Buffer Solutions (pH meter)	Mettler Toledo GmbH, Schwerzenbach, Switzerland	51302068
LS columns	Miltenyi Biotech GmbH, Bergisch Gladbach	130-042-401
Medoject Needles (18G)	Chirana T Injecta, Stara Tura, Slovakia	CH18112SB
Microliter Filter Tips (10, 200, 1000 µL)	STARLAB International GmbH, Hamburg	S1120-3810, S1120-1810, S1120-8810, S1126-7810
Microliter Syringe ™ (50 µL)	Hamilton Bonaduz AG, Bonaduz, Switzerland	80565/00
Microliter Tip Stack (200 µL)	STARLAB International GmbH, Hamburg	S1111-1206
Millex® Sterile Filter Unit (33 mm; 0.45 µm)	Merck Millipore Ltd., Tullagreen, Ireland	SLHV033RS
MiniPROTEAN precast gel (4-20%)	Bio-Rad Laboratories GmbH, Munich	456-1093
MultiScreen® 96-well plate	Merck Millipore Ltd., Tullagreen, Ireland	MAHAS4510
Parafilm "M" Laboratory Film	Bemis Flexible Packaging, Neenah, WI, USA	PM-996
PCR SingleCap 8-SoftStrips 0.2 ml	Biozym Scientific GmbH, Hessisch Oldendorf	710970
Petri dish (10 cm)	Greiner Bio-One GmbH, Frickenhausen	616201
Polystyrene Round Bottom Tube (14 mL)	Corning Inc. New York, USA	352059
Primaria cell culture flasks (T75, T150)	Corning Inc. New York, USA	353810, 353112
Propan/ Butan	CAMPINGAZ GmbH, Hattersheim	C206GLS
PVDF-Membran Immobilon-P	Merck KGaA, Darmstadt	IPVH00010
Reaction Tubes DNA LoBind (1.5 mL)	Eppendorf AG, Hamburg	0030108-051
Reaction Tubes Safe Lock (0.5, 1.5, 2.0 mL)	Eppendorf AG, Hamburg	0030121-023, 0030120-086, 003120-094
Reagent reservoir 50ml	Corning Inc. New York, USA	4870
Sekusept™ PLUS	Ecolab Deutschland GmbH, Monheim am Rhein	30 309 10
SIGMA™ Cell Scraper	Sigma-Aldrich Chemie GmbH, Munich	SIAL0010-100EA
Ultracentrifuge tube Ultra Clear™ (14 mL)	Beckman Coulter Ireland Inc., Galway, Ireland	344060
ViCell Sample Cup 4ml	Beckman Coulter Ireland Inc., Galway, Ireland	383721
X-tracta Disposable Gel Extraction Tool	STARLAB International GmbH, Hamburg	N2000-0025

2.2 Kits

Table 7 – List of Kits

Kit	Company	Catalog Number
BD Cytofix/ Cytoperm™ Plus	Becton Dickinson, Franklin Lakes, USA	555028
CD4+ T-cell isolation kit mouse	Miltenyi Biotech Inc., Auburn, CA, USA	130-104-454
CD8a+ T-cell isolation kit mouse	Miltenyi Biotech Inc., Auburn, CA, USA	130-104-075
Dneasy® Blood & Tissue Kit	QIAGEN GmbH, Hilden	69506
EndoFree® Plasmid Maxi Kit	QIAGEN GmbH, Hilden	12362
Human IFNγ ELISA MAX™ Deluxe Set	BioLegend, San Diego, CA, USA	430104
human IFNγ ELISpot^{BASIC}	MABTECH, Nacka Strand, Sweden	3420-2A
human TNFα ELISpot^{BASIC}	MABTECH, Nacka Strand, Sweden	3510-2A
MinElute® PCR Purification Kit	QIAGEN GmbH, Hilden	28004
Mouse Cell Depletion Kit	Miltenyi Biotech Inc., Auburn, CA, USA	130-104-694
NucleoSpin® Gel and PCR Celan-up	Macherey-Nagel GmbH & Co KG, Düren	740609.50
QIAprep® Spin Miniprep Kit	QIAGEN GmbH, Hilden	27106
RNA 6000 Nano	Agilent Technologies Inc., Santa Clara, CA, USA	5067-1511
Rneasy Mini RNA	QIAGEN GmbH, Hilden	74104
Tumor dissociation Kit, Human	Miltenyi Biotech Inc., Auburn, CA, USA	130-095-929
Tumor dissociation Kit, Mouse	Miltenyi Biotech Inc., Auburn, CA, USA	130-096-730

2.3 Machines

Table 8 – Hardware and machines

Product	Company
2100 Bioanalyzer	Agilent Technologies Inc., Santa Clara, CA, USA
37℃ incubator	Heraeus Instruments
Analytical scale Quintix124-1S	Sartorius Lab Instruments GmbH & Co KG
BD HTS	Becton Dickinson, Franklin Lakes, USA
BioRad GenePulser Xcell	Bio-Rad Laboratories GmbH, Munich
Biorad PowerPac Basic	Bio-Rad Laboratories GmbH, Munich
Bioreader 5000 F-beta	BIO-SYS GmbH, Karben
BVC professional (S2 environment)	Vacuubrand GmbH & Co KG, Wertheim
Cell cultre flows (Safe2020, MaxiSafe2020)	Thermo Fisher Scientific, Waltham, MA, USA
Centrifuge 5810, 5810R, 5424, 5424R	Eppendorf AG, Hamburg
CO_2 incubator Heracell 150i & 240i	Thermo Fisher Scientific, Waltham, MA, USA
CoolCell®	Corning Inc. New York, USA
CTL ImmunoSpot®	Cellular Technology Ltd., Cleveland, OH, USA
DNA gel printer	INTAS Science Imaging GmbH, Göttingen
EnVision 2104 Multilabel Reader	Perkin Elmer, Waltham, MA, USA
Eppendorf thermomixer comfort	Eppendorf AG, Hamburg
Flow cytometer BD LSRFortessa	Becton Dickinson, Franklin Lakes, USA
Freezer -20 ℃	Liebherr-International Deutschland GmbH, Biberach a.d. Riß
Freezer -80 ℃	Eppendorf AG, Hamburg
Fridge	Liebherr-International Deutschland GmbH, Biberach a.d. Riß
Fujifilm Las-3000	Fujifilm, Tokio, Japan
Gel electrophoresis chambers	Biometra GmbH, Göttingen
GenePulser Xcel (+CE module)	Bio-Rad Laboratories GmbH, Munich
Heidolph Polymax 1040	Heidolph Instruments GmbH, Schwabach
INTAS UV-System	INTAS Science Imaging GmbH, Göttingen
Integra Vacusafe	Integra Biosciences AG, Zizers, Switzerland
Intensilight C-HGFI	Nikon Corporation, Tokio, Japan
Laboratory glass bottles	Schott AG, Mainz
MACS Mix	Miltenyi Biotech GmbH, Bergisch Gladbach
Magnet Stand	Miltenyi Biotech GmbH, Bergisch Gladbach
Mercury Lamp (HB-10101AF)	Nikon Corporation, Tokio, Japan
Microliter Pipettes	Eppendorf AG, Hamburg
MidiMACS Magnets	Miltenyi Biotech GmbH, Bergisch Gladbach
Minitron 37℃ shaker	Infors AG, Bottmingen, Switzerland
Nanodrop8000	Thermo Fisher Scientific, Waltham, MA, USA
neoVortex® Mixer	neoLab Migge GmbH, Heidelberg
Nikon DIAPHOT300	Nikon Corporation, Tokio, Japan
Nikon Eclipse TS100	Nikon Corporation, Tokio, Japan
Nikon Power Unit (12V; 100W)	Nikon Corporation, Tokio, Japan
Optima™ L-90K Ultracentrifuge	Beckman Coulter GmbH, Krefeld
Optima™ XPN-80 Ultracentrifuge	Beckman Coulter GmbH, Krefeld
PerfectBlueTM “semi-dry” electro blotter	VWR International GmbH, Darmstadt
pH Electrode SE 100 N	Knick Elektronische Messgeräte GmbH & Co KG; Berlin
pH meter 766 Calimatic	Knick Elektronische Messgeräte GmbH & Co KG; Berlin
Pipetboy-Sterilfilter 0.45	Integra Biosciences AG, Zizers, Switzerland
Plate washer EL406	BioTek Instruments GmbH, Bad Friedrichshall
PrimoVert Light Microscope	Carl Zeiss AG, Oberkochen
Professional Trio Thermocycler	Biometra GmbH, Göttingen
PyroMark Q24	QIAGEN GmbH, Hilden
Scale Kern 572	Kern & Sohn GmbH, Balingen
SDS PAGE chambers	Bio-Rad Laboratories GmbH, Munich
SW40Ti ultracentrifuge rotor	Beckman Coulter GmbH, Krefeld
Tissue dissociator gentleMACS Octo Dissociator	Miltenyi Biotech GmbH, Bergisch Gladbach
Vi-CELL® XR cell counter and viability analyzer	Beckman Coulter GmbH, Krefeld
Waterbath	GFL Gesellschaft für Labortechnik mbH, Burgwedel
Wessamat Perfect Ice Micro Cubes	Friedrich Wolf GmbH, Heidelberg

2.4 Chemicals and reagents

Table 9 – List of reagents

Reagent	Ingredient	Amount
4x Laemmli buffer	Bio-Rad Medical Diagnostics GmbH, Dreieich	1610747
Ammonium Persulfate	MP Biomedical LLC, Solon, OH, USA	802811
Ampicillin (sodium salt)	Sigma-Aldrich Chemie GmbH, Munich	A0166-25G
BD FACSClean	Becton Dickinson, Franklin Lakes, USA	340345
BD FACSFlow	Becton Dickinson, Franklin Lakes, USA	342003
BD FACSRinse	Becton Dickinson, Franklin Lakes, USA	340346
BSA - Type H1	GERBU Biotechnik GmbH, Heidelberg	10630100
Calcium chloride	Sigma-Aldrich Chemie GmbH, Munich	C7902-500G
CHAPS	AppliChem GmbH, Darmstadt	A1099.0005
Clarity Western ECL substrate kit	Bio-Rad Laboratories GmbH, Munich	170-5060
cOmplete protease inhibitor	Roche Diagnostics GmbH, Mannheim	11836153001
Corning® Matrigel®	neoLab Migge GmbH, Heidelberg	356231
COULTER® CLENZ Cleaning Agent	Beckman Coulter Ireland Inc., Galway, Ireland	8448222
COULTER® ISOTON® II Diluent	Beckman Coulter Ireland Inc., Galway, Ireland	8448011
CountBright™ absolute counting beads	Life Technologies GmbH, Darmstadt	C36950
D-Glucose	Carl Roth GmbH & Co KG, Karlsruhe	X997.2
di-Sodium Hydrogen Phosphate	Carl Roth GmbH & Co KG, Karlsruhe	T877.1
Ethanol (absolute)	Thermo Fisher Scientific, Waltham, MA, USA	E/0650DF/C17
Ethidium bromide	AppliChem GmbH, Darmstadt	A1152.0010
GeneRuler™ DNA Ladder Mix	Thermo Fisher Scientific, Waltham, MA, USA	SM0331
HEPES	EMD Millipore Corp., Billerica, MA, USA	391338-100GM
Hydrochloric acid (37%)	VWR International GmbH, Darmstadt	20252290
Isopropanol	Thermo Fisher Scientific, Waltham, MA, USA	P/7500/PC17
Kanamycine Sulfate	Carl Roth GmbH & Co KG, Karlsruhe	T832.2
LB broth (Lysogeny Broth)	Sigma-Aldrich Chemie GmbH, Munich	L3022
LB-Agar	Sigma-Aldrich Chemie GmbH, Munich	L2897
Methanol	Thermo Fisher Scientific, Waltham, MA, USA	M/4000/PC17
n-Octyl-β-D-Glucopyranoside	AppliChem GmbH, Darmstadt	A1010.0001
PageRuler™ prestained protein ladder 10 to 180 kDa	Thermo Fisher Scientific, Waltham, MA, USA	26616
Phenylmethylsulfonylfluorid	Carl Roth GmbH & Co KG, Karlsruhe	6367.4
Potassium chloride	Carl Roth GmbH & Co KG, Karlsruhe	6781.1
Retronectin®	TaKaRa Bio Inc., Kusatsu, Japan	T100B
rm-IL21	AIMM Therapeutics, Amsterdam, Netherlands	—
RNase-ZAP™	Sigma-Aldrich Chemie GmbH, Munich	R2020
Rotiphorese® Gel 30	Carl Roth GmbH & Co KG, Karlsruhe	3029.1
SIGMAFAST™ BCIP®/NBT	Sigma-Aldrich Chemie GmbH, Munich	B5655-25TAB
Sodium chloride	Sigma-Aldrich Chemie GmbH, Munich	31434
Sodium Deoxycholate	Sigma-Aldrich Chemie GmbH, Munich	D6750-10G
Sodium hydroxide (solution)	Thermo Fisher Scientific, Waltham, MA, USA	35256-1L
Sulfuric acid (96 %)	Carl Roth GmbH + Co. KG, Karlsruhe	4623.3
TEMED	Carl Roth GmbH & Co KG, Karlsruhe	2367.3
Tris buffered saline (10x TBS)	Bio-Rad Laboratories GmbH, Munich	170-6435
Tris/Glycine Buffer (10x TG)	Bio-Rad Laboratories GmbH, Munich	161-0771
Tris/Glycine/SDS Buffer (10x TGS)	Bio-Rad Laboratories GmbH, Munich	161-0772
Trypan Blue solution	Sigma-Aldrich Chemie GmbH, Munich	T8154-100ML

2.5 Molecular biology and western blot reagents

All enzymes were already supplied with the respective reaction buffers and supplements. Enzymatic reactions were set up and performed according to the manufacturers guidelines.

Table 10 – List of molecular biology reagents

Reagent	Company	Catalogue Number
ApaI	Thermo Fisher Scientific, Waltham, MA, USA	ER1411
BglII	Thermo Fisher Scientific, Waltham, MA, USA	ER0081
BsmBI/ Esp3I	Thermo Fisher Scientific, Waltham, MA, USA	ER0451
BveI/ BspMI	Thermo Fisher Scientific, Waltham, MA, USA	ER1741
dNTP mix (10 mM)	Thermo Fisher Scientific, Waltham, MA, USA	R0191
EcoRI	Thermo Fisher Scientific, Waltham, MA, USA	ER0271
EndoH	New England Biolabs GmbH, Ipswich, MA, USA	P0702S
FastAP	Thermo Fisher Scientific, Waltham, MA, USA	EF0654
FastDigest BveI/ BspMI	Thermo Fisher Scientific, Waltham, MA, USA	FD1744
FastDigest Eco31I/ BsaI	Thermo Fisher Scientific, Waltham, MA, USA	FD0293
FastDigest NotI	Thermo Fisher Scientific, Waltham, MA, USA	FD0593
HindIII	Thermo Fisher Scientific, Waltham, MA, USA	ER0501
Library Efficiency DH5α Competent Cells	Life Technologies GmbH, Darmstadt	18263012
MyTaq™ HS Mix	Bioline Reagents Ltd.	BIO-25045
NheI	Thermo Fisher Scientific, Waltham, MA, USA	ER0975
NotI	Thermo Fisher Scientific, Waltham, MA, USA	ER0595
Nuclease free water	Thermo Fisher Scientific, Waltham, MA, USA	R0581
Pfu DNA Polymerase	Thermo Fisher Scientific, Waltham, MA, USA	EP0501
PNGaseF	New England Biolabs GmbH, Ipswich, MA, USA	P0704S
SOC medium	Thermo Fisher Scientific, Waltham, MA, USA	15544034
T4 DNA Ligase	Thermo Fisher Scientific, Waltham, MA, USA	EL0014
T4 Polynucleotide Kinase (T4 PNK)	Thermo Fisher Scientific, Waltham, MA, USA	EK0031

2.6 Cell lines

Table 11 – List of cell lines used during this work.

Cell line	Organism	Tissue	Medium	Provider	Reference	Comment
ø-NX Ampho	human	kidney	ø-NX	ATCC® CRL-3213™	[308–310]	$CD8^+$; MMULV (gag-pol^+& env^+)
771 B cells	mouse	B cell	B cell	AG Ossendorp (LUMC Leiden)	[311, 312]	MCF1233 MuLV-transformed
BOK	mouse	fibroblast	BOK	Schoenberger/ Offringa	[313, 314]	B7-1^+, SigOVA(257-264)$^+$, H2-Kb^+
CD40L L cells	mouse	fibroblast	B cell	AIMM Therapeutics	—	Expresses CD40L
HEK293T	human	kidney	ø-NX	ATCC® CRL-3216™	[315]	Expresses SV40 large T antigen
KBV623	human	B cell	B cell	AG Heemskerk (LUMC Leiden)	[316]	EBV immortalized
T2	human	B and T cell hybrid	T2	ATCC® CRL-1992™	[317]	TAP1$^-$; TAP2$^-$; LMP2$^-$; LMP7$^-$
TIPC102	human	pancreas/ PDX derived	PaCo	AG Sprick (DKFZ)	—	Grows only in Primaria Flask
TIPC102_A2	human	pancreas/ PDX derived	PaCo + G418	AG Will (GPCF - DKFZ)	—	HLA-A02:01 transduced; neo^R
TIPC113	human	pancreas/ PDX derived	PaCo	AG Sprick (DKFZ)	—	Grows only in Primaria Flask
TIPC222	human	pancreas/ PDX derived	CSC	—	—	—
TIPC222_CIITA	human	pancreas/ PDX derived	CSC + G418	AG Will (GPCF - DKFZ)	—	CIITA transduced; neo^R
TIPC253_Bcell	human	B cell	B cell	AIMM Therapeutics	[318]	Bcl-6/XL immortalized; GFP^+
TIPC275_Bcell	human	B cell	B cell	AIMM Therapeutics	[318]	Bcl-6/XL immortalized; GFP^+

2.7 Cell culture solutions and reagents

Table 12 – List of cell culture products

Product	Company	Catalog Number
100x sodium pyruvate (100 mM)	Life Technologies GmbH, Darmstadt	11360039
100x Streptomycin-Penicillin (10000 units/ml) (Pen/Strep)	Thermo Fisher Scientific, Waltham, MA, USA	15140-122
12-O-Tetradecanoylphorbol-13-acetate (PMA)	Sigma-Aldrich Chemie GmbH, Munich	P-1585
2-Mercaptoethanol, 50 mM (1000X)	Life Technologies GmbH, Darmstadt	31350-010
ACK (Ammonium-Chloride-Potassium) lysing buffer	Lonza Group Ltd, Basel, Switzerland	10-548E
Advanced DMEM/ F12	Life Technologies GmbH, Darmstadt	12634
AIM V	Life Technologies GmbH, Darmstadt	12055091
Albumin from bovine serum (BSA)	Sigma-Aldrich Chemie GmbH, Munich	A9418-100G
BSA 20% (Albumax I solution)	Life Technologies GmbH, Darmstadt	11020-039
Collagenase Type IV	Life Technologies GmbH, Darmstadt	17104-019
DMEM, high glucose (Dulbecco's Modified Eagle Media)	Life Technologies GmbH, Darmstadt	41965-039
DMSO Hybri-max sterile filtered	Sigma-Aldrich Chemie GmbH, Munich	D2650-100ML
DNase I	AppliChem GmbH, Darmstadt	A3778
Dulbeccos Phosphate buffered saline (+ Calciumchloride)	Sigma-Aldrich Chemie GmbH, Munich	D8662-24x500ml
DynaBeads® Human T-Activator CD3/CD28	Life Technologies GmbH, Darmstadt	11131D
Ethylenediaminetetraacetic acid (EDTA)	Sigma-Aldrich Chemie GmbH, Munich	1233508
Fetal bovine serum (FBS superior)	Biochrom GmbH, Berlin	S 0615
Ficoll Paque Plus	GE Healthcare Bio-Science AB, Uppsala, Sweden	AM/17144003/000001
Fungizone/ Amphotericin B	Life Technologies GmbH, Darmstadt	15290018
G418 disulfate salt solution	Sigma-Aldrich Chemie GmbH, Munich	G8168-10ML
Gentamicin	Life Technologies GmbH, Darmstadt	15750060
Glucose 45%	Sigma-Aldrich Chemie GmbH, Munich	G8769
Glucose solution (200 g/L)	Life Technologies GmbH, Darmstadt	A24940-01
Glutamine	Life Technologies GmbH, Darmstadt	25030024
GolgiPlug™	Becton Dickinson, Franklin Lakes, USA	555029
GSH (L-Glutathione reduced)	Sigma-Aldrich Chemie GmbH, Munich	G6013-5G
Heparine 2 mg/mL	Sigma-Aldrich Chemie GmbH, Munich	H3149
HEPES buffer solution (1 M)	Life Technologies GmbH, Darmstadt	H0887-100ml
Human Serum Albumin (20%)	CSL Behring GmbH, Marburg	L0744411A
Human Serum Type AB (male)	Sigma-Aldrich Chemie GmbH, Munich	H4522-100ML
HyClone H2O	GE Healthcare Bio-Science AB, Uppsala, Sweden	SH3052902
Hygromycin B	Life Technologies GmbH, Darmstadt	10687010
IGFR3 (LONG(R) R3 IGF-1, HUMAN)	Sigma-Aldrich Chemie GmbH, Munich	I1271-1MG
IMDM (Iscove's Modified Dulbecco's Media)	Life Technologies GmbH, Darmstadt	12440053
Ionomycin	Sigma-Aldrich Chemie GmbH, Munich	I-3909
L-Glutamine	Life Technologies GmbH, Darmstadt	25030-024
Lipid Mix	Life Technologies GmbH, Darmstadt	11905-031
Medium199	Thermo Fisher Scientific, Waltham, MA, USA	31150022
MEM NEAA (100X)	Life Technologies GmbH, Darmstadt	11140-035
N2 Supplement	Life Technologies GmbH, Darmstadt	18045-070
Opti-MEM® Rreduced serum medium (1X)	Life Technologies GmbH, Darmstadt	31985047
Phytohaemagglutinin (PHA)	Sigma-Aldrich Chemie GmbH, Munich	L-8754
Proleukin® S	Novartis Pharma AG, Basel, Switzerland	2238131
Recombinant human basic FGF	PeproTech Germany, Hamburg	100-18B
Recombinant human EGF	PeproTech Germany, Hamburg	AF-100-15
Recombinant Human FGF-10	PeproTech Germany, Hamburg	AF-100-26
Recombinant Human IFNγ	Becton Dickinson, Franklin Lakes, USA	554617
Recombinant Human Nodal	R&D Systems, Minneapolis, MN, USA	3218-ND-025/CF
Recombinant Human β2 Microglobulin	Becton Dickinson, Franklin Lakes, USA	551089
RPMI 1640 Medium	Life Technologies GmbH, Darmstadt	52400025
β-MercaptoEthanol	Life Technologies GmbH, Darmstadt	31350-010
StemPro Accutase	Life Technologies GmbH, Darmstadt	A11105-01
Trace Elements A	VWR International GmbH, Darmstadt	MDTH25-021-CI
Trace Elements B	VWR International GmbH, Darmstadt	MDTH25-022-CI
Trace Elements C	VWR International GmbH, Darmstadt	MDTH25-023-CI
Trypan Blue Solution (Cell Culture)	Sigma-Aldrich Chemie GmbH, Munich	T8154-100mL
Tween-20	AppliChem GmbH, Darmstadt	A1389.0500
UltraPure™ 0.5 M EDTA pH8	Thermo Fisher Scientific, Waltham, MA, USA	15575020
Water (f.i. or cell culture grade)	Life Technologies GmbH, Darmstadt	A12873-01
X-Vivo 15	Lonza Group Ltd, Basel, Switzerland	BE02-060Q

2.8 Antibodies and markers

2.8.1 Fluorescence antibodies and markers

Table 13 – Flow cytometry antibodies and reagents for human cells

Marker	Fluorophore	Clone	Supplier	Catalogue Number	Amount per sample [µL]
HLA-DR, DP, DQ	FITC	Tu39	Becton Dickinson, Franklin Lakes, USA	563591	2.5
CD3	BV711	OKT3	BioLegend, San Diego, CA, USA	317328	2.5
CD4	APC-Cy7	SK3	BioLegend, San Diego, CA, USA	344616	1.0
CD8	Alf-700	HIT8a	BioLegend, San Diego, CA, USA	300920	2.5
CD271 (NGFR)	APC	ME20.4	BioLegend, San Diego, CA, USA	345108	3.0
FLAG	APC	L5	BioLegend, San Diego, CA, USA	637308	4.0
HLA-A, B, C	FITC	W6/32	BioLegend, San Diego, CA, USA	311410	2.5
CD326 (EpCAM)	APC-Vio770	HEA-125	Miltenyi Biotech Inc., Auburn, CA, USA	130-101-161	2.5
HLA-A2	FITC	BB7.2	BioLegend, San Diego, CA, USA	343304	2.0
TNF-α	APC	MAb11	BioLegend, San Diego, CA, USA	502912	4.0
IFN-γ	PE	B27	Becton Dickinson, Franklin Lakes, USA	559327	5.0
mTCR-β	BV421	H57-597	BioLegend, San Diego, CA, USA	109229	3.0
CD4	BV510	OKT4	BioLegend, San Diego, CA, USA	317443	2.0
FLAG	APC	L5	BioLegend, San Diego, CA, USA	637308	3.0
Dextramer (HLA-A2_Mart1)	PE	—	Immudex, Copenhagen, Denmark	WB2162_PE	10.0
Dextramer (HLA-A2_neg)	PE	—	Immudex, Copenhagen, Denmark	WB2666_PE	10.0

Table 14 – Flow cytometry antibodies and reagents for mouse cells

Marker	Fluorophore	Clone	Supplier	Catalogue Number	Amount per sample [µL]
CD45.1	BV711	A20	BioLegend, San Diego, CA, USA	110739	0.5
CD45.2	PE/ Dazzle594	104	BioLegend, San Diego, CA, USA	109846	0.5
H2-K_b	APC	AF6-88.5	BioLegend, San Diego, CA, USA	116518	0.5
H2-K_b- SIINFEKL	PE	25-D1.16	BioLegend, San Diego, CA, USA	141603	0.5
CD3	APC	17A2	BioLegend, San Diego, CA, USA	100236	0.1
CD8a	APC-Cy7	53-6.7	BioLegend, San Diego, CA, USA	100714	0.1
CD4	Pacific Blue	RM4-5	BioLegend, San Diego, CA, USA	100531	0.1

Table 15 – Additional flow cytometry reagents

Product	Company	Catalogue Number
Fixable LIVE/ DEAD cell marker Aqua	Thermo Fisher Scientific, Waltham, MA, USA	L34957
Fixable LIVE/ DEAD cell marker 488	Thermo Fisher Scientific, Waltham, MA, USA	L23101
Zombie Violet™ Fixable Viability Kit	BioLegend, San Diego, CA, USA	423113
5(6)-Carboxyfluorescein diacetate N-succinimidyl ester (CFSE)	Sigma-Aldrich Chemie GmbH, Munich	21888

2.8.2 Western blot

Table 16 – Western blot antibodies

Marker	Host	Company	Catalogue Number	Dilution
α-GAPDH	rabbit	GeneTex Inc., Irvine, CA, USA	GTX100118	1:1000
α-FLAG (M2)	mouse	Sigma-Aldrich Chemie GmbH, Munich	F1804	1:1000
α-rabbit-HRP	goat	SantaCruz Biotechnology Inc., Dallas, TX, USA	sc-2004	1:20.000
α-mouse-HRP	goat	SantaCruz Biotechnology Inc., Dallas, TX, USA	sc-2005	1:20.000

2.8.3 Additional

Table 17 – Additional antibody formats

Marker	Isotype	Company	Catalogue Number
HLA-DP,DQ,DR	CR3/43	Dako Denmark A/S, Glostrup, Denmark	M0775
Ultra-LEAF™ HLA-A,B,C	W6/32	BioLegend, San Diego, CA, USA	311428
CD3	OKT3	Life Technologies GmbH, Darmstadt	16-0037-85
CD28	CD28.2	Thermo Fisher Scientific, Waltham, MA, USA	16-0289-85

2.9 Buffers and media

Table 18 – List of media used for cell culturing. (part1) (# = as described in [319]).

Medium	Ingredient (Stock concentration)	Amount	Comments
T2	RPMI	500 mL	
	FCS	50 mL	
ø-NX culture medium	DMEM	500 mL	
	NEAA	5 mL	
	Pen/Strep	5 mL	
Cryomedium	FCS	45 mL	
	DMSO	5 mL	
B cell medium	IMDM	500 mL	
	L-Glutamine (200 mM)	5 mL	
	FCS	50 mL	
	Pen/Strep	5 mL	
CSC Medium	Advanced DMEM/ F12	500 mL	
	B27 Supplement	10 mL	
	L-Glutamine (200 mM)	5 mL	
	Glucose (200 g/L)	15 mL	
	Heparine (12 mg/mL)	500 µL	
	HEPES (1 M)	2.5 mL	
	Pen/Strep	5 mL	
PaCo medium#	Advanced DMEM/ F12	500 mL	
	N2 Supplement	5 mL	
	L-Glutamine (200 mM)	5 mL	
	GSH (2mg/mL)	250 µL	Stock in H_20
	human basic FGF (250 µg/ mL)	250 µL	Stock in PBS + 1% BSA
	human EGF (100 µg/ mL)	200 µL	Stock in PBS + 1% BSA
	IGFR3 (1 mg/ mL)	5 µL	Stock in 10 mM HCl
	β-mercapto ethanol	1 mL	
	water	25 mL	
	10x PaCo Master Mix	8.45 mL	
10x PaCo Master Mix#	Glucose (45 %)	17 mL	
	Trace Elements A	2.5 mL	
	Trace Elements B	5 mL	
	Trace Elements C	5 mL	
	BSA - Albumax I solution (20 % w/V)	15 mL	Stock in PBS
	Heparine (2 mg/ mL)	5 mL	
	Lipid Mix	10 mL	
	HEPES (1 M)	25 mL	

Table 19 – List of media used for cell culturing (part 2)

Medium	Ingredient (Stock concentration)	Amount	Comments
Transport medium	X-Vivo 15*	140 mL	
	HSA	20 mL	
	Fungizone (250 µg/ mL)	20 mL	
	Gentamicin (50 mg/ mL)	80 µL	
	Pen/Strep	20 mL	
TIL culture medium I	X-Vivo15*	1000 mL	*Supplemented with either:*
	Fungizone (250 µg/ mL)	10 mL	2% Human AB serum *or* 2% HSA
	Gentamicin (50 mg/ mL)	400 µL	*and*
	Pen/Strep	10 mL	600 IU/ mL human IL-2
OT culture medium	DMEM	500 mL	
	FCS	50 mL	
	β-mercapto ethanol	500 µL	
	HEPES (1 M)	5 mL	
	Sodium pyruvate	5 mL	
	Pen/ Strep	5 mL	
BOK culture medium	DMEM	500 mL	
	FCS	50 mL	
	Pen/Strep	5 mL	
	G418	300 µg/ mL	
	Hygromycin B	300 µg/ mL	
TIL-medium	X-vivo 15*	1000 mL	*Supplemented with:*
	HSA	100 mL	300 IU/ mL human IL-2
	Pen/Strep	10 mL	

* Due to issues with the production and delivery X-vivo15 was later replaced with a mix of RPMI1640 and AIM-V (50% each).

Table 20 – List of bacterial growth media. *SOC medium was delivered with the Library Efficiency DH5α bacteria.

Buffer	Ingredient	Amount
LB Medium	ddH2O	800 mL
	LB broth	16 g
LB agar	ddH2O	400 mL
	LB agar	14 g
*SOC medium**	Tryptone	2%
	Yeast extract	0.5%
	Sodium chloride	10 mM
	Potassium chloride	2.5 mM
	Magnesium chloride	10 mM
	Magnesium sulfate	10 mM
	Glucose	20 mM

Table 21 – List of additional buffers used

Buffer	Ingredient (Stock concentration)	Amount/ Concentration	Comment
FACS buffer	PBS	500 mL	
	BSA	2.5 g	
	EDTA	2 mM	
2x HBS	ddH_2O	—	
	NaCl	274 mM	
	KCl	10 mM	
	Na_2HPO_4	1.4 mM	
	D-Glucose	15 mM	
	HEPES	42 mM	
Lysis Buffer	PBS	5.25 mL	*CHAPS later changed for:*
	CHAPS	0.6% [w/V]	n-Octyl-β-D-Glucopyranoside (1% [w/V])
	PMSF (100 mM)	52 µL	Sodium Deoxycholate (0.25% [w/V])
	cOmplete protease inhibitor	1 Tablet	*to avoid clogging of the spectrometer*
ELISpot-wash buffer	PBS	500 mL	
	Tween-20	0.05% [V/V]	
ELISpot-blocking buffer	X-Vivo15	10 mL	
	HSA (20%)	500 µL	
Transfer buffer	10x TG	100 mL	
	Methanol	200 mL	
	H_2O	700 mL	
TBS buffer	10x TBS	100 mL	
	H_2O	900 mL	
SDS running buffer	10x TGS	100 mL	
	H_2O	900 mL	
TBE buffer (10x)	Tris-Base	540 g	
	Boric Acid	275 g	
	EDTA (0.5 M)	200 mL	
	H_2O	5000 mL	

2.10 Primers

Primers were ordered from Sigma Aldrich as 100 µM, HPLC purified stock solutions in H_2O.

Table 22 – List of regular sequencing primers. *Primer kindly provided by Dr. M. Volkmar and used by J. Rebmann during PyroSequencing.

Primer name	Sequence	Tm [°C]
pMP71_forward	CGTCTTGTCTGCTGCAGCAT	67.1
pMP71_reverse	AGAGGTTGATTAACAGGAACAGAGCGT	68.8
Lampum_Fsh	TATAGCGGCCGCGCTAGCATGGCTGCCCCTGGCAG	74.2
Lampum_R	TATGAATTCTCAGATGGTCTGGTAGCCGGCGTG	64.9
Lamp1_αBveI_F	CATGACCTTCGATCTGCCCAGCGACGCC	67.7
Lamp1_αBveI_R	CGTCGCTGGGCAGATCGAAGGTCATGT	65.7
DBY_F1	GCTGTACACCACCGCCGAGGAGCTGG	68.4
DBY_F2	CCGGCATCGGCATCCTGAC	61.4
DBY_F3	CGTGATCCTGGGCGTGTGCC	63.7
DBY_F4	CCCCCCACATCGAGAACTTCAGCGACAT	65.3
DBY_F5	CGACATGGGCGAGATCATCATGGGCAACAGC	66.9
DBY_R1	CGTCGCTGTTGCCCATGATGATCTCGCCCA	68.2
DBY_R2	TGTCGATGTCGCTGAAGTTCTCGATGTG	61.8
DBY_R3	GGGGGGGCACACGCC	63.9
DBY_R4	CAGGATCACGGTCAGGATGC	57.9
DBY_R5	CGATGCCGGCCAGCTCCTC	63.8
DBY_R6	GGCGGTGGTGTA	56.0
LAMP-Hind-F	GAAGCTTCCGTCTCGGACGAG	59.6
LAMP-Apa-R	AAGGGCCCTCAGATGGTCTG	59.2
LAMP-G390R-F	CCGTGGGCAGAGCCCTGGCTGGAC	70.0
LAMP-G390R-R	CAGGGCTCTGCCCACGGC	64.7
LAMP-L395K-F	GGCTGGAAAGGTGCTGATCGTGC	62.8
LAMP-L395K-R	TCAGCACCTTTCCAGCCAGGGC	64.4
LAMP-GLtoRK-F	CCGTGGGCAGAGCCCTGGCTGGAAAGGTGCTGATCGTGC	73.8
LAMP-GLtoRK-R	TCAGCACCTTTCCAGCCAGGGCTCTGCCCACGGC	73.7
Ova-F1	GCTGCTGGAACAGCTGGAAAGCATTATTAACTTTGAAAAAC	63.3
Ova-F2	TGACCGAATGGACCAGCCTGAAAATTAGCCAG	64.5
Ova-F3	GCGGTGCATGCGGCGCATGCGGAAATTAAC	68.7
Ova-F4	GAAGCGGGCCGCGAAGTGGTGGGCAGC	72.6
Ova-R1	CGTCGCTGCCCACCACTTCGCGGCCCGCTTC	74.4
Ova-R2	GTTAATTTCCGCATGCGCCGCATGCACCGCCTGG	71.0
Ova-R3	CTAATTTTCAGGCTGGTCCATTCGGTCAGTTTTTC	62.0
Ova-R4	AAAGTTAATAATGCTTTCCAGCTGTTCCAG	57.8
CIITA_F1	GCCTCCCAACATCTCCAGAC	68.0
CIITA_F2	CGGCTTCTCCATGGAGCAG	69.0
CIITA_R1	ACACAGCTGAGTCCCACGAG	70.0
CIITA_R2	TGCTCCATGGAGAAGCCG	68.0
pcDNA1090_R	TCCAGGGTCAAGGAAG	60.0
pcDNA1061_R	CAAACAACAGATGGCTG	58.0
pcDNA802_F	TCTATATAAGCAGAGCTCTC	57.0
pcDNA830_F	TAGAGAACCCACTGCTTAC	61.0
TanCon_F	CCATGCACCTGCGAGAGC	70.0
TanCon_R	CTCATCACACCTGCTCTCC	65.0
HLA-A2_Seq	CGGAGCTCGTGGAGACCAG	71.0
A2_attB1_F_Seq	TGTACAAAAAAGCAGGCTTAACCATG	66.0
A2_attB1_F	GGGGACAAGTTTGTACAAAAAAGCAGGCTTAACCATGGCGCCCCGAACC	83.0
A2_attb2_R	GGGGACCACTTTGTACAAGAAAGCTGGGTTTCACACTTTACAAGCTGTGAGAGACAC	80.0
Spec_PyroRBio*	[Btn]TACCTACCCACCAAAATCAACAAGG	67.0
Spec_PyroF*	TGGATCTTATATGTAGAGCCCATCAGG	67.0
Spec_PyroS1*	ATATGTAGAGCCCATCAGG	60.0
GBAS_S1*	AGGAACCATGATTGAATG	56.0
DTNBP_S1*	TTCTCTACCTCCTCAAAACT	59.0
ATAD2_S1*	AAAAATCTCTCCATAATCAC	54.0
RASSF6_S1*	GCTTTCTTACCTCCTGTT	58.0
FILIP1L_S1*	CCTTTTTTGGAGTGACA	56.0

Table 23 – List primer pairs for mutation validation. *Primer pair kindly provided by Dr. M. Volkmar for PCR amplification of the respective mutated gene later sequenced by pyrosequencing using the S1 primers found in table 22.

Patient	Gene	Mutation	Forward	Tm [°C]	Reverse	Tm [°C]	Product Length [bp]
TIPC102	FOXJ2	D4G	ACTTGCCCCCAGTATTTTCGT	59.9	GGGGGAGCCAGTCTATGGAG	61.1	106
	MAP2K4	G294R	ATAGACCCAAGCGCATCACG	60.5	AACGAACGGGGAAGTCTGAT	59.0	160
	CDC16	L447V	AGCAGTTACCCTGGCCTTGT	61.4	GATGCTGATTTTATCTGAGCAGCC	60.3	340
	LRP12	R330H	TCCCCTTGCAGCATTCACTT	59.8	TGGGAACATTGACTGCCTTGA	59.8	373
	FILIP1L*	F109V	CCTCTAACACCTTTTTTGGAGTGA	55.3	[Btn]CGAGATGAGGTCATAGGCATTTTA	55.0	100
	ATAD2*	R913C	GGCTTAGCAGCTTGTTTTAGAATT	54.8	[Btn]AACCATTGTAAGTTGGGGATCAT	54.6	190
	GBAS*	G203D	CACAGAAGAACTAACAAACCAAATC	53.5	[Btn]CCCTAGAATTAACACTATGGCCTAA	54.3	140
	DTNBP1*	A123V	CCCACATAAGTCTTCCAGATGC	55.6	[Btn]TGATTGAGGATTCTGACTTTTGAGG	55.4	125
	RASSF6*	A238V	GGCAGCAAACTGTAGCACTCT	57.8	[Btn]AGTCCCCAGGATTTTGCTCT	55.6	100
	KRAS*	G12D	CATTATTTTTATTATAAGGCCTGC	49.2	[Btn]CAAAATGATTCTGAATTAGCTGT	50.3	120
TIPC113	TLE4	S48G	TTCGCCTGTGATGTGGGCTA	61.5	ATACCTTTGTGACGCCCCCA	61.4	256
	PGM3	L156F	TGCCTTTCCATATCGGCCAC	60.4	TGACACAAAAGGATTTGTCACCC	59.6	184
	KIFC1	P435L	TTTGCCTATGGCCAGACAGG	60.0	GGTCCCGGACAGTCTCATTG	60.1	196
	SARM1	F591L	TGTCTTCATCAGCTACCGCC	59.8	GGTCTTGCATGCACTTGTCC	59.7	282
	CDH1	R90W	GATTGCACCGGTCGACAAAG	59.8	GCGCACTAAAACAACAGCGA	60.0	258
	UGT1A6	H54N	TAGCACTTTGGGGCATGGTT	59.8	TCTTGGTCATACGGCACTGG	59.7	202
	CDKN2A	P114R	GCTCTCAGGGTACAAATTCTCAGAT	60.4	TCTGGCAGGTCATGATGATGGG	62.1	353
	FAM193B	I530V	GAGGGGAGCCCAAAGTCAAA	59.8	AAAGACTCCATCCGTGCCAG	60.0	181
	DCAF6	A242V	CAGAGGAAGAACCTCTACTGGAAA	59.4	CGTGCTGTATCATCTTTCGGG	59.1	325
	KRAS*	G12V	CATTATTTTTATTATAAGGCCTGC	49.2	[Btn]CAAAATGATTCTGAATTAGCTGT	50.3	120
TIPC222	AGPAT6	T344I	TATCTGGGGTAAAGGGCCAAC	59.4	AGTGTGTACCATCGGAGGTC	58.8	166
	ANKRD32	L1010R	CAGCAACTTGAATTTGGCTCCT	59.7	ATCAAGGCCTCAGTGTGTACC	59.7	284
	AUTS2	R1154C	CCTGCTAAGGAACGACCCG	60.1	GATAGTGCATGCTGGGGAGT	59.5	302
	BARD1	R150Q	AGGCTGGGTTTGCACTGAAG	60.8	GAGCTCCATGTGGGAGCAATA	59.8	198
	CEP44	A153T	ATACACCTGTGACTGGGAACTC	59.4	GCCACTGATATCAACGCCAAC	59.9	319
	CSNK1A1	E60D	CTACCCACTTCCCCATTCCG	59.8	TCTTTCCCCTGCAGGAAGTG	59.6	182
	DDX5	R263S	CTTCTTTTGGCCAAGTCGCA	59.3	TGCAACACCTGGAAGACTGAT	59.5	280
	KDM6B	P272S	TCTCCTAGACTGGCCTTCCC	60.0	CCATGCAGGGTACTCCACAG	60.1	157
	KLHL13	R336M	TGGGGGCTAACGATTTCCAC	60.0	TGCAGCCAGTTATGCAGTCA	59.9	153
	KPNA7	P371S	TCTTCAGAATGGAACGCCCC	60.0	CTCCTGCAACACAACAAGCC	59.9	313
	KRAS*	G12D	CATTATTTTTATTATAAGGCCTGC	49.2	[Btn]CAAAATGATTCTGAATTAGCTGT	50.3	120
	N4BP2	D1482N	CTTGGTTGGACATACTGGGC	58.5	AAACCAGAATCAGAGACAGTAGCTT	59.9	236
	PIK3CA	I788F	GCCACTGTGGTTGAATTGGG	59.6	TGGCTTTCAGTAGTTTTCATGGT	58.5	179
	PPM1D	N242S	TCTCTGAACAGGAATTTTGGCT	57.9	AGTGAGTCGAGGTCGTTTCC	59.4	218
	TROAP	M465L	CGCATCGGTATCCTGCAACA	60.8	CACTCCTCTGGAAGACAGGG	59.1	227
TIPC236	CCDC88C	F27L	CCATGCAACCTTCCACTCCA	60.2	GGGAGAGCTTTGGACCGTTT	60.2	254
	CDKN2A	G55V	CATCTATGCGGGCATGGTTAC	59.1	TCTACACAAGCTTCCTTTCCGT	59.6	358
	COPS7A	T224M	TGGCTGTAGCAGACAACCAG	59.9	GCCCTTTGAGGCTTTCTTGC	60.0	230
	KRAS*	G12D	CATTATTTTTATTATAAGGCCTGC	49.2	[Btn]CAAAATGATTCTGAATTAGCTGT	50.3	120
	N4BP1	M173T	CCTGTGGCAGCATTCTGTGTA	60.6	ATTGGCCTTCTTGGCATCAGA	59.9	323
	PRKACB	W185S	ACTTTGGGTTTGCCAAAAGAGT	59.1	AAAGTCCATAGGGATGCATGT	57.0	151
	RBL2	V539A	GACACACTTTGCACTCACTC	56.9	GAAAAAGTGACGACCTCAAGGC	60.0	191
	SLC43A1	V86M	GAAGCAGGCACTGTGGAGAC	60.9	AGCAGGACGAGATGCTCAAC	60.1	239
	TGFBRAP1	T121M	CGCCTGTGCTGTAATTGTGG	59.8	TTCAAGAAGCCCGTGAACGA	59.8	367

2.11 Peptides

Peptides were ordered from, and synthesized by, M. Koch from the AG Eichmüller, DKFZ Heidelberg. Finished products were received as 2 - 4 mg aliquots of lyophilized peptide. Quality of the HPLC purified peptides was routinely assessed by M. Koch using electronspray ionization mass spectrometry.

Table 24 – List of non-patient derived peptides

Peptide	Sequence	MW (monoisotopic) [Da]	Reference
NEF 136-145	PLTFGWCYKL	1226.62	[320]
GAG 77-85	SLYNTVATL	980.52	[320]
NEF 73-82	QVPLRPMTYK	1231.67	[320]
GAG 20-28	RLRPGGKKK	1038.68	[320]
NEF 120-128	YFPDWQNYT	1232.51	[320]
GAG 240-249	TSTLQEQIGW	1161.57	[320]
EBV	GLCTLVAML	919.49	[321]
Mart1	ELAGIGILTV	984.59	[171]
Mart1_long	KGHGHSYTTAE*ELAGIGILTV*LGVLLLIG	3044.73	
HY	HIENFSDIDMGE	1405.58	[316, 322]
HY_long	EATGSNCPP*HIENFSDIDMGE*IIMGNIELT	3246.45	
SIINFEKL	SIINFEKL	962.54	[323]
OVA_MHC-II	ISQAVHAAHAEINEAGR	1772.89	[324]
CSNK1A1	GLFGDIYLAI	1080.59	[325]
GAS7	SLADEAEVYL	1108.53	[325]
HAUS3	ILNAMIAKI	985.60	[325]

Table 25 – Predicted patient peptides for TIPC102. Highlighted amino acids indicate the respective position of the mutation within the predicted epitope.

Peptide	Sequence	MW (monoisotopic) [Da]
FILIP1L_1	ALLEAQYG**V**	962.51
FILIP1L_2	LALLEAQYG**V**	1075.59
FILIP1L_6	ALLEAQYG**V**V	1061.58
ATAD2_1	FI**C**DYGEIFNV	1318.58
FILIP1L_3	LLEAQYG**V**	891.46
FILIP1L_4	DLALLEAQYG**V**	1190.61
FILIP1L_5	LALLEAQYG**V**V	1174.65
DTNBP1_1	MTANLTHLE**V**	1127.55
FOXJ2	**G**LESSLTSI	905.46
RASSF6_1	FALHIIF**V**T	1059.60
RASSF6_2	FALHIIF**V**	958.55
MAP2K4_1	SL**R**ITLYEL	1106.62
KRAS_G12D	KLVVVGA**D**GV	955.559
CDC16	VTVDKWEP**V**	1071.54
DTNBP1_2	SMTANLTHLE**V**	1214.58
LRP12_1	KLL**H**VLTAF	1040.62
LRP12_2	KLL**H**VLTA	893.55
ATAD2_2	ELFI**C**DYGEI	1200.52
MAP2K4_2	SL**R**ITLYELA	1177.66

Table 26 – Predicted patient peptides for TIPC113. Highlighted amino acids indicate the respective position of the mutation within the predicted epitope.

Peptide	Sequence	MW (monoisotopic) [Da]
KIFC1_1	I**L**RALRHLFSV	1323.81
SARM1_1	V**L**IDVEKLEA	1127.64
SARM1_2	QLHGFSV**L**I	1012.57
SARM1_3	LQLHGFSV**L**I	1125.65
KRAS_G12V	KLVVVGA**V**GV	939.61
UGT1A6_1	VLSDRG**N**EI	1001.51
CDKN2A	RL**R**VDLAEEL	1212.68
SARM1_4	QLHGFSV**L**IDV	1226.67
UGT1A6_2	VLSDRG**N**EIV	1100.58
KIFC1_2	**L**RALRHLFSV	1210.73
SARM1_5	LQLHGFSV**L**	1012.57
FAM193B	**V**NLDLSPLTL	1083.62
DCAF6	MV**V**RFIPSHL	1197.67

Table 27 – Predicted patient peptides for TIPC222. Highlighted amino acids indicate the respective position of the mutation within the predicted epitope.

Peptide	Sequence	MW (monoisotopic) [Da]
AGPAT6_3	FEIGA**I**VYPV	1106.60
KLHL13_1	AI**M**SDTTHLV	1086.54
KLHL13_2	AI**M**SDTTHL	987.47
PIK3CA_1	WLNWENPD**F**M	1350.57
KLHL13_3	I**M**SDTTHLVT	1116.55
AGPAT6_1	SFEIGA**I**VYPV	1193.63
KDM6B	GLATS**S**PFQL	1019.53
KLHL13_4	I**M**SDTTHLVTL	1229.63
BARD1	KMWFSP**Q**SKKV	1364.73
CEP44	KIS**T**EAVGV	902.51
AGPAT6_4	EIGA**I**VYPV	959.53
KLHL13_5	TAI**M**SDTTHLV	1187.59
KRAS_G12D	KLVVVGA**D**GV	955.57
PIK3CA_2	**F**MSELLFQN	1127.53
AGPAT6_2	FEIGA**I**VYPVA	1177.64
DDX5	MLDMGFEPQI**S**	1266.56
PPM1D	VMNKSGV**S**RV	1075.58
AUTS2	HLDERE**C**LHML	1394.64
ANKRD32	LLD**R**YAGNI	1033.56

2.12 Software and bioinformatic tools

Table 28 – Software and bioinformatic tools

Software	Company
GraphPad Prism 6.0	GraphPad Software Inc., La Jolla, CA, USA
Wallac EnVision Manager version 1.12	Perkin Elmer, Waltham, MA, USA
FlowJo v10.4.1	FlowJo LLC, Ashland, OR, USA
BD FACSDivaTM software version 6.2	Becton Dickinson (BD) GmbH, Heidelberg
Serial Cloner (Version 2.6.1)	Serial Basics Software
SnapGene®Viewer (Version 4.1)	GSL Biotech, Chicago, USA
Integrative Genomics Viewer	Broad Institute, USA
ImageJ	National Institute of Health, Bethesda, USA
Inkscape	Free Software Foundation, Boston, USA
LyX - The Document Processor	http://www.lyx.org/
HUSAR/GCG (Release 4.0)	Genomics and Proteomics Core Facility (DKFZ), Heidelberg
MacOS (Version 10.12.6; Sierra)	Apple Inc., Cupertino, USA
Microsoft Office	Microsoft Corporation, Redmond, USA
CTL Immunospot Software (V 5.0)	Cellular Technology Ltd., Cleveland, OH, USA
Vi-CELL XR Cell Viability Analyzer 2.03	Beckman Coulter Ireland Inc., Galway, Ireland
Motic Image Plus 2.0^{ML}	Motic China Group Co. Ltd., Xiamen, China
Image Reader LAS-3000 (V 2.21)	Fujifilm, Tokio, Japan
Multigauge	Fujifilm, Tokio, Japan
Intas GDS	Intas Science Imaging Instruments GmbH, Göttingen
NanoDrop 8000 Operating Software (V 2.3.2)	Thermo Fisher Scientific, Waltham, MA, USA

3 Methods

3.1 Patient material

3.1.1 Sample collection

Resected tumor tissue and blood samples of pancreatic cancer patients were obtained from the European Pancreas Center Heidelberg. Informed written consent was obtained from all patients prior to sample collection. The study was approved by the local ethics committee and conducted in accordance with the declaration of Helsinki [326].

3.1.2 Patient selection

Patients were primarily selected based on the availability of exome and transcriptome data of the primary tumor and/ or xenograft. Depending on the screening approach, additional requirements had to be met to include a patient. In case of the expression based screening system, expanded TILs, recognizing the autologous tumor had to be available in sufficient amounts. For the development of the long peptide screening system, blood or spleen samples were needed for the generation of immortalized B cells. To set up the targeted proteomics screening system, patients had to be HLA-A02:01$^+$ and the respective PDX derived cell line was needed.

3.2 Cell Culture

When working with virus producing cells, viral suspensions or EBV immortalized cell lines, all experiments and cell cultures were performed in the central S2 facility of the German Cancer Research Center (DKFZ). Cells immortalized with EBV were washed twice with PBS and either fixed (4% formaldehyde) or irradiated prior to transfer to an S1 facility.

3.2.1 Processing of primary pancreatic tumor tissue

Freshly resected tumor was kept in transport medium during transfer from the operating theatre to the laboratory. Afterwards, tumor tissue was immediately minced and several pieces (27 mm^3each) snap frozen to -196 °C for RNA and DNA extraction. A slice from the middle of the tumor piece (16 mm^2) was embedded in Tissue-Tek®for histological analyses.
Residual pieces were used for *in vitro* expansion of TILs and xenograft generation.

3.2.2 *In vitro* expansion of tumor infiltrating lymphocytes

TIL cultures were set up from fresh tumor tissue as previously described[279, 327]. Briefly, the expansion was split into two parts and performed as follows:

1. Day 0 - 14:

   For an initial expansion, tumor pieces (1 mm^3) were transferred to a 24-well plate. Per well 1 mL TIL culture medium I (+ 2% HSA), containing 6000 U/mL recombinant IL-2, and

one piece of tumor were incubated. After 24h half of the medium was exchanged. TIL growth was monitored frequently and expanding wells were pooled on day 14. One part of the TIL pool was cryopreserved, the other part was used for further rapid expansion to either day 28 or day 42.

2. Day 14 onwards:

   In order to generate larger amounts, the pre-expanded TILs were put on a rapid expansion protocol [279]. PBMCs of three different allogenic donors were thawed, irradiated with 40 Gy, pooled at equal amounts and adjusted to 3x10^8 cells/mL in TIL culture medium I (+ 2% human AB serum). Afterwards, 100 µL pooled PBMCs, 1x10^7 cells/donor, were transferred to each standing T25 flask together with 1x10^5 TILs, 30 ng/mL α-CD3 (OKT3) and 20 mL TIL culture medium I (+ 2% human AB serum).
   The next day another 5 mL TIL culture medium I (+ 2% human AB serum), containing 1500 U/mL recombinant IL-2, were added to the culture, resulting in a final concentration of 300 U/mL recombinant IL-2 per flask.
   On day five of rapid expansion half of the medium was carefully removed, without disturbing the cell layer, and replaced by the same amount of fresh TIL culture medium I (+ 2% human AB serum), containing 600 U/ml recombinant IL-2.
   The following days, growth was frequently monitored and cells split 1:1 into new culture flasks if necessary.
   After 14 days of rapid expansion TILs were harvested, analyzed by flow cytometry and cryopreserved. Whenever necessary, this part could be repeated to expand TILs to a maximum of 42 days.

3.2.3 Cell centrifugation

During regular cell culture, tissue digest, washing and after fixation cells were pelleted for 6 min at 350 xg. For regular flow cytometry stainings, cells were pelleted for 2 min at 700xg unless stated otherwise.

3.2.4 Cell count and viability assessment

Cell number and viability was monitored using a Vi-CELL™ XR cell counter (Beckman Coulter). For each sample 450 µL PBS were mixed with 50 µL cell suspension and acquired using the machines default settings. In the S2 facility and to counter check Vi-CELL results, cell concentration and viability were assessed using a hemocytometer. Here, the cell suspension was mixed in a 1:10 ratio with trypan blue, applied to the hemocytometer and two sets of corner squares counted. The cell concentration was calculated as follows:

$$[Cells]_{initial} = 10000 * \frac{\sum counted\,cells}{2} * Dilution\ factor\ (cells/mL) \quad (1)$$

3.2.5 Cell irradiation

Cells were irradiated using a GammaCell1000 (Atomic Energy of Canada Limited). Here, cells were placed in 15 mL reaction tubes in 5 - 10 mL fresh culture medium, placed inside the

irradiation chamber and exposed to the desired amount of radiation. Due to radioactive decay, the time of exposure had to be slightly adjusted every six month according to the data sheet provided by the administrative department “Strahlenschutz und Dosimetrie (W060)” of the DKFZ.

3.2.6 Cryopreservation and revival

For cryopreservation and storage, cells were pelleted, resuspended in 5 mL PBS and cell number, as well as viability were assessed. Cells were again pelleted and adjusted to the desired concentration in cryomedium. Afterwards, 500 µL cell suspension were transferred to each cryo vial and cells cooled down by -1 °C/min using CoolCell® freezing containers (BioCision) for 24 h at -80 °C. Afterwards, cells were transferred to -196 °C for long term storage.
Upon use, cells were put into a 37° C water bath for 3 min, carefully resuspended by adding 1 mL pre-warmed culture medium and transferred directly into 10 mL pre-warmed culture medium. The suspension was pelleted, washed once with 10 mL pre-warmed culture medium, counted and the cell number adjusted to the desired concentration for later use.

3.2.7 Culture and passaging of eukaryotic cells

Cells were generally kept and incubated at 37° C, 5% CO_2 and 95% relative humidity unless stated otherwise. Adherent cells were split at 85 - 90% confluency by washing once with 5 - 10 mL PBS and detached using StemPro Accutase (Thermo Fisher Scientific) according to the manufacturers protocol. Cells were taken up in fresh culture medium, viability was assessed and the desired amount of cells seeded in fresh culture flasks. Accutase was chosen for passaging, since most PDX derived cell lines appeared sensitive to trypsin-EDTA dissociation and were lost upon reseeding.
Stably transduced PDX derived cell lines were constantly cultured in the presence of the respective selection antibiotic. Bcl-6/XL immortalized B cell lines were cultured as previously described [**?**]. Briefly, the cells were cultured in B cell medium supplemented with 50 ng/mL rm-IL-21 and irradiated (50 Gy) murine L cell fibroblasts, stably expressing CD40L.
Suspension cells were pelleted, taken up in 5 mL fresh culture medium, viability was assessed and cells were distributed to new culture flasks at the desired concentrations.

3.2.8 Generation of PDX derived cell lines

Cell lines for patients TIPC102 and TIPC113 were kindly provided by the group of M. Sprick and grown in PaCo medium.
For other cell lines the resected xenograft was minced, transferred to 20 mL PBS (+ 1% Pen/Strep) and centrifuged for 5 min at 110 xg. The pellet was washed twice with 25 mL PBS (+1% Pen/Strep) at the same speed. Afterwards, it was resuspended in 20 mL Medium 199 followed by the addition of 120 µL $CaCl_2$ (sterile stock at 25 mM in H_2O), as well as 1 mL Gibco® Collagenase Type IV (sterile stock at 40 mg/mL), and incubated for 2.5 h at 37° C. The digested suspension was passed through a 100 µm strainer, washed with 10 mL PBS and the

cells taken up in 12 mL CSC medium. Subsequently, the suspension was transferred to a T75 flask and growth monitored frequently.

3.2.9 Purification of PDX derived cell lines

PDX derived cell lines were routinely tested for mouse cell contamination by pyrosequencing. Primers for the amplification of species specific single nucleotide polymorphisms (SNPs) were designed and provided by Dr. M. Volkmar. In a first step, adherent, PDX derived cultures revealing different cellular phenotypes were separated by differential trypsinisation. For this, the cells were washed once with PBS. Afterwards, 5 mL StemPro Accutase (Thermo Fisher Scientific) were added to each flask, the culture incubated for 3-4 min @ 37℃ and constantly monitored under the microscope. Once the first phenotype detached, the supernatant was collected, the flask washed once with 5 mL PBS and fresh accutase added to the flask to detach the remaining population. In general, two cultures were generated by this approach. One detaching early (after 3 - 5 min) and the other detaching considerably late (10 - 20 min). Collected cells were seeded in separate new flasks and species origin determined by pyrosequencing. Primers used for pyrosequencing were designed by Dr. M. Volkmar and covered a small region within the catalytic subunit gamma of the protein phosphatase 1 (PPP1CC) encoding for three interspecies SNPs (NCBI references: human = NG_030325; mouse = AH006785). Cell lines tested positive for contamination were afterwards purified by flow cytometry sorting. Here, the respective cell lines were treated with 330 U/mL IFNγ for 48 h prior to bulk cell sorting. Cells were sorted for the 5% highest, living population of human MHC-I positive cells into fresh CSC medium. The sorted population was washed once with 10 mL CSC medium, taken up in fresh medium and plated in a T25 flask.

3.2.10 Isolation of mononuclear cells from peripheral blood

Buffy coats were provided by the DRK Blutspendedienst Mannheim and the IKTZ Heidelberg gGmbH. Peripheral blood mononuclear cells (PBMC) were isolated by gradient centrifugation using Ficoll-Paque PLUS (GE Healthcare). The blood was distributed to 50 mL reaction tubes (7.5 - 10 mL blood per tube), 35 mL PBS was added and the suspension mixed by pipetting. Afterwards, the suspension was carefully underlaid with 10 mL ficoll solution and centrifuged for 22 min at 800 xg with acceleration and break turned off to avoid disruption of the gradient. The plasma layer was carefully removed and the lymphocyte layer transferred to a fresh 50 mL reaction tube. The suspension was filled up to 50 mL with PBS and pelleted for 7 min at 450 xg. Subsequently, the pellet was washed twice with 50 mL PBS, resuspended in 30 mL PBS and cell number, as well as viability were assessed. Cells were aliquoted and cryopreserved until use.

3.3 Mouse Work

All mouse work was performed under the approval of the German Cancer Research Center (DKFZ) in accordance with federal, state and local guidelines. Organ extractions were

performed under permit number DKFZ303 and xenograft generation under permit number G-222/15.

3.3.1 Mouse lines used

Ly5.1 [B57BL/6-Ptprc^{a}][328], OTI [C57BL/6-Tg(TcraTcrb)1100Mjb/J][329], OTII [B57BL/6-Tg(TcraTcrb) 425Cbn/J][330] and NSG™ [NOD.Cg-Prkdc^{scid}Il2rg^{tm1Wjl}/SzJ][331] mice were bred in-house and originated from the Jackson Laboratory. Mice were housed in a SPFP facility with 12h light/ dark cycle at 25° C and 40 - 60% humidity. Up to 6 mice were kept per individually ventilated container with food and water being provided *ad libitum*.

3.3.2 Organ extraction and cell purification

For T cell and splenocyte isolation mice were sacrificed, spleen and lymph nodes (axillary, inguinal and mesenteric) resected and immediately put in cold PBS. Organs were meshed through a 100 µm strainer, the strainer flushed with 10 mL cold PBS and the cells pelleted. The supernatant was discarded and lymph node pellets resuspended in 15 mL PBS. Splenocytes were resuspended in 5 mL ACK-buffer (Lonza) and incubated for 5 min on ice to lyse erythrocytes. The lysis was stopped by adding 10 mL PBS. Cell suspensions from lymph nodes and spleen were rinsed through a 40 µm strainer, the strainer flushed with 10 mL PBS and the suspensions pelleted. Afterwards, cells were resuspended in 5 mL FACS buffer and cell numbers, as well as viability, were assessed.
To retrieve pure CD4 (OTII) or CD8 (OTI) T cells, the isolated suspensions were purified by negative selection using either a CD4+ or the CD8a+ T cell isolation kit (Miltenyi Biotec) following the manufacturers instructions. Purified populations were later used for T cell proliferation analyses.

3.3.3 Xenograft generation, control and harvest

Digest of resected tumor tissue was performed using the human Tumor Dissociation Kit (Miltenyi Biotec), following the manufacturers instructions. Briefly, digestion solution was prepared, containing 4.7 mL RPMI1640, 200 µL Enzyme H, 100 µL Enzyme R and 25 µL Enzyme A and transferred to a gentleMACS C tube (Miltenyi Biotec). Tumor tissue was minced and added to the digestion solution. gentleMACS C tubes were placed onto gentleMACS Octo Dissociator with heater (Miltenyi Biotec) and digested using the pre-installed program 37C_h_TDK3. Afterwards, a cell strainer (100 µm) was placed inside a 50 mL reaction tube and pre-rinsed with 5 mL PBS. The digested tissue suspension was applied to the strainer, followed by an additional 10 mL PBS to wash the strainer. Subsequently, the cells were pelleted, supernatant removed and cells taken up in 10 mL fresh PBS. Cell number and viability were assessed, the cells pelleted again and the cell concentration adjusted to 2 x 10^7 cells/mL in PBS. For each injection 100 µL cell suspension were mixed with 100 µL matrigel® matrix (Corning) and constantly kept on ice until injection to avoid solidification. Prior to injection the right flanks of the mice were shaved and disinfected with 70% ethanol. Per mouse 200 µL of the cell suspension (2x10^6 cells) were injected subcutaneously, cranial to the right hind leg using a 26G needle.

Tumor volume was assessed in three dimensions once per week using a caliper. At 1000 mm^3 mice were sacrificed and the tumor tissue resected.

3.4 Immune and biochemical assays

3.4.1 Flow cytometry

In general, multiparametric flow cytometry stainings were subdivided into three consecutive parts applied as far as needed for the respective assay. For each sample up to $1x10^6$ cells were placed per sample in a 96-well V-bottom plate. All staining steps were performed in the dark. Samples were acquired in a final volume of 200 µL FACS-buffer using an LSRFortessa flow cytometer (BD Bioscience). Analysis was performed using the FlowJo software package (Treestar).

1. *Dead cell staining:*

   For all samples, cells were first stained with a marker to distinguish live and dead cell populations. Cells were washed once with PBS and taken up in the respective amount of dead cell marker in PBS. Samples were incubated for 15 min at 4 °C, diluted with 100 µL FACS-buffer, pelleted and washed twice with 200 µL FACS-buffer. Afterwards, either extracellular staining was performed or, in the case of GFP transfection/ -duction, cells were taken up in FACS-buffer and directly analyzed.

2. *Extracellular staining:*

   Antibody master mixes were prepared in FACS-buffer, 20 µL were distributed to each sample and incubated for 30 min at 4 °C. Subsequently, the samples were washed twice with 200 µL FACS-buffer and either directly analyzed or stained for intracellular cytokines.

3. *Intracellular staining:*

   To perform intracellular cytokine staining the pre-stained samples were fixed using 100 µL BD Cytofix/ Cytoperm™ (4.2% formaldehyde [w/w], BD Biosciences) and incubated for 30 min at 4 °C. Cells were washed twice with 200 µL Perm/Wash™ buffer (BD Biosciences). In order to avoid disruption of the cells, centrifugal forces were lowered from here on to 350 xg for 6 min during the washing steps. Afterwards, cells were stained with 20 µL antibody master mix prepared in Perm/Wash™ buffer, incubated for 30 min at 4 °C and washed twice with 200 µL Perm/Wash™ buffer. All samples were washed one additional time with 200 µL FACS-buffer and subsequently analyzed.

For certain assays cells were stained with CFSE prior to assay setup. Here, respective cells were pelleted for 6 min at 350 xg, washed once with 10 mL PBS and up to $2x10^7$cells were taken up in 1 mL 5 µM CFSE in PBS. Subsequently, the tubes were covered in aluminum foil and gently rocked for 15 min at RT. One volume of FCS was added and the suspension incubated for 2 min at RT. Afterwards, 10 mL culture medium was added and the cells incubated for 5 min on ice. Viability was again measured to account for cell loss upon staining and the cells adjusted to the desired concentration.

3.4.2 Peptide pulse of target cells

Here, target cells were pulsed with 10 µg/mL of the respective peptide unless stated otherwise. For this, up to 2.5 x 10^6 cells were taken up in 200 µL of the respective culture medium and another 50 µL culture medium, containing 25 µg/mL peptide of interest, were added. Suspensions were incubated at 37℃ for 1 h, washed once with 10 mL of the respective assay medium and taken up in assay medium at the desired concentration.

3.4.3 Murine T cell proliferation analyses

Antigen induced activation of murine T cells (OTI and OTII) was assessed by proliferation using a CFSE dilution [332]. Samples were set up using 1x10^5 CFSE labeled effector cells and 5x10^4 (OTI setup) or 1x10^5(OTII setup) target cells in 200 µL OT culture medium. Samples containing only T cells served as negative controls. For positive controls T cells were either activated unspecifically using 20 ng/mL PMA and 50 µg Ionomycine or antigen specific by co-incubation with BOK cells (OTI) or peptide pulsed, congenic (CD45.1$^+$) splenocytes (OTII). Cell division was assessed by flow cytometry after 48 - 96 h (OTI - 48 and 72 h; OTII - 72 and 96 h). Total cell numbers were assessed using CountBright™ Absolute Counting Beads (Invitrogen) according to the manufacturers protocol.

3.4.4 HLA-binding assay

TAP-deficient T2 cells were harvested, washed once with serum free RPMI1640 medium and adjusted to 2x10^6 cells/mL. For each sample 100 µL of the cells were seeded per well into 96-well U-bottom plates. Peptides were pre-diluted to 20 µg/mL in serum free RPMI1640 and 100 µL were added to each sample. In total five plates, each containing the same sample layout, were prepared. Four plates were incubated over night at 25° C and 5% CO_2, the last plate was incubated at 37° C and 5% CO_2 until harvest. Upon 16h cold pre-incubation, three of the plates were transferred to 37° C and 5% CO_2 in 2h intervals. Two hours after the last plate was put to 37° C all samples were transferred to 96-well V-bottom plates, washed once with PBS, stained and analyzed for HLA-A2 surface presentation in the living cell population. From the point of transfer to the 96-well V-bottom plates, samples were constantly kept at 4℃. Further characterization of increased HLA-A2 stabilization upon temperature increase was performed by addition of 5 µg/mL Brefeldin A (BD GolgiPlug™; BD Biosciences) to each sample directly before transfer to 37° C.

3.4.5 Cytokine production and secretion assessment

Wells containing only T cells served as negative controls. For positive controls T cells were either unspecifically stimulated with 1 µg/mL Phytohaemagglutinin (PHA) or in the case of T cell receptor transductions co-incubated with peptide pulsed target cells.

1. *ELISpot:*

   ELISpot analyses were performed using either the Human IFNγ ELISpot^{BASIC} (ALP) kit (MabTech) or Human TNFα ELISpot^{BASIC} (ALP) kit (MabTech). Capture antibodies (IFNγ:

1-D1K; TNFα: TNF3/4) were diluted in PBS (IFNγ: 1:500; TNFα: 1:250) and coated to 96-well MAHAS4510 filter plates (75 µL/well) one day prior to co-culture set up. Plates were incubated over night at 4℃. The next day plates were washed six times with 180 µL sterile ELISpot-wash buffer and blocked with ELISpot-blocking buffer for 120 min at 37° C. In the meantime the effector and target cell suspensions were prepared. MHC blocking was performed by pre-incubating the respective target cells with 10 µg/mL blocking antibody for 1 h at 37℃. Target cells were irradiated with 100 Gy prior to setup of co-culture. Plates were washed once with 180 µL X-vivo15 medium, $0.5x10^5$ target and $2x10^5$ effector cells were setup in triplicates and incubated for 48 h at 37° C. Following co-incubation the plates were washed six times with 180 µL ELISpot-wash buffer. The second antibodies (IFNγ: 7-B6-1 biotin; TNFα: TNF5-biotin) were pre-diluted in PBS +1% HSA (IFNγ: 1:1000; TNFα: 1:500), 75 µL added to each well and the plates incubated for 2 h at RT. Plates were again washed six times with 180 µL ELISpot-wash buffer and 75 µL/ well Streptavidin-ALP (1:1000 in PBS + 1% HSA) were added, followed by 1 h incubation at RT. The supernatant was discarded and the plates washed three times with 180 µL ELISpot-wash buffer followed by two washes with 180 µL PBS. Development of the spots was performed using one SIGMAFAST™ BCIP®/NBT tablet, dissolved in 10 mL water. 75 µL of the solution were added to each well and the plates incubated in the dark at RT until first spots became visible. Reactions were stopped under running tab water, the plates dried and analyzed using an ImmunoSpot® S6 MACRO (Cellular Technology Limited). Samples with significantly higher spot counts than the respective controls were considered positive.

2. *ELISA:*

   Each assay was set up in triplicates by plating $0.5x10^4$ effector and $1x10^5$ target cells per well in a 96-well U-bottom plate in a total volume of 200 µL. Plates were spun down at 130 xg for 1 min and incubated for 20 h at 37℃. Co-culture supernatants were carefully transferred to a fresh 96-well U-bottom plate and analyzed using the Human IFNγ ELISA MAX™ kit (BioLegend) according to the manufacturers protocol. Wash steps were fully automated using an EL406 Combination Washer Dispenser (BioTek). Depending on the target cells, supernatants were pre-diluted in Assay Diluent (BioLegend) to stay in the linear range of detection (table 29). Absorbance at 450 nm was measured with an EnVision 2104 Multilabel Reader (PerkinElmer).

Table 29 – Routine, target dependent supernatant dilutions.

Target cells	Supernatant predilution
B-cells	1:100
TILs	1:10

3. *Intracellular cytokine staining:*

   Co-cultures were set up using $0.5x10^5$ target and $2x10^5$ effector cells in a total volume of 200 µL. When working with autologous target cells, these were labeled with CFSE prior to set up of the co-cultures to later distinguish them from the effector population. Samples were spun down at 130 xg for 1 min and incubated for 1 h at 37℃. Subsequently, 1 µg/mL

GolgiPlug/ Brefeldin A (BD Bioscience) was added, the cells spun down at 130 xg for 1 min and incubated for another 5 h. Subsequently, samples were transferred to a 96-well V-bottom plate and stained for flow cytometric analyses.

3.4.6 Polyacrylamide gel electrophoresis

HEK293T cells were transfected by $CaPO_4$co-precipitation. Cells were lysed in 1x Laemmli buffer (+5% β-mercaptoethanol) and whole protein concentration assessed by photospectrometry using a NanoDrop 8000 Photospectrometer (Thermo Fisher Scientific). Deglycosylation was performed by transferring 40 µg whole protein per sample to a 1.5 mL reaction tube. Each sample was diluted 1:1 with H_2O and mixed with 1.5 µL of the respective 10x deglycosylation buffer (G5 = EndoH; G7 = PNGaseF). In the case of PNGaseF, 1.5 µL NP40 (10% stock) was added to the reaction mix. Afterwards, 0.2 µL Deglycosylase (EndoH or PNGaseF; New England Biolabs) was added, each sample filled up to 15 µL total volume, the reaction mixtures were incubated for 1 h at 37° C and another 5 µL 4x Laemmli buffer (+5% β-mercaptoethanol) were added. Untransfected cells and untreated lysates served controls.
Samples, as well as a protein ladder, were loaded to a 4-20 % gradient SDS gel and run at 60 V for 15 min, followed by 60 min at 15 mA per gel in SDS running buffer.

3.4.7 Western Blot & Protein detection

Protein was performed using a semi-dry blotting system. PVDF membranes were prepared by incubating for 15 sec in methanol, 2 min in deionized water and 5 min in transfer buffer. Blotting was performed for 1.5 h with 100 mA (per gel) at RT.
Membranes were blocked with 5% BSA (Gerbu) in TBS buffer for 1 h at RT on a shaker. Afterwards, each membrane was washed for 5 min with TBS buffer and transferred to a 50 mL reaction tube. Primary antibodies, mouse-α-FLAG (1:1000) and rabbit-α-GAPDH (1:10000), were added in 5% BSA in TBS buffer per membrane, incubated over night at 4℃ while rotating and the membranes washed three time with TBS buffer (+0.1% Tween-20) for 10 min. Secondary antibodies, goat-α-mouse-HRP and goat-α-rabbit-HRP (each 1:20000), were added in TBS buffer (+0.1% Tween-20) and incubated for 60 min at RT while rotating the tubes. Subsequently, each membrane was washed three time for 10 min with TBS buffer (+0.1% Tween-20), followed by one wash with TBS buffer for 10 min.
Membranes were covered with Clarity™ Western ECL Substrate (BioRad) and immediately analyzed using a LAS-3000 (Fujifilm Life Science). Quantification was performed using ImageJ 1.51s [333].

3.5 Molecular biologic methods

3.5.1 Design of Lamp1 constructs

The different Lamp1 constructs were designed together with M. Lemberg. The full length, canonical Lamp1 sequence (UniProtKB - P11279-1) was retrieved from UniProt [334]. A 3xFLAG tag was added directly C-terminal to the ER localization sequence, between amino

acid residues 28 and 29. Two BsmBI restriction sites, the first reverse and the second forward oriented, were used to introduce the desired antigenic sequences between amino acid residues 377 and 378, N-terminal to the transmembrane domain. The final construct was codon optimized for *H. sapiens* and ordered via the Invitrogen GeneArt® Gene Synthesis service (Thermo Fisher Scientific). Afterwards, the candidate destabilizing mutations were introduced in the transmembrane domain via site directed mutagenesis by PCR. The generated constructs were further adapted for each round of system validation as follows:

1. *General functionality:*

   Inserts were prepared using four overlapping primer pairs encoding the two ovalbumin peptides SIINFEKL (H-2K^b-restricted) and ISQAVHAAHAEINEAGR (I-A^b-restricted). Prior to ligation, each primer pair was dimerized and phosphorylated separately (table 30), leading to primer dimers with matching 3' and 5' sticky ends. Here, the samples were incubated in a Thermocycler for 1 h at 37 °C, followed by 5 min incubation at 95 °C and cooling to 10 °C. Afterwards, the dimerized primer pairs were ligated**,** creating an antigen encoding insert with 3' and 5' overhang for insertion into BsmBI digested , dephosphorylated (32) Lamp1 constructs.

Table 30 – Sample setup for the generation of phosphorylated primer dimers

	Amount (µL)
10 mM ATP	1
PNK Buffer A	2
1 µM Primer (forward & reverse)	1
Nuclease free water	14
T4 PNK	1

Table 31 – Sample setup for primer dimer ligation

	Amount (µL)
Each primer pair	2
0.1 M DTT	1
10 mM ATP	0.5
Nuclease free water	12
T4 DNA Ligase	2.5

2. *Translation into human setting:*

   An insert encoding the HLA-A02:01 restricted Mart1 epitope (ELAGIGILTV), as well as the DDX3Y/HY epitope (HIENFSDIDMGE), interspaced by two BveI restiction sites, the first reverse and the second forward oriented, was introduced into the Lamp1 constructs. Target vectors, as well as inserts were digested using BsmBI (table 32), followed by construct ligation.

Table 32 – General protocol for BsmBI digests of inserts and target vectors

	Target vector	Insert
Template	150 ng	15 ng
Buffer Tango	2 µL	2 µL
100mM DTT	0.2 µL	0.2 µL
BsmBI	1 µL	1 µL
Nuclease free water	10.9 µL	15.8 µL
FastAP	0.5 µL	—
Total volume	20 µL	20 µL

3. *Patient Screening:*

   The native, codon optimized sequence of Lamp1 contained one additional BveI restriction site, which was removed by site directed mutagenesis using PCR.
   Introduction of patient derived constructs was performed by restriction digest of target vector and inserts using BveI (table 33), followed by construct ligation.

Table 33 – Restriction digest patient constructs

	Target Vector	Insert
Template	100 ng	1000 ng
Buffer O	2 µL	2 µL
50x Oligo Mix	0.4 µL	0.4 µL
BveI	1 µL	1 µL
Nuclease free water	15.6 µL	15.6 µL
FastAP	0.5 µL	—
Total volume	20 µL	20 µL

3.5.2 Design of tandem patient constructs

The mRNA RefSeq accession numbers (NM_) [335] of validated mutations from exome and transcriptome analyses were used to retrieve 30mer wild type amino acid sequences, with the mutation site at position 16, from UniProt [334]. The respective mutated sequences were reverse translated and codon optimized for *H. sapiens* using Serial Cloner 2.6 (SerialBasics).
Up to six 30mer sequences were put back-to-back, resulting in 180 amino acid long tandem constructs. The full length constructs were flanked 3' and 5' by BveI restriction sites, the first reverse and the second forward oriented, and ordered via the Eurofins Genomics Gene Synthesis service in pEX-A128 vector backbones.

3.5.3 Preparation of bacterial growth media

Media and plates used to grow bacteria were based on lysogeny broth (LB). All media were autoclaved directly after preparation and stored at 4℃ until use. In all cases ampicillin (100 µg/mL) was used for selection. Upon use, all media and plates were handled in close proximity to a bunsen burner.

1. *Setup of liquid cultures*:

   For liquid cultures 2% ([$\frac{w}{V}$]) LB in deionized water was used. Directly prior to use the selection antibiotic was added and the solution stirred to evenly distribute it.

2. *Setup of LB-agar plates*:

   LB-agar stocks contained 3.5% ([$\frac{w}{V}$]) LB-agar in deionized water. Prior to use solidified stocks were heated in a microwave until no solid agar was visible and cooled back down to be hand warm at RT while stirring. Afterwards the selection antibiotic was added, the mixture shortly stirred to receive an even solution and the medium distributed to 10 cm petri dishes. Upon solidification the plates were stored at 4℃ until use.

3.5.4 Transformation of competent bacteria

Chemically competent E. coli DH5α bacteria were thawed for 20 min on ice. For each sample 50 µL of the bacterial suspension were mixed with 100 ng plasmid DNA for re-transformations or 5 µL ligation mix. When working with ligation mixes fresh bacteria were used. For re-transformation, refrozen - according to the manufacturers instructions - bacteria could be used. After addition of plasmid DNA the suspensions were incubated for 30 min on ice. To perform the heat shock the reaction mixes were put into a Thermomixer, pre-heated to 42℃, for 40 sec followed by 2 min incubation on ice. Subsequently, 500 µL SOC medium were added and samples were incubated on a shaker for 50 min at 37℃ for bacterial recovery. Afterwards, the bacterial suspensions were spun down for 3 min at 2400 xg, the majority of supernatant discarded and the pellet resuspended the residual medium. Resuspended bacteria were streaked onto LB-agar plates containing the respective selection antibiotic.

3.5.5 Plasmid DNA purification

Depending on the desired amount and application plasmid DNA was purified using two different approaches. Concentrations of all purified plasmid solutions were measured by photo spectrometry using a NanoDrop 8000 Photospectrometer (Thermo Fisher Scientific).
Following protocols were applied:

1. *Small scale purification*:

   Desired bacterial clones were picked late in the afternoon, placed in 5 mL LB-medium containing the respective selection antibiotic and incubated for 14 - 16 h. Afterwards the bacteria were pelleted for 7 min at 2400 xg. Plasmid DNA was then purified using the QIAprep Spin Miniprep kit (Qiagen) according to the manufacturers instructions.

2. *Large scale purification (endotoxin free)*:

   Since the plasmids derived from large scale purifications were later used for transfections and transductions an endotoxin free purification was chosen.
   Colonies were picked early in the morning, placed in 5 mL LB-medium containing the respective selection antibiotic and incubated for 6 - 8 h. Afterwards the pre-culture was

diluted 1:1000 in 200 mL LB-medium containing the respective selection antibiotic, incubated for 14 - 16h and pelleted for 30 min at 2400 xg. Plasmid DNA was performed using the Endofree Plasmid Maxi kit (Qiagen) according to the manufacturers instructions. Plasmid DNA pellets were resolubilized in TE-buffer provided by the kit.

3.5.6 Restriction digest

Digests of plasmid DNA and PCR products were performed using recombinant restriction enzymes in their respective buffer system (RE-buffer). Sample master mixes, containing the respective buffer, restriction enzymes, nuclease free water and in some cases oligo additives, were prepared according to the manufacturers instructions.
In general, two sets of digests were performed during this work:

1. *Target vector digest*:

   Here, target vector, pre-diluted in nuclease free water, was mixed with the respective digestion master mix. The reaction mix was incubated for 16 h at 37℃. Afterwards, the linearized target vector was dephosphorylated by adding FastAP, gently mixing the solution by pipetting and incubated it for an additional 30 - 60 min at 37℃. The dephosphorylation reaction was stopped by heat inactivation for 15 min at 85℃. The received digestion product was later used for construct ligation.

2. *Insert digest*:

   DNA fragments to be inserted into target vectors were digested without dephosphorylation. The respective reaction mixes were incubated for 16 h at 37℃. Digested inserts were purified by gel extraction, precipitated and later used for ligation with the target vector.

3.5.7 Agarose gel electrophoresis

Gels were prepared by mixing 1x TBE buffer with the desired amount of agarose (table 34) in an erlenmeyer flask and heating up the suspension in a microwave to create an even mixture. Afterwards 10 µL ethidium bromide solution was added, the mixture gently stirred and poured into a gel preparation chamber. A sample comb was added and the gel polymerized at RT. In the meantime the samples were prepared by mixing 10 µL sample with 2 µL loading dye (6x). Gels were loaded with the prepared samples and 10 µL GeneRuler DNA ladder mix™ (Thermo Fisher Scientific) for size control. Gels were run for 60 min at 100 V in 1x TBE buffer.

Table 34 – Size dependent agarose gel densities

Product size	TBE buffer [mL]	Agarose [g]	Gel density (% [w/V])
<500 bp	130	2.60	2
500 - 1000 bp	130	1.95	1.5
1000 bp	130	1.30	1

3.5.8 Gel extraction

Directly after agarose gel electrophoresis gels were illuminated with long wave UV light (366 nm) and bands of interest cut out using an X-tracta Disposable Gel Extraction Tool (STARLAB). The gel pieces were placed in pre-tared 1.5 mL reaction tubes and weighed. DNA was extracted from the gel pieces using a Nucleospin® Gel and PCR Clean-up kit (Macherey-Nagel) following the manufacturers instructions.

3.5.9 DNA precipitation

Precipitation was performed whenever a switch of buffer was needed. For most instances this was the case after gel extraction and subsequent construct ligation.
The DNA solution of interest was filled up to 40 µL with nuclease free water. Afterwards 10% ($[\frac{V}{V}]$) 5 M NaCl was added to the solution followed by 300 µL ethanol. The reaction mixture was incubated for 30 min at -20 °C and afterwards spun down for 30 min at 20.000 xg and 4 °C. Supernatant was removed, the pellet washed once with 70% ethanol (diluted with nuclease free water) to remove excess salt and spun down for 5 min at 20.000 xg and 4 °C. The supernatant was again discarded, the pellet air dried and resuspended in the buffer of choice.

3.5.10 Construct ligation

Inserts and target vectors retrieved from sequential digests were ligated using T4 DNA ligase. Digested and dephosphorylated target vectors were mixed with the complete amount of digested and purified insert, T4 ligase buffer (10x) and filled up to 28.5 µL with nuclease free water. Afterwards, 1.5 µL T4 DNA ligase were added to the mix, each sample homogenized by gentle pipetting and incubated for 2 h at RT. Then the samples were transferred to 4 °C for at least 24 h before using them for transformation of competent bacteria.

3.5.11 Primer design

All primers used during this work were ordered as 100 µM HPLC purified stock solutions from Sigma Aldrich. In the case of pyrosequencing, primers were ordered with a 5' biotiylation.

1. *For cell line mutation validation*:

   Genomic sequences surrounding the mutated position 200 - 300 bp to each side were retrieved from the UCSC Genome Browser [336] for reference genome GRCh37/hg19 [337]. Extracted sequences were analyzed for ideal primer pairs with NCBI-primer BLAST [338], initially using default settings. For sequences yielding off-target amplicons the default settings (Max T_m difference and # total mismatches) were adjusted. Optimal primer pairs, most specific for the given loci, were chosen and ordered.

2. *For PCR, sanger sequencing and pyrosequencing:*

   Sequencing primer for regular construct analysis and PCR amplifications were designed using the respective target sequence as a template. For sanger sequencing, primers were

chosen between 80 - 100 bp up- or downstream of the region of interest. Each primer was monitored for melting temperature and hairpin formation using IDT Oligo Analyzer 3.1 [339]. Primer pairs for pyrosequencing were designed and provided by Dr. M. Volkmar.

3.5.12 Polymerase chain reaction

Polymerase chain reactions (PCRs) were performed in different ways based on the needs of the PCR product. Primer stocks were pre-diluted to 5 µM in nuclease free water. All PCR products were analyzed by agarose gel electrophoresis prior to use in follow up assays.

1. *Subcloning and site directed mutagenesis:*

   Amplification for subcloning and site directed mutagenesis was performed with Pfu DNA polymerase, using a touchdown PCR program (table 35). Primers for full length construct amplification included restriction sites for ligation of the PCR product into the respective target vector.
   Site directed mutagenesis PCRs were generally split into two parts using four different primers. Two primers covering the substitution codon of choice and two primers to amplify the full length construct. In a first step, both strands were amplified up to and from the substitution site. Afterwards, the full length, mutated construct was generated.
   Master mixes, containing 0.5 µL dNTP mix (10mM stock), 2.5 µL Pfu-buffer (10x, with $MgSO_4$), 1 µL of each primer, 2 ng template DNA, 1 µL Pfu-polymerase and 18 µL nuclease free water were used for each amplification. The final PCR products were purified by gel electrophoresis, digested and ligated into the target vector of choice.

Table 35 – Standard construct amplification PCR program for subcloning and site directed mutagenesis

Step	Temperature [°C]	Time [sec]	Cycles
Initial denaturation	95	120	1
Denaturation	95	20	10
Annealing	65 $\Rightarrow$ 55 (ΔT = -1)	30	10
Extension	72	120 per kb	10
Denaturation	95	20	15
Annealing	55	30	15
Extension	72	120 per kb	15
Final extension	72	600	1
Pause	10	∞	—

2. *Colony PCR:*

   Colony PCRs were routinely performed to pre-select positive bacterial colonies from construct ligations prior to sending for sequencing. Here, PCR master mixes were prepared containing 8 µL MyTaq™ HS Mix (Bioline), 7 µL nuclease free water and 1 µL of each primer. Per sample 16 µL of the master mix were placed in PCR stripes. Afterwards, colonies were picked, the toothpick shortly stirred in the respective reaction tube and residual bacteria plated onto a fresh LB-agar plate to re-grow the selected colony. The respective empty vector served as negative control.

Sequences of interest were amplified (table 36) and PCR products analyzed by agarose gel electrophoresis.

Table 36 – Standard colony PCR program

Step	Temperature [°C]	Time [sec]	Cycles
Initial denaturation/ Lysis	95	180	1
Denaturation	95	15	25
Annealing	63	30	25
Extension	72	60 per kb	25
Final extension	72	600	1
Pause	10	∞	—

3. *Cell line mutation validation and pyrosequencing:*

   For sufficient PCR product sequencing, larger amounts of amplified sequences were needed. Thus, the total volume for these reactions was 50 µL. For each sample 25 µL MyTaq™ HS Mix (Bioline), 16 µL nuclease free water, 3.5 µL of each primer and 60 ng template DNA were mixed. After PCR amplification (table 37), samples used for mutation validation by sanger sequencing were purified using the MinElute PCR purification kit (Qiagen) following the manufacturers instructions. Samples used for pyrosequencing were directly used.

Table 37 – Standard mutation validation and pyrosequencing PCR program

Step	Temperature [°C]	Time [sec]	Cycles
Initial denaturation/ Lysis	95	120	1
Denaturation	94	20	45
Annealing	58	30	45
Extension	72	60 per kb	45
Final extension	72	300	1
Pause	10	∞	—

3.5.13 Sequencing of plasmid DNA and PCR products

1. *Sanger Sequencing*

   Sequencing reactions were performed by the Eurofins Tube Sequencing service. Template DNA from plasmid purifications or PCR amplifications was provided following the manufacturers instructions. When using non-standard primers - not available at Eurofins Genomics - these were always provided in a separate tube. For result analysis the sequencing chromatograms were inspected and the received sequences checked using Serial Cloner 2.6 (SerialBasics).

2. *Pyrosequencing*

   Loci of interest were amplified by PCR using biotinylated primers for later immobilization of the PCR product to streptavidin-coated sepharose beads. Pyrosequencing was performed by J. Rebmann using a PyroMark Q24 (Qiagen), following the manufacturers instructions.

3.5.14 Transient transfection

1. *Using Electroporation*

   For electroporation experiments a GenePulser XCell™ (BioRad) was used. All experiments were performed using cuvettes with a 4 mm gap width. A suspension of 5x10^6 cells and 12 µg total plasmid DNA in 400 µL OptiMEM was prepared for each sample. Pulse optimization (see table 38) for each cell line was performed using eGFP-N1 [340] as fluorescence marker. After the pulse, cells were carefully taken out of the cuvette using a pasteur pipette, placed in 5 mL pre-warmed culture medium per well of a 6-well plate and incubated over night. Electroporation efficiency for living, GFP transfected cells was assessed by flow cytometry.

Table 38 – B cell line dependent, optimal electroporation conditions

Cell line	Shape	Voltage [V]	Capacitance [µF]	Number of pulses
771 B cells	exponential decay	200	500	1
KBV623 B cells	exponential decay	250	750	1
TIPC253 B cells	exponential decay	250	750	1
TIPC275 B cells	exponential decay	250	750	1

2. *Using Calcium phosphate co-precipitation*

   One day prior to transfection cells were seeded. On the day of transfection the supernatant was removed, fresh culture medium was added and cells incubated at 37° C and 5% CO_2 for at least 20 min to stabilize the mediums pH. In the meantime the transfection solutions were brought to room temperature. Solutions were mixed by adding the $CaCl_2$/DNA mix to 2x HBS buffer under rigorous pipetting (see table 39). The mix was immediately added to the cells, evenly distributed and incubated for 6 - 8 h at 37℃. Afterwards the supernatant was discarded and fresh culture medium was added to the cells.

Table 39 – Calculation table for $CaPO_4$ co-precipitation. Calculations are given for single wells. Solutions need to be tested each time they are prepared.

Dish	Medium [mL]	Solution A	Solution B			Amount per well/ dish [µL]
		2x HBS [µL]	$CaCl_2$ (2.5 M) [µL]	DNA [µg]	H_2O ad [µL]	
6-well	2	60	6	2	60	120
10 cm	10	300	30	10	300	600

3.5.15 Genomic DNA extraction

Purification of genomic DNA from cell lines and tumor tissue was performed using the DNeasy® Blood & Tissue Kit (Qiagen) according to the manufacturer's instructions.

3.5.16 Tumor RNA extraction

For RNA extraction frozen tissue samples were constantly kept on dry ice during transportation. The tissue pieces were homogenized using a pestle. RNA was extracted using the RNeasy®

Mini Kit (Qiagen) following the producers manual. RNA was quantified using a Qubit (LifeTechnologies) and quality was assessed using a BioAnalyzer 2100 (Agilent) with the RNA 6000 Nano Kit (Agilent), both following the respective manufacturers protocol.

3.5.17 Exome and Transcriptome analyses

Next generation sequencing data was collected in the context of the HIPO-15 and HIPO-K28E projects. Patient sample identifier were provided by the sample processing lab (SPL) of the Heidelberg Center for Personalized Oncology (HIPO). Prior to sample preparation, concentrations were assessed via Qubit (LifeTechnologies), following the manufacturers protocol. Total RNA and genomic DNA samples were were adjusted to the desired concentrations in fresh nuclease free water and transferred to the SPL on dry ice.
Whole exome and RNA sequencing were performed by the Genomics and Proteomics core facility (GPCF) of the DKFZ. Sequencing was performed on an Illumina HiSeq4000 using following submission parameters:

Table 40 – Total RNA and genomic DNA sample submission parameters

Provided Analyte	Application Type	Sequencing Type	Total Amount [µg]
Genomic DNA	Low Input Exome - Version 6 without UTRs	HiSeq 4000 Paired-End 100 bp	500
Total RNA	RNA-Seq	HiSeq 4000 Paired-End 100 bp	1500

Analysis of exome and transcriptome data was performed using the Heidelberg Unix Sequence Analysis Resources (HUSAR) program package. Genome Reference Consortium Human Build 37 (GRCh37/ hg19) [337] was used as the reference genome for all primary and germline sample analyses during this work. A human-mouse hybrid reference genome (provided by Dr. M. Volkmar) was applied to all xenograft samples in order to reduce read misalignment of mouse cell derived reads.
Raw sequencing data of primary tumors, xenograft and germline were retrieved from the GPCF and prepared for mutation calling, as well as filtering, using to following script (kindly provided by Dr. M. Volkmar) in the HUSAR environment.
Reads were aligned to the respective reference genome using the Burrows-Wheeler Alignment Tool (BWA)[341, 342] align function:

1. For the first read file:

```
bwa aln -t 4 reference.fa sampleXYZ_read1.fastq.gz >
   sampleXYZ_read1.sai
```

2. For the second read file:

```
bwa aln -t 4 reference.fa sampleXYZ_read2.fastq.gz >
   sampleXYZ_read2.sai
```

Both indexed read files (*sampleXYZ_read1.sai* and *sampleXYZ_read2.sai*) were further merged to a paired-end alignment SAM file using the BWA sampe function:

```
bwa sampe reference.fa sampleXYZ_read1.sai sampleXYZ_read2.sai
   sampleXYZ_read1.fastq.gz sampleXYZ_read2.fastq.gz > sampleXYZ.sam
```

The generated Sequence Alignment/Map (SAM) files were sorted and converted to their respective binary counterparts using Picard tools[343] SortSam function:

```
java -Djava.io.tmpdir=[path to temporary directory] -jar $NGSUTILDIR/
    java/SortSam.jar INPUT=[working directory]/sampleXYZ.sam OUTPUT=[
    working directory]/sampleXYZ_sorted.bam SORT_ORDER=coordinate
```

Readgroups were added to each sorted Binary Alignment/Map (BAM) using Picard tools AddOrReplaceReadGroups function:

```
java -jar $NGSUTILDIR/java/picard-tools-1.78/AddOrReplaceReadGroups.jar
    INPUT=[working directory]/sampleXYZ_sorted.bam OUTPUT=[working
    directory]/sampleXYZ_AddedReadGroup.bam RGLB=TIPC91GPCF1 RGPL=
    Illumina RGPU=1 RGSM=TIPC91GPCF
```

Duplicate reads in the sorted BAM files were marked as originating from the same DNA fragment without removing them using Picard tools MarkDuplicates tool:

```
java -Djava.io.tmpdir=[path to temporary directory] -jar $NGSUTILDIR/
    java/picard-tools-1.78/MarkDuplicates.jar INPUT=[working directory]/
    sampleXYZ_AddedReadGroup.bam OUTPUT=[working directory]/
    sampleXYZ_markdup.bam METRICS_FILE=TIPC091GPCF_markdup.metrics
    REMOVE_DUPLICATES=false ASSUME_SORTED=true VALIDATION_STRINGENCY=
    LENIENT CREATE_INDEX=true
```

Creation of targets for re-alignment around indels was performed using the Genome Analysis Toolkit (GATK)[344–346] RealignerTargetCreator (RTC):

```
java -jar GATK.jar -T RealignerTargetCreator -R reference.fa -I
    sampleXYZ_markdup.bam -known 1000genomes_gold_standard.indels.hg19.
    vcf -o RTC_sampleXYZ.intervals
```

Local realignment of target regions around indels retrieved from RTC was performed using the GATK IndelRealigner function, to decrease overall base mismatches across all reads:

```
java -jar GATK.jar -T IndelRealigner -R reference.fa -I
    sampleXYZ_markdup.bam -targetIntervals RTC_sampleXYZ.intervals -known
     1000genomes_gold_standard.indels.hg19.vcf -o sampleXYZ_markdup_indel
    -realigned.bam
```

Base quality score recalibration (BSQR) was performed using the GATK BaseRecalibrator, in order to increase variant call accuracy:

```
java -jar GATK.jar -T BaseRecalibrator -R reference.fa -I
    sampleXYZ_markdup_indel-realigned.bam -knownSites 1000genomes.high-
    confidence-SNPs.hg19.vcf -o sampleXYZ_recal.data.grp
```

RealignmentTargetCreator and BaseRecalibrator output files were then merged using the GATK PrintReads function resulting in a coordinate sorted output BAM file:

```
java -jar GATK.jar -T PrintReads -R reference.fa -I
    sampleXYZ_markdup_indel-realigned.bam -BQSR sampleXYZ_recal.data.grp
    -o sampleXYZ_markdup_indel-realigned-recal.bam
```

Afterwards, the sequencing sample data from tumor and xenograft were compared to the germline sample for calling of point mutations by MuTect[347]:

```
java -jar MuTect-1.1.4.jar --analysis_type MuTect --reference_sequence
   reference.fa --dbsnp dbSNP_build144_GRCh37.13_chr.vcf --
   downsampling_type NONE --input_file:normal
   sampleXYZ_Germline_markdup_indel-realigned-recal.bam --input_file:
   tumor sampleXYZ_Tumor_markdup_indel-realigned-recal.bam --out
   sampleXYZ_Tumor_MutectSNV_stats.txt --coverage_file
   coverage_sampleXYZ.wig.txt --vcf sampleXYZ_Tumor_Mutect.vcf
```

The output files were then filtered for MuTect quality control passed mutations using the GATK SelectVariants tool:

```
java -jar GATK.jar -T SelectVariants -R reference.fa --variant
   sampleXYZ_Mutect.vcf -o sampleXYZ_Mutect_filterPASSed.vcf -ef
```

Transcriptome read depth was manually assessed using the Integtrative Genomics Viewer (IGV)[348, 349]. Mutations covered with up to as little as a single mutated read were extracted for further analyses.
All expressed, mutated genes were compared to their respective overall expression in the PDAC tumor tissue derived subset of National Center for Biotechnology Information's (NCBI) Gene Expression Omnibus (GEO)[350, 351] DataSet Record GDS4336[352, 353] (accession number GSE28735).

3.5.18 HLA genotyping

Patient HLA typing, seq2HLA [354] was performed using either raw RNASeq or whole exome sequencing data.

3.6 Retroviral transduction

3.6.1 Virus production and transduction

Described here are the steps from seeding of virus producing cells to final transduced cell product in a day-by-day manner, since this process takes one week to receive the final transduced cell product.

- Day 1: ø-NX-Ampho cells were seeded at 0.25x10^6 cells per well in 2 mL ø-NX culture medium in a 6-well plate. One 6-well plate yielded enough virus for one transduction of 3x10^6 cells.
- Day 2: ø-NX-Ampho cells were transfected using the $CaPO_4$method. A 24-well plate was coated with 500 µL PBS, containing 5 µg/mL αCD3 (OKT3) and 1 µg/mL αCD28, for 2 h at 37° C. Afterwards the supernatant was removed, up to 2x10^6T cells in TIL-medium, containing 300 U/mL IL-2, were added to each well and rested for 48 h.
- Day 3: In the late afternoon supernatant was removed from the transfected ø-NX-Ampho cells and 3 mL fresh ø-NX culture medium per well was added. In addition cells transfected with a GFP construct were screened for transfection efficiency using a fluorescence microscope. Afterwards the cells were incubated for another 14 - 16 h. The late

timepoint for medium exchange was chosen to reduce the amount of empty virus particles as much as possible. To later co-localize virus particles and target cells, 6-well plates (non-cellculture treated) were coated with 1 mL RetroNectin (25 µg/mL in PBS) and incubated over night at 4 °C. Here one well is need for the transduction of up to $3x10^6$ target cells.

- Day 4: RetroNectin was taken up, pooled and transferred to fresh 6-well plates (non-cellculture treated), which were in turn again incubated over night at 4 °C. Empty wells were blocked with 1 mL 2% BSA (in PBS) for 30 min at RT. Afterwards the solution was discarded and each well washed once with 1 mL PBS. On this day the ø-NX-Ampho cells should have a confluency of 90 - 95%. Virus containing supernatant was taken up from up from the ø-NX-Ampho cells and filtered (0.45 µm) to remove excess cellular debris, resulting in 18 mL viral supernatant. Moving on, this suspension was split into two parts.

  1. *Direct transduction*:

     PBS was removed from the RetroNectin coated, blocked plates and 3 mL of viral suspension was added to each well. Plates were immediately centrifuged for 90 min at 2000 xg and 32 °C. The pre-rested target cells were resuspended, adjusted to $1x10^6$cells/mL in TIL-culture medium, containing 400 U/mL IL-2 and 4 µg/mL protamin sulfate. Afterwards the supernatant was removed from the virus coated plates and 3 mL of the cell suspension was added to each well. Subsequently, the target cells were spun onto the virus for 30 min at 130 xg and 32 °C followed by over night incubation.

  2. *Concentration by ultra-centrifugation*:

     Ultra centrifuge tubes were rinsed with 70% ethanol and dried in a laminar flow hood. Afterwards the residual viral supernatants were added, the tubes balanced and the virus concentrated by ultra-centrifugation for 2 h at 111.200 xg (25.000 rpm) in an SW40Ti rotor and 4°C. The supernatant was discarded and the virus reconstituted over night at 4 °C with 500 µL PBS.

- Day 5: RetroNectin from the pre-coated plates was discarded and the plates washed once with 1 mL PBS. The concentrated virus was reconstituted by addition of another 500 µL PBS and careful pipetting. Afterwards the viral suspension was added to the RetroNectin coated, blocked plate and spun onto the it for 90 min at 2000 xg and 32 °C. The supernatant was removed, the target cells from day 4 directly transferred to the new plates, centrifuged onto the virus for 30 min at 130 xg and 32 °C and incubated for 48 - 60 h. Incubation over the weekend and harvest on Monday morning did not appear to harm target cell activation or transduction efficiency.

- Day 7-8: Cells were resuspended and washed twice with PBS. Afterwards, the cells were directly used for assay setup or kept in TIL-culture medium, containing 50 U/mL IL-2, for up to 3 days. Transduction efficiency was monitored by flow cytometry.

3.6.2 Stable cell line generation

Generation of CIITA or HLA-A02:01 transduced, PDX derived cell lines was performed by the Genomics and Proteomics core facility of the DKFZ. Briefly, 5x10^5 cells/well were seeded in 6-well plates and adhered over night. The next day the cells were transferred to the core facility together with the respective culture medium. In general, cells were ready for pick up and transfer to an S1 environment about 48 h later. For antibiotic selection 500 µg/mL G418 was routinely used and directly added to the culture medium during medium exchange. When splitting confluent cultures, the cells were plated and adhered over night in absence of G418 to avoid loss of the culture. After 24h the medium was changed for fresh culture medium, containing 500 µg/mL G418.
Generation of Bcl-6/XL immortalized B cell lines from patients peripheral blood or spleen was performed by AIMM Therapeutics (Amsterdam) under a material transfer agreement (MTA).

3.7 Mass spectrometry

3.7.1 Epitope binding prediction

Binding predictions for HLA-A02:01 were performed using netMHC4.0 [355, 356]. Search parameters were restricted for 8mer - 12mer sequences with thresholds for strong (0.5% rank) and weak (2% rank) binders. Input sequences were retrieved from UniProt [334] as 30mer amino acid sequences with the mutation at position 15 using the mRNA RefSeq accession number (NM_) [335] received from exome and transcriptome analyses. Epitope sequences with an affinity < 1000 nM were retrieved and synthetic peptides were generated.

3.7.2 Peptide synthesis and handling

The respective sequences were synthesized via solid phase synthesis, purified by HPLC and controlled by electronspray ionization mass spectrometry by M. Koch. Aliquots of lyophilized peptides were constantly kept at -20 °C. Upon solubilization peptides were first brought to RT to avoid moisture uptake from the air. Afterwards, peptides were resolubilized in sterile DMSO at 10 mg/mL working stocks and aliquots kept at -20 °C until use. To avoid repeated freeze-thaw cycles, working aliquots were prepared fresh for each experiment series.

3.7.3 Lysate generation for mass spectrometry

Due to the expected low abundance of naturally processed and presented HLA-A02:01 bound neoepitopes within PDX derived cell lines, up to 45 cell culture dishes (10 cm) were prepared for lysis. In the case of antigen overexpression in HEK293T cells 10 culture dishes were already sufficient for neoepitope detection. All samples were acquired as biological triplicates.
Cell lines were seeded at 1x10^6 cells per 10 cm dish in the respective culture medium. HEK293T cells were transfected with the respective constructs by $CaPO_4$ co-precipitation. At 80 - 85% confluency, medium was changed to fresh culture medium containing 330 U/mL IFNγ and cells incubated for another 48 h. HEK293T cells were at 60 - 70% confluency at the time of medium

exchange and IFNγ addition, as they grew comparably faster. Transfection efficiency, in the case of HEK293T monitored by GFP, and HLA-A2 upregulation upon IFNγ treatment was assessed by flow cytometry. Prior to starting the lysis, lysis buffer, PBS, cell scraper and collection tubes were pre-cooled to 4 °C. Culture dishes were taken out of the incubator and immediately put on ice. It was crucial to constantly keep the dishes in contact with the ice to reduce possible peptide degradation. Culture medium was removed, each plate rinsed with 5 mL PBS and the PBS completely removed to avoid sample dilution. Afterwards 1 mL of lysis buffer was used for lysis of four 10 cm dishes ($\approx$4x10^7 cells) by adding the buffer to the first plate, scraping off the cells and transferring the suspension to the next dish to repeat the process. Lysates were collected, aliquoted to 2 mL tubes and cellular debris was pelleted for 30 min at >20.000 xg and 4 °C. Afterwards up to 5 mL supernatant were pooled and stored at -80 °C until submission for mass spectrometry analyses.

3.7.4 Mass spectrometry analyses

All lysates and lyophilized peptides were transferred to the group of PD Dr. Dr. A. Riemer on dry ice. HLA pulldown, peptide elution and mass spectrometry analyses were performed by them as previously described [357].

3.8 Generation of flow cytometry data

3.8.1 Flow Cytometry Panels

Table 41 – Flow cytometry panels applied for mouse cell experiments. Stainings for the different markers were performed as described in the method section. Amounts used for each marker can be found in the material section.

Staining	Marker	Fluorophore	Panel setup (Volume [µL])	
			H2-K^b-SIINFEKL	OT Assay
CFSE	CFSE	CFSE	—	✓
Dead cell staining	DCM_Aqua	Aqua	✓	✓
	DCM_ZV	Zombie Violet	—	—
	DCM_488	488	—	—
Extracellular	CD45.1	BV711	—	✓
	CD45.2	PE/ Dazzle594	—	✓
	H2-K$_b$	APC	✓	—
	H2-K$_b$- SIINFEKL	PE	✓	—
	CD3	APC	—	✓
	CD8a	APC-Cy7	—	✓
	CD4	Pacific Blue	—	✓
Additional	GFP	GFP	✓	—

Table 42 – Flow cytometry panels applied for human cell experiments. Stainings for the different markers were performed as described in the method section. Amounts of each marker can be found in the material section. (✓) = Seperate samples with either of the antibodies used.

Staining	Marker	Fluorophore	Panel setup				Transduction			
			T cell	MHC expression	T Cell Activation	Cell line contamination	3xFLAG	DMF5	HY TCR	GFP
CFSE	CFSE	CFSE	—	—	✓	—	—	—	—	—
Dead cell staining	DCM_Aqua	Aqua	✓	—	—	✓	✓	✓	—	—
	DCM_ZV	Zombie Violet	—	✓	✓	—	—	—	—	✓
	DCM_488	488	—	—	—	—	—	—	✓	—
Extracellular	CD3	BV711	✓	—	✓	—	—	—	—	—
	CD4	APC-Cy7	✓	—	✓	—	—	—	—	—
	CD8	Alf-700	✓	—	✓	—	—	—	—	—
	CD271 (NGFR)	APC	—	—	—	—	—	—	✓	—
	FLAG	APC	—	—	—	—	—	—	—	—
	CD326 (EpCAM)	APC-Vio770	—	—	—	✓	—	—	—	—
	HLA-A2	FITC	—	(✓)	—	—	—	—	—	—
	HLA-A, B, C	FITC	—	(✓)	—	—	—	—	—	—
	HLA-DR, DP, DQ	FITC	—	(✓)	—	—	—	—	—	—
	mTCR-β	BV421	—	—	—	—	—	✓	—	—
	CD4	BV510	—	—	—	—	—	—	—	—
	FLAG	APC	—	—	—	—	✓	—	—	—
Intracellular	TNF-α	APC	—	—	✓	—	—	—	—	—
	IFN-γ	PE	—	—	✓	—	—	—	—	—
Additional	GFP	GFP	—	—	—	—	—	—	—	✓

3.8.2 Gating strategies

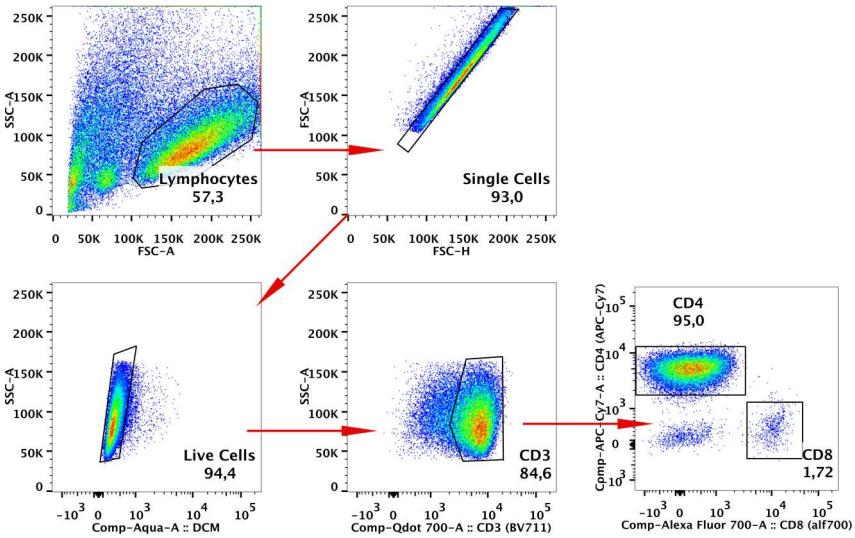

Figure 13 – Gating strategy to determine $CD4^+$/ $CD8^+$ ratios in bulk expanded TIL populations. Applying the T cell panel.

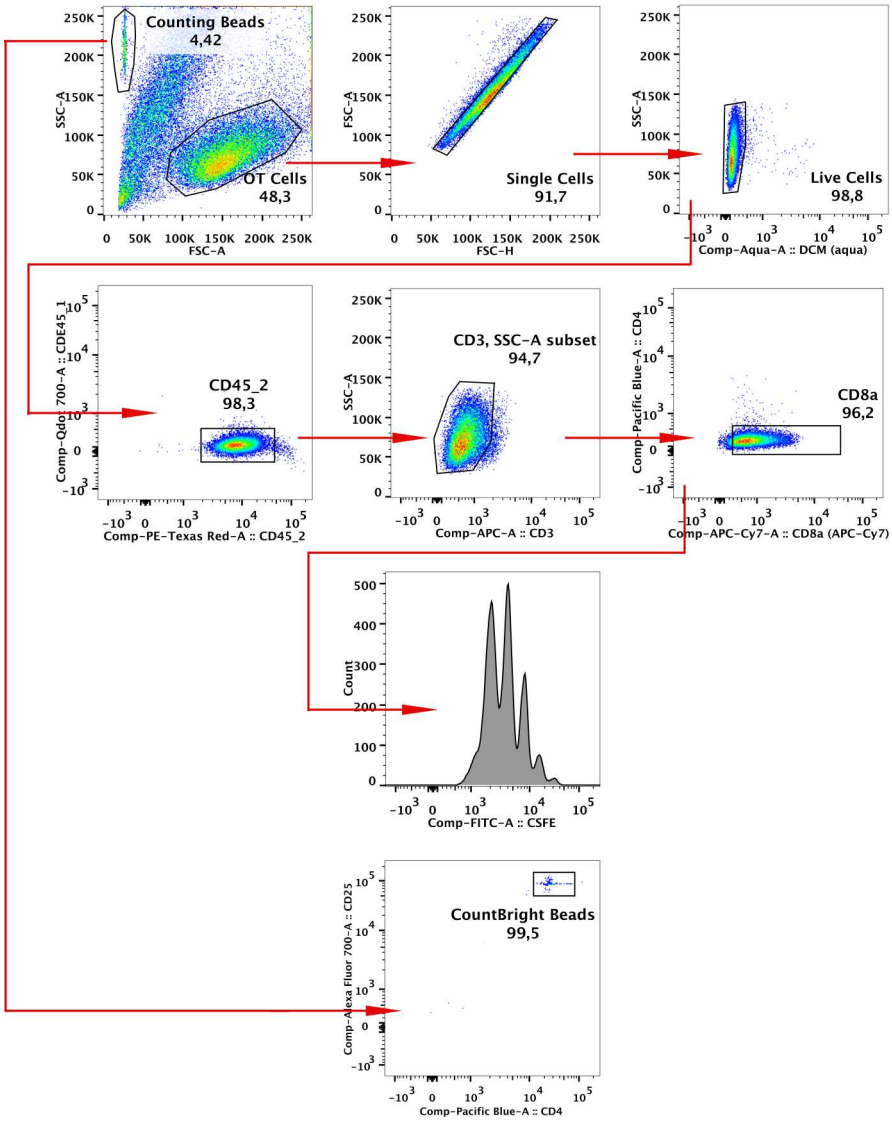

Figure 14 – Gating strategy for the OT proliferation assays. Applying the OT assay panel.

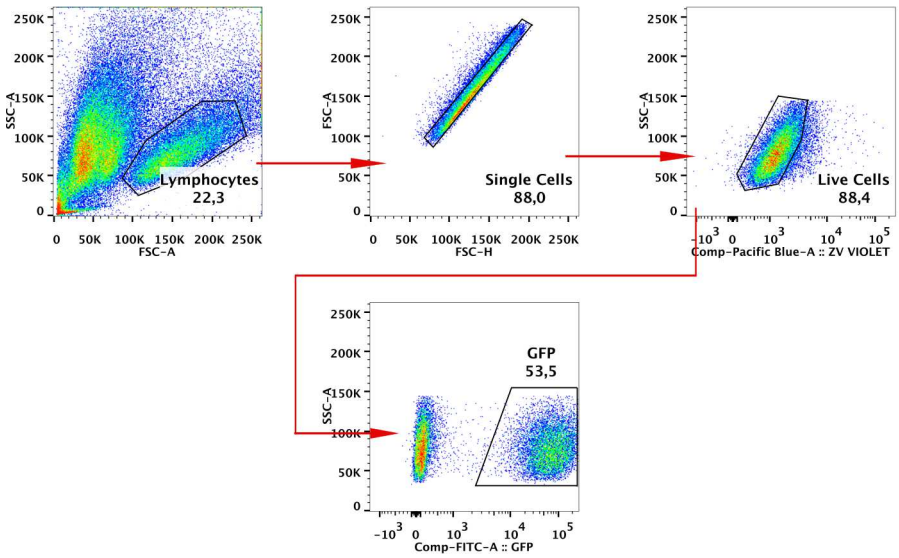

Figure 15 – Gating strategy to asess the GFP transduction efficiency. Applying the GFP transduction panel.

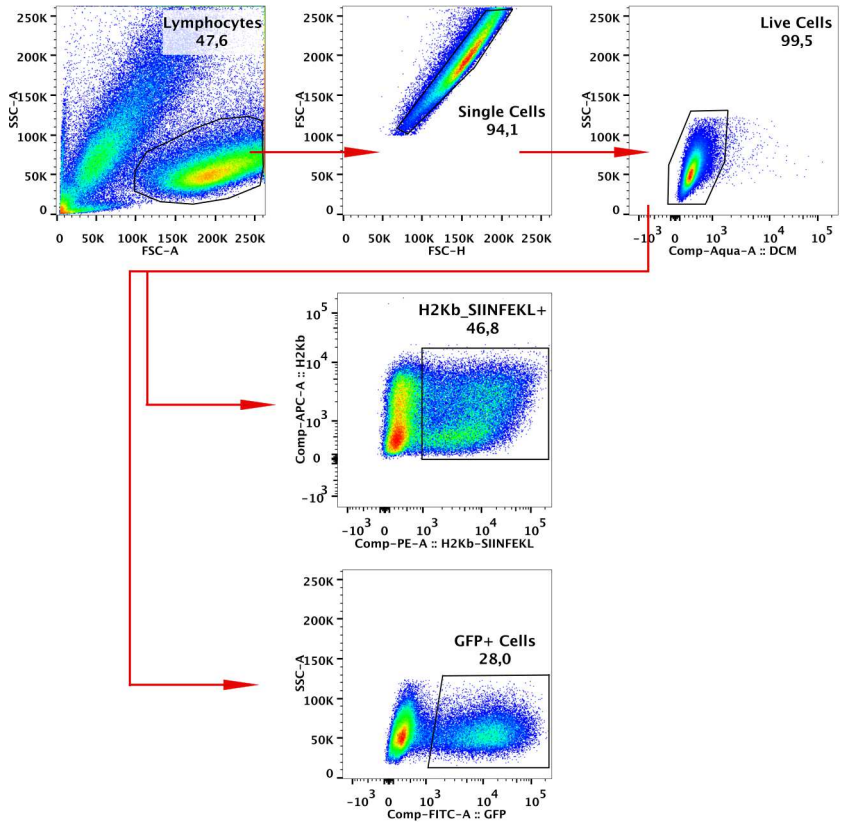

Figure 16 – Gating strategy for the H2-K^b-SIINFEKL surface staining. Applying the H2-K^b-SIINFEKL panel.

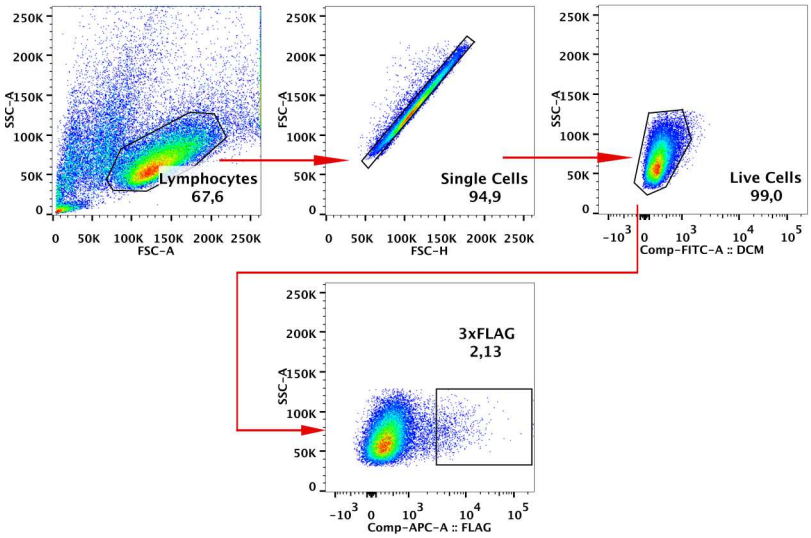

Figure 17 – Gating strategy to asess the Lamp1 transduction efficiency. Applying the 3xFLAG transduction panel.

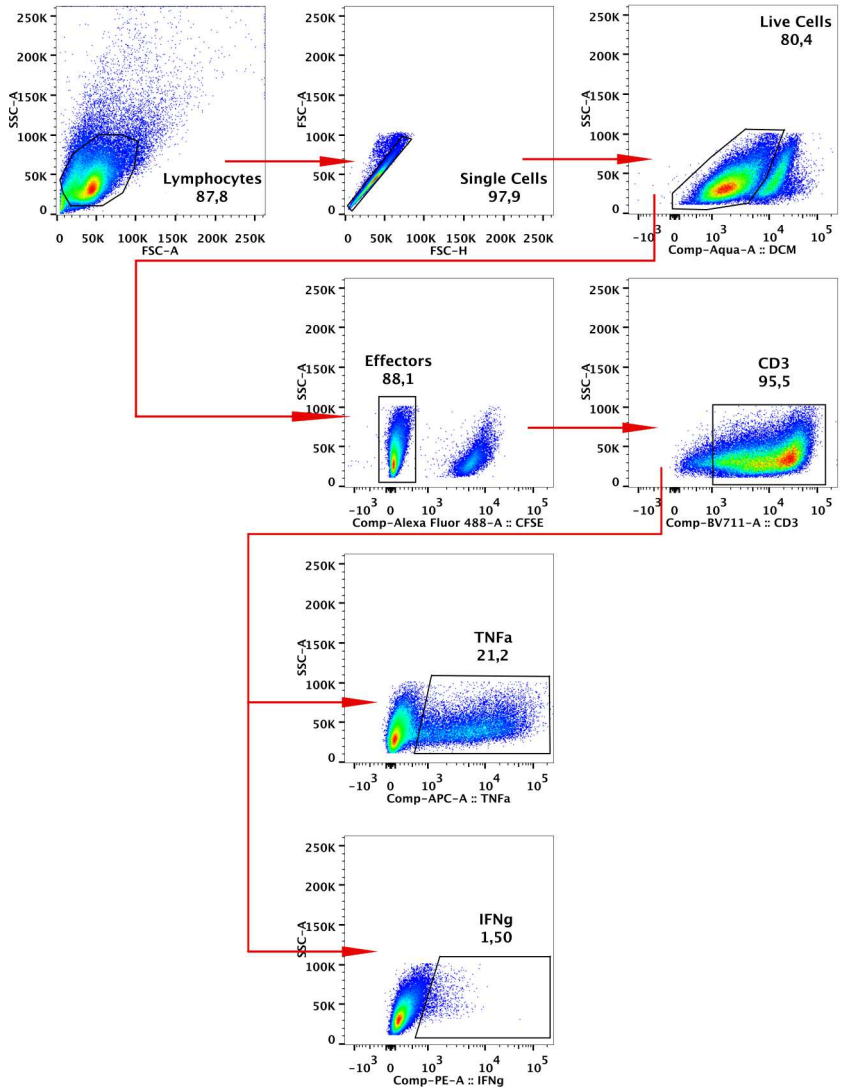

Figure 18 – Gating strategy for monitoring human T cell activation in an autologous setting. Applying the T cell activation panel.

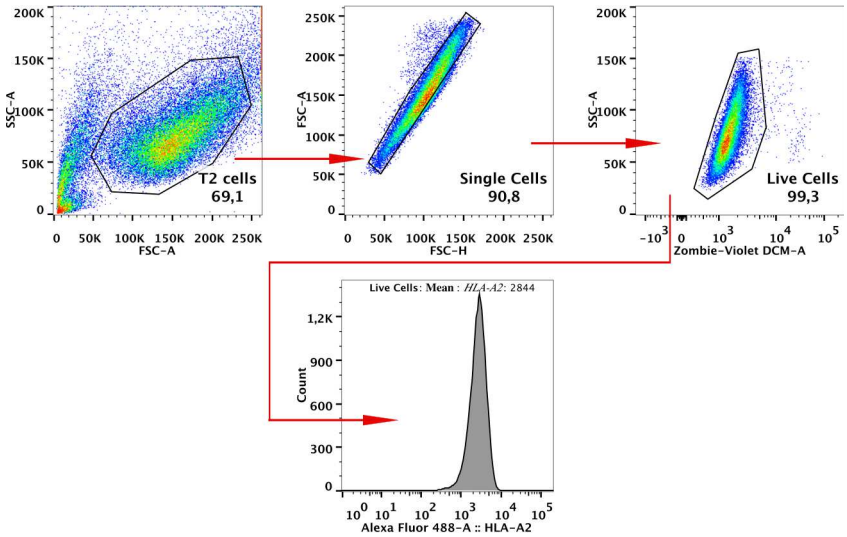

Figure 19 – Gating strategy to assess peptide dependent HLA-A2 stabilization. Applying the MHC expression panel with the HLA-A2_FITC antibody.

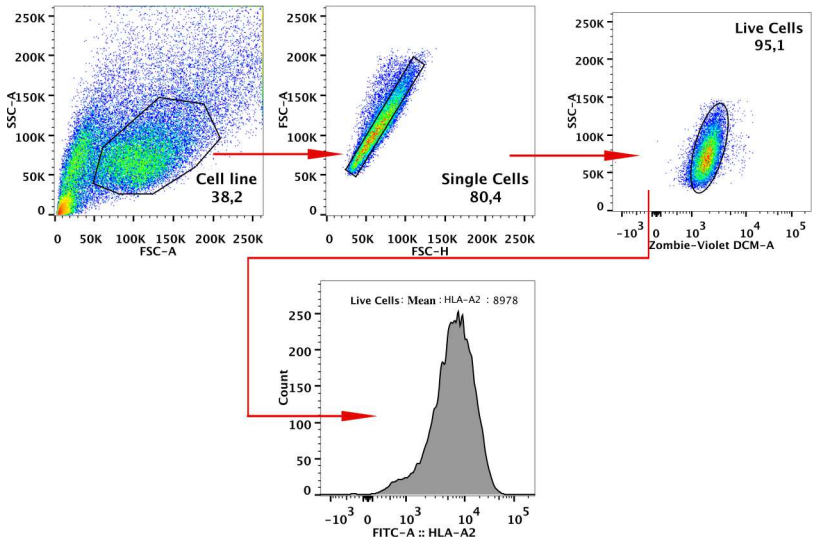

Figure 20 – Gating strategy to assess HLA-A2 upregulation on PDX derived cell lines. Applying the MHC expression panel with the HLA-A2 antibody.

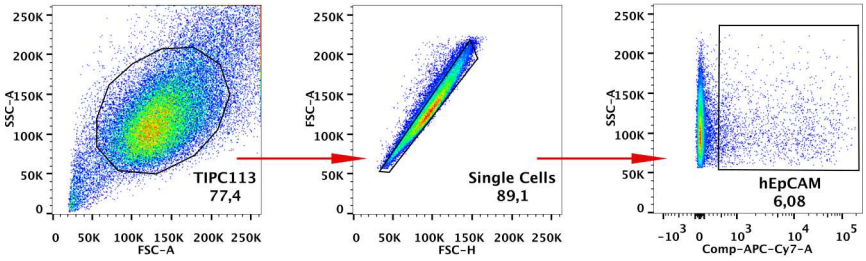

Figure 21 – Gating strategy to visualize phenotypic differences in mouse contaminated cell lines. Applying the cell line contamination panel.

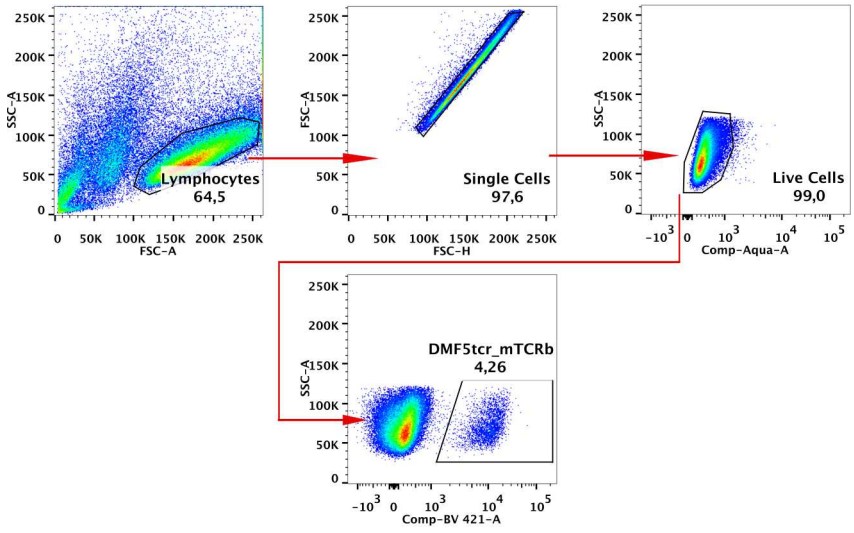

Figure 22 – Gating strategy to asess the DMF5 TCR transduction efficiency. Applying the DMF5 transduction panel.

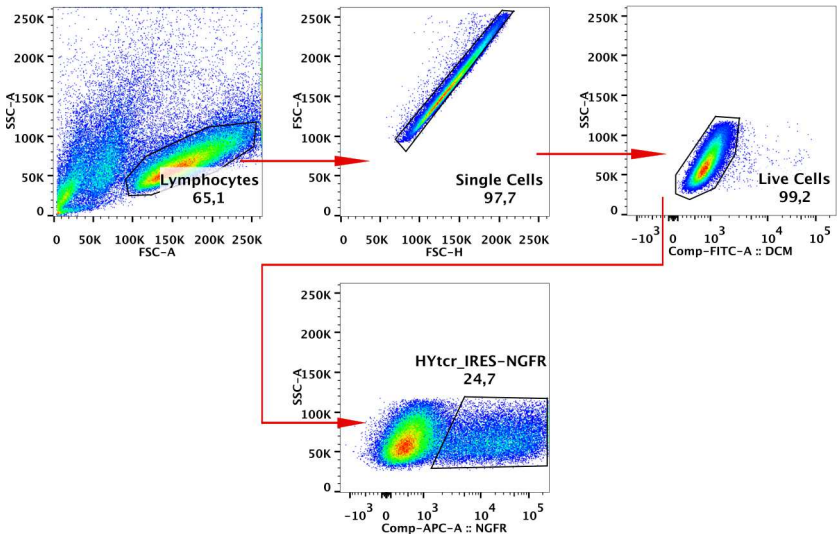

Figure 23 – Gating strategy to asess the HY TCR transduction efficiency. Applying the HY TCR transduction panel.

3.9 Statistical analyses

Statistical analyses and plotting of graphs was performed using GraphPad Prism 7 for Mac OS X, GraphPad software, La Jolla California USA, www.graphpad.com. For the statistical analyses applied during this work, unpaired t-test and One-way ANOVA with Tukey's multiple comparison post-hoc multiple comparisons test were used.

4 Results

4.1 Strategies towards the identification of TIL-target epitopes in PDAC

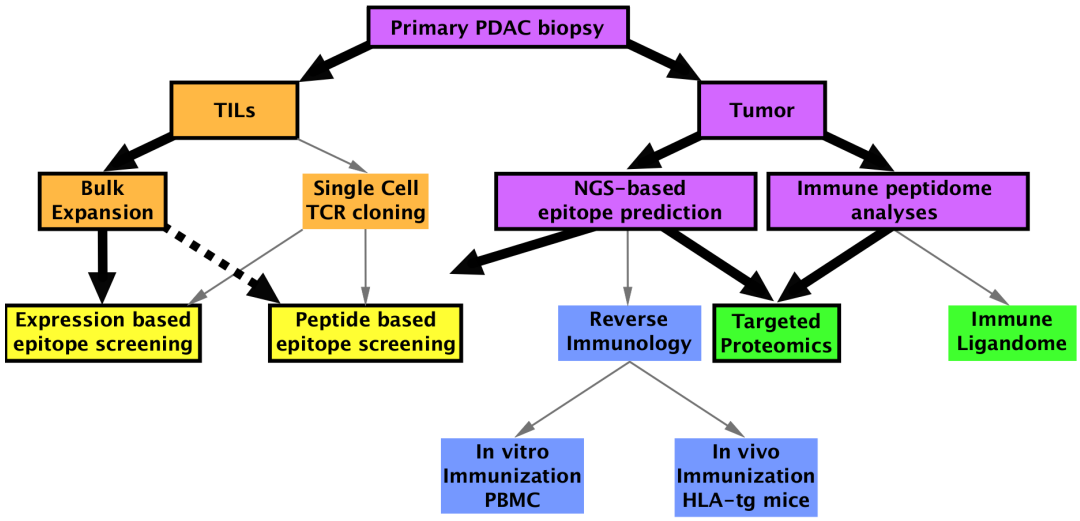

Figure 24 – Complementary strategies for the identification of TIL-target epitopes in PDAC. For the identification of immunogenic antigens, our main focus was on the validation of an expression based screening approach. In the case of direct identification of antigens presented on the surface of tumor cells, we focussed on a targeted proteomics protocol. The main methodologies validated during this work are highlighted (black arrows).

In order to examine the specificity of PDAC tumor infiltrating lymphocytes (TILs), a general framework of complementary methodologies can be applied, depending on the starting material used (see figure 24). Applying these methodologies to primary PDAC biopsies, this thesis focused on two main strategies (see figure 24; highlighted by black arrows). On the one hand on the assessment of immunogenic antigens recognized by PDAC TILs and on the other hand on the direct identification of antigens presented at the tumor cell surface. Regarding tumor recognition by TILs, two functional approaches for the identification of immunogenic antigens may be used which either focus on *in vitro* expanded TILs, or single cell cloned T cell receptors (TCRs) [141, 143, 144, 358]. However, as the identification of tumor reactive TCRs from single cells currently remains challenging and cost intensive, we used *in vitro* expanded TILs for the implementation of our antigen screening system in this thesis. Especially, since expanded PDAC TILs have been shown to recognize their autologous tumor [279]. Furthermore, the use of an expression-based or a peptide-based epitope screening were shown to be useful tools for the identification of immunogenic antigens [146, 175]. Here, we decided to implement an expression-based screening system, as this approach best resembles the physiological processing and presentation of relevant antigens. Given the overall low number of mutations found in PDAC tumors, in combination with a frequent infiltration of tumor reactive T cells - to a slightly higher extent by $CD4^+$ than $CD8^+$ cells -, we chose to develop a system, that could potentially target antigens into the MHC-I, as well as the MHC-II antigen presenting pathway. This allowed us to screen for $CD4^+$ and $CD8^+$ T cell restricted epitopes in an unbiased (i.e. MHC independent) fashion.

The tumor material itself can be used to analyze its genetic profile by next-generation sequencing, an important step in the process of antigen identification, as it yields crucial information

on the malignancies' gene expression profile and tumor mutanome. Based on this, the identified alterations can afterwards either be used to screen for immunogenic antigens (i.e. using TILs), to predict potential antigens for *in vitro* / *in vivo* immunization (i.e. reverse immunology) or to directly identify previously predicted epitopes, presented on the tumor cell surface (i.e. by targeted mass spectrometry). In this thesis, we decided to focus on the direct identification of antigens presented on the tumor cell surface, using a targeted mass spectrometry approach. The advantage of this targeted approach, allowing for a highly sensitive detection of low abundant and weaker binding epitopes, was recently shown by the group of PD Dr. Dr. A. Riemer [357].

4.2 Patient characteristics

4.2.1 Patient sample-sets relevant for this study

In order to design screening methodologies to identify PDAC derived neoepitopes, we analyzed the available patient material for screening eligibility. For this, we defined the minimal criteria the patient material had to fulfill to be used for the envisioned approaches. In the case of the expression based screening, large numbers of expanded TILs, exome and transcriptome data, as well as patient derived xenografts (PDX) had to be available. For the targeted proteomics approach, PDX derived cell lines from HLA-A02:01$^+$ patients in combination with the respective exome and transcriptome data were needed. These criteria led to a total of four patients that were eligible for an initial application of the screening approaches (table 43; underlined patients). Out of these patients, three (TIPC102, 222 & 236) could be used for the expression based screening approach and all four (TIPC102, 113, 222 and 236) for the targeted proteomics approach. Material of selected patients not meeting the selection criteria (TIPC079, 091, 253 and 275), was used to set up and validate our screening methodologies.

Table 43 – Patient material used to setup the neoepitope screening pipeline. Patients highlighted (underlined) fullfilled the criteria needed for neoepitope screening by either of the assays indicated. Material from the residual patients was used for validation and setup of the neoepitope identification pipeline. Indicators: ✓ = used in the context of this subproject; + = available/ positive; – = unavailable/ negative.

Patient	Setup and Validation	Expression based	MS based	NGS data	TILs	PDX	Cell line	HLA-A2$^+$
TIPC079	✓			+	+	–	–	+
TIPC091	✓			+	+	–	–	–
TIPC102		✓	✓	+	+	+	–	+
TIPC113			✓	+	–	+	+	+
TIPC222		✓	✓	+	+	+	+	+
TIPC236		✓	✓	+	+	+	–	+
TIPC253	✓			+	–	+	–	+
TIPC275	✓			–	+	+	–	–

4.2.2 Assessment of patient specific mutations

The selected set of tumors was analyzed for the expression of non-synonymous single nucleotide variants (nsSNV). These mutations were of special interest, as they are tumor specific

and the respective T cell pool is unaffected by central tolerance. For this, exome and transcriptome data of the primary tumors, and of low passage PDX samples, were collected, analyzed and compiled (figure 25). In the case of TIPC113, no primary tumor transcriptome data could be acquired, due to low RNA quality of the collected sample. In total, the data revealed an average mutational burden of 80.5 nsSNVs per tumor (range: 72 - 99) (figure 25). However, looking at the matched transcriptome data, only approximately 33% (average: 27.75 nsSNV; range: 22 - 39 nsSNV) of these nsSNVs were actually expressed in the respective tumor samples (figure 25 & table S3-S6).
To establish the targeted proteomics approach, it was necessary to also predict possible HLA-A02:01 binding epitopes from the fraction of expressed nsSNVs and validate their presence in the respective PDX derived cell line (figure 25). This resulted in an average of 11 expressed nsSNVs (range: 9 - 15) per primary tumor for which potentially HLA-A02:01 binding epitopes could be predicted by netMHC4.0 (figure 25 & table S10-S13). Of these mutations, an average of 7 nsSNVs (range: 1 - 11) were later found to still be present in the PDX-derived cell line (figure 25 & table S14-S17). In this context the cell line of TIPC236 needs to be highlighted, since the mutation validation in this cell line revealed mostly wild type loci, with only the KRAS_G12D mutation still present (table S17). Therefore implying, that there was a potential mix-up of this sample during the generation of the PDX-derived cell line. Thus, this patient was excluded from the targeted proteomics screening approach.

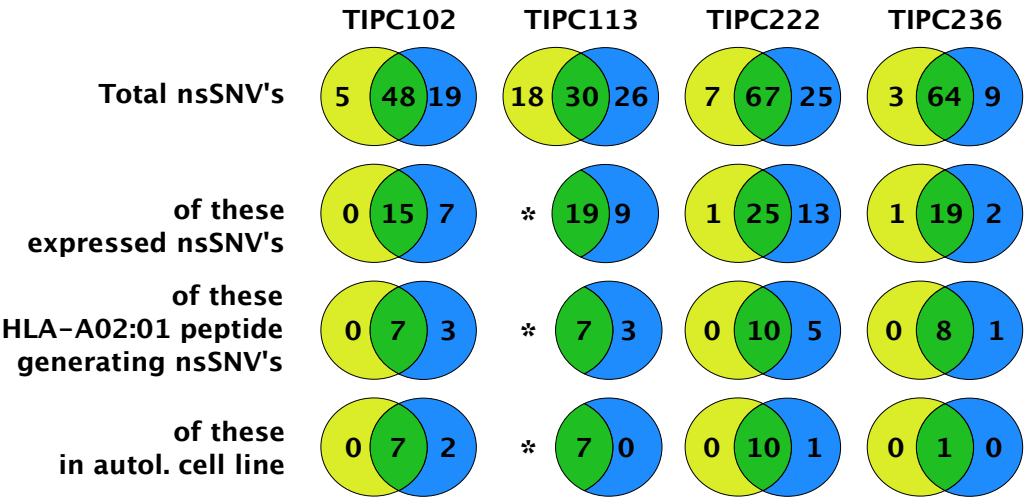

Figure 25 – Schematic summary of the exome and transcriptome analyses of patient samples used for neoantigen prediction. Yellow circles represent the number of primary tumor unique mutations and blue circles xenograft unique mutations. The green overlap indicates the number of mutations found in both primary tumor and xenograft. *For TIPC113 only xenograft transcriptome data was available and the expression of primary tumor unique mutations could not be assessed. nsSNV = non synonymous single nucleotide variant. Detailed summaries can be found in table S3-S6

4.3 Development of an expression based screening system

Due to the overall low number of non-synonymous mutations found in pancreatic cancer, it is crucial that not a single immunogenic epitope is missed by the applied screening methodology. Moreover, both, $CD8^+$ and $CD4^+$ T cells, were shown to be important for an anti tumor T cell response ([142, 144, 220, 221]). Therefore, a screening system capable of simultaneously detecting MHC-I and MHC-II restricted epitopes is desirable, in order to cover the complete range

of potentially immunogenic antigens. Based on this idea, we chose lysosome-associated membrane glycoprotein 1 (Lamp1; UniProtKB - P11279-1) as a starting point for the development of such a screening system. In particular, we were aiming to make use of the subcellular localization of Lamp1 to the endocytic compartment. This translocation is achieved by a combination of an N-terminal signal peptide (residues 1 – 28), leading to the translation into the endoplasmic reticulum (ER), and a C-terminal cytosolic sorting motif (residues 406 – 417; motif Tyr-X-X-Ile), responsible for lysosomal translocation of Lamp1 [359–361]. It was previously shown, that full length Lamp1 is capable of targeting antigens to the endocytic compartment, leading to presentation on MHC-II molecules and antigen specific $CD4^+$ T cell activation [362, 363]. Moreover, truncated variants, encoding only the signal peptide, the antigen of interest and the sorting motif, were shown to induce antigen specific T cell activation [364, 365]. Due to unknown folding of the introduced poly-peptide sequences, however, we expected such reduced screening constructs to be more negatively affected by the introduction of larger antigen constructs. Thus, we chose to modify full-length Lamp1 to simultaneously shuttle antigens into the MHC-I and MHC-II pathway.

4.3.1 Lamp1 construct design

In order to design our expression based screening system, we analyzed the single-spanning transmembrane helix of Lamp1 for the introduction of destabilizing residues to induce a protein fallback into the endoplasmic reticulum via ER-associated degradation (ERAD) mediated by intramembrane rhomboid proteases [366]. By introducing such a destabilization we were aiming to obtain a construct that would overcome sole MHC-II antigen presentation and result in a balanced MHC-I/ MHC-II antigen presentation. We identified two distinct residues (G390 & L395), that were most likely to destabilize the helix and cause early degradation of Lamp1 (figure 26). To test our hypothesis we generated two constructs encoding the single destabilizing mutations (G390R and L395K) and one construct combining both mutations (figure 26). The respective antigens used to screen for MHC-I and MHC-II presentation were consecutively introduced N-terminally of the transmembrane helix, between residues L377 & D378 (figure 26). During each step of the system's development we took along minigenes – known for efficient MHC-I antigen presentation [146] – containing only the respective MHC-I and MHC-II epitopes and devoid of translocation sequences, as a benchmark of T cell activation (figure 26C).
In the following paragraphs the different constructs will be referred to as Wild Type for the non-modified construct, Mut390/ Mut395 for the respective single mutants and MutGLRK for the double mutant.

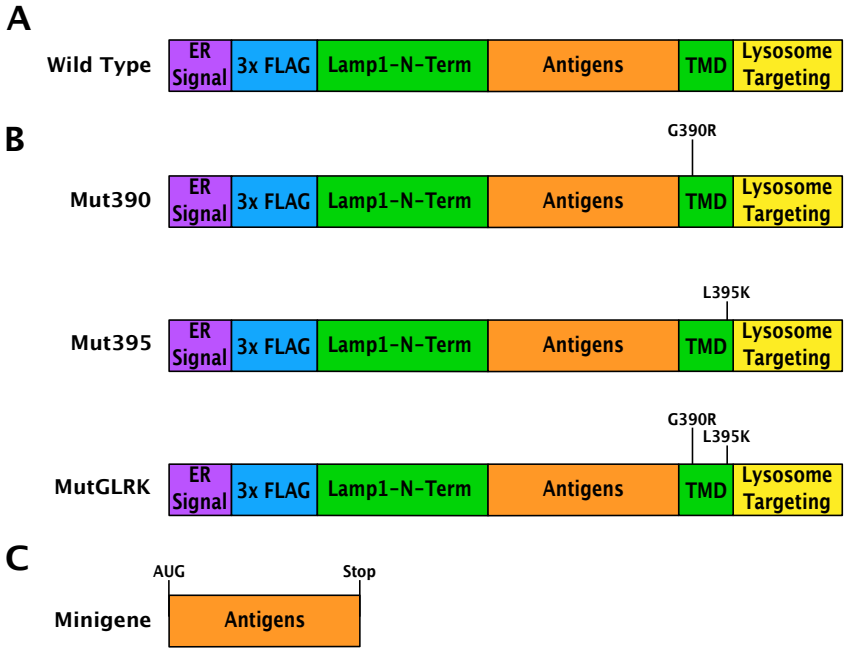

Figure 26 – General construct design for the establishment of the expression based screening system. Shown are the wild type Lamp1 construct (A) and the three transmembrane domain (TMD) destabilizing variants (B), as well as the minigene design used as benchmark (C). Each Lamp1 constuct contains the native ER localization sequence of Lamp1 followed by a 3xFLAG tag for later detection of the protein. Antigens used for specific activation of $CD8^+$ and $CD4^+$ T cells during the systems funcionality validation were introduced N-terminally to the TMD. Lysosomal targeting was achieved by using the native Lamp1 lysosomal targeting sequence. The minigene construct is devoid of any signal sequence.

4.3.2 Functionality validation of the expression based screening system

For an initial test of the functionality and effects of the destabilization on antigen specific T cell activation, we used murine, ovalbumin-specific OT-I/ OT-II transgenic T cells as a readout system. Antigen presentation was achieved by inserting two ovalbumin epitopes, namely SIINFEKL (H-$2K^b$-restricted) and ISQAVHAAHAEINEAGR (I-A^b-restricted), into our Lamp1 variants combined with transfection of the resulting constructs into the murine 771 B cell line (H-$2K^{b+}$ and I-A^{b+}, see material section). Co-culture of transfected 771 B cells with ovalbumin specific $CD8^+$ (OT-I; SIINFEKL specific) [329] and $CD4^+$ (OT-II; ISQAVHAAHAEINEAGR specific) [330] murine T cells allowed to screen for presentation of antigens via the MHC-I/ MHC-II pathway.

During these experiments we could not observe significant differences in antigen specific $CD8^+$ T cell activation between the different Lamp1 constructs (figure 27), suggesting that Lamp1, independent of our modifications, efficiently introduced peptides into the MHC-I pathway. Here, the formation of defective ribosomal products (DRiPs) of the Lamp1 construct might already serve as an early source of MHC-I restricted antigen formation ([367, 368]). As expected, the minigene was capable of specifically activating the OT-I cells (figure 27). Looking at MHC-II restricted T cell activation, however, we could show the advantage of our Lamp1 screening system over regular minigene constructs, which were incapable of translocating antigens to the MHC-II compartment (figure 28). Furthermore, we could show a decrease in $CD4^+$ T cell activation by our double mutant Lamp1 variant (MutGLRK) compared to the Wild Type construct,

whereas the single mutants were still capable of activating OT-II cells (figure 28).
Taken together, we could not observe a significant advantage of the TMD destabilizing Lamp1 variants over its wild type form, when looking at the induction of a balanced antigen specific T cell activation. Furthermore, the double mutant (MutGLRK) even resulted in an undesired abrogation of $CD4^+$ T cell activation compared to wild type Lamp1, making it the least favorable construct for neoepitope screening in this context. Nevertheless, we could show, that the advantage of a Lamp1 based screening approach, compared to a minigene based one, lies in the increased shuttling of antigens into the MHC-II pathway. Thus, we had a functional approach to express and screen antigens restricted to the MHC-I, as well as MHC-II antigen presenting pathway.

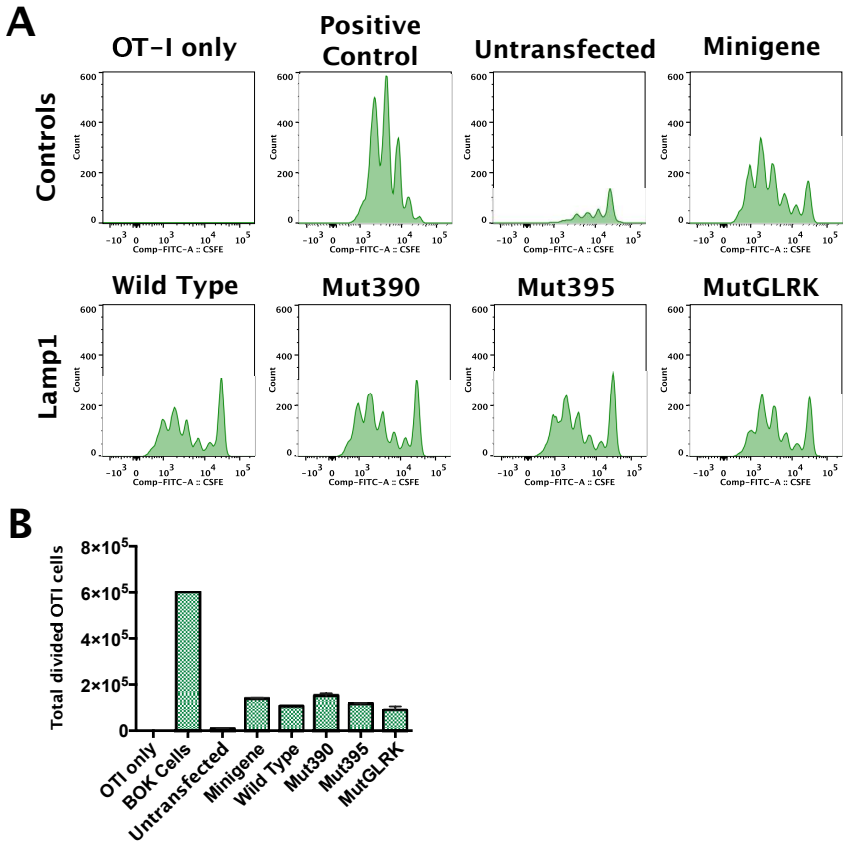

Figure 27 – Validation of MHC-I restricted antigen presentation of the Lamp1 screening system. (A) Antigen specific activation of OT-I cells monitored by CFSE dilution. For the positive control, SIINFEKL expressing BOK cells (B7-1^+, SigOVA(257-264)$^+$, H2-Kb^+ MEC-1 cell line [313, 314]) were used to induce antigen specific T cell activation. Untransfected 771 B cells served as negative controls to monitor background T cell proliferation. Lamp1 and minigene constructs were transfected into 771 B cells by electroporation. Readout was performed after 72h coincubation of CFSE labeled OT-I cells and $5x10^4$ of the respective target cells. (B) Analysis of numbers of divided OT-I cells in each sample after 72h incubation. Total cell numbers were assessed by normalization to the aquired number and volume of CountBright™ beads. A representative experiment of n = 4 biological experiments is shown. Experiments were performed as technical duplicates.

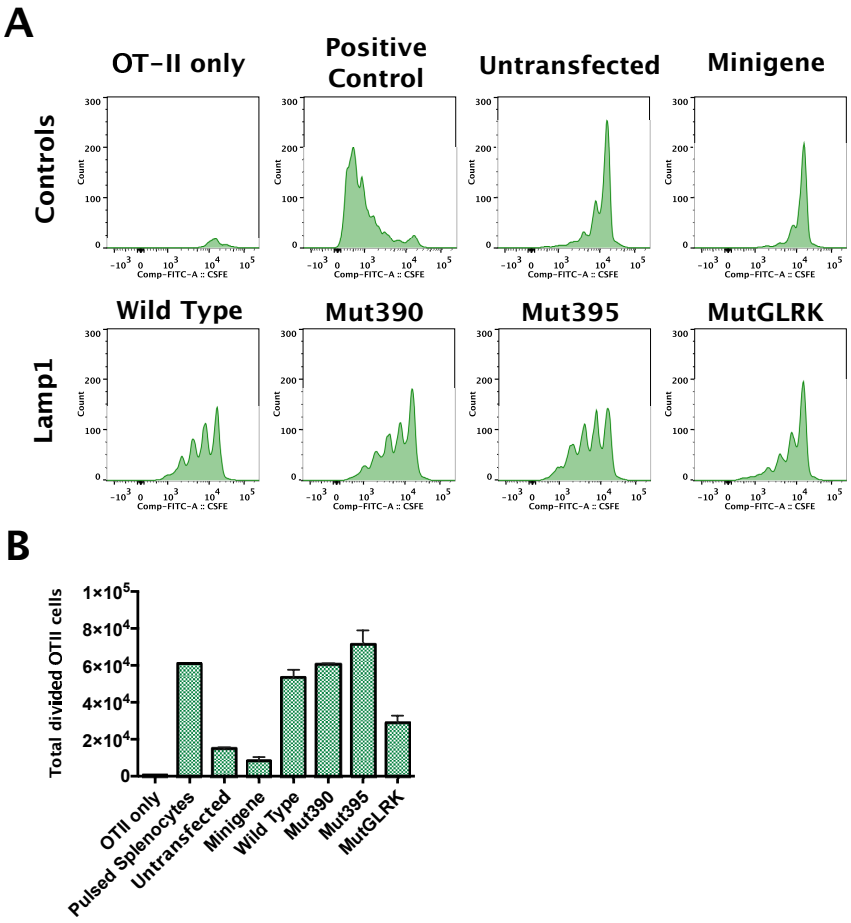

Figure 28 – Validation of MHC-II restricted antigen presentation of the Lamp1 screening system. (A) Antigen specific activation of OT-II cells monitored by CFSE dilution. Peptide pulsed (5 µg/ mL OVA_MHC-II peptide), congeneic (CD45.1$^+$) splenocytes were used as positive control for antigen specific T cell activation. Lamp1 and minigene constructs were transfected into 771 B cells by electroporation. Readout was performed after 96h coincubation of CFSE labeled OT-II cells and 1x10^5 of the respective target cells. (B) Analysis of numbers of divided OT-II cells in each sample after 96h incubation. Total cell numbers were assessed by normalization to the aquired number and volume of CountBright™ beads. A representative experiment of n = 4 biological experiments is shown. Experiments were performed as technical duplicates.

4.3.3 Validation of expanded PDAC derived TILs as antigen presenting cells

After the validation of the systems functionality in murine cells, we set out to confirm this functionality in a fully autologous human setting. Due to the difficulty of obtaining professional antigen presenting cells from PDAC patients, we tested and used *in vitro* expanded TILs as a source of autologous APCs for our screening approach. This approach was supported by the fact, that activated human T cells are known to express functional MHC-I and MHC-II on their surface [369–371] (figure 29A). In addition, we were able to obtain TILs from most PDAC patients in large numbers, as previously described [279].

To set up the screening system in the human setting, we used two T cell receptors (TCRs) with known antigen specificity and transduced these into TILs from patient TIPC079, expressing both HLA alleles needed for the presentation and recognition of the antigens of interest (table S2). In particular, we used a Mart1-specific TCR (DMF5) recognizing E(A/L)AGIGILTV bound to HLA-A02:01 [372] and a DDX3Y/ HY specific TCR specific for HIENFSDIDMGE

presented on HLA-DQB01:05 [316]. Since the TIL population of TIPC079 contained mainly $CD4^+$ T cells (figure S1), it should be noted, that the Mart1 TCR used here is known to potently activate T cells in a CD8-independent manner [372]. For antigen presentation, we generated a sequence encoding both epitopes, elongated by their native sequence (Mart1–HY: YTTAEELAGIGILTVILGV–CPPHIENFSDIDMGEIIMGN), using it either as a minigene or introducing it into our different Lamp1 constructs. The resulting gene constructs were transduced into autologous TILs, generating the autologous APC population.

We could show that in the human setting the introduction of transmembrane domain (TMD) destabilizing mutations into Lamp1 leads to a significant increase in MHC-I restricted T cell activation compared to the Wild Type variant (figure 29D). In addition, these destabilizations did not interfere with the MHC-II restricted T cell response (figure 29F), even though the double mutant construct (MutGLRK) revealed a slight decrease in MHC-II restricted T cell activation (figure 29F). As in the murine system, the Lamp1-based screening system displayed superior MHC-II restricted T cell activation compared to the minigene construct (figure 29F).

Taken together, we could show the functionality of the Lamp1 based screening approach, using PDAC derived TILs as autologous antigen presenting cells. In addition, these results show the advantage of our Lamp1 screening system over the use of regular minigenes. The functionality validation of the Lamp1 screening system revealed that the Mut395 construct was overall the most robust in balanced MHC-I and MHC-II restricted T cell activation (table 44). Thus, this construct was chosen as the starting point to screen for patient derived neoepitopes in the context of PDAC.

Table 44 – Summary of the Lamp1 screening system validation. Depicting the potency of MHC-I and MHC-II restricted T cell activation during each step of the systems validation. +/++/+++: Objective strength of T cell activation above background from weak to strong; –: Activation on background level. Each experimental set was performed as biological triplicates.

Effector cells	Antigen presenting cell		Lamp1 construct				
			Minigene	Wild Type	Mut390	Mut395	MutGLRK
OTI OTII	771 B cell line	MHC-I MHC-II	++ –	++ ++	++ ++	++ ++	++ –
human PBMC	KBV623 cell line	MHC-I MHC-II	+ –	+ ++	++ ++	++ ++	+++ +
PDAC TIL	PDAC TIL	MHC-I MHC-II	++ –	+ ++	++ ++	+++ +++	+++ +

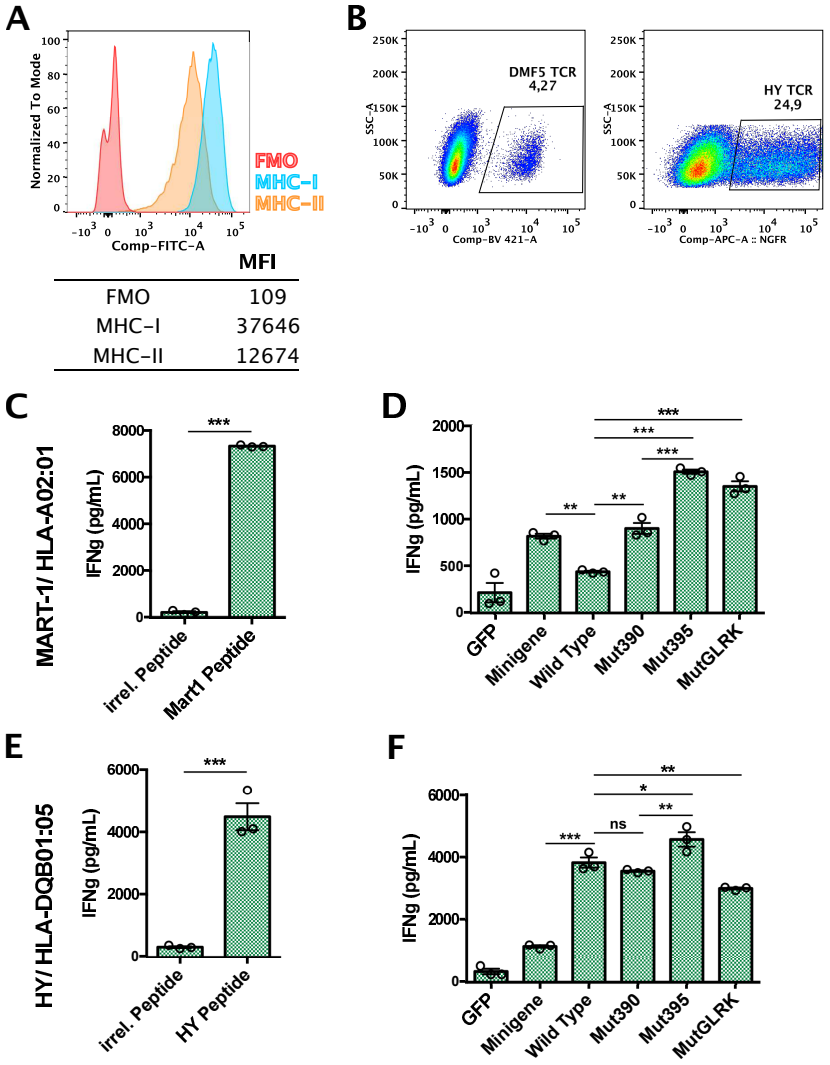

Figure 29 – Lamp1 destabilization leads to a balanced CD4$^+$/CD8$^+$ T cell activation. (A) Surface expression of MHC-I and MHC-II on TILs of TIPC079. (B) Transduction efficiency of both antigen specific TCRs. Detection of DMF5 TCR transduction efficiency was performed using an α-mouseTCR-β_BV421 antibody. HY TCR transduction efficiency was assessed via the expression of truncated NGFR using a α-NGFR_APC antibody. (C/E) Antigen specific activation of TCR transduced TILs for the DMF5 TCR (C) and HY TCR (E). Untransduced, autologous TILs were pulsed with 10 µg/mL of the respective, synthetic peptide. Irrelevant peptide either represented HY peptide (C) or Mart1 peptide (E). (D/F) Influence of the Lamp1 expression system and minigene on MHC-I (D) and MHC-II (F) restricted antigen specific T cell activation. Co-incubation was performed using 0.5x10^4 TCR transduced effector and 1x10^5 of the respective target cells per sample. T cell activation was assessed by ELISA in technical triplicates. Shown is one representative experiment of n = 3 biological replicates. Statistical analysis of the peptide results was performed using an unpaired t-test, while for the Lamp1 samples a One-way ANOVA with post-hoc Tukey's multiple comparisons test was used.

4.3.4 Generation and validation of patient derived constructs

Since the introduction of larger multi-epitope sequences in close proximity to the transmembrane helix of Lamp1 could lead to a disruption of the antigen processing and presentation, we included the Mart1 and HY epitopes in each further construct. This allowed us to control the functional integrity of each construct after the introduction of patient derived antigens, using the Mart1 and HY specific TCRs as previously described (figure 30).

Patient specific multi-epitope constructs were designed by analyzing the respective exome and transcriptome data for all expressed mutations (figure 25). Sequences encoding up to six mutations were introduced into our Mut395 construct (figure 30 and table S7-S9). Each mutation was encoded by nucleotides encompassing 30 amino acids with the mutation at position 16, surrounded by the native sequence (figure 30). For mutations close to the protein's N- or C-terminus, the position of the mutation could slightly differ. In order to minimize the generation of artificial epitopes, due to the decreased spacing between two mutations, we decided to place the latter sequences either in the first (mutation close to N-term) or last (mutation close to C-term) position of the respective multi-epitope construct (table S7-S9).
Altogether, we generated 15 patient-derived tandem constructs for a set of three patients, based on the mutations expressed in the primary tumor and xenograft (table S3, S5-S9). All 15 patient constructs generated were capable of shuttling antigens into the MHC-I, as well as the MHC-II antigen presenting pathway (figure 31 and 32).

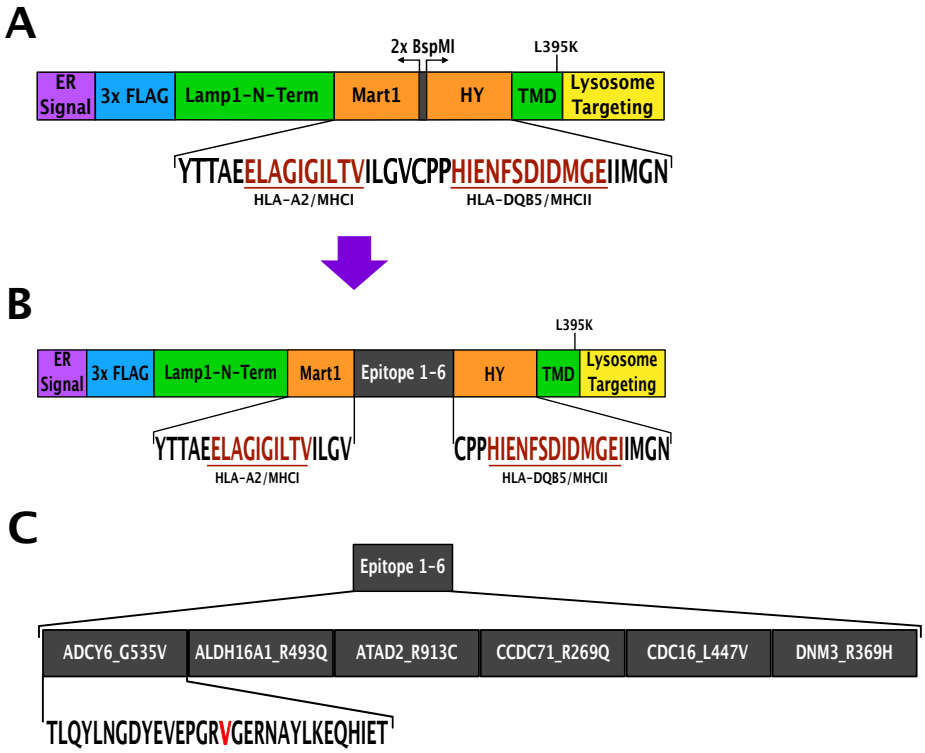

Gene	Mutation	Mutation location	Mutated sequence
ADCY6	G535V	chr12:49170065	TLQYLNGDYEVEPGRVGERNAYLKEQHIET
ALDH16A1	R493Q	chr19:49967929	PDGLYEYLRPSGTPAQLSCLSKNLNYDTFG
ATAD2	R913C	chr8:124351668	KPHSALPEEVQELFICDYGEIFNVQLPDKE
CCDC71	R269Q	chr3:49200836	HQSKTNRATGSPSVRQMKGGSALGTKTAQA
CDC16	L447V	chr13:115027386	IKAIGNEVTVDKWEPVLNNLGHVCRKLKKY
DNM3	R369H	chr1:172011262	LELSGGAKINRIFHEHFPFEIVKMEFNEKE

Figure 30 – Schematic overview of the adaptation of the Lamp1_Mut395 construct for patient derived epitope screening. (A) Layout of the empty Lamp1_Mut395 construct. (B) Lamp1_Mut395 general layout after introduction of patient derived, multi-epitope constructs. (C) multi-epitope construct setup example from TIPC102 (Construct 1). The table indicates the respective gene and mutation, the chromosomal location of the nsSNV, as well as the mutated sequences used for the setup of this specific construct. For data from all patients, see table S3 - S9.

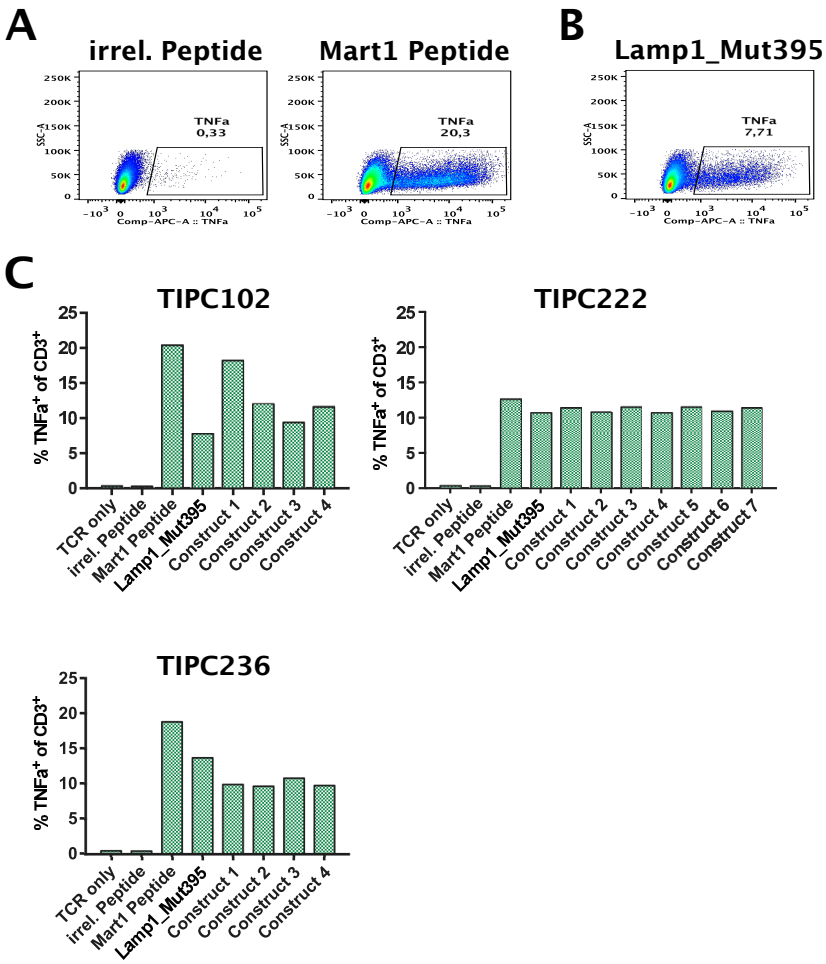

Figure 31 – MHC-I antigen presentation functionality of the Lamp1_Mut395 system after introducing patient derived, multi-epitope constructs. (A) Antigen specific activation of DMF5 TCR transduced TILs against peptide pulsed, autologous APCs. Here, the HY peptide (HIENFSDIDMGE) was used as irrelevant control. (B) Antigen specific, class-I restricted activation of DMF5 TCR transduced TILs against empty Lamp1_Mut395 transduced, autologous TILs. The empty Lamp1_Mut395 construct (figure 30) served as a baseline control for the systems functionality. (C) Summary of the MHC-I restricted, antigen specific activation of DMF5 TCR transduced TILs against the various patient derived, multi-epitope constructs encoding Lamp1_Mut395 constructs.
Staining was performed using the T cell activation panel. Activation was monitored by TNFα expression in the $CD3^+$ effector ($CFSE^-$) population via intracellular cytokine staining. Day 42 TILs from patient TIPC079 were used for transduction of the TCR and Lamp1 constructs. Peptides were pulsed onto GFP transduced d42 TILs. Experiments were performed seperately for each patient.

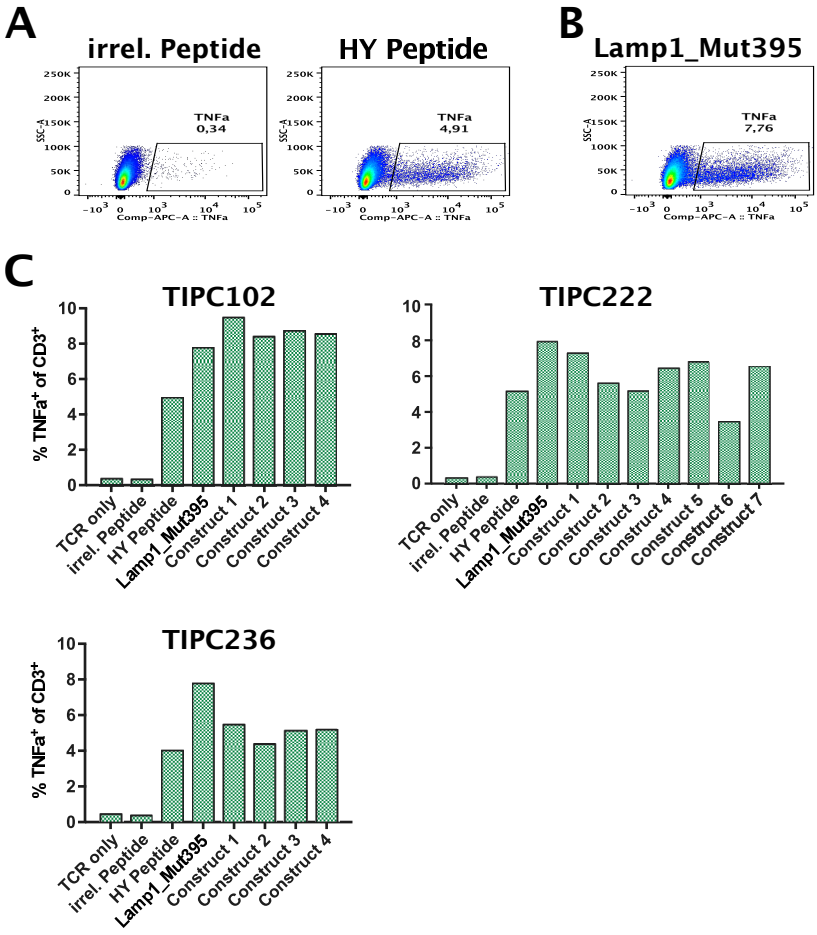

Figure 32 – MHC-II antigen presentation functionality of the Lamp1_Mut395 system after introducing patient derived, multi-epitope constructs. (A) Antigen specific activation of HY TCR transduced TILs against peptide pulsed, autologous APCs. Here, the Mart1 short peptide (ELAGIGILTV) was used as irrelevant control. (B) Antigen specific, class-II restricted activation of HY TCR transduced TILs against empty Lamp1_Mut395 transduced, autologous TILs. The empty Lamp1_Mut395 construct (figure 30) served as a baseline control for the systems functionality. (C) Summary of the MHC-II restricted, antigen specific activation of HY TCR transduced TILs against the various patient derived, multi-epitope constructs encoding Lamp1_Mut395 constructs.
Staining was performed using the T cell activation panel. Activation was monitored by TNFα expression in the $CD3^+$ effector ($CFSE^-$) population via intracellular cytokine staining. Day 42 TILs from patient TIPC079 were used for transduction of the TCR and Lamp1 constructs. Peptides were pulsed onto GFP transduced d42 TILs. Experiments were performed seperately for each patient.

4.3.5 Screening of patient TIL using multi-epitope constructs

After assessing the functionality of each patient derived Lamp1 construct, we went on to screen the respective patient TILs for recognition of the encoded mutations. For this, minimally expanded TILs (expanded for 28 days) from patients TIPC102, 222 and 236 were used as responder T cells against the respective patients' Lamp1 multi-epitope constructs. The Lamp1 constructs were transduced into excessively expanded (expanded up to 42 days) TILs from the same patient to generate the autologous APC population. For each patient, the transduction efficiencies of the Lamp1 constructs had to be estimated on the basis of GFP and TCR transduction efficiency, since we could not directly assess the transduced Lamp1 using its N-terminal 3x-FLAG tag (figure S5 and S6). Since each patient of this cohort was HLA-$A2^+$, the presence and functionality of each Lamp1 construct was monitored, within the screening experimetns,

by coincubation of the autologous APCs with Mart1 TCR (DMF5) transduced TILs. In accordance with the previously published assays to describe recognition of the autologous tumor by PDAC TILs, we measured the secretion of IFNγ to describe antigen specific TIL reactivity [279]. Overall, screening of TIPC 102 revealed little to no reactivity against the patient derived xenograft and no reactivity against any of the patient derived mutations (figure 33B - D). Importantly, the transfection of the multi-epitope constructs was successful, as the MART-1 epitope encoded by each construct was recognized by DMF5 TCR transduced T cells (figure 33B and D). It should be noted that the control sample used to test the Mart1 TCR functionality during these experiments was negative, due to loss of HLA-A02:01 in the xenograft (figure 47B).
For patient TIPC222, we had access to responder TILs from two distinct tumor sites (222.2 and 222.3). However, we could neither show recognition of the autologous xenograft, nor reactivity against any of the mutation encoding Lamp1 constructs (figure 34B - E).
Screening TILs from patient TIPC236 initially appeared more promising, revealing reactivity against the autologous tumor (figure S4B & D and figure 35B & D). In addition, the IFNγ ELISpot revealed responder TIL reactivities against all mutation encoding Lamp1 constructs (figure 35C and D). When we tried to confirm this finding, we included a TNFα ELISpot for an additional functionality readout. However, the TNFα ELISpot could not confirm results of the IFNγ readout (figure 35C and D), therefore indicating that the reactivities seen in the IFNγ ELISpot might be artifacts.
Taken together, we could not show the recognition of mutation derived epitopes by expanded TIL populations from PDAC patients. However, it should be kept in mind that the overall response rate of these cells against the autologous tumor was previously shown to be rather low ($\approx$1.5%), indicating that the chances of finding neoepitope reactive T cells in bulk expanded TILs from PDAC patients is generally low [279]. Nevertheless, these findings do not rule out the initial presence of tumor reactive T cells in pancreatic cancer. They rather show, that the identification of tumor reactive TILs should start at an earlier stage of tumor material processing (e.g. *ex vivo* single cell TCR sequencing of TILs), to avoid the loss of initially tumor reactive T cell clones during *in vitro* culture. Furthermore, it should be kept in mind that, though nsSNVs might harbor an elegant source of potentially immunogenic neoepitopes, they only represent a limited pool of recognizable antigens. Thus, widening the window of screened epitopes to antigens derived from peptide and RNA editing or to over-expressed self-antigens might overcome this limitation. Furthermore, the negative result of the TNFα ELISpot indicates, that the T cell activation marker panel used for these screenings should be enlarged to include more than the previously applied IFNγ single readout. In addition, the use of autologous TILs as antigen presenting cells should be reconsidered for patients with access to professional APCs, as these could be more potent in complete T cell activation.

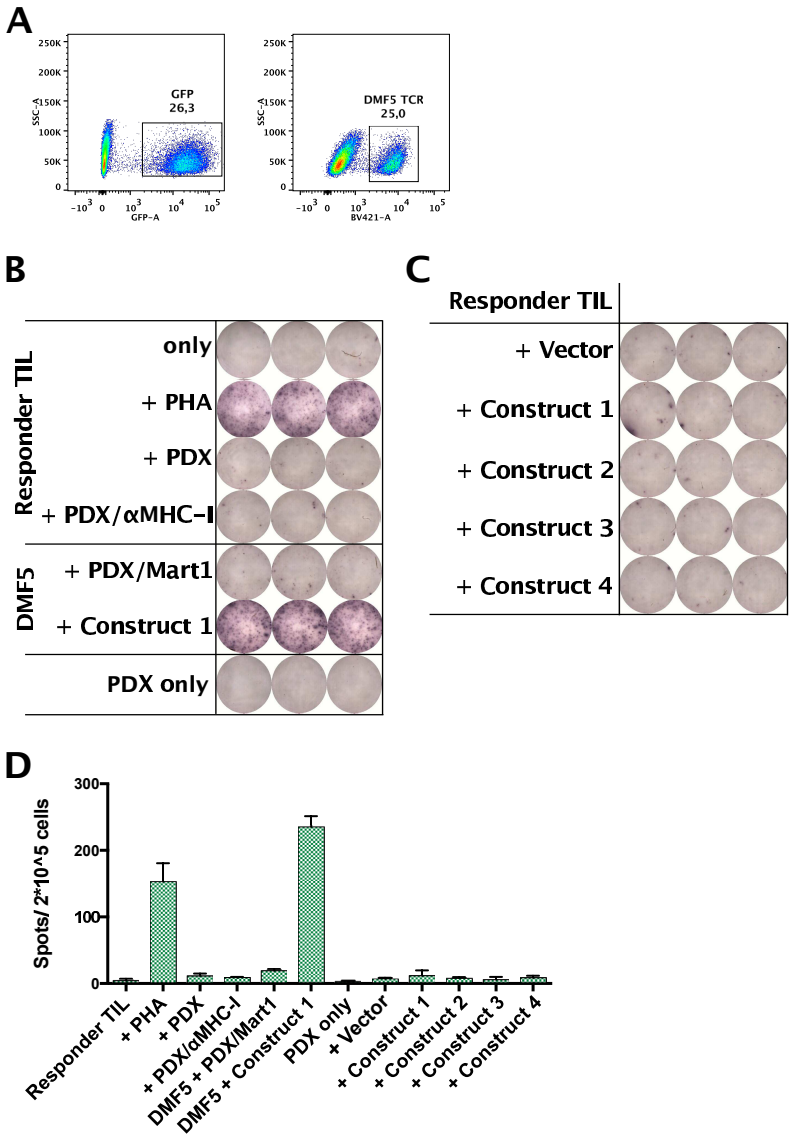

Figure 33 – Screening for patient specific neoepitope reactivity by bulk expanded TILs from patient TIPC102. (A) Transduction efficiency assessment of TIPC102 autologous APCs and DMF5 TCR transduced TILs. A combination of GFP and DMF5 TCR served as rough indicator for overall transduction efficiency during the experiments. (B and C) Assessment of responder TIL reactivity by IFNγ ELISpot. (B) Control samples monitoring the background reactivity and general T cell functionality after unspecific activation with PHA. In addition, reactivity against the autologous xenograft was assessed. Mart1 TCR (DMF5) transduced TILs were used to monitor functional antigen presentation and presence of each Lamp1 construct (only shown for multi-epitope construct 1; representative for all constructs used). Functionality of the DMF5 TCR was assessed by pulsing the xenograft with Mart1 peptide. PDX = autologous xenograft. PDX/αMHC-I = MHC-I blocked autologous xenograft. PDX/Mart1 = Mart1 peptide pulsed (Mart1 – ELAGIGILTV), autologous xenograft. (C) Screening for responder TIL reactivity against Lamp1 construct expressing autologous APCs. Vector Control = Lamp1_Mut395 screening construct without patient mutations (figure 30). Construct 1 - 4 = Patient mutation encoding Lamp1 constructs (see table S3 and S7). (D) Spot count for each technical triplicate during one experiment. The screen was performed as biological duplicate. Statistical analysis of results was performed using a One-way ANOVA with post-hoc Tukey's multiple comparisons test.

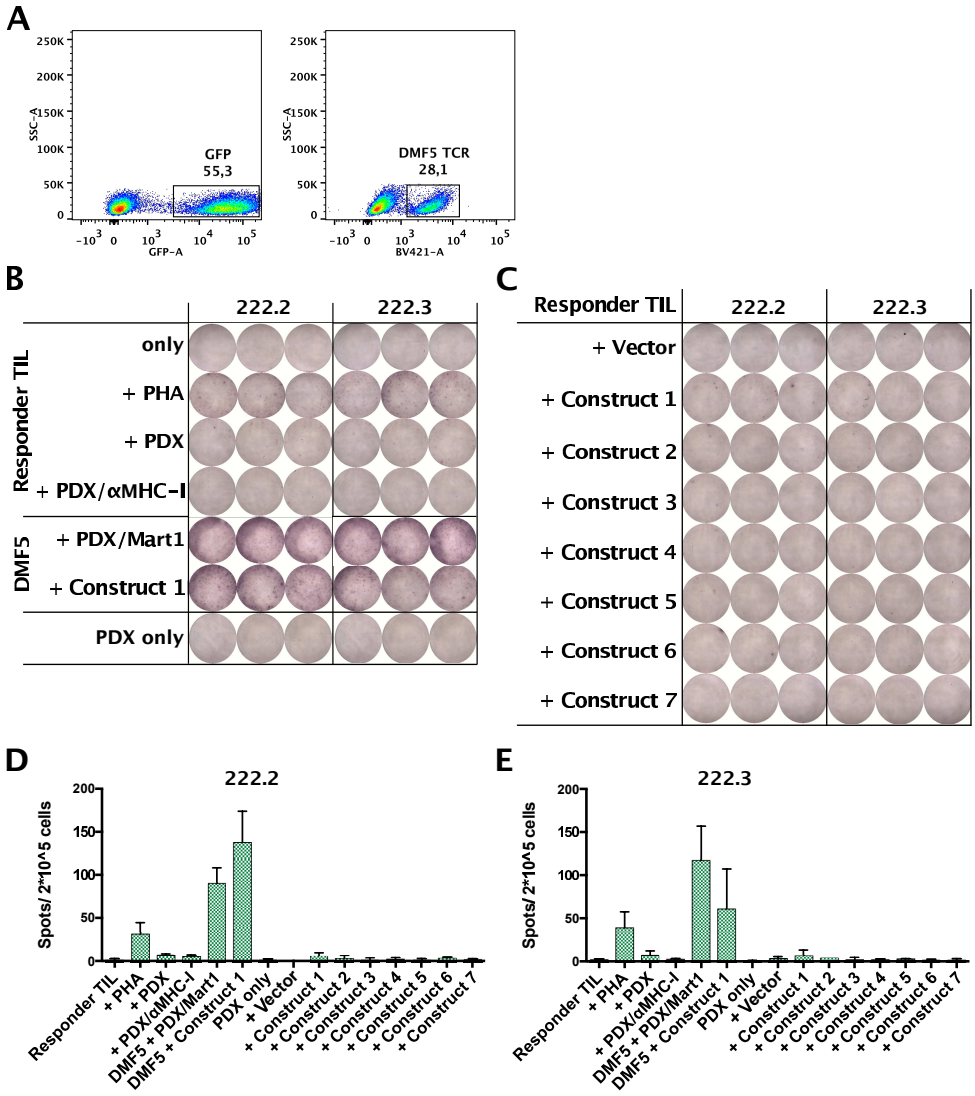

Figure 34 – Screening for patient specific neoepitope reactivity by bulk expanded TILs from patient TIPC222. (A) Transduction efficiency assessment of TIPC222 autologous APCs and DMF5 TCR transduced TILs. A combination of GFP and DMF5 TCR served as rough indicator for overall transduction efficiency during the experiments. (B and C) Assessment of responder TIL reactivity by IFNγ ELISpot. Samples 222.2 and 222.3 indicate expanded TIL cultures from two different locations of the autologous tumor material. (B) Control samples monitoring the background reactivity and general T cell functionality after unspecific activation with PHA. In addition, reactivity against the autologous xenograft was assessed. Mart1 TCR (DMF5) transduced TILs were used to monitor functional antigen presentation and presence of each Lamp1 construct (only shown for multi-epitope construct 1; representative for all constructs used). Functionality of the DMF5 TCR was assessed by pulsing the xenograft with Mart1 peptide. PDX = autologous xenograft. PDX/αMHC-I = MHC-I blocked autologous xenograft. PDX/Mart1 = Mart1 peptide pulsed (Mart1 – ELAGIGILTV), autologous xenograft. (C) Screening for responder TIL reactivity against Lamp1 construct expressing autologous APCs. Vector Control = Lamp1_Mut395 screening construct without patient mutations (figure 30). Construct 1 - 7 = Patient mutation encoding Lamp1 constructs (see table S5 and S8). (D) Spot count for each technical triplicate during one experiment. The screen was performed once. Statistical analysis of results was performed using a One-way ANOVA with post-hoc Tukey's multiple comparisons test.

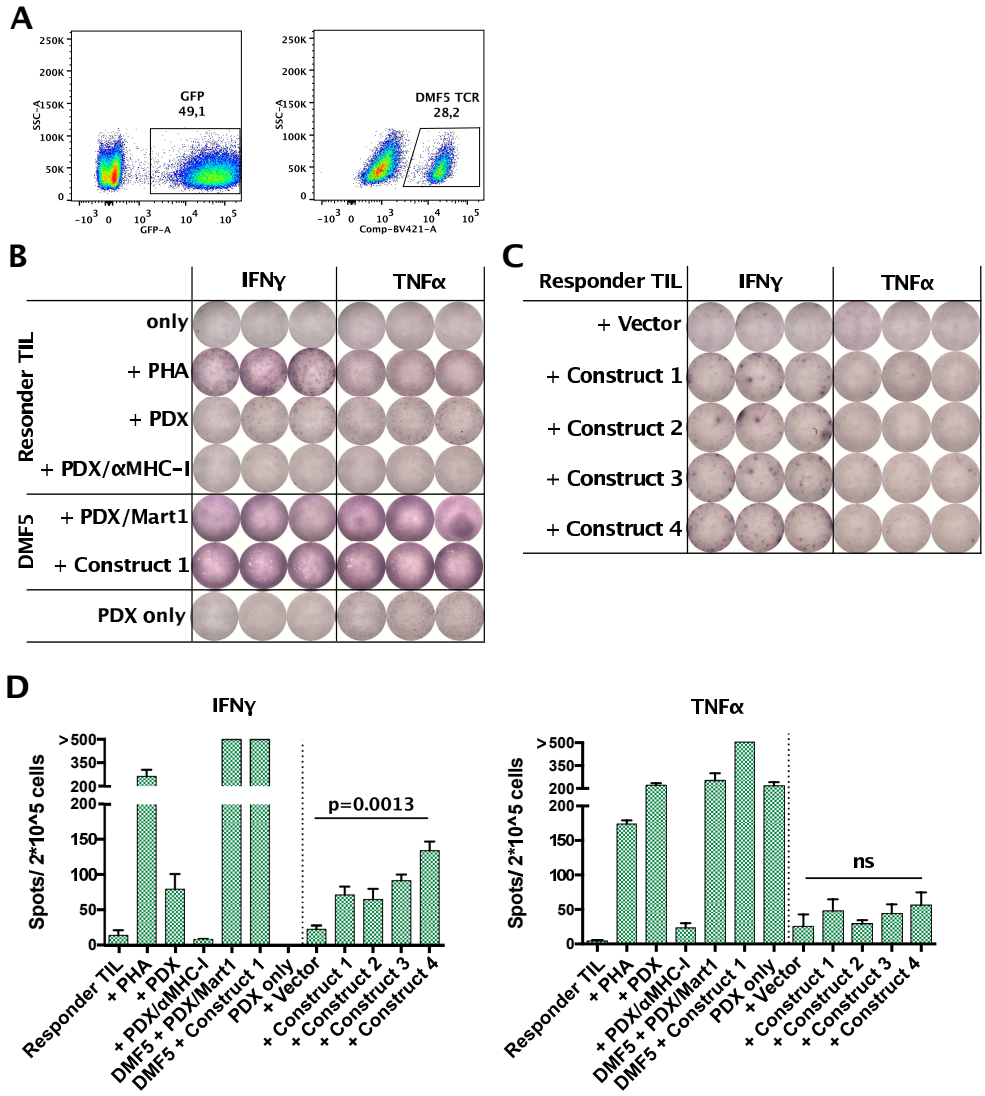

Figure 35 – Screening for patient specific neoepitope reactivity by bulk expanded TILs from patient TIPC236. (A) Transduction efficiency assessment of TIPC236 autologous APCs and DMF5 TCR transduced TILs. A combination of GFP and DMF5 TCR served as rough indicator for overall transduction efficiency during the experiments. (B and C) Assessment of responder TIL reactivity by IFNγ and TNFα ELISpot. (B) Control samples monitoring the background reactivity and general T cell functionality after unspecific activation with PHA. In addition, reactivity against the autologous xenograft was assessed. Mart1 TCR (DMF5) transduced TILs were used to monitor functional antigen presentation and presence of each Lamp1 construct (only shown for multi-epitope construct 1; representative for all constructs used). Functionality of the DMF5 TCR was assessed by pulsing the xenograft with Mart1 peptide. PDX = autologous xenograft. PDX/αMHC-I = MHC-I blocked autologous xenograft. PDX/Mart1 = Mart1 peptide pulsed (Mart1 – ELAGIGILTV), autologous xenograft. (C) Screening for responder TIL reactivity against Lamp1 construct expressing autologous APCs. Vector Control = Lamp1_Mut395 screening construct without patient mutations (figure 30). Construct 1 - 4 = Patient mutation encoding Lamp1 constructs (see table S6 and S9). (D) Spot count for each technical triplicate during one experiment. The upper default detection limit of the counting software was 500 spots/ well. The IFNγ ELISpot was performed as biological duplicate. The TNFα ELISpot was measured once, in parallel with the second IFNγ ELISpot screening, to further evaluate reactivities seen in the IFNγ readout. Statistical analysis of results performed using a One-way ANOVA with post-hoc Tukey's multiple comparisons test.

4.3.6 Alternative neoepitope screening approaches for PDAC

Comparison of the Lamp1 screening system to a MITD expression system

In 2017, Sahin and coworkers (BioNTech) published an RNA-based vaccine construct capable of inducing neoantigen specfic $CD4^+$ and $CD8^+$ T cell activation, leading to reduced post resection disease recurrence in melanoma patients [176]. For this vaccination study they made use of a gene construct - distinct from our expression vector - capable of directing T cell epitope presentation to MHC-I and -II. In the case of their vector, we decided to compare the efficiency of the two constructs for MHC-I/ -II antigen presentation to check if the BioNTech construct would be more efficient. Based on published information, we generated a construct encoding the N-terminal signal peptide (SP) and MHC-I transmembrane domain (MITD) [252] used in their RNA vaccination constructs and compared it to our Lamp1 based screening system (figure 36). For this approach, each gene construct was introduced into TILs from patient TIPC079 and encoded the Mart1 and HY epitopes to monitor MHC-I, as well as MHC-II restricted T cell activation. In addition, Mart1 TCR and HY TCR transduced TILs served again as responder T cell population. Moreover, we wanted to assess the stability of each systems functionality upon the introduction of larger multi-epitope constructs. Here, we introduced two patient derived multi-epitope constructs (TIPC102_TC1 and TIPC102_TC2) in between the Mart1 and HY epitopes to monitor their influence on antigen specific T cell activation.
Our results indicate that both systems are equally efficient in simultaneously inducing MHC-I, as well as MHC-II restricted T cell activation (figure 37C and 38C). In addition, the introduction of larger multi-epitope constructs did not appear to disrupt this functionality in either of the two approaches (figure 37C and 38C).
In view of these findings, we decided to continue with the Lamp1 screening approach, as we had already extensively validated this system, which worked well in our hands.

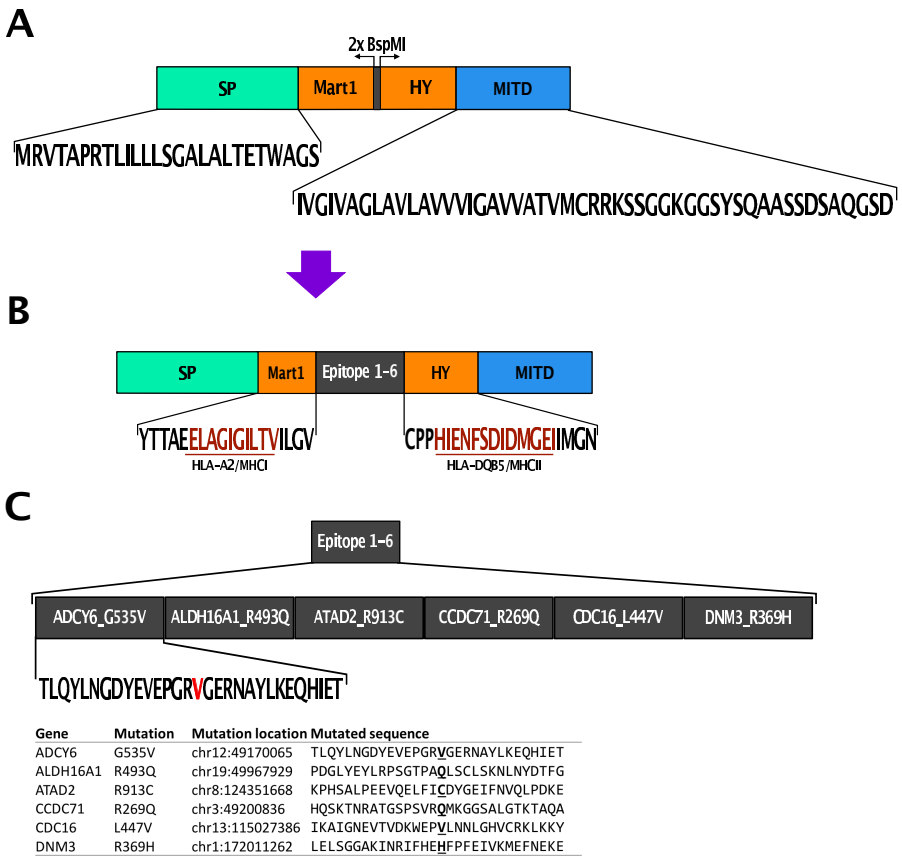

Gene	Mutation	Mutation location	Mutated sequence
ADCY6	G535V	chr12:49170065	TLQYLNGDYEVEPGRVGERNAYLKEQHIET
ALDH16A1	R493Q	chr19:49967929	PDGLYEYLRPSGTPAQLSCLSKNLNYDTFG
ATAD2	R913C	chr8:124351668	KPHSALPEEVQELFICDYGEIFNVQLPDKE
CCDC71	R269Q	chr3:49200836	HQSKTNRATGSPSVRQMKGGSALGTKTAQA
CDC16	L447V	chr13:115027386	IKAIGNEVTVDKWEPVLNNLGHVCRKLKKY
DNM3	R369H	chr1:172011262	LELSGGAKINRIFHEHFPFEIVKMEFNEKE

Figure 36 – Schematic overview of the MITD construct design. (A) Layout of the empty MITD construct. Sequences for the signal peptide (SP) and MHC-I transmembrane domain (MITD) were retreived from [252]. (B) MITD construct after the insertion of patient derived multi-epitope constructs. (C) multi-epitope construct setup example from TIPC102 (Construct 1) used for one of the tested MITD constructs. The table indicates the respective gene and mutation, the chromosomal location of the nsSNV, as well as the mutated sequences used for the setup of this specific construct (compare to table S3 & S7)

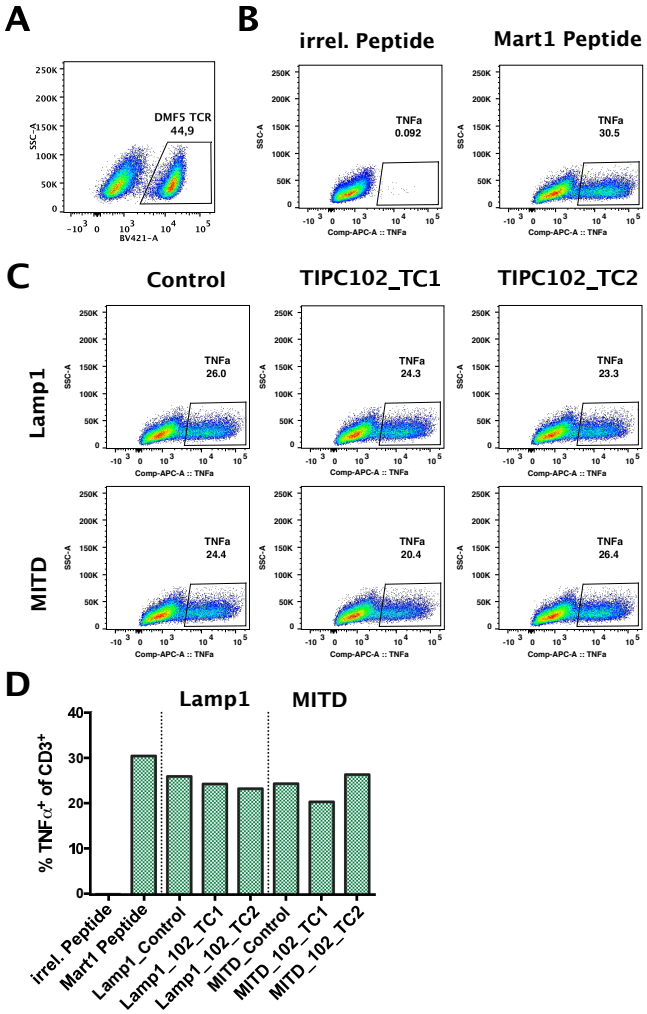

Figure 37 – Comparison of MHC-I restricted T cell activation between the Lamp1 expression system and the MITD construct. (A) Transduction efficiency of the DMF5 TCR. Detection was performed using an α-mouseTCR-β_BV421 antibody. (B) Antigen specific DMF5 TCR transduced T cell acitvation. Autologous, peptide pulsed TILs served as target cells. The irrelevant peptide is represented by the HY short peptide (HIENFSDIDMGE). (C) Antigen specific activation of DMF5 transduced TILs by autologous TILs transduced with the respective expression system. Activation was monitored by TNFα expression in the $CD3^+$ effector ($CFSE^-$) population via intracellular cytokine staining. (D) Summary of the MHC-I restricted, antigen specific activation of DMF5 TCR transduced TILs against the respective expression system. Lamp1_Control = Lamp1_Mut395 screening construct without patient multi-epitope constructs (figure 30); MITD_Control = MITD construct without patient multi-epitope constructs (figure 36). TIPC102_TC1 and TIPC102_TC2 represent the respective expression system combined with multi-epitope constructs from patient TIPC102. Day 42 TILs from patient TIPC079 were used for transduction. Peptides were pulsed onto GFP transduced d42 TILs.

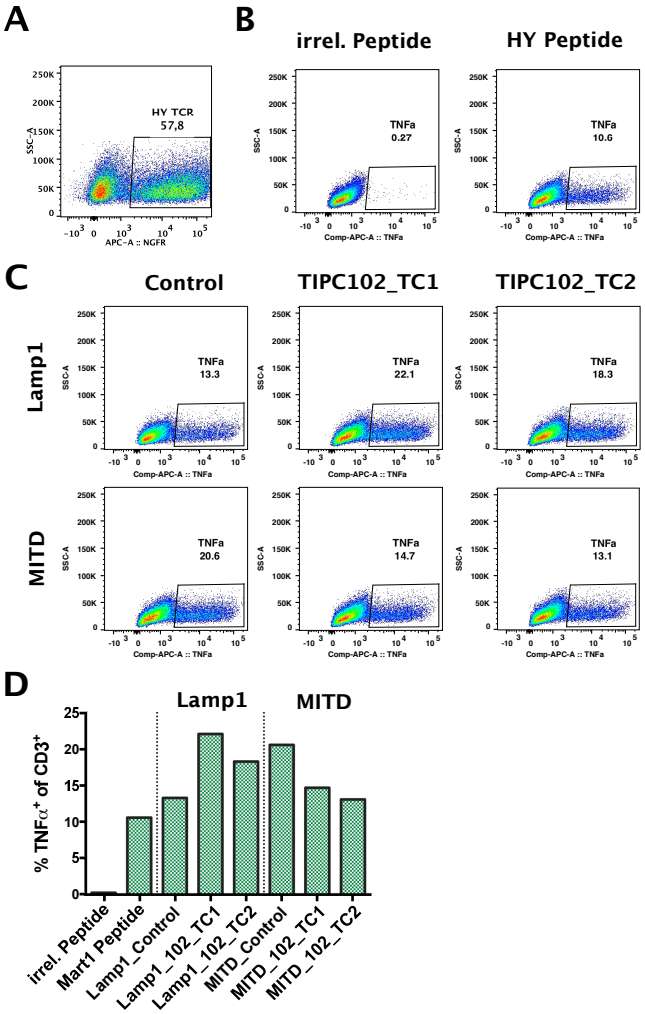

Figure 38 – Comparison of MHC-II restricted T cell activation between the Lamp1 expression system and the MITD construct. (A) Transduction efficiency of the HY TCR. Detection was performed using an α-NGFR_APC antibody. (B) Antigen specific HY TCR transduced T cell acitvation. Autologous, peptide pulsed TILs served as target cells. The irrelevant peptide is represented by the Mart1 short peptide (ELAGIGILTV). (C) Antigen dependent activation of HY transduced TILs by autologous TILs transduced with the respective expression system. Activation was monitored by TNFα expression in the $CD3^+$ effector ($CFSE^-$) population via intracellular cytokine staining. (D) Summary of the MHC-II restricted, antigen specific activation of HY TCR transduced TILs against the respective expression system. Lamp1_Control = Lamp1_Mut395 screening construct without patient multi-epitope constructs (figure 30); MITD_Control = MITD construct without patient multi-epitope constructs (figure 36). TIPC102_TC1 and TIPC102_TC2 represent the respective expression system combined with multi-epitope constructs from patient TIPC102. Day 42 TILs from patient TIPC079 were used for transduction. Peptides were pulsed onto GFP transduced d42 TILs.

Comparison of the Lamp1 screening system to peptide pulsed, autologous B cells

One way to overcome the fact that autologous, expanded TIL might not be the best possible APC would be the use of immortalized B cells for patient samples where we have access to an adequate source of B cells (e.g. resected spleen or blood). Unfortunately, access to autologous spleen or blood samples from patients was rather limited. To test an alternative screening approach, we used spleen samples from two patients (TIPC253 and 275) for the immortalization of B cells. We successfully over-expressed antiapoptotic endogenous proteins (Bcl-6/XL) to immortalize the B cells as previously described [175, 318], since overexpression of Bcl-6/XL

in B cells was recently shown to significantly reduce background T cell activation compared to commonly used EBV immortalized B cells, when screening for neoepitope reactive T cells in a peptide-based screening approach [175].
We tested the applicability of the Lamp1 based screening approach in Bcl-6/XL immortalized B cells. Furthermore, we compared the Lamp1 system to the use of synthetic peptide-based screening approaches applied when using B cells as APCs [175]. Mart1 (DMF5) and HY TCRs transduced TILs from patient TIPC091 were used as responder T cells. Immortalized B cells from TIPC253 were used as positive controls for antigen presentation, as this patient expressed both HLA-A02:01 and HLA-DQB01:05, needed for presentation and recognition of our antigens (table S2), whereas B cells from TIPC275 served as negative control, since this patient expressed neither HLA-A02:01 nor HLA-DQB01:05 (table S2). To use the B cell lines as APCs, we either pulsed them with the Mart1 or HY core peptides, an elongated version of these or transduced them with our Lamp1_Mut395 screening construct. Here, the elongated peptides were used to monitor a potential loss of T cell responses in the context of peptide processing and cross-presentation.
The results first and foremost revealed, that the Lamp1 screening system is still functional in simultaneous MHC-I and MHC-II antigen presentation when introduced into immortalized B cells (figure 39 and 40). We could further show a loss of antigen specific T cell reactivity against elongated, MHC-I restricted peptides compared to the core epitope recognized by the TCR (figure 39), most likely due to a limited capability of antigen cross presentation by the B cells into MHC-I [373]. In the context of the Lamp1 system, however, elongated epitope variants could still induce MHC-I restricted T cell reactivities (figure 39). In the case of MHC-II restricted responses, the core HY peptide, as well as its elongated version, and the Lamp1 system appeared equally potent in T cell activation (figure 40). Background reactivity of the HY TCR against TIPC253 B-cells was observed as could have been expected, as these cells derive from a male patient potentially expressing endogenous HY antigen.
Taken together, these results enlarge the pool of potential autologous APCs that could be used with the Lamp1 based screening approach. In addition, the Lamp1 screening system appeared superior to a peptide based screening approach, when looking at MHC-I restricted epitopes. Here, the use of too large or falsely designed peptides will certainly result in overlooking of potential immunogenic epitopes, whereas the use of long peptides seems less critical for the detection of MHC-II restricted epitopes.

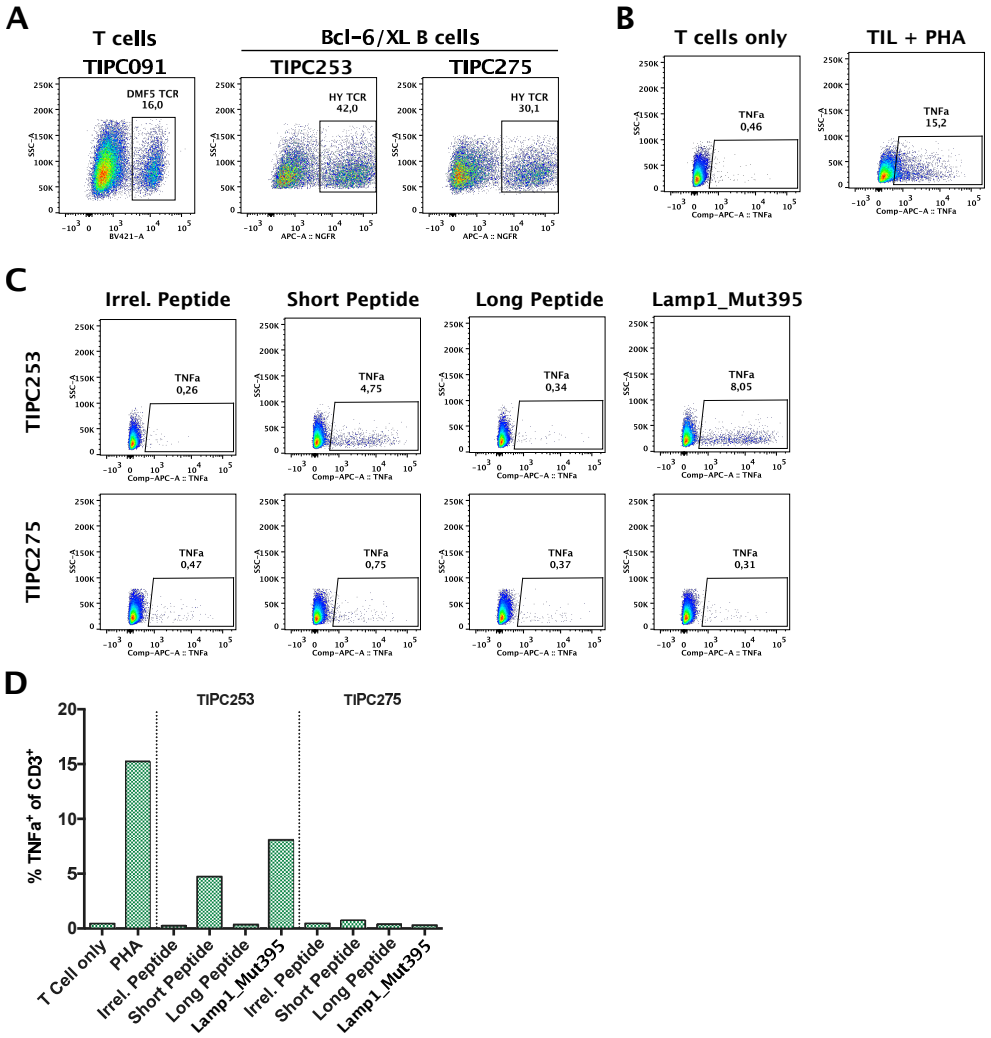

Figure 39 – Comparing MHC-I restricted T cell activation between a peptide based and the Lamp1 screening system. (A) Assessment of transduction efficiency. DMF5 TCR was transduced into expanded TILs from patient TIPC091. Transduction efficiency of immortalized B cells was monitored by HY TCR control transduction. Staining of the DMF5 TCR was performed using an α-mouseTCR-β_BV421 antibody. HY TCR expression was monitored using an α-NGFR_APC antibody. (B and C) Monitoring activation of DMF5 TCR transduced TILs from patient TIPC091. (B) Assessment of the general functionality of the TCR transduced effector cells by unspecific activation with 1 µg/ mL PHA. (C) Reactivity of DMF5 TCR transduced TILs against the respective peptide or the empty Lamp1_Mut395 construct (see figure 30). B-cell lines were pulsed for 20h with 20 µg/ mL of the peptide as described in [175] or transduced with the empty Lamp1_Mut395 construct (see figure 30). The HY peptide served as irrelevant peptide control. (D) Summary of antigen specific reactivities. Reactivities were assessed by intracellular cytokine staining on TNFα. Peptides used Mart1 = ELAGIGILTV; Mart1_long = KGHGHSYTTAE*ELAGIGILTV*LGVLLLIG; HY = HIENFSDIDMGE.

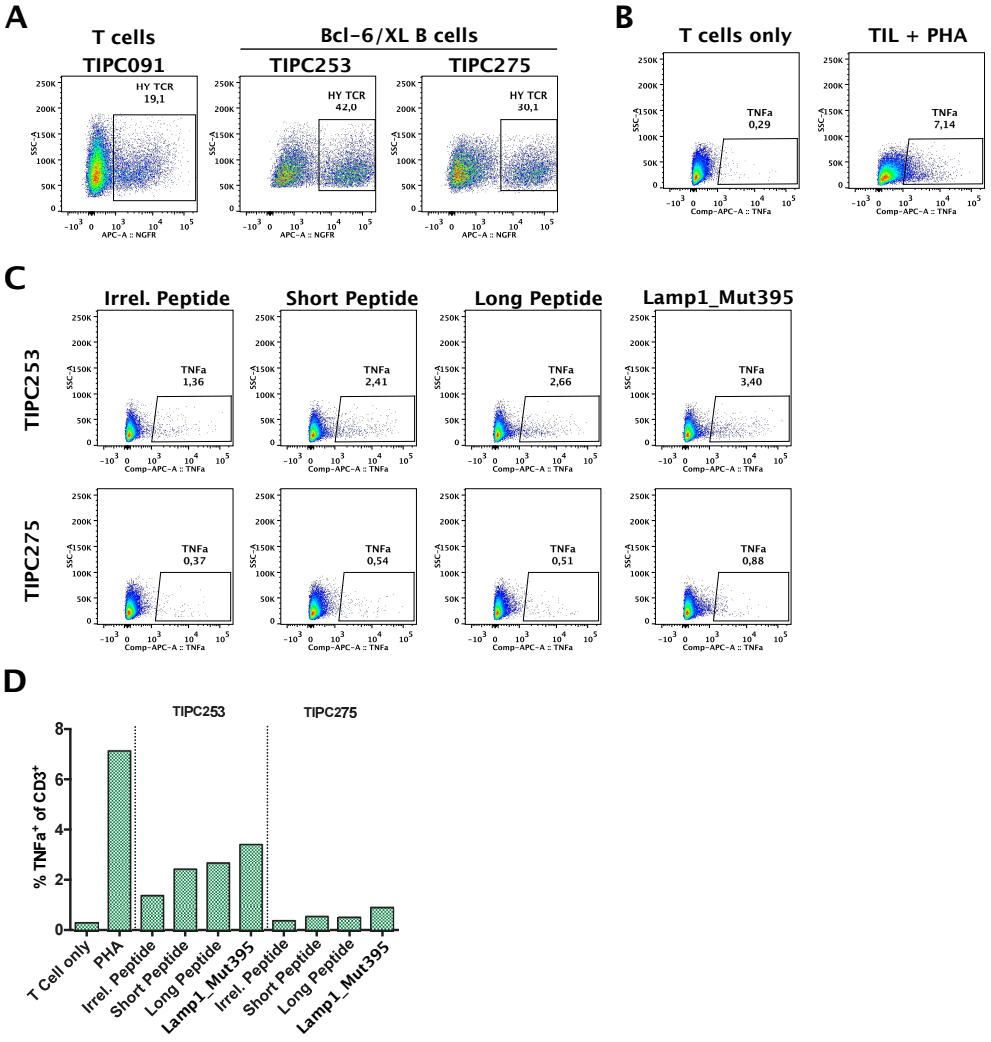

Figure 40 – Comparing MHC-II restricted T cell activation between a peptide based and the Lamp1 screening system. (A) Assessment of transduction efficiency. HY TCR was transduced into expanded TILs from patient TIPC091. Transduction efficiency of immortalized B cells was monitored by HY TCR control transduction. Staining was performed using an α-NGFR_APC antibody. (B and C) Monitoring activation of HY TCR transduced TILs from patient TIPC091. (B) Assessment of the general functionality of the TCR transduced effector cells by unspecific activation with 1 µg/ mL PHA. (C) Reactivity of HY TCR transduced TILs against the respective peptide or the empty Lamp1_Mut395 construct (see figure 30). B-cell lines were pulsed for 20h with 20 µg/ mL of the peptide as described in [175] or transduced with the empty Lamp1_Mut395 construct (see figure 30). The Mart1 peptide served as irrelevant peptide control. (D) Summary of antigen specific reactivities. Reactivities were assesed by intracellular cytokine staining on TNFα. Peptides used HY = HIENFSDIDMGE; HY-long = EATGSNCPP*HIENFSDIDMGE*IIMGNIELT; Mart1 = ELAGIGILTV.

4.3.7 Effects of Lamp1 destabilizing mutations on antigen trafficking and presentation

In order to get a better understanding of the underlying effects on antigen presentation upon destabilization of Lamp1, we monitored MHC-I antigen presentation and subcellular localization of our different Lamp1 constructs.

Destabilization of Lamp1 leads to an increase in MHC-I restricted antigen presentation

To obtain an insight into the influence of Lamp1 destabilization on MHC restricted antigen presentation, we directly monitored the surface presentation of the respective antigens. For

this, we co-transfected the ovalbumin antigen (SIINFEKL; H-2K^b-restricted and ISQAVHAA-HAEINEAGR; I-A^b-restricted) encoding Lamp1 constructs, as well as GFP for transfection control (figure 41A), into the murine 771 B cell line. MHC-I restricted surface expression of SIINFEKL was monitored using a H-2K^b-SIINFEKL specific antibody. In the case of MHC-II restricted antigen presentation, however, there was no I-A^b-Ovalbumin specific antibody available and we could not assess the surface presentation of ISQAVHAAHAEINEAGR.
We could show that MHC-I antigen presentation was not significantly increased by either of the single mutants compared to wild type Lamp1 (figure 41B and C). However, the combination of both TMD destabilizing mutations revealed a significant increase in MHC-I restricted antigen presentation, indicating an improved early degradation of this construct (figure 41B and C).

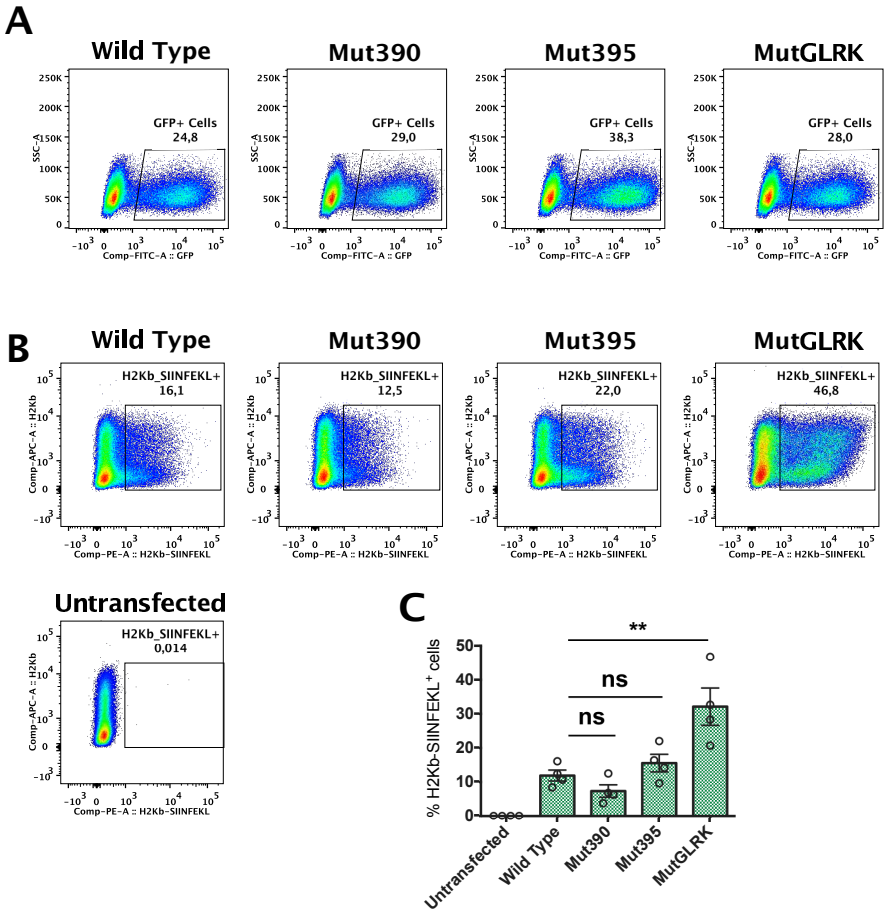

Figure 41 – Destabilization of the Lamp1 expression system results in increased MHC-I antigen presentation. (A) Transfection efficiency control by cotransfection of 771 B cells with pEGFP_N1 and the respective ovalbumin antigen encoding Lamp1 constructs. (B) Monitoring the influence Lamp1 destabilitzation on surface the presentation of SIINFEKL using a H2-Kb-SIINFEKL_PE specific antibody. (C) Summary of the influence on MHC-I antigen presentation upon Lamp1 destabilization. n=4 biological replicates. Statistical analysis of results performed using a One-way ANOVA with post-hoc Tukey's multiple comparisons test.

Effects of TMD destabilization on subcellular localization

Another aspect influencing antigen presentation upon TMD destabilization of Lamp1 is the subcellular localization of the protein in combination with an early protein degradation. Thus, we analyzed the increase in early protein degradation resulting from the TMD destabilization by

monitoring protein accumulation (signal at 45 kDa) upon proteasome inhibition using the small molecule inhibitor MG132. In addition, we examined the subcellular localization of our different Lamp1 variants, by taking advantage of the high number of N-linked gylcosylation sites (18 in total) spread over the whole luminal domain of Lamp1 [360]. Due to glycan maturation in the golgi network, Lamp1 should become resistant to EndoH digest upon shuttling from the ER through the golgi and to the MHC-II compartment. Thus, comparing EndoH digested to PNGaseF digested Lamp1 (signal at 120 kDa) in turn reveals the portion of protein passing the golgi network. Since experiments were independent of surface antigen presentation, we used HEK293T cells for the expression of the different Lamp1 constructs.

Proteasome inhibition did not reliably lead to Lamp1 accumulation, despite the presence of over-expressed, incompletely processed (EndoH sensitive) protein (figure 42). However, our results indicate, that the introduction of TMD destabilizing mutations can lead to a disruption of subcellular trafficking of Lamp1. While the MutGLRK construct appeared to mainly reside in the ER, both single mutants, as well as the wild type variant still appeared to cross the golgi network (figure 42).

These results suggest that Lamp1 TMD destabilization is not critical for shuttling antigens into the MHC-I presentation pathway, due to the accumulation of highly overexpressed protein in the ER. Nevertheless, the introduction of these mutations appears to influence MHC-II restricted antigen presentation by disrupting the subcellular trafficking of the protein.

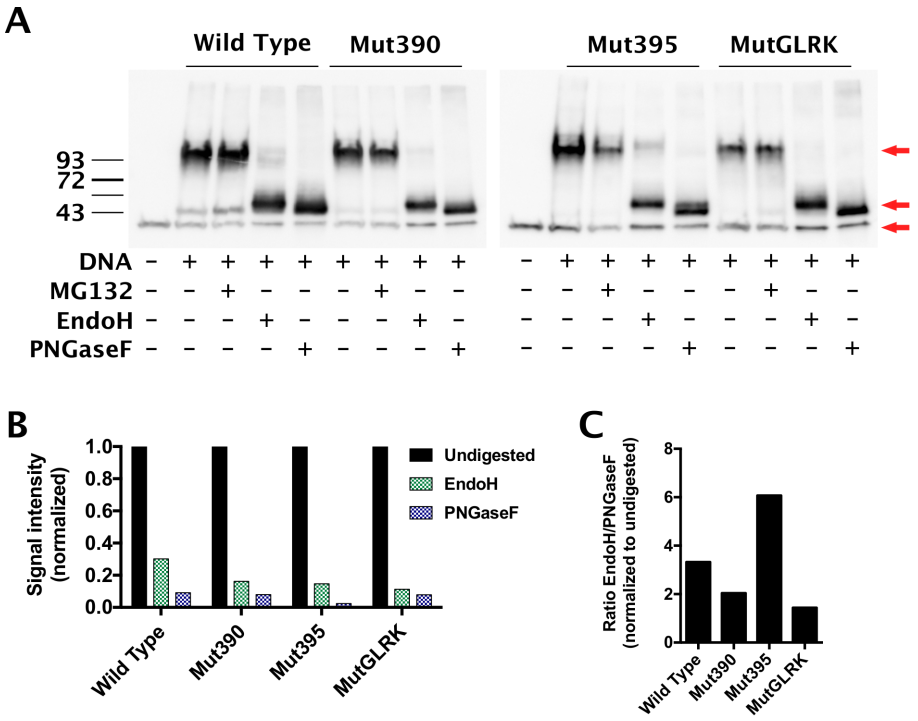

Figure 42 – Destabilization of Lamp1 indicates disruption of subcellular trafficking. A) Analysis of subcellular trafficking of the respective Lamp1 construct by western blot. Arrows indicate: Top = EndoH resistant Lamp1; Middle = EndoH sensitive Lamp1 and Bottom = loading control (GAPDH). B) Analysis of EndoH resistant and PNGaseF sensitive Lamp1 signal intensities (120 kDa). Signal intensities were first normalized to the loading control. Quantification was performed by normalization to the signal intensity of the non-deglycosylised sample. C) Ratio of normalized signal intensities of EndoH to PNGaseF digested Lamp1. The Lamp1 constructs were introduced into HEK293T cells via Calcium phosphate coprecipitation. A representative experiment of n=3 biological replicates is shown.

4.4 Using targeted proteomics to identify PDAC neoepitopes

An alternative method to identify mutation derived epitopes is direct identification of antigens presented on the tumor cell surface by mass spectrometry [180, 181, 357]. In this context, Bassani-Sternberg and coworkers could recently show the potential benefit (i.e. antigen specific T cell priming) and current hurdles (i.e. sensitivity) of direct neoepitope identification from resected melanoma tissue using an untargeted (MHC allele independent) screening approach [181]. Since the success of such an untargeted approach seems highly dependent on state-of-the-art technologies - which are currently difficult to access - combined with the risk of missing low abundant epitopes, we aimed for a targeted mass spectrometry approach to verify the presentation of predicted mutation-derived epitopes. The advantage of such a targeted proteomics approach, looking for low abundant and weaker binding epitopes, was recently shown by the group of PD Dr. Dr. A. Riemer [357]. By combining epitope-derived reference spectra with mass spectrometry data of a samples HLA-ligandome we aimed to directly identify PDAC-derived epitopes.

In cooperation with the group of PD Dr. Dr. A. Riemer, we set up a pipeline to identify neoepitopes presented on the surface of pancreatic cancer cells (figure 43). For the initial testing of the pipeline we focused on neoepitopes predicted to bind HLA-A02:01, keeping the current limitations of epitope prediction algorithms in mind [182, 183].

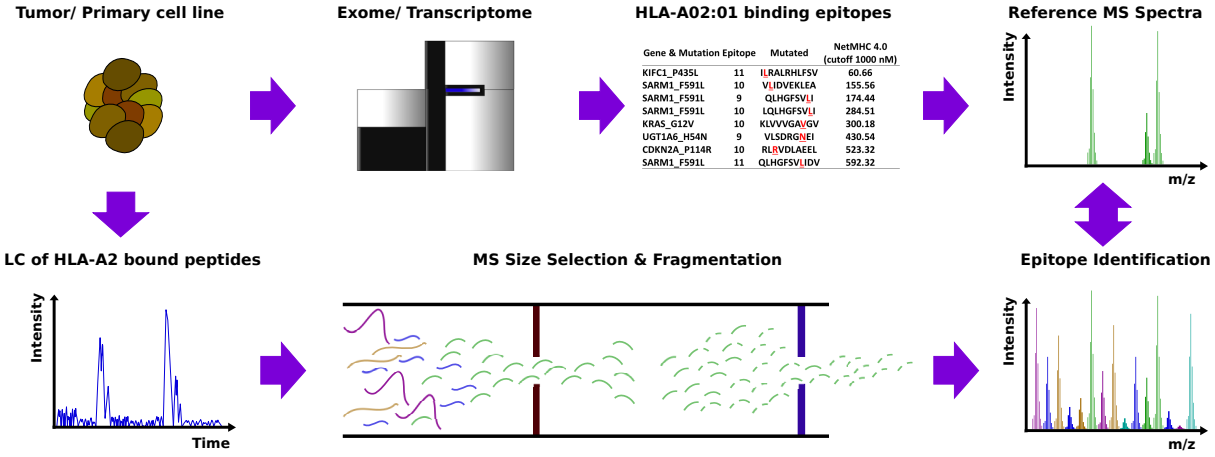

Figure 43 – Schematic overview of the targeted proteomics approach.

4.4.1 Validation of the targeted proteomics pipeline by detection of overexpressed epitopes

In order to test the setup and sensitivity of the screening pipeline, we initially screened a set of well characterized HLA-A02:01 binding epitopes, which we over-expressed in HEK293T cells. The epitopes chosen for this approach (CSNK1A1: GLFGDIYLAI; GAS7: SLADEAEVYL; HAUS3: ILNAMIAKI) were previously shown to be restricted to HLA-A02:01 and immunogenic in melanoma patients [325]. However, to validate their binding to HLA-A02:01 we applied two assays monitoring either their general HLA-binding in combination with the HLA:peptide complex stability over time (low stringency assay) or by measuring the formation of stable HLA:peptide complexes at a physiological temperature (high stringency assay). Here, peptides binding to HLA-A02:01 at a physiological temperature indicate an increased likelihood of

these epitopes to be endogenously processed and presented at the cell surface. Therefore, these epitopes might be more relevant in an actual anti-tumor T-cell response.
For the low stringency assay we induced the accumulation and potential stabilization of HLA-A02:01 at the cell surface by pre-incubating TAP-deficient T2 cells together with the respective peptide at a low temperature (25° C for 16 h), as previously described [374, 375]. Afterwards, the cells were transferred to a higher temperature (37° C) for different time spans, leading to an increased internalization of unstable HLA-A02:01. Peptide-stabilized MHC molecules remained on the cell surface for an extended period of time, allowing the assessment of epitopes binding to and stabilizing HLA-A02:01 over time (figure 44A - C). Furthermore, the high stringency assay was performed by co-incubation of each peptide with TAP-deficient T2 cells at 37° C over night, indicating a strong and lasting stabilization of HLA-A02:01(figure 44D & E). To control and compare the binding strength of each peptide, we took along well characterized viral reference peptides [320, 321], three binding (EBV, GAG77-85 and NEF136-145) and four not binding (GAG20-28, NEF73-82, GAG240-249 and NEF120-128) to HLA-A02:01 during each assay (figure 44B and E). Taken together, we could validate HLA-A02:01 binding of all three melanoma epitopes (figure 44C), with GAS7 showing the strongest binding among these (figure 44D and E).
Based on this, we screened for the endogenous presentation and detectability of these epitopes using direct identification by targeted mass spectrometry. We first designed two minigene constructs expressing all three epitopes, either as elongated versions of the epitopes (figure 45A) or the core sequences separated by a triple alanine linker (figure 45B). These constructs were transfected into HEK293T cells, followed by a 48 h IFNγ treatment of the cells to increase the overall antigen processing and HLA-A02:01 surface expression (figure 46A and B). Afterwards, the cells were lysed, the HLA-A02:01-bound peptides extracted and analyzed for the presence of the three melanoma epitopes by comparing the mass spectrometry data of HLA-A02:01 bound epitopes to the reference spectra of the respective synthetic peptide. We could detect two (GAS7 and HAUS3) of the three epitopes presented on the surface of transfected HEK293T cells (figure 46D - F). Looking at the differences in detectability of both, the GAS7 and the HAUS3, epitopes, the GAS7 epitope was detected with a higher abundance than the HAUS3 epitope (figure 46D). Here, the increased detectability of the GAS7 peptide, compared to the HAUS3 peptide, likely derives from physico-chemical properties influencing the peptides behavior during acquisition (e.g. polarity), which is also seen when measuring both synthetic peptides at equimolar concentrations (figure 46C). In combination with suboptimal antigen processing, this difference in epitope abundance likely led to the loss of detectability of the HAUS3 epitope in the 25mer gene construct (figure 46D). The third epitope (CSNK1A1) was neither detectable as a synthetic peptide nor in the biological sample.
Taken together, these results indicate that we now have a functional pipeline to detect HLA-A02:01 binding epitopes using targeted mass spectrometry. In addition, the validation of HLA-A02:01 binding might be a critical step in this pipeline, considering that epitopes used for future patient screenings might not bind as well as previously predicted. Furthermore, an enhanced stabilization of HLA-A02:01 at 37° C might indicate a stronger MHC binding and result in a higher chance to detect these epitopes by mass spectrometry. This hypothesis was supported by the correlation of the enhanced HLA-A02:01 binding of the GAS7 epitope at 37° C with a higher abundance in the mass spectrometry readouts, compared to the HAUS3 epitope.

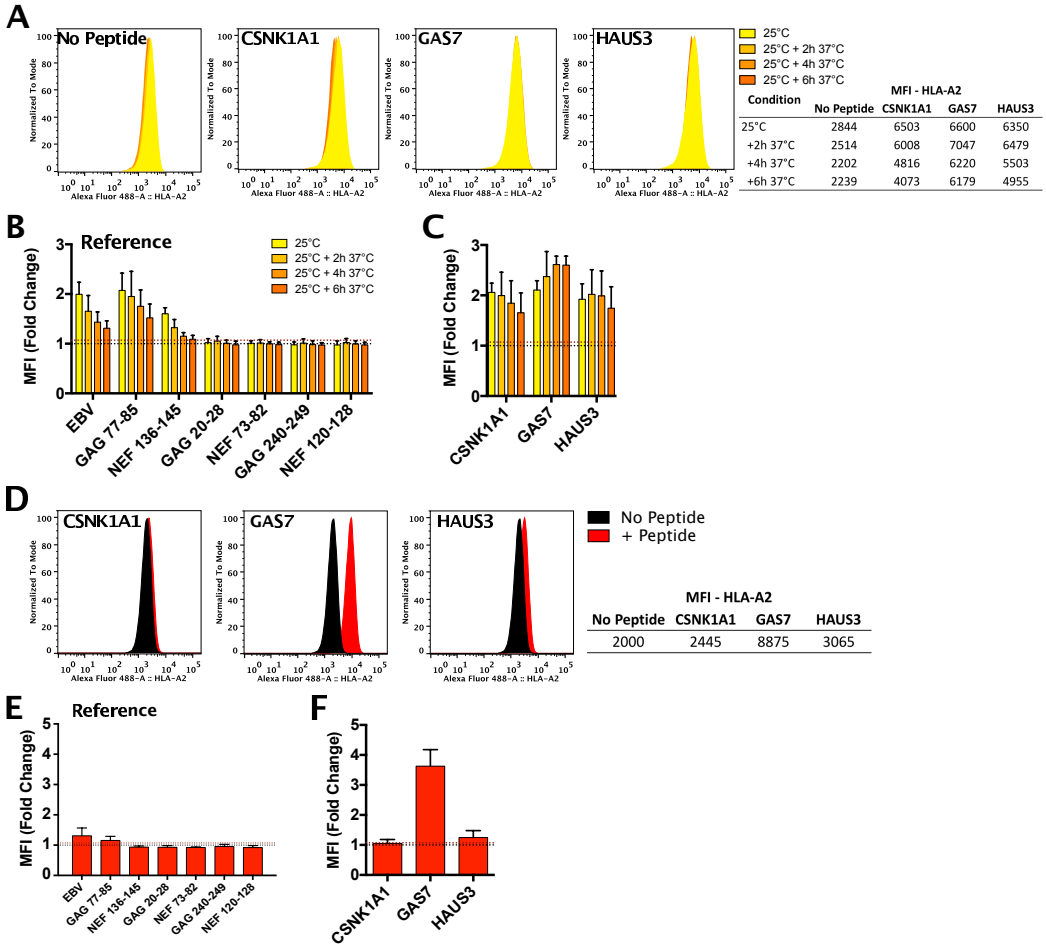

Figure 44 – Assessing HLA-A2 binding of the overexpressed epitopes. (A) Analysis example for peptide derived HLA-A2 stabilization on T2 cells upon increase of incubation temperature. (B and C) Analysis of HLA-A2 stabilization on T2 cells by 10 µg/mL of the respective pepitde compared to a matched sample without peptide. Colour scale indicates the time incubated at 37°C. Mean fluorescence intensity (MFI) change of the peptide sample to a DMSO treated sample was assessed. (D) Analysis example HLA-A02:01 stabilization after coincubation of T2 cells with the respective peptide over night at 37°C. (E) MFI change in HLA-A2 surface stabilization by the respective peptide compared to a DMSO sample. Reference Peptides: HLA-A02:01 binders: EBV = GLCTLVAML; GAG77-85 = SLYNTVATL; NEF136-145 = PLTFGWCYKL. Non-HLA-A02:01 binders: GAG20-28 = RLRPGGKKK; NEF73-82 = QVPLRPMTYK; GAG240-249 = TSTLQEQIGW; NEF120-128 = YFPDWQNYT. Melanoma peptides: CSNK1A1 = GLFGDIYLAI; GAS7 = SLADEAEVYL; HAUS3 = ILNAMIAKI. Each peptide was measured as biological triplicate.

Figure 45 – Gene construct design for the detection of overexpressed HLA-A02:01 binding epitopes. Two versions were designed encoding three previously published HLA-A02:01 binding epitopes (see [325]) fused head-to-tail into the pcDNA3.1 vector. (A) The 25mer variant encoding each core epitope, elongated N- and C-terminally by its native sequence, with the published mutation at position 13 (arrow). (B) The minimal variant encoding the core sequences of the published epitopes connected by triple alanine linkers.

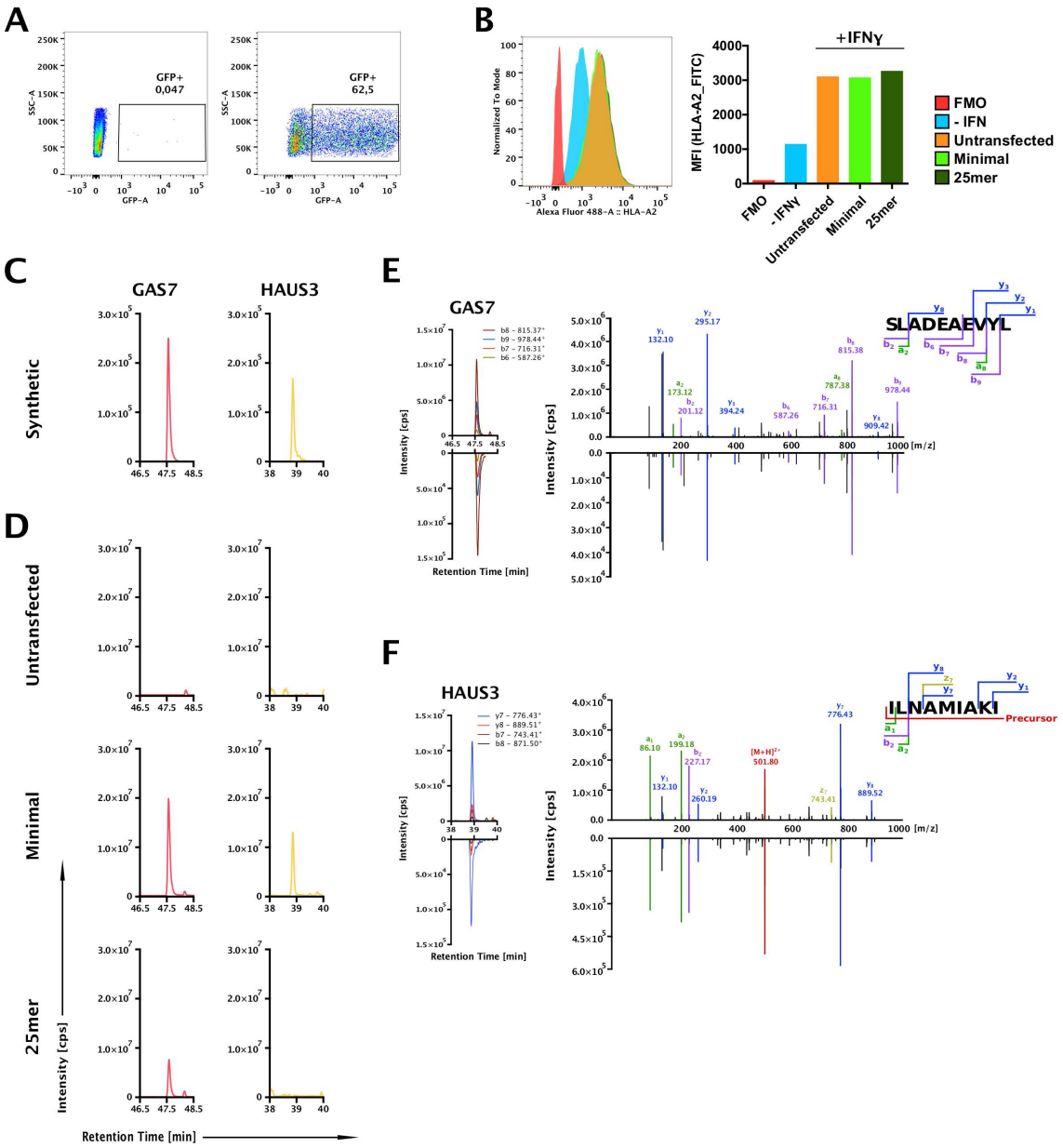

Figure 46 – Detection of overexpressed HLA-A02:01 epitopes using a targeted mass spectrometry approach. (A) Transfection efficiency of HEK293T cells using $CaPO_4$ co-precipitation. Efficiency was assessed by GFP expression in a seperate sample three days after transfection, on the day of cell lysate generation. (B) Upregulation of HLA-A2 upon 48 h IFNγ treatment of HEK293T cells. (C and D) Total ion chromatograms of the respective synthetic peptides at equimolar concentrations (C) and the HLA-A2 pulldown samples (D). (E and F) Extracted-ion chromatograms for measured MS^3 fragment transitions and their underlying MS^3 spectra in the pulldown samples (top) and the synthetic peptides (bottom) of the GAS7 (E), as well as HAUS3 (F) epitopes. Fragments are indicated with their respective m/z ratio.

4.4.2 Selection of patient samples to screen for presentation of neoepitopes

In order to validate the targeted proteomics pipeline with patient samples, we identified a set of four patients who were HLA-A02:01$^+$ with exome and transcriptome data, as well as a growing cell line available (TIPC102, 113, 222 and 236). Of these, TIPC236 was later excluded as we could not validate the mutations, identified in the primary tumor and xenograft, in the cell line (table S17; table 43). For the remaining patients we confirmed HLA-A02:01 surface expression, as well as its upregulation upon treatment of each xenograft derived cell line with IFNγ for 48 h (figure 47).

Notably, we encountered two examples of immune editing influencing the HLA-A02:01 surface expression in cell lines TIPC102 and 222. In the case of TIPC102, xenograft expansion led to the outgrowth of a clone devoid of the chromosome 6 p-arm encoding for HLA-A02:01 (figure 47B). Since this patient initially expressed HLA-A02:01, we decided to reintroduce the HLA molecule, generating a cell line stably expressing HLA-A02:01 (figure 47A). For the TIPC222 cell line we could identify a general unresponsiveness to the IFNγ treatment, caused by a functional loss of JAK2 during xenograft expansion (figure 47D and E). Nevertheless, due to a reasonably high endogenous expression of HLA-A02:01, we decided to include this patient for the targeted proteomics approach. The cell line of patient TIPC113 did not reveal any abnormality affecting HLA-A02:01 expression or upregulation (figure 47C).

These results demonstrate the necessity of testing each xenograft derived cell line for functional HLA-A02:01 expression. The high incidence of abnormalities calls for a deeper characterization (i.e. validation of mutations) of every cell line after xenograft expansion, due to the outgrowth of certain subclones.

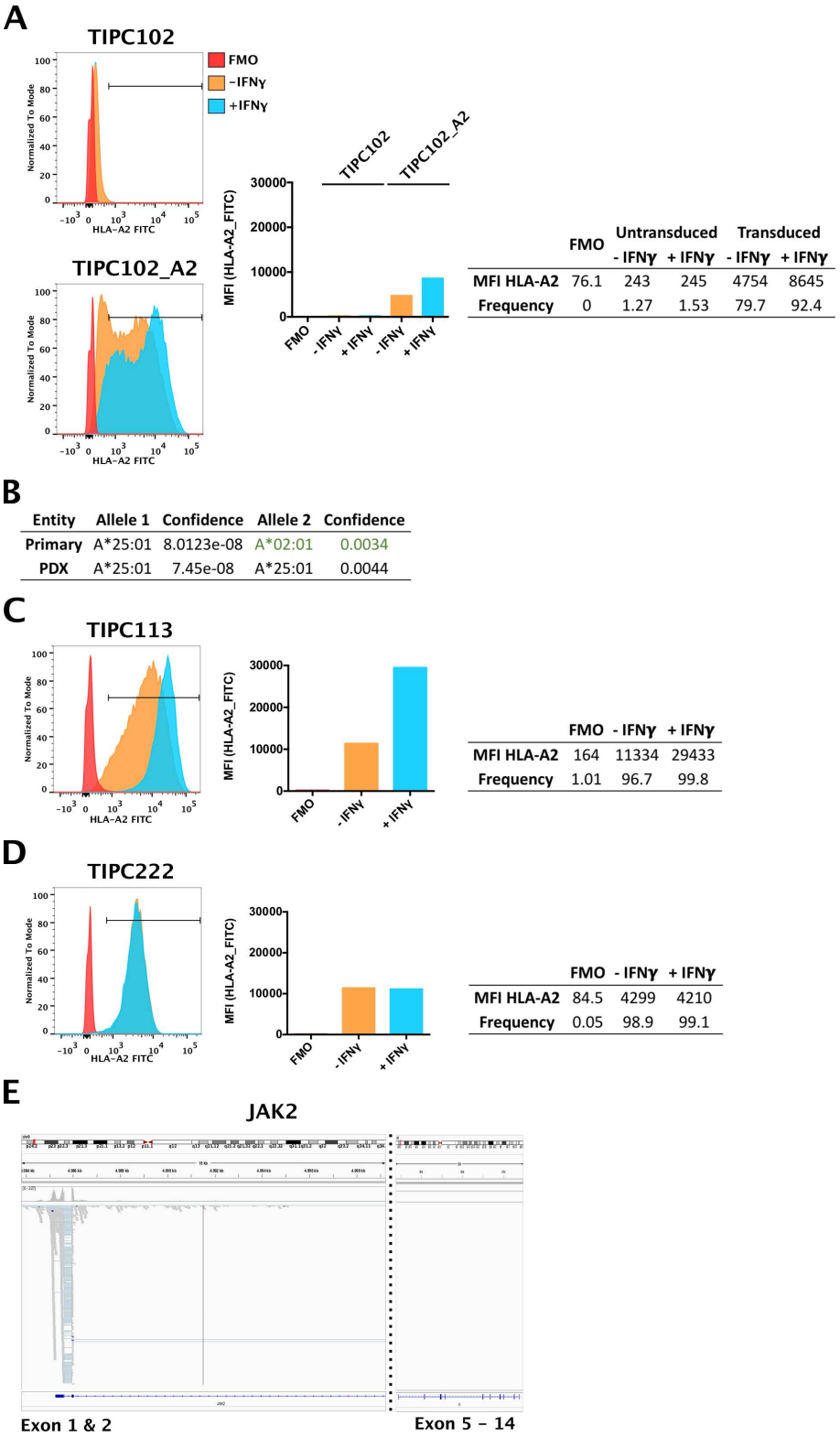

Entity	Allele 1	Confidence	Allele 2	Confidence
Primary	A*25:01	8.0123e-08	A*02:01	0.0034
PDX	A*25:01	7.45e-08	A*25:01	0.0044

	FMO	Untransduced		Transduced	
		- IFNγ	+ IFNγ	- IFNγ	+ IFNγ
MFI HLA-A2	76.1	243	245	4754	8645
Frequency	0	1.27	1.53	79.7	92.4

	FMO	- IFNγ	+ IFNγ
MFI HLA-A2	164	11334	29433
Frequency	1.01	96.7	99.8

	FMO	- IFNγ	+ IFNγ
MFI HLA-A2	84.5	4299	4210
Frequency	0.05	98.9	99.1

Figure 47 – Upregulation of HLA-A2 on cell lines upon IFNγ treatment. Shown are PDX derived cell lines selected for the targeted mass spectrometry approach. (A) HLA-A2 suface expression of TIP102 before (top) and after (bottom) stable transduction with HLA-A02:01. (B) Loss of HLA-A*02 locus in TIPC102 upon xenograft passaging. (C) Increase of HLA-A2 surface expression in the TIPC113 cell line after IFNγ treatment. (D) Unresponsivness of TIPC222 cell line to IFNγ treatment. (E) TIPC222 transcriptome analysis of the JAK2 locus. Shown is the read coverage of exon 1 & 2, as well as exons 5 - 14, in the xenograft transcriptome. (FACS plot colors: red = FMO; orange = no IFNγ; blue = 330 U/mL IFNγ).

4.4.3 Prediction of HLA-A02:01 binding epitopes from expressed mutations

Using the exome and transcriptome data of three patients (TIPC102, 113 and 222), we analyzed the expressed mutations for potential HLA-A02:01 binding epitopes using netMHC 4.0 with an affinity cut-off of 1000 nM. Overall, these predictions revealed mutations generating one or more HLA-A02:01 binding epitopes, as well as mutations yielding no binding epitopes within the given binding affinity range of <1000 nM (example in table 45). Compiling these results led to a total of 51 epitopes (range 13 - 19) within 27 mutations (range 7 - 11) across all three patients (table S10 - S12). Approximately 40.1% of the expressed mutations (range 35.7 - 45.4%) led to predicted HLA-A02:01 binding epitopes within the applied affinity range (figure 25).

Table 45 – Example for the prediction of HLA-A2 binding epitopes from expressed nsSNVs. Shown here for patient TIPC102 samples. The predicted affinity cutoff for the mutated epitope was set to $\leq$1000 nM. Posititions of amino acid changes are highlited in bold & underlined. Lists of predicted HLA-A02:01 binding epitopes for all patients can be found in the table S10 - S13.

Gene	Mutation	Location	Sequence	Length	Predicted affinity [nM]
ADCY6	G535V	chr12:49170065	—	—	—
ALDH16A1	R493Q	chr19:49967929	—	—	—
ATAD2	R913C	chr8:124351668	FI**C**DYGEIFNV	11	32.2
			ELFI**C**DYGEI	10	807.4
CCDC71	R269Q	chr3:49200836	—	—	—
CDC16	L447V	chr13:115027386	VTVDKWEP**V**	9	502.1
DNM3	R369H	chr1:172011262	—	—	—
DOCK1	E1316	chr10:129201400	—	—	—
DTNBP1	A123V	chr6:15615618	MTANLTHLE**V**	10	297.4
			SMTANLTHLE**V**	11	594.9
FILIP1L	F109V	chr3:99648801	ALLEAQYG**V**	9	4.3
			LALLEAQYG**V**	10	22.1
			ALLEAQYG**V**V	10	28.9
			LLEAQYG**V**	8	173.2
			DLALLEAQYG**V**	11	174.9
			LALLEAQYG**V**V	11	288.2
FOXJ2	D4G	chr12:8192439	**G**LESSLTSI	9	312.2
GBAS	G203D	chr7:56052562	TMIEW**D**NYWA	10	44.1
			GTMIEW**D**NYWA	11	758.3
GNG2	P60L	chr14:52433368	—	—	—
KRAS	G12D	chr12:25398284	KLVVVGA**D**GV	10	498.0
LIMCH1	T760K	chr4:41673607	—	—	—
LPIN1	M78I	chr2:11907930	—	—	—
LRP12	R330H	chr8:105509791	KLL**H**VLTAF	9	655.1
			KLL**H**VLTA	8	779.2
MAP2K4	G294R	chr17:12028677	SL**R**ITLYEL	9	436.5
			SL**R**ITLYELA	10	854.8
NFKBIZ	G405E	chr3:101572584	—	—	—
NR1I2	G36R	chr3:119526203	—	—	—
NSD1	L2063F	chr5:176715855	—	—	—
RASSF6	A238V	chr4:74447542	FALHIIF**V**T	9	312.4
			FALHIIF**V**	8	329.7
SRGAP2D	Q97R	chr1:121116733	—	—	—

4.4.4 Validation of mutations present in xenograft derived cell lines

Following HLA-A02:01 binding epitope prediction, we validated the underlying mutations, found in the primary tumor and xenograft, in each respective xenograft-derived cell line, to avoid screening of mutations lost due to the outgrowth of certain subclones (i.e. as a result of tumor heterogeneity). We first identified the mutated locus from the exome and transcriptome data. Based on this, we designed primer pairs to amplify and sequence the respective mutated locus (figure 48). For three of the patients (TIPC102, 113 and 222) the majority of HLA-A02:01 epitope yielding mutations (average: 80%; range: 70 - 90%) were still present in the respective cell line (table S14 - S16). As mentioned before, this step of validation revealed the absence of most mutations, except for KRAS_G12D, in the cell line of patient TIPC236 (table S17). Thus, we excluded this cell line from any additional experiments, due to a likely sample mix-up during cell line generation.

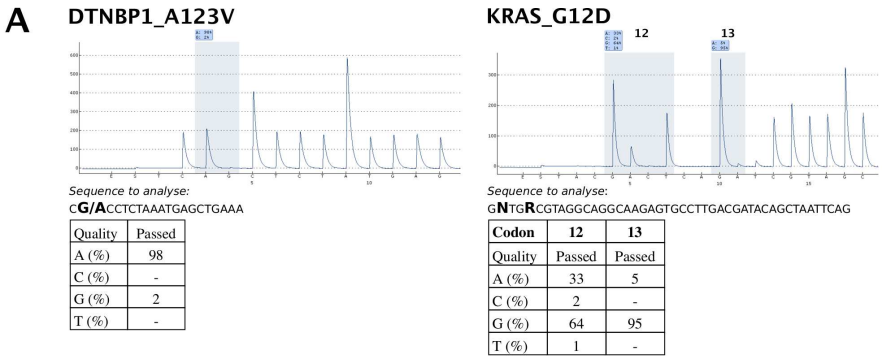

C

Gene	Mutation	Exome MAF Primary	Exome MAF PDX	RNASeq MAF (read count)	Pyro Sequencing*	Sanger Sequencing
ATAD2	R913C	0.190	0.422	42 % (39 of 92reads)	49% mutated	heterozygous
CDC16	L447V	0.416	0.996	100 % (99 mutant reads)	--	homozygous mutated
DTNBP1	A123V	--	0.979	90 % (9 of 10reads)	98% mutated	--
FILIP1L	F109V	0.159	0.646	71 % (5 of 7reads)	70% mutated	--
FOXJ2	D4G	0.217	0.538	47 % (9 of 19reads)	--	heterozygous
GBAS	G203D	--	0.289	26 % (14 of 54reads)	--	wild type
KRAS	G12D	0.228	0.495	40 % (22 of 55reads)	33% mutated	--
LRP12	R330H	--	0.300	75 % (3 of 4reads)	--	heterozygous
MAP2K4	G294R	0.369	1.0	100 % (23 mutant reads)	--	homozygous mutated
RASSF6	A238V	0.235	0.635	60 % (76 of 126reads)	69% mutated	--

Figure 48 – Example of the assessment of patient specific mutations in the PDX derived cell line. Shown here for the cell line TIPC102_A2. Using either pyrosequencing (A) or sanger sequencing (B) to assess the presence of mutations in the respective cell line. (C) Summary of the mutation validation results for the TIPC102_A2 cell line. Detailed lists for validated mutations in the cell lines used for the targeted proteomics approach can be found in table S14 - S17.

4.4.5 Validation of HLA-A02:01 binding of predicted patient epitopes

In order to avoid screening of predicted epitopes that do not truly bind to HLA-A02:01, we validated each peptide using both T2 cell-based HLA-A02:01 stabilization assays - see results section 4.4.1 - (figure 49 and 50). We could show, that the majority of predicted epitopes (average 88.8%; range 76.9 - 100%) bound with varying strength to HLA-A02:01, using the low stringency assay (figure 49C - E). In addition, the correlation between predicted binding affinity and experimentally determined epitope binding was poor (figure 49C - E and table S10 - S12). Compared to the viral reference peptides, the predicted patient epitopes could be further divided into four groups. The first group of peptides stabilized HLA-A02:01 as good as the reference peptides and induced lasting complex formation (e.g. ATAD2; figure 49 C). The second group of epitopes revealed HLA-A02:01 stabilization comparable to the reference peptides (e.g. FILIP1L_2; figure 49 C). The third group of peptides weakly bound to HLA-A02:01, resulting in a fast complex internalization (e.g. FOXJ2; figure 49 C). The last group of peptides did not bind to HLA-A02:01 (e.g. LRP12_1; figure 49 C). Furthermore, the high stringency assay revealed a small set (average: 20.9%; range: 15.4 - 31.6%) of 9 epitopes forming strong peptide:MHC complexes at physiological temperatures (figure 50C - E). This strong HLA-A02:01 binding correlated with the first group of peptides identified by the low stringency assay (figure 49 C-E and 50 C - E). Due to the strong and lasting formation of peptide:MHC complexes at physiological temperature, this small set of 9 epitopes (highlighted in figure 50C - E) was considered to include the best candidates for mass spectrometry analyses. However, as we are currently lacking further information on epitope characteristics essential for the detection by this targeted MS approach, we decided to screen all epitopes exceeding a general HLA binding and stabilization at 25° C beyond one standard deviation of the non-HLA-A02:01 binding reference epitopes (figure 49; σ = 0.07 indicated by the red line).

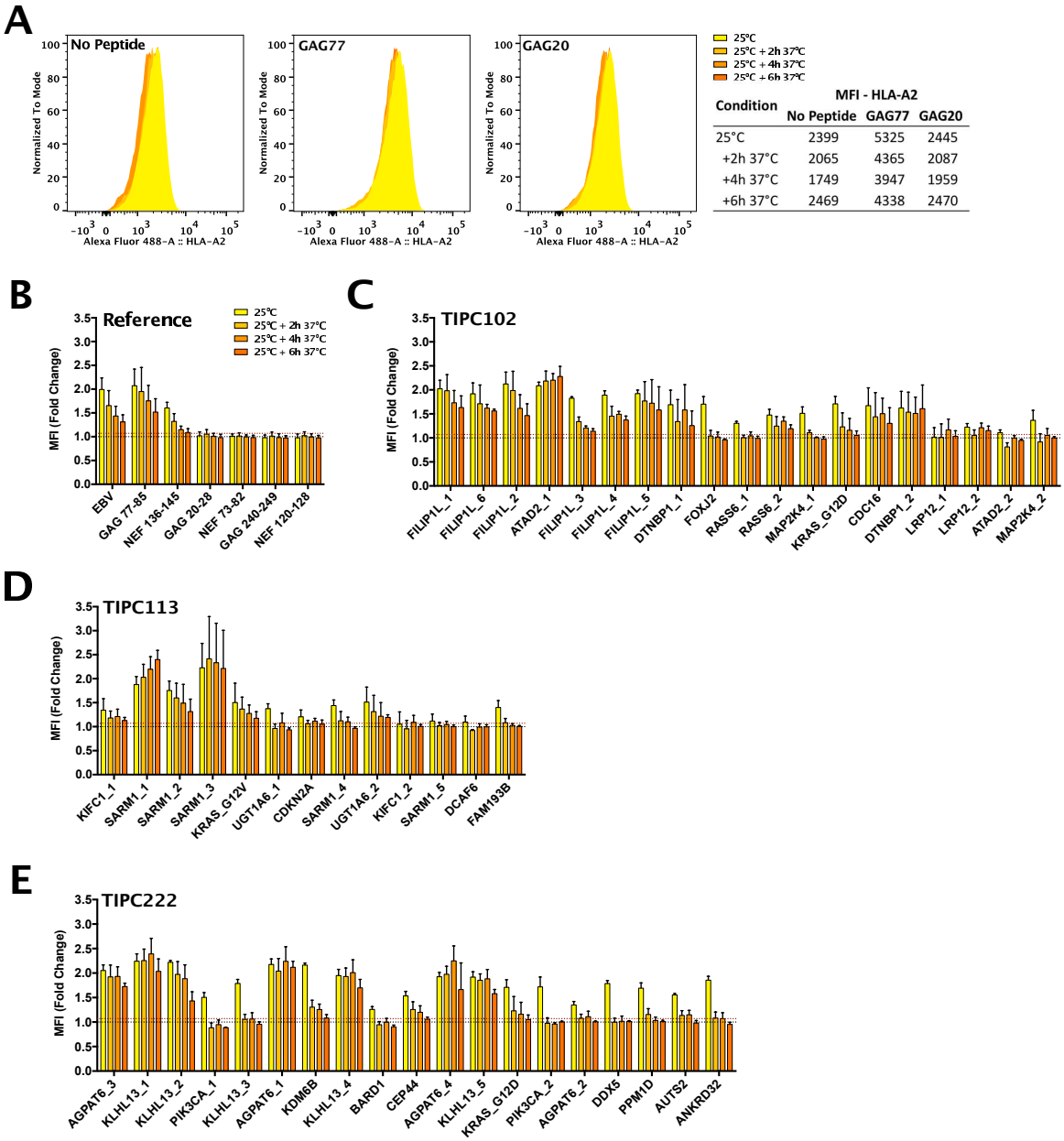

Condition	MFI - HLA-A2		
	No Peptide	GAG77	GAG20
25°C	2399	5325	2445
+2h 37°C	2065	4365	2087
+4h 37°C	1749	3947	1959
+6h 37°C	2469	4338	2470

Figure 49 – Assessing HLA-A2 binding of predicted epitopes. (A) Analysis example for peptide derived HLA-A2 stabilization on T2 cells over time at 37° C. (B-E) HLA-A2 MFI fold change of epitope pulsed T2 cells compared to the respective DMSO control sample was used to assess HLA-A2 binding. (B) HLA-A2 stabilization profile of the control peptides used in each experiment. (C - E) HLA-A2 stabilization of the various predicted peptides for the patient indicated. Peptides are sorted by decreasing predicted binding affinity. Dotted lines indicate normalization to DMSO sample (black line; MFI fold change = 1) and the standard deviation of the four non HLA-A2 binding control peptides (red line; σ = 0.07). All peptides were measured as biological triplicates.

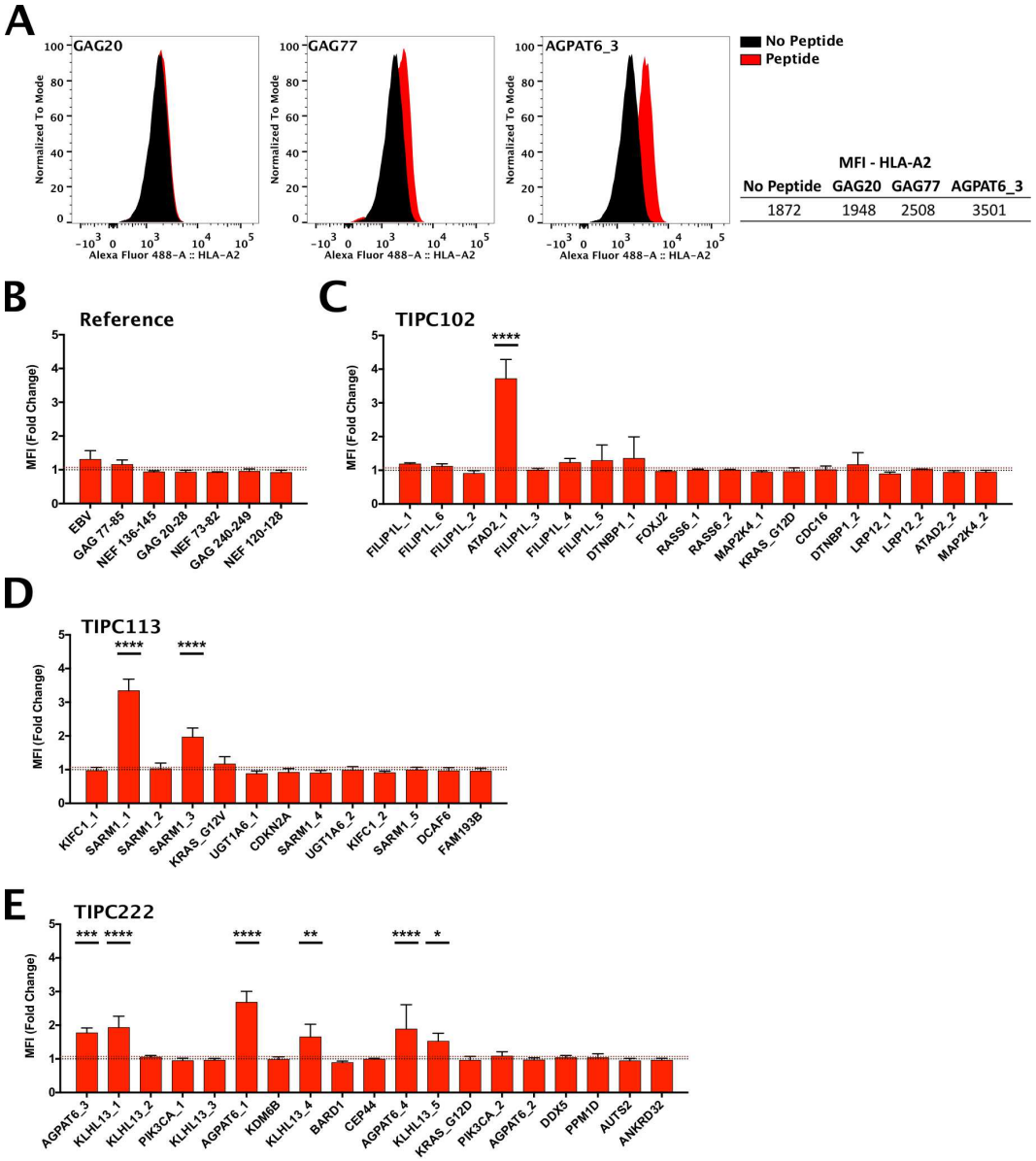

Figure 50 – Assessment of strong HLA-A2 binding peptides at 37° C. (A) Visualization of HLA-A2 stabilization on T2 cells by two of the control peptides and one predicted peptide (ATAD2_1; TIPC102) after over night incubation at 37° C. (B-E) HLA-A2 MFI fold change compared to the respective DMSO sample was used to assess HLA-A2 binding. (B) Stabilization of HLA-A2 by the control peptides. (C - E) HLA-A2 stabilization of the various predicted peptides for the patient indicated. Peptides are sorted by decreasing predicted binding affinity. Dotted lines indicate normalization to DMSO sample (black line; MFI fold change = 1) and the standard deviation of the four non HLA-A2 binding control peptides (red line; $\sigma = 0.07$). All peptides were measured as biological triplicates. Statistical analysis of results performed using a One-way ANOVA with post-hoc Tukey's multiple comparisons test. Asterisks indicate significance compared to DMSO sample.

4.4.6 In depth analysis of strong HLA-A02:01 binding epitopes

After we found that only a small set of predicted epitopes led to an enhanced stabilization of HLA-A02:01, we wanted to get a better understanding of the underlying mechanisms of this stabilization. Using the T2-based assay, we analyzed the peptide dependent stabilization of *de novo* synthesized HLA-A02:01 by blocking its transport to the cell surface with Brefeldin A upon transfer of the samples to 37° C. Here, the absence or suboptimal binding of stabilizing

peptides would result in the internalization of unstable HLA molecules, resulting in an overall decrease of HLA-A02:01 surface presentation. We tested each of the eight previously identified epitopes showing the strongest MHC binding (figure 50C - E) for their capabilities of stabilizing *de novo* synthesized HLA-A02:01.

We could show that some epitopes indeed directly stabilize *de novo* synthesized HLA molecules, indicated by a decrease in HLA-A02:01 surface presentation following the addition of Brefeldin A (figure 51A and C). These effects were most prominent for the peptides SARM1_1 and AGPAT6_4 (figure 51A and C). In addition, these results show a prolonged HLA-A02:01 stabilization by some epitopes, indicating a lasting surface presentation of the respective neoepitopes (figure 51C).

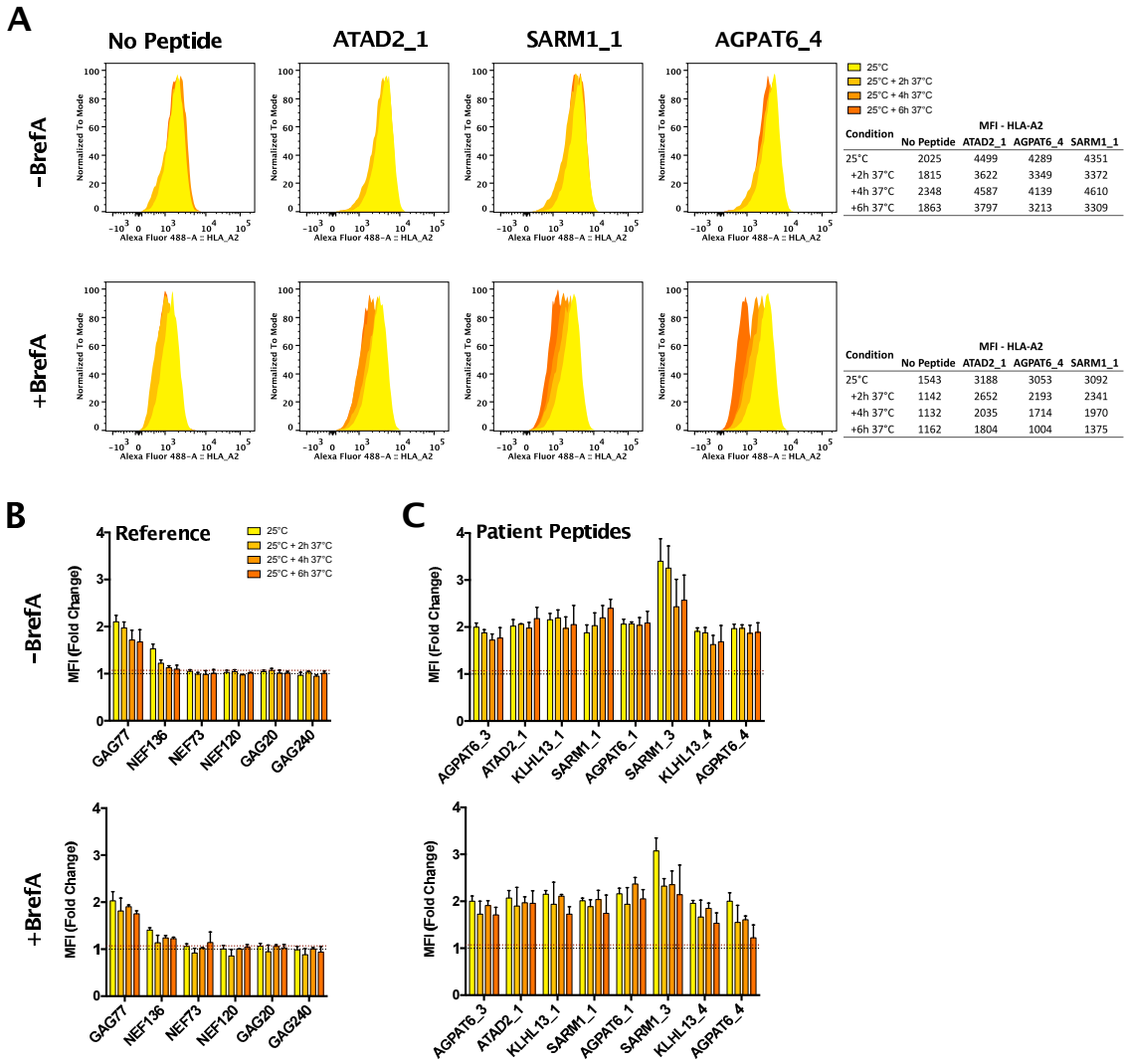

Figure 51 – Brefeldin A treatment indicates direct stabilization of *de novo* synthesized HLA-A2 by strong binding peptides. (A) Effect of HLA-A2 stabilization in DMSO and peptide samples in the absence or presence of 5 µg/ mL Brefeldin A upon increase of incubation temperature. (B and C) Effect of HLA-A2 stabilization by the control peptides (B) and selected strong binding peptides (assessed in figure 50) (C). MFI increase compared to the respective DMSO sample was used to assess HLA-A2 binding. Peptides are sorted by decreasing predicted binding affinity. Dotted lines indicate normalization to DMSO sample (black line; MFI fold change = 1) and the standard deviation of the four non HLA-A2 binding control peptides (red line; $\sigma = 0.07$). All peptides were measured as biological triplicates.

4.4.7 Detection of epitopes on xenograft derived cell lines

To validate the targeted MS-based screening approach for PDAC patient samples, we generated whole cell lysates from three PDX-derived cell lines (TIPC102_A2, 113 and 222) and gave the samples to the group of PD Dr. Dr. A. Riemer. We were not able to detect any of the in total 45 validated HLA-A02:01 binding epitopes in these samples. These results do not rule out the presence of immunogenic neoepitopes on PDAC tumor cells. The problems of epitope detection might rather result from technical issues (i.e. limit of detection by MS) in combination with low antigen abundance on the cell surface and the subsequent loss during sample processing. Moreover, the use of current standard epitope prediction algorithms (i.e. NetMHC4.0) and affinity cut-offs introduces additional limitations on the choice of epitopes screened. Therefore, the current technical issues, as well as the prediction bias, should be thoroughly revised during future applications of the targeted proteomics pipeline.

5 Discussion

Pancreatic cancer still forms a disease with no cure available. Currently the majority of pancreatic cancer patients experiences relapse within less than 24 months post surgery and ultimately succumbs to the disease [38, 39]. The limited progression in increasing the overall survival of PDAC patients by various treatment regimen reveals a high unmet medical need to combat this malignancy.
In this context, the increasing clinical relevance of neoepitope specific T cell therapies against various solid malignancies, including those with low mutational burden, represents a promising approach for the treatment of PDAC [142–145, 264]. Still, it should be kept in mind that, while the specificity of neoepitope reactive T cells appears highly effective, targeting single epitopes in the context of MHC-I antigen presentation likely results in immunoediting and leads to escape by the tumor due to selective pressure [144]. Therefore, the use of multi-epitope reactive T cells, including both $CD4^+$ and $CD8^+$ cells, could offer a remedy to the single epitope immune evasion [253]. In this context, especially the use of multi-epitope RNA vaccination was shown to be effective in suppressing disease recurrence in metastatic melanoma [176]. This approach might also be considered to counter tumor recurrence in patients with primary resectable pancreatic cancer, when applied as adjuvant treatment. Nevertheless, a functional proof of TIL reactivity against characterized PDAC epitopes is still missing. The presented thesis focused on the development of screening methodologies to hopefully provide this missing information.
The implementation of an epitope screening approach for PDAC patients is supported by the recognition of autologous, xenograft-derived tumor material by *in vitro* expanded PDAC TILs [279]. Furthermore, despite the low and mainly patient specific mutational landscape, it was recently shown bioinformatically that PDAC frequently contains potentially immunogenic neoepitopes [178]. Therefore, we validated two screening methodologies, which can be applied to identify and characterize the frequency, as well as the origin of antigens recognized by PDAC TILs. Both methodologies may be employed to overcome the current lack of functional information on immunogenic antigens recognized by PDAC TILs. Taken together, this study may provide the foundation for the screening of immunogenic antigens in larger pancreatic cancer patient cohorts, facilitating insights into the applicability of antigen specific T cell therapies in the context of PDAC in the future.

5.1 Development of an expression based screening system

Until now, most studies focussed on the characterization of either MHC-I (i.e. tandem minigenes) or MHC-II (i.e. long peptides) restricted antigens recognized by the respective tumor reactive T cell population [142–145, 175]. In the context of the low mutational burden of pancreatic cancer in combination with a frequent infiltration of tumor reactive T cells, we developed a screening system capable of identifying MHC-I and MHC-II epitopes in parallel, independent of the HLA type of the patient. Furthermore, due to the restricted access to professional APCs from PDAC patients, we focussed the application of this system on using autologous TILs as APCs, as we were able to expand these to large numbers. This approach was supported by the functional expression of both, MHC-I and MHC-II, on the surface of activated human T-cells [369, 371].

We developed an expression-based screening system based on the protein Lamp1, since it was previously shown that full length chimeric Lamp1:antigen proteins are able to induce antigen specific $CD4^+$ T cell responses [362]. However, this rendered the risk that MHC-I epitopes could be missed, as the introduced antigens may preferably be processed through the MHC-II pathway. Working from here, the modification of two candidate residues in its transmembrane domain led to a destabilization of Lamp1, increasing the presentation of incorporated MHC-I restricted epitopes, while keeping the MHC-II antigen presentation functional (figure 29). We showed that these TMD destabilizing mutations induced a disruption of subcellular Lamp1 trafficking through the golgi network (figure 42). Thus, we could increase the MHC-I antigen presentation by destabilization of the Lamp1 transmembrane domain, which was likely induced by an increased ER associated degradation (i.e. by intramembrane proteases [366]) of the protein. Furthermore, our single mutant construct Lamp1_Mut395 was the most robust in simultaneous MHC-I and MHC-II antigen presentation (table 44) and was therefore used for patient epitope screenings.
In addition, our Lamp1 screening approach appeared equally potent in shuttling antigens into both, the MHC-I and MHC-II presentation pathway, compared to a RNA vaccine construct recently published by Sahin and coworkers [176, 253] (figure 37 and 38).
We futher compared the functionality of the Lamp1 system with short (core epitopes) and long synthetic peptides (30mer) loaded onto APCs. Here, we were able to highlight the advantage of an expression-based screening approach over an approach focussing on synthetic peptides (figure 39 and 40). While the use of synthetic peptides to screen for MHC-II restricted antigens seems feasible, it appears suboptimal for screening MHC-I restricted epitopes, especially, when using suboptimal or long peptides during these approaches, as potential antigen specific responses could be missed (figure 39).
Because of the afore-mentioned clinical relevance of mutation derived epitopes as targets of TIL reactivity [142–145, 176], we focussed our screening approach on expressed neoepitopes identified by exome and transcriptome analyses of the primary tumor, as well as low passage patient derived xenografts. Furthermore, we chose to work with *in vitro* expanded TILs as responder populations, as these populations were previously described to recognize their autologous tumor [279] and currently form the most commonly used population for adoptive T cell therapy [142, 144, 145, 261, 264, 358]. For the small cohort used in this work, we could only detect weak to no recognition of the autologous tumor by the TILs (figure 33 - 35). Furthermore, we were not able to show TIL reactivity against any of the mutations encoded by the expression based system (figure 33 - 35).
Taken together, these results indicate certain considerations need to be taken into account for future applications of the expression based screening system. On the one hand, bulk expanded TILs might not yield the optimal material to screen for neoepitope specific responses. Here, insights into the initial T cell repertoire within the primary tumor, focussing on the identification of tumor reactive T cell receptors of large T cell clones, might yield greater success to later identify the recognized epitopes. In addition, a loss of large tumor reactive T cell clones during unspecific *in vitro* expansion would further support such an approach [279, 376]. On the other hand, keeping in mind the overall low frequency of tumor reactive TILs ($\approx$1%) in the expanded population [279], the sole focus on mutation derived epitopes might be another reason for the poor screening outcome within this study. For future large scale screening approaches

one should further consider taking into account additional sources of antigens, such as InDels (base insertion/ deletion) [377, 378], over-expressed self-antigens [172, 247, 264], as well as cancer testis antigens, and epitopes derived from RNA editing [379–383] and peptide splicing [384–387], as these yield additional potential targets of TIL reactivity in the context of PDAC and other cancers.

5.2 Using targeted proteomics to identify PDAC neoepitopes

Another key question to be answered in the context of PDAC is the tumors capability to present mutation-derived epitopes. One way to address this question is the direct characterization of neoantigens presented on the surface of tumor cells using mass spectrometry. In combination with exome-based *in silico* epitope prediction, it is now possible to detect neoepitopes presented on the cell surface by targeted mass spectrometry [179–181, 357, 388]. In order to apply these findings to pancreatic cancer, we established a pipeline based on the targeted identification of previously predicted, mutation derived epitopes. Even though, pancreatic cancer was previously bioinformatically described to frequently yield potential neoepitopes, the overall cell surface abundance of these is currently not known [178].
Therefore, we validated a streamlined mass spectrometry pipeline, based on known control epitopes (figure 44 and 46), which can be applied to directly identify PDAC epitopes.
Following the basic workflow validation by the melanoma epitopes, we identified a small cohort of four PDAC patients for an initial application of the pipeline. For the screening of patient-derived material, however, the initial pipeline had to be adapted to include the validation of HLA-A02:01 surface presentation and upregulation by IFNγ on the tumor cells (figure 47), as well as validation of cell line purity (figure S7) and the presence of mutations after xenograft passaging (table S14 - S17). We could validate HLA-A02:01 binding for the majority of the predicted epitopes, with a minor fraction of the epitopes revealing strong and lasting HLA-stabilization (figure 49 and 50). Deeper characterization of the strongest HLA-A02:01 binding patient epitopes (figure 50) indicated a direct binding and stabilization of *de novo* synthesized MHC molecules on the cell surface (figure 51). The final targeted mass spectrometry screening of PDAC epitopes from three patients did not confirm HLA-A02:01 surface presentation for any of the peptides tested. This result does not rule out the presence of immunogenic antigens on the surface of PDAC cells, but merely indicates the need of further optimization of the protocols procedure.
Here, several adaptations should be considered: First of all, we validated the presence of each mutation in the respective patient cell line on the DNA level. However, silencing of mutated loci is missed with this approach, resulting in unnecessary screening of unexpressed mutations. Thus, it might be worthwhile to include a mutation validation on the RNA level, to ensure functional expression of the respective mutations in each cell line and thus only screen for mutations truly expressed. In addition, we validated the targeted mass spectrometry sensitivity on over-expressed epitopes, that may not represent physiological antigen abundance within a cell line. Thus, the sensitivity of the mass spectrometry protocol should be further refined with a cell line expressing known immunogenic epitopes. Here, especially the patient-derived melanoma cells expressing the three melanoma epitopes used for validation of this targeted proteomics pipeline would be of interest [325], as these cells were shown to induce antigen specific T cell

activation against physiological levels of the respective epitopes. This readout would in the end yield the necessary information on the sensitivity of the targeted proteomics approach in the context of physiological levels of known immunogenic epitopes.
Taken together, we show the development of a pipeline that can be applied to directly identify antigens on the surface of xenograft-derived cell lines. By implementing a first proof of principle approach, using over-expressed melanoma antigens, we carefully monitored each step necessary for a streamlined and straight forward screening of patient-derived antigens. An application of this pipeline to a small patient cohort revealed certain issues (i.e. immune editing, detection sensitivity) and chances for improvement, that should be kept in mind and tested in future screenings. Furthermore, the protocol implemented here might allow for the functional characterization of the origin (e.g. mutation-derived or over-expressed self antigens), as well as frequency, of potentially immunogenic antigens in the context of PDAC.

5.3 Concluding remarks and Outlook

In summary, we show the development of an expression-based screening system with the advantage of an HLA independent, simultaneous identification of MHC-I and MHC-II restricted epitopes in a fully autologous system. In addition, this methodology has the advantage of an unbiased screening for immunogenic epitopes, independent of artificial epitope prediction algorithms. Moreover, we describe an initial protocol including the minimum prerequisites needed for the screening of an enlarged patient cohort. It should be noted that the negative results during the screening of the initial small patient cohort in this work do not rule out the general recognition of tumor-derived antigens by PDAC TILs. These results merely emphasize the complexity and difficulty of identifying targets of TIL reactivity in the context of PDAC.
The presented work highlights that *in vitro* expanded PDAC TILs may not represent an optimal T-cell population to characterize immunogenic target antigens in PDAC. Here, using single cell cloned TCRs from primary PDAC tissue instead might, indeed, be a more promising approach, as these TCRs resemble the initial T-cell repertoire more accurately. In this case the most dominant T-cell clones would be of special interest, as they are most likely to be tumor reactive. Furthermore, a combination of cloned TCRs showing reactivity against their autologous tumor with the expression-based screening might then reveal the functional proof of concept currently needed to move forward with a T-cell based therapy for PDAC patients. However, even if these *in vitro* experiments yield positive results, they do not provide information on PDAC directed T-cell responses in a complex tumor microenvironment. For this, a pre-clinical *in vivo* assessment of TCR functionality against the autologous tumor (e.g. PDX model) would probably achieve the most reliable results. Assuming these pre-clinical experiments are successful, the next step would be to assess the safety of the most dominant TCR clones in a small patient cohort to monitor the frequency of potential off-target effects (e.g. self-antigen reactivity). The results of such a trial will be crucial to apply a T-cell based therapy to a greater cohort of PDAC patients. Importantly, since the short therapeutic window for PDAC patients might not allow for an epitope characterization prior to the start of the treatment. Nevertheless, once the chosen TCRs appear to induce tumor regression or disease stabilization, the antigen identification might be performed afterwards.
In conclusion, the pipelines and screening modalities developed in the course of the presented

thesis may be applied to achieve further insight into and functional proof of the antigens recognized by PDAC TILs, therefore laying the foundation for the functional applicability of T-cell based therapy in PDAC patients.

6 Supplementary Data

6.1 Patient characteristics

6.1.1 General information

Table S1 – Patient characteristics of the cohort used for this study. *Tumor content of the tissue sample received for xenograft generation and TIL expansion. T cell tumor infiltrate calculations, based on immunohistochemistry stainings, were kindly provided by C. Lauenstein, as previously described [279].

Patient	Gender	Diagnosis (Location)	TNM-Stage	Grade	R-classification	Neoadjuvant	Tumor Content* [%]	T cell tumor infiltrate		
								CD3/mm^2	CD8/mm^2	FoxP3/mm^2
079	female	PDAC (whole organ)	T3/N1/M0	N/A	R1	Chemo	95	256.56	42.82	103.38
091	male	PDAC (whole organ)	T3/N1/M0	G2	R1	—	100	162.96	101.06	18.85
102	female	PDAC (whole organ)	T3/N3/M1	G2	R1	—	65	262.46	14.73	71.11
113	male	PDAC (tail)	T3/N0/M1	G2	R0	—	90	222.96	44.36	173.66
222	male	PDAC (head)	T3/N3/M0	G3	R1	—	50	438.35	378.42	358.50
236	female	PDAC (whole organ)	T3/N3/M1	G2	R1	—	100	280.83	3.31	N/A
253	male	PDAC (tail)	T3/N3/M0	G3	R1	—	100	N/A	5.56	6.57
275	female	PDAC (head)	T3/N3/M0	G3	R1	—	90	374.88	21.29	247.98

6.1.2 Patient HLA Typing

Table S2 – HLA typing of the patient cohort used for this work. Allele 1 and 2 represent the most likely HLA-alleles of the patient. p-value indicates the confidence score of correct read mapping between the true HLA allele and background noise. Values converging to 0 represent an increase in confidence. N/A = reads could not be mapped to a specific HLA allele above background.

Patient			Allele 1	p-value	Allele 2	p-value
TIPC079	MHC-I	A	A*03	6.65e-05	A*02	0.00614
		B	B*18	0.00146	B*35	0.03462
		C	C*04	2.57e-06	C*12	0.29450
	MHC II	DQA	A1*01	1.29e-12	A1*05	0.32802
		DQB	B1*05	0.05419	B1*03	0
		DRB	B1*01	0.00095	B1*11	0.13036
TIPC091	MHC-I	A	A*34	0.00196	A*11	0.00661
		B	B*35	5.67e-05	B*07	0.02532
		C	C*04	0.00221	C*15	0.03976
	MHC II	DQA	A1*05	0.18852	A1*01	0.24163
		DQB	B1*02	0.00557	B1*05	0.24548
		DRB	B1*03	0.01622	B1*01	0.05113
TIPC102	MHC-I	A	A*25	1.748e-09	A*02	0.00420
		B	B*39	0.00017	B*13	1.68e-05
		C	C*06	0.01815	C*12	0.12397
	MHC II	DQA	A1*05	0.06901	A1*01	0.32802
		DQB	B1*02	0.01256	B1*05	0.42202
		DRB	B1*03	0.07152	B1*01	0.08453
TIPC113	MHC-I	A	A*25	0.00047	A*02	0.00762
		B	B*13	8.90e-12	B*27	0.00012
		C	C*01	0.07024	C*02	0.01983
	MHC II	DQA	A1*01	7.15e-05	A1*02	0.24175
		DQB	B1*02	0.01707	B1*05	0.32804
		DRB	B1*01	0.00285	B1*07	0.01430
TIPC222	MHC-I	A	A*01	1.70e-05	A*02	0.02454
		B	B*08	0.07709	B*39	0.00856
		C	C*12	0.00505	C*07	0.02530
	MHC II	DQA	A1*01	6.83e-12	A1*05	0.32899
		DQB	B1*05	0.01226	B1*02	0.42202
		DRB	B1*16	0.07197	B1*03	0.08998
TIPC236	MHC-I	A	A*03	0.00042	A*02	0.02379
		B	B*27	0.00279	B*07	0.00264
		C	C*02	4.12e-03	C*07	0.02582
	MHC II	DQA	A1*01	2.33e-09	A1*04	0.53423
		DQB	B1*06	0.00568	B1*04	0.42202
		DRB	B1*08	0.31896	B1*15	0.09091
TIPC253	MHC-I	A	A*24	0.01071	A*02	0.01354
		B	B*13	2.42e+00	B*58	0.00182
		C	C*06	0.01283	C*03	0.03700
	MHC II	DQA	A1*01	0.01054	A1*02	0.32802
		DQB	B1*05	0.00051	B1*02	0
		DRB	B1*01	0.00060	B1*07	0.20127
TIPC275	MHC-I	A	A*01	0.00155	A*29	0.13250
		B	B*08	2.73e-05	B*08	0.00906
		C	C*07	0	C*07	0.00011
	MHC II	DQA	A1*05	0.00063	A1*05	0.05748
		DQB	B1*02	N/A	B1	N/A
		DRB	B1*03	7.17e-08	B1*12	0.62962

6.1.3 Composition of bulk expanded TILs

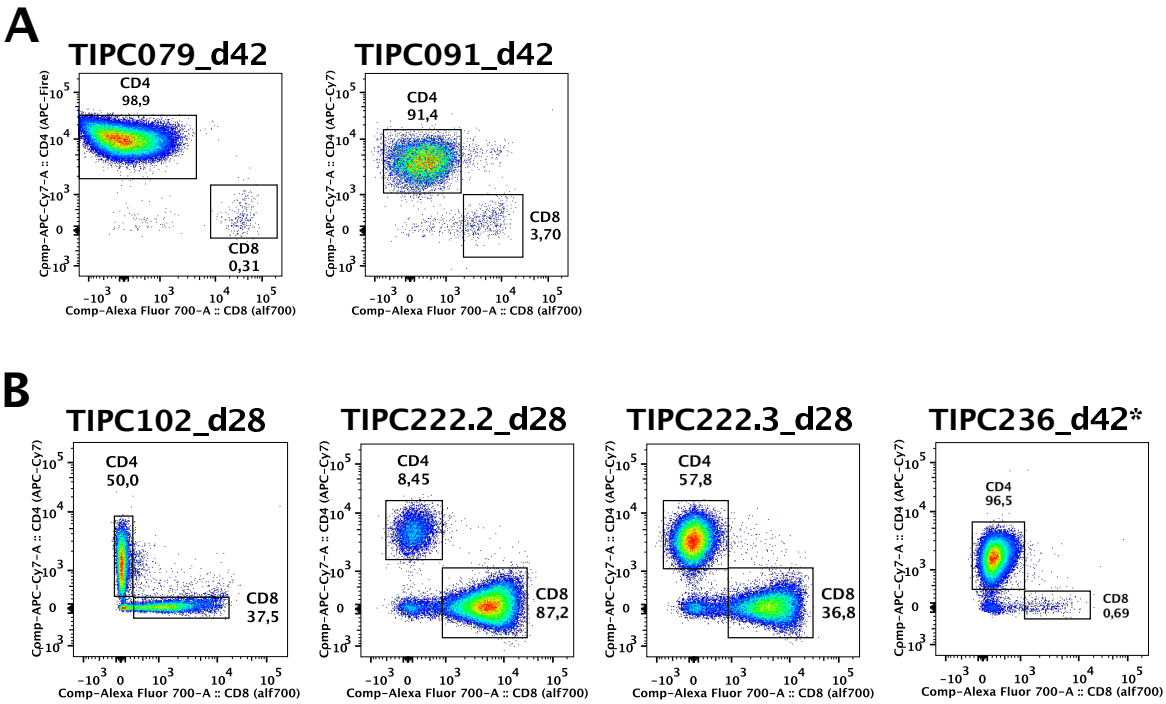

Figure S1 – CD4⁺/ CD8⁺ composition of bulk expanded TIL populations (d28/42 = TILs expanded for 28 or 42 days) used during this study. (A and B) Patient TILs used to establish the expression based screening pipeline (A) and screen for neoepitope reactivity (B). Stainings were performed using the T cell panel. *For TIPC236 the data of d28 bulk expanded cells was unfortunately lost and could not be restored without unnecessary thawing of patient material.

6.1.4 Exome and transcriptome analyses

Table S3 – Expressed mutations identified from the exome and transcriptome data of TIPC102. Highlighted amino acid in mutated sequence indicates the position of the mutated residue. *indicates the first or last amino acid residue of the respective protein.

Gene	Mutation	NCBI Reference	Mutation Location	Mutated sequence	Tumor MAF exome	PDX MAF exome	RNASeq MAF (read count)	Expression percentile (GDS4336)
ADCY6	G535V	NM_015270	chr12:49170065	TLQYLNGDYEVEPGRVGERNAYLKEQHIET	0.221	0.478	89% (8 of 9 reads)	81st
ALDH16A1	R493Q	NM_153329	chr19:49967929	PDGLYEYLRPSGTPAQLSCLSKNLNYDTFG	0.193	0.345	2 mutant reads	57th
ATAD2	R913C	NM_014109	chr8:124351668	KPHSALPEEVQELFICDYGEIFNVQLPDKE	0.190	0.422	42% (39 of 92 reads)	75th
CCDC71	R269Q	NM_022903	chr3:49200836	HQSKTNRATGSPSVRQMKGGSALGTKTAQA	0.191	0.355	50% (1 of 2 reads)	70th
CDC16	L447V	NM_003903	chr13:115027386	IKAIGNEVTVDKWEPVLNNLGHVCRKLKKY	0.416	0.996	100% (99 mutant reads)	92nd
DNM3	R369H	NM_015569	chr1:172011262	LELSGGAKINRIFHEHFPFEIVKMEFNEKE	0.154	0.620	75% (3 of 4 reads)	44th
DOCK1	E1316K	NM_001380	chr10:129201400	AEQYENEMFDYEQLSKLLKKQAQFYENIVK	0.223	0.571	52% (25 of 48 reads)	91st
DTNBP1	A123V	NM_032122	chr6:15615618	IADLESMTANLTHLEVSFEEVENNLLHLED	—	0.979	90% (9 of 10 reads)	83rd
FILIP1L	F109V	NM_182909	chr3:99648801	KAEKMDLALLEAQYGVVTPKKVLEALQRDA	0.159	0.646	71% (5 of 7 reads)	64th
FOXJ2	D4G	NM_018416	chr12:8192439	*MASGLESSLTSIDWLPQL	0.217	0.538	47% (9 of 19 reads)	31st
GBAS	G203D	NM_001483	chr7:56052562	ELRSYQLRPGTMIEWDNYWARAIRFRQDGN	—	0.289	26% (14 of 54 reads)	83rd
GNG2	P60L	NM_053064	chr14:52433368	AKEDPLLTPVPASENLFREKKFFCAIL*	0.248	0.460	1 mutant read	60th
KRAS	G12D	NM_004985	chr12:25398284	*MTEYKLVVVGADGVGKSALTIQLIQNHFVD	0.228	0.495	40% (22 of 55 reads)	89th
LIMCH1	T760K	NM_014988	chr4:41673607	NSQVDSPSSEKSPVMKPQFKFWAWDPEEER	—	0.592	53% (24 of 45 reads)	61st
LPIN1	M78I	NM_145693	chr2:11907930	KVVDIEINGESVDLHIKLGDNGEAFFVQET	—	0.253	14% (6 of 42 reads)	84th
LRP12	R330H	NM_013437	chr8:105509791	VKIYDGLEENPHKLLHVLTAFDSHAPLTVV	—	0.300	75% (3 of 4 reads)	75th
MAP2K4	G294R	NM_003010	chr17:12028677	ASRQGYDVRSDVWSLRITLYELATGRFPYP	0.369	1.00	100% (23 mutant reads)	76th
NFKBIZ	G405E	NM_031419	chr3:101572584	MASDSSNTSLPFSNMENPMNTTQLGKSLFQ	0.212	0.621	76% (77 of 101 reads)	93rd
NR1I2	G36R	NM_003889	chr3:119526203	ESVPGKPSVNADEEVRGPQICRVCGDKATG	—	0.249	5% (1 of 20 reads)	48th
NSD1	L2063F	NM_022455	chr5:176715855	IKAGTELTFNYNLECFGNGKTVCKCGAPNC	0.208	0.477	46% (32 of 70 reads)	87th
RASSF6	A238V	NM_177532	chr4:74447542	KIENSPQDFALHIIFVTGEQRRLKKTDIPL	0.235	0.635	60% (76 of 126 reads)	62nd
SRGAP2D	Q97R	NM_001271887	chr1:121116733	RQAKYTENKLKAIKARNEYLLALEATNASV	—	0.107	55% (12 of 22 reads)	97th

Table S4 – Expressed mutations identified from the exome and transcriptome data of TIPC113. Highlighted amino acid in mutated sequence indicates the position of the mutated residue. *indicates the first or last amino acid residue of the respective protein.

Gene	Mutation	NCBI Reference	Mutation Location	Mutated sequence	Tumor MAF exome	PDX MAF exome	RNASeq MAF (read count)	Expression percentile (GDS4336)
ABCA12	Y629C	NM_015657	chr2:215866305	AAKTIDEMEREAKRLCKSNELPGSVIFKLP	0.093	0.455	1 mutant read	32nd
AGMO	P414L	NM_001004320	chr7:15405161	MFLMLYRFGHLKPLVLSLSSAFEIVFSICI	0.079	0.274	14% (2 of 14 reads)	44th
ANXA2	T208N	NM_004039	chr15:60644641	QDARDLYDAGVKRKGNDVPKWISIMTERSV	—	0.424	51%(2278 of 4455 reads)	99th
BRAT1	L168R	NM_152743	chr7:2583524	QGDSSLFVASAASQLRVHVLALSMRGGAEG	—	0.624	73%(8 of 11 reads)	60th
CDH1	R90W	NM_004360	chr16:68835677	FKVGTDGVITVKRPLWFHNPQIHFLVYAWD	—	0.034	12%(134 of 1097 reads)	95th
CDKN2A	P114R	NM_000077	chr9:21971017	RAGARLDVRDAWGRLRVDLAEELGHRDVAR	0.120	1.00	100%(7 of 7 reads)	51st
DCAF6	A242V	NM_018442	chr1:167962500	RATGNYAGRGTTGMVVRFIPSHLNNKSCRV	0.100	0.286	38%(106 of 280 reads)	91st
FAM193B	I530V	NM_001190946	chr5:176951894	LPPSNLSGSSEQQPDVNLDLSPLTLGSPQN	0.144	0.181	20%(8 of 41 reads)	62nd
GUCY1A3	E246K	NM_000856	chr4:156632053	VEVSLMPPCFHNDCSKFVNQPYLLYSVHMK	0.120	1.00	100%(12 of 12 reads)	89th
KIFC1	P435L	NM_002263	chr6:33373176	MEGGPGGDPQLEGLILRALRHLFSVAQELS	0.110	0.404	42%(14 of 33 reads)	53rd
KLF4	W435R	NM_004235	chr9:110248169	HTGEKPYHCDWDGCGRKFARSDELTRHYRK	0.092	1.00	99%(362 of 365 reads)	76th
KRAS	G12V	NM_004985	chr12:25398284	*MTEYKLVVVGAVGVGKSALTIQLIQNHFVD	0.122	0.411	49%(69 of 142 reads)	89th
MAP6	M598T	NM_033063	chr11:75298753	DEGPMVSASVKDQGPIVSAPVKDQGPIVPA	0.108	0.518	1 mutant read	49th
NEMF	L1070F	NM_004713	chr14:50251377	LSRNIPGKVKVSAPNFLNVKRK*	0.153	0.480	54%(91 of 168 reads)	79th
PEX16	A20S	NM_004813	chr11:45939305	RLLGLRYQEYVTRHPSATAQLETAVRGFSY	0.179	0.635	50%(7 of 14 reads)	55th
PGM3	L156F	NM_015599	chr6:83892687	IDGVTVLGGQFHDYGFLTTPQLHYMVYCRN	—	0.357	39%(35 of 90 reads)	84th
RPS6KA1	D44V	NM_001006665	chr1:26872522	QTSLPVPGPGSGPQRVSDEGVLKEISITHH	—	1.00	1 mutant read	71st
SARM1	F591L	NM_015077	chr17:26715411	ASLLKVHLQLHGFSVLIDVEKLEAGKFEDK	—	0.476	52%(17 of 33 reads)	55th
TLE4	S48G	NM_007005	chr9:82188700	DRIKEEFQFLQAQYHGLKLECEKLASEKTE	—	0.989	92%(12 of 13 reads)	69th
TMC4	Y109H	NM_144686	chr19:54673367	RRAHRQRNASRDQVVHGSGTKTDRWARLLR	0.098	0.434	45%(120 of 265 reads)	83rd
TMEM8A	V416I	NM_021259	chr16:425414	TISLRANKTEMRNETIVVACVNAASPFLGF	0.110	0.529	47%(60 of 128 reads)	79th
TP53	C275Y	NM_000546	chr17:7577114	SSGNLLGRNSFEVRVYACPGRDRRTEEENL	0.177	1.00	100%(137 of 137 reads)	77th
UGT1A6	H54N	NM_001072	chr2:234601810	WLSMKDIVEVLSDRGNEIVVVVPEVNLLLK	0.100	0.437	59%(48 of 82 reads)	62nd
XPNPEP1	S548T	NM_020383	chr10:111630542	GVGSFLNVHEGPCGITYKTFSDEPLEAGMI	0.084	0.556	53%(273 of 513 reads)	93rd
ZNF28	R589Q	NM_006969	chr19:53303332	TGEKPYKCKVCDKAFQRDSHLAQHQRVHTG	—	0.103	1%(1 of 173 reads)	73rd

Table S5 – Expressed mutations identified from the exome and transcriptome data of TIPC222. Highlighted amino acid in mutated sequence indicates the position of the mutated residue. *indicates the first or last amino acid residue of the respective protein.

Gene	Mutation	NCBI Reference	Mutation Location	Mutated sequence	Tumor MAF exome	PDX MAF exome	RNASeq MAF (read count)	Expression percentile (GDS4336)
AGPAT6	T344I	NM_178819	chr8:41472545	TSVMMFKKGSFEIGAIVYPVAIKYDPQFGD	0.133	0.962	100%(388 of 388 reads)	92nd
ANKRD32	N938D	NM_032290	chr5:94030652	KEELFAITKIEDTVEDFHAQAEKHFHYQQL	0.111	0.923	100%(22 of 22 reads)	41st
ANKRD32	L1010R	NM_032290	chr5:94030869	SHKETTSVHTDWLLDRVAGNIKTLQKLPHI	0.139	0.983	100%(47 of 47 reads)	41st
AUTS2	R1154C	NM_015570	chr7:70255662	PRREHERGGHLDERECLHMLREDYEHTRLH	0,19	0.437	43%(32 of 75 reads)	60th
BARD1	R150Q	NM_000465	chr2:215646149	DAGNKKNSIKMWFSPQSKKVRYVVSKASVQ	0.163	0.359	33%(15 of 46 reads)	67th
C8orf47	P115L	NM_173549	chr8:99101589	STEKTQPGEGLEESGLPQPGGKEDAPAAEG	0.2	0.544	47%(59 of 125 reads)	51st
CACNA1C	V2052I	NM_199460	chr12:2797733	TPPATPGSRGWPPQPIPTLRLEGVESSEKL	—	0.386	50%(3 of 6 reads)	63rd
CDC27	I493P	NM_001114091	chr17:45219311	GYLALCSYNCKEAINPLSHLPSHHYNTGWV	0.082	—	0% (1 of 280 reads)	87th
CEP44	A153T	NM_001040157	chr4:175225470	SSGKSEPPLGNEKISTEAVGVDISGRFMTS	0.204	0.404	52%(38 of 73 reads)	57th
CMYA5	A3318V	NM_153610	chr5:79034541	GEGESVDHVETVGNVVMQKKAPITEDVRVA	0.14	0.967	1 mutant read	39th
CPSF1	D1275N	NM_013291	chr8:145619364	FMVDNAQLGFLVSDRNRNLMVYMYLPEAKE	0.147	0.445	39%(279 of 714 reads)	70th
CPSF2	V535F	NM_017437	chr14:92624010	TKCISTTESIEIKARFTYIDYEGRSDGDSI	0.113	0.628	53%(206 of 388 reads)	95th
CSNK1A1	E60D	NM_001892	chr5:148929688	VKLESQKARHPQLLYDSKLYKILQGGVGIP	—	0.494	52%(371 of 708 reads)	98th
DDX5	R263S	NM_004396	chr17:62499327	DEADRMLDMGFEPQISKIVDQIRPDRQTLM	0.158	0.242	20%(679 of 3456 reads)	99th
GAK	D1222V	NM_005255	chr4:843849	QDLAKDTDPLKLKLLYWIEGKERNIRALLS	—	0.231	17%(205 of 1241 reads)	81st
IL17RE	R519C	NM_153483	chr3:9956449	ALLTLLGVVLALTCRCPQSGPGPARPVLLL	0.232	0.940	99%(219 of 220)	56th
IMPA2	T143M	NM_014214	chr18:12014310	LEFGVIYHCTEERLYMGRRGRGAFCNGQRL	0.186	0.612	76%(524 of 694 reads)	69th
KDM6B	P272S	NM_001080424	chr17:7750239-	PPPPPPPPLPGLATSSPFQLTKPGLWSTLH	0.203	1.0	100%(17 of 17 reads)	67th
KLHL13	R336M	NM_033495	chrX:117043623	MPYMQPVMQSDRTAIMSDTTHLVTLGGVLR	—	0.381	64%(21 of 33 reads)	40th
KLHL13	F301S	NM_033495	chrX:117043728	LMTPQELINYVQTVDSMRTDNTCVNLLLEA	—	0.398	59%(23 of 39 reads)	40th
KPNA7	P371S	NM_001145715	chr7:98782575	PCHHIQQLLAYDVLPSLVALLKNGEFKVQK	—	0.043	8%(7 of 88 reads)	46th
KRAS	G12D	NM_033360	chr12:25398284	*MTEYKLVVVGADGVGKSALTIQLIQNHFVD	0.203	0.603	68%(315 of 461 reads)	89th
LIG1	I707B	NM_000234	chr19:48626460	EFVFATSLDTKDIEQNAEFLEQSVKDSCEG	0.226	0.985	100%(265 of 265 reads)	61st
MAPRE2	S222Y	NM_001143827	chr18:32707002	SRPSSAKRASSSSGSAYKSDKDLETQVIQLN	0.198	0.988	100%(203 of 203 reads)	83rd
N4BP2	D1482N	NM_018177	chr4:40127867	KLLKTLTASEMLPLLNHWNTQTKKVSLREI	—	0.413	46%(11 of 24 reads)	67th
PCDHGB7	D184N	NM_018927	chr5:140797976	KYQLSPNEYFSLVEKNNPDGGKYPELVLQK	0.084	0.320	28%(11 of 39 reads)	43rd
PCLO	V927M	NM_014510	chr7:82764087	ITDAPKSQPTTPQETMTGKLFGFGASIFSQ	—	0.213	2 mutant reads	34th
PDLIM1	M61V	NM_020992	chr10:97031457	IGDVITAIDGENTSNVTHLEAQNRIKGCTD	0.133	0.486	55%(460 of 840 reads)	94th
PIK3CA	I788F	NM_006218	chr3:178942555	SSAKRPLWLNWENPDFMSELLFQNNEIIFK	0.188	0.460	55%(54 of 98 reads)	92nd
PPM1D	N242S	NM_003620	chr17:58711237	RIEGLGGSVMNKSGVSRVVWKRPRLTHNGP	0.174	0.313	27%(23 of 86 reads)	68th
RALBP1	P628R	NM_006788	chr18:9535850	WRGGAVQPPRDGVLERKAAKEQPKAGKEPA	0.136	0.569	69%(153 of 223 reads)	88th
SMARCA2	R1531Q	NM_139045	chr9:2191317	SVKVKIKLNKKDDKGQDKGKGKKRPNRGKA	—	0.155	20%(76 of 376 reads)	89th
STEAP1	T64S	NM_012449	chr7:89790224	TAHADEFDCPSELQHSQELFPQWHLPIKIA	—	0.032	2%(9 of 439 reads)	66th
TP53	H20D	NM_001276699	chr17:7578395	QSQHMTEVVRRCPHDERCSDSDGLAPPQHL	0.254	0.985	99%(550 of 551 reads)	77th
TROAP	M465L	NM_005480	chr12:49724021	VGGQCVPLNGGSSLDLVELQPLLTEISRTL	—	0.344	40%(49 of 121 reads)	43rd
TSKU	T121P	NM_001258210	chr11:76507021	RLRYLESLDLSHNGLPALPAESFTSSPLSD	0.156	0.463	47%(358 of 752 reads)	89th
UQCRC2	V358L	NM_003366	chr16:21987512	QATAAGDVIKAAYNQLKTIAQGNLSNTDVQ	—	0.417	40%(602 of 1511 reads)	97th
WDR43	R252Q	NM_015131	chr2:29140767	LSGAVHDRLLNVWQVQSENKEKSAVMSFTV	—	0.193	18%(105 of 597 reads)	89th

Table S6 – Expressed mutations identified from the exome and transcriptome data of TIPC236. Highlighted amino acid in mutated sequence indicates the position of the mutated residue. *indicates the first or last amino acid residue of the respective protein.

Gene	Mutation	NCBI Reference	Mutation Location	Mutated sequence	Tumor MAF exome	PDX MAF exome	RNASeq MAF (read count)	Expression percentile (GDS4336)
CCDC88C	F27L	NM_001080414	chr14:91883162	FLQSPLVTWVKTFGPLGSGSQDNLTMYMDL	0.205	0.450	39%(21 of 54 reads)	73rd
CDKN2A	G55V	NM_001195132	chr9:21971194	APNSYGRRPIQVMMMVSARVAELLLLHGAE	0.341	0.994	99%(886 of 889 reads)	51st
CIC	R190H	NM_015125	chr19:42791588	SALPKERDSSSEKDGHSPNKREKDHIRRPM	0.364	0.609	62%(141 of 228 reads)	68th
COPS7A	T224M	NM_001164095	chr12:6839869	IESEVANLKKTIKVTMAAAAAATSQDPEQH	0,22	0.519	46%(240 of 517 reads)	80th
IGSF3	M75T	NM_001542	chr1:117158899	YLPSSPEREVQIVSTTDSSFPYAIYTQRVR	0.062	—	0% (1 of 244 reads)	48th
KCTD5	G215S	NM_018992	chr16:2752447	EFLCVVSKELHNTPYSTASEPSEKAKILQE	0.256	0.467	50%(227 of 455 reads)	79th
KRAS	G12D	NM_033360	chr12:25398284	*MTEYKLVVVGADGVGKSALTIQLIQNHFVD	0.255	0.488	42%(121 of 287 reads)	89th
LCA5	T596A	NM_001122769	chr6:80197029	RNSMEKLSKDGVDLIARKEKKANLMEQLFG	0.373	0.515	58%(22 of 38 reads)	58th
N4BP1	M173T	NM_153029	chr16:48596036	REFKQFVEAHADNYTTDLLILPTSLKKELL	0.218	0.493	48%(171 of 360 reads)	85th
PCDHGA10	A582V	NM_018913	chr5:140794487	LYPALPTDGSTGVELVPRSAEPGYLVTKVV	0.209	0.496	50%(2 of 4 reads)	43rd
PLXNB2	D766N	NM_012401	chr22:50722387	SKLHVTLYNCSFGRSNCSLCRAANPDYRCA	0.272	0.543	52%(680 of 1299 reads)	89th
PRKACB	W185S	NM_001242858	chr1:84663455	QVTDFGFAKRVKGRTSTLCGTPEYLAPEII	0.237	0.508	46%(391 of 853 reads)	81st
RBL2	V539A	NM_005611	chr16:53498193	EQDAFHRSLLACCLEAVTFSYKPPGNFPFI	0.238	0.440	52%(134 of 259 reads)	95th
RORC	R57Q	NM_005060	chr1:151789268	HYGVITCEGCKGFFRQSQRCNAAYSCTRQQ	0.292	0.480	45%(24 of 53 reads)	61st
SLC43A1	V86M	NM_001198810	chr11:57268701	QQDEMLNLGFTIGSFMLSATTLPLGILMDR	0.276	0.441	46%(11 of 24 reads)	71st
SMARCA4	G784R	NM_001128848	chr19:11123700	YNNNLNGILADEMGLRKTIQTIALITYLME	0.351	0.984	99%(243 of 245 reads)	81st
SMG7	A38T	NM_001174061	chr1:183486881	FKNQITTLQQQAKNRTNPNRSEVQANLSLF	0.233	0.500	46%(117 of 253 reads)	80th
SYBU	E423K	NM_001099752	chr8:110587860	DTMADGLSLEEQVTGKCADRELLVGDSIAN	0.242	0.424	52%(51 of 99 reads)	65th
SYNE1	A5379V	NM_033071	chr6:152640038	LTEATNHRQNIEKMAVEQKEKYLGLYTILP	—	0.404	40%(2 of 5 reads)	72nd
TGFBRAP1	T121M	NM_001142621	chr2:105924397	NLEPVPSGARIKGAAMFALNENPVSGDPFC	—	0.090	20%(14 of 71 reads)	73rd
TNXB	G3330R	NM_019105	chr6:32016191	VSGLDPARKYKFLLFRLQNGKRHGPVPVEA	0.303	0.448	25%(1 of 4 reads)	51st
TP53	H20R	NM_001276699	chr17:7578394	KQSQHMTEVVRRCPHRERCSDSDGLAPPQH	0.406	0.992	10%(164 of 164 reads)	77th
WDR45B	D86G	NM_019613	chr17:80585155	GGKKPKYPPNKVMIWGDLKKKTVIEIEFST	0.235	0.427	47%(642 of 1359 reads)	94th

6.2 Expression based screening system

6.2.1 Validation of Lamp1 functionality in human B cells

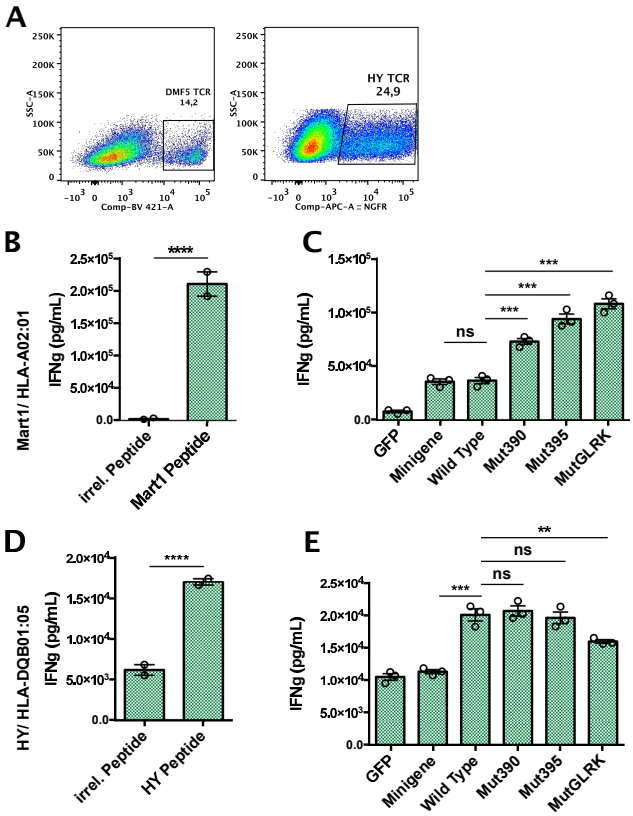

Figure S2 – Validation of Lamp1 functionality in human B cells. (A) Transduction efficiency of both antigen specific TCRs into donor PBMC. Detection of DMF5 TCR transduction efficiency was performed using an α-mouseTCR-β_BV421 antibody. HY TCR transduction efficiency was assessed by expression of truncated NGFR using a α-NGFR_APC antibody. Both TCRs shown in the $CD3^+$ population (B/D) Antigen specific activation of TCR transduced PBMCs for the DMF5 TCR (B) and HY TCR (D). Untransfected B cells (KBV623) were pulsed with 10 µg/mL of the respective, synthetic peptide. Irrelevant peptide either represented HY peptide (B) or Mart1 peptide (D). (C/E) Influence of the Lamp1 expression system and minigene on MHC-I (C) and MHC-II (E) restricted antigen specific T cell activation. Co-incubation was performed using $0.5x10^4$ TCR transduced PBMCs and $1x10^5$ of Lamp1 transfected B cells per sample. T cell activation was assessed by ELISA in technical triplicates. Lamp1 was introduced into the B cells by electroporation. Shown is one representative experiment of n = 3 biological replicates. Statistical analysis of the peptide results was performed using an unpaired t-test, while for the Lamp1 samples a One-way ANOVA with post-hoc Tukey's multiple comparisons test was used.

6.2.2 Setup of Lamp1 multi-epitope constructs

The Lamp1 multi-epitope encoding constructs were designed by first fusing the sequences found in table S3, S5 and S6 head-to-tail, followed by introducing the resulting tandem constructs into the Lamp1_Mut395 screening system as depicted in figure 30. For TIPC113 no constructs were generated, since bulk expanded TILs from this patient neither recognized the autologous xenograft, nor the PDX derived cell line.

Table S7 – Lamp1 tandem construct setup for TIPC102. Indicated are the respective positions of each mutation in the final construct. The indicated mutations are encoded by the mutated sequences found in table S3.

Tandem Construct	Encoded mutations (by position)					
	1	2	3	4	5	6
1	ADCY6_G535V	ALDH16A1_R493Q	ATAD2_R913C	CCDC71_R269Q	CDC16_L447V	DNM3_R369H
2	FOXJ2_D4G	DOCK1_E1316K	DTNBP1_A123V	FILIP1L_F109V	GBAS_G203D	GNG2_P60L
3	KRAS_G12D	LIMCH1_T760K	LPIN1_M78I	LRP12_R330H	MAP2K4_G294R	NFKBIZ_G405E
4	NR1I2_G36R	NSD1_L2063F	RASSF6_A238V	SRGAP2D_Q97R	—	—

Table S8 – Lamp1 tandem construct setup for TIPC222. Indicated are the respective positions of each mutation in the final construct. The indicated mutations are encoded by the mutated sequences found in table S5.

Tandem Construct	Encoded mutations (by position)					
	1	2	3	4	5	6
1	AGPAT6_T344I	ANKRD32_N938D	ANKRD32_L1010R	AUTS2_R1154C	BARD1_R150Q	C8orf47_P115L
2	CACNA1C_V2052I	CEP44_A153T	CMYA5_A3318V	CPSF_D1275N	CPSF2_V535F	CSNK1A1_E60D
3	DDX5_R263S	GAK_D1222V	IL17RE_R519C	IMPA2_T143M	KLHL13_R336M	CDC27_I493P
4	KRAS_G12D	KDM6B_P272S	KLHL13_F301S	KPNA7_P371S	LIG1_I707N	—
5	MAPRE2_S222Y	N4BP2_D1482N	PCDHGB7_D184N	PCLO_V927M	PDLIM1_M61V	—
6	PIK3CA_I788F	PPM1D_N242S	RALBP1_P628R	SMARCA2_R1531Q	STEAP1_T64S	—
7	TP53_H20D	TROAP_M465L	TSKU_T121P	UQCRC2_V358L	WDR43_R252Q	—

Table S9 – Lamp1 tandem construct setup for TIPC236. Indicated are the respective positions of each mutation in the final construct. The indicated mutations are encoded by the mutated sequences found in table S6.

Tandem Construct	Mutation position in the construct					
	1	2	3	4	5	6
1	KRAS_G12D	CCDC88C_F27L	CDKN2A_G55V	CIC_R190H	COPS7A_T224M	KCTDS_G215S
2	LCA5_T596A	N4BP1_M173T	PCDHGA10_A582V	PLXNB2_D766N	PRKACB_W185S	RBL2_V539A
3	RORC_R57Q	SLC43A1_V86M	SMARCA1_G784R	SMG7_A38T	SYBU_E423K	SYNE1_A5379V
4	TGFBRAP1_T121M	TNXB_G3330R	TP53_H20R	WDR45B_D86G	IGSF3_M75T	—

6.2.3 Screening of patient derived constructs

The remaining screening results of samples where a duplicate measurement yielded conclusive results are given in the following figures. For TIPC222 the repeated screening was inconclusive, as the responder TIL samples revealed reactivities indistinguishable from remaining signals. Thus, this approach was not included in this work.

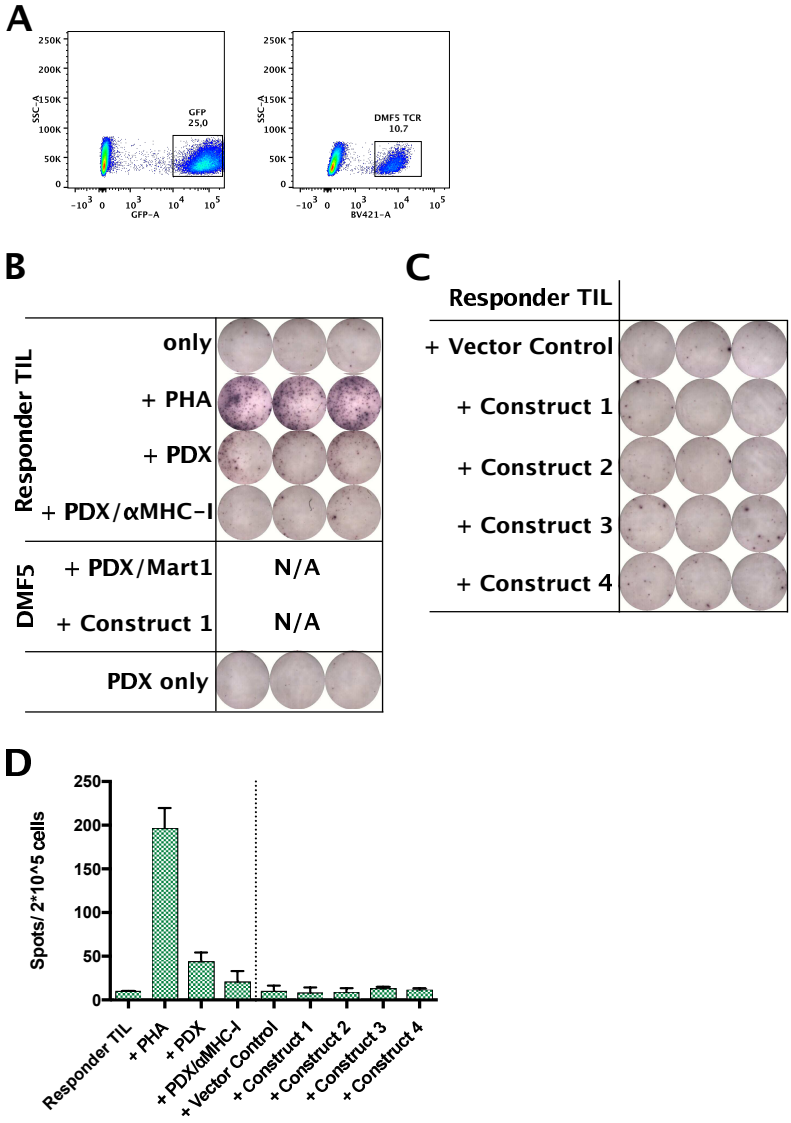

Figure S3 – Additional screening for patient specific neoepitope reactivity by bulk expanded TILs from patient TIPC102. (A) Transduction efficiency assessment of TIPC102 autologous APCs and DMF5 TCR transduced TILs. A combination of GFP and DMF5 TCR served as rough indicator for overall transduction efficiency during the experiments. (B and C) Assessment of responder TIL reactivity by IFNγ ELISpot. (B) Control samples monitoring the background reactivity and general T cell functionality after unspecific activation with PHA. In addition, reactivity against the autologous xenograft was assessed. PDX = autologous xenograft. PDX/αMHC-I = MHC-I blocked autologous xenograft. (C) Screening for responder TIL reactivity against Lamp1 construct expressing autologous APCs. Vector Control = Lamp1_Mut395 screening construct without patient mutations. Construct 1 - 4 = Patient mutation encoding Lamp1 constructs. (D) Spot count for each technical triplicate during one experiment. The screen was performed as biological duplicate. Statistical analysis of results was performed using a One-way ANOVA with post-hoc Tukey's multiple comparisons test.

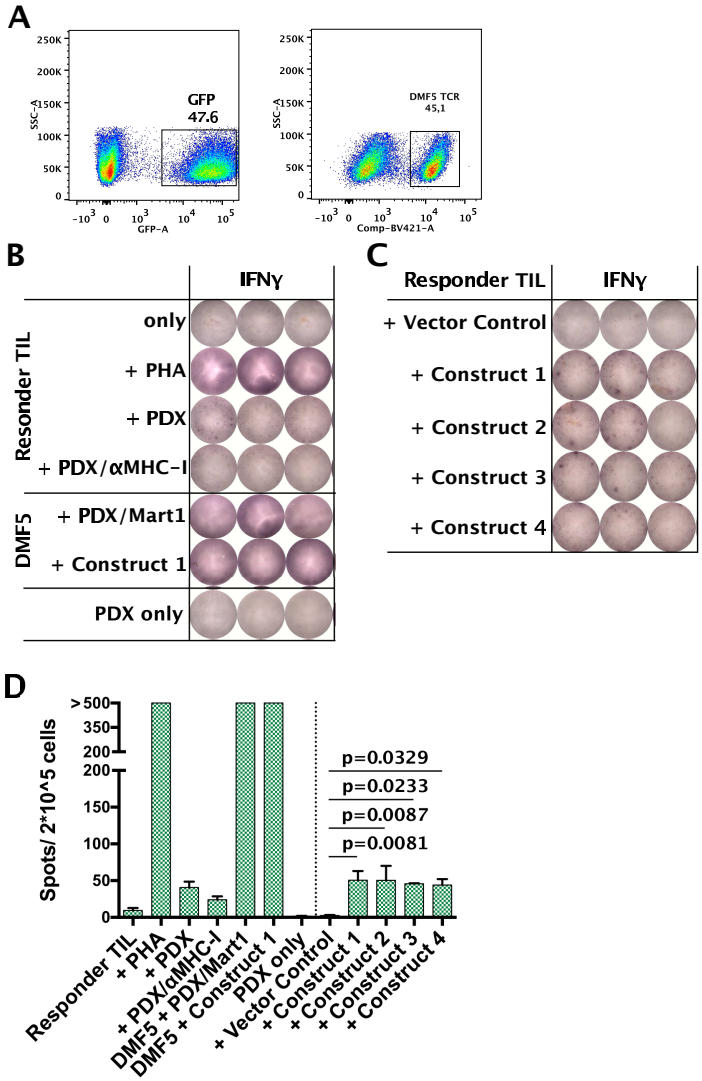

Figure S4 – Additional screening for patient specific neoepitope reactivity by bulk expanded TILs from patient TIPC236. (A) Transduction efficiency assessment of TIPC236 autologous APCs and DMF5 TCR transduced TILs. A combination of GFP and DMF5 TCR served as rough indicator for overall transduction efficiency during the experiments. (B and C) Assessment of responder TIL reactivity by IFNγ and TNFα ELISpot. (B) Control samples monitoring the background reactivity and general T cell functionality after unspecific activation with PHA. In addition, reactivity against the autologous xenograft was assessed. Mart1 TCR (DMF5) transduced TILs were used to monitor functional antigen presentation and presence of each Lamp1 construct. Functionality of the DMF5 TCR was assessed by pulsing the xenograft with Mart1 peptide. PDX = autologous xenograft. PDX/αMHC-I = MHC-I blocked autologous xenograft. PDX/Mart1 = Mart1 peptide pulsed (Mart1 – ELAGIGILTV), autologous xenograft. (C) Screening for responder TIL reactivity against Lamp1 construct expressing autologous APCs. Vector Control = Lamp1_Mut395 screening construct without patient mutations. Construct 1 - 4 = Patient mutation encoding Lamp1 constructs. (D) Spot count for each technical triplicate during one experiment. The upper default detection limit of the counting software was 500 spots/ well. The IFNγ ELISpot was performed as biological duplicate. The TNFα ELISpot was measured once, in parallel with the second IFNγ ELISpot screening, to further evaluate reactivities seen in the IFNγ readout. Statistical analysis of results performed using a One-way ANOVA with post-hoc Tukey's multiple comparisons test.

6.2.4 Assessment of Lamp1 transduction efficiency by 3xFLAG tag

Initially the 3xFLAG tag included in our Lamp1 screening system was supposed to serve as a transfection or transduction marker. However, we were not able to reliably detect Lamp1 after introduction into the cells. An initial attempt to stain the 3xFLAG tag intracellularly could not indicate any Lamp1 population (figure S5).
Considering that Lamp1 could potentially traffic throughout the cell, we expected it to also reach the cell surface. Therefore, we later performed a surface staining, that appeared to detect a small portion of introduced Lamp1 control vector (figure S6A). Nevertheless, this population decreased after the introduction of patient derived tandem constructs (figure S6B).

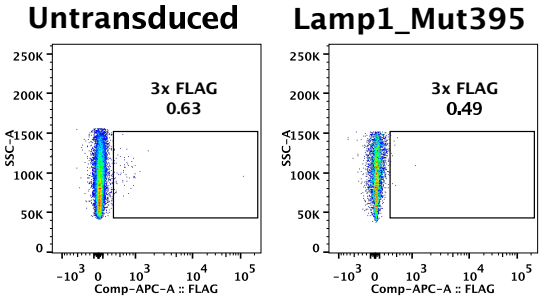

Figure S5 – Assessment of Lamp1 transduction efficiency by intracellular staining. Lamp1_Mut395 was transduced into TILs from patient TIPC079. 3xFLAG tag staining was performed by intracellular staining. The experiment was performed as biological triplicate.

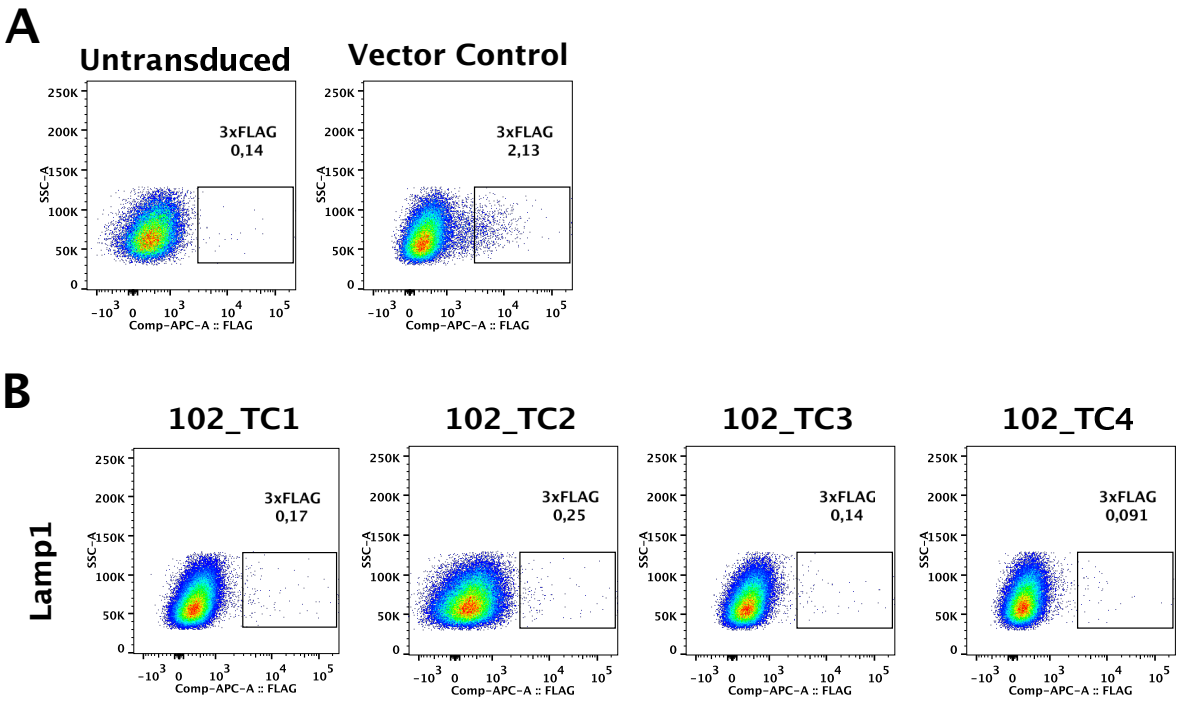

Figure S6 – Assessment of Lamp1 transduction efficiency by surface staining. (A) Control samples. Vector control = Lamp1_Mut395 empty construct (see figure 30). (B) Lamp1 tandem construct transduction efficiency. 3xFLAG tag staining was performed on the cell surface. Here, tandem constructs from TIPC102 were used. All constructs were transduced into TILs from patient TIPC079. The experiment was performed as biological triplicate.

6.3 Targeted proteomics

6.3.1 Prediction of HLA-A02:01 binding epitopes from patient samples

Table S10 – HLA-A02:01 epitope prediction for expressed mutations of patient TIPC102. Mutated positions are highlited in bold & underlined. Peptides sorted by predicted binding affinity of the mutated epitope to HLA-A02:01. The respective peptide name is derived from the mutated gene followed by an arbitrary running number.

Peptide name	Sequence	Length	Predicted affinity [nM]		RNASeq MAF & Read Count	Expression percentile (GDS4336)
			mutated	wild type		
FILIP1L_1	ALLEAQYG**V**	9	4.3	320.4	71% (5 of 7 reads)	64th
FILIP1L_2	LALLEAQYG**V**	10	22.1	2555.3	71% (5 of 7 reads)	64th
FILIP1L_6	ALLEAQYG**V**V	10	28.9	14.2	71% (5 of 7 reads)	64th
ATAD2_1	FI**C**DYGEIFNV	11	32.2	39.4	42% (39 of 92 reads)	75th
FILIP1L_3	LLEAQYG**V**	8	173.2	13795.7	71% (5 of 7 reads)	64th
FILIP1L_4	DLALLEAQYG**V**	11	174.9	12300.6	71% (5 of 7 reads)	64th
FILIP1L_5	LALLEAQYG**V**V	11	288.2	101.4	71% (5 of 7 reads)	64th
DTNBP1_1	MTANLTHLE**V**	10	297.4	3067.6	90% (9 of 10 reads)	83rd
FOXJ2	**G**LESSLTSI	9	312.1	10691.9	47% (9 of 19 reads)	31st
RASSF6_1	FALHIIF**V**T	9	312.4	126.7	60% (76 of 126 reads)	62nd
RASSF6_2	FALHIIF**V**	8	329.8	2448.6	60% (76 of 126 reads)	62nd
MAP2K4_1	SL**R**ITLYEL	9	436.5	63.3	100% (23 mutant reads)	76th
KRAS_G12D	KLVVVGA**D**GV	10	498.0	506.9	40% (22 of 55 reads)	89th
CDC16	VTVDKWEP**V**	9	502.1	1924.7	100% (99 mutant reads)	92nd
DTNBP1_2	SMTANLTHLE**V**	11	594.9	5871.5	90% (9 of 10 reads)	83rd
LRP12_1	KLL**H**VLTAF	9	655.1	1215.2	75% (3 of 4 reads)	75th
LRP12_2	KLL**H**VLTA	8	779.2	1539.4	75% (3 of 4 reads)	75th
ATAD2_2	ELFI**C**DYGEI	10	807.5	2863.2	42% (39 of 92 reads)	75th
MAP2K4_2	SL**R**ITLYELA	10	854.8	564.9	100% (23 mutant reads)	76th

Table S11 – HLA-A02:01 epitope prediction for expressed mutations of patient TIPC113. Mutated positions are highlited in bold & underlined. Peptides sorted by predicted binding affinity of the mutated epitope to HLA-A02:01. The respective peptide name is derived from the mutated gene followed by an arbitrary running number.

Peptide name	Sequence	Length	Predicted affinity [nM]		RNASeq MAF & Read Count	Expression percentile (GDS4336)
			mutated	wild type		
KIFC1_1	I**L**RALRHLFSV	11	60.6	5149.4	42% (14 of 33 reads)	54th
SARM1_1	V**L**IDVEKLEA	10	155.5	9209.6	52% (17 of 33 reads)	55th
SARM1_2	QLHGFSV**L**I	9	174.4	77.0	52% (17 of 33 reads)	55th
SARM1_3	LQLHGFSV**L**I	10	284.5	133.8	52% (17 of 33 reads)	55th
KRAS_G12V	KLVVVGA**V**GV	10	300.2	506.9	49% (69 of 142 reads)	89th
UGT1A6_1	VLSDRG**N**EI	9	430.5	178.1	59% (48 of 82 reads)	62nd
CDKN2A	RL**R**VDLAEEL	10	523.3	487.6	100% (7 of 7 reads)	51st
SARM1_4	QLHGFSV**L**IDV	11	592.3	749.1	52% (17 of 33 reads)	55th
UGT1A6_2	VLSDRG**N**EIV	10	785.8	863.5	59% (48 of 82 reads)	62nd
KIFC1_2	**L**RALRHLFSV	10	792.2	1689.8	42% (14 of 33 reads)	54th
SARM1_5	LQLHGFSV**L**	9	902.6	13661.6	52% (17 of 33 reads)	55th
FAM193B	**V**NLDLSPLTL	10	916.2	572.5	20% (8 of 41 reads)	62nd
DCAF6	MV**V**RFIPSHL	10	971.9	642.5	38% (106 of 280 reads)	92nd

Table S12 – HLA-A02:01 epitope prediction for expressed mutations of patient TIPC222. Mutated positions are highlited in bold & underlined. Peptides sorted by predicted binding affinity of the mutated epitope to HLA-A02:01. The respective peptide name is derived from the mutated gene followed by an arbitrary running number.

Peptide name	Sequence	Length	Predicted affinity [nM]		RNASeq MAF & Read Count	Expression percentile (GDS4336)
			mutated	wild type		
AGPAT6_3	FEIGA**I**VYPV	10	22.7	35.3	100% (388 of 388 reads)	94th
KLHL13_1	AI**M**SDTTHLV	10	45.5	632.3	64% (21 of 33 reads)	40th
KLHL13_2	AI**M**SDTTHL	9	84.8	9698.3	64% (21 of 33 reads)	41st
PIK3CA_1	WLNWENPD**F**M	10	122.9	948.9	55% (54 of 98 reads)	92nd
KLHL13_3	I**M**SDTTHLVT	10	174.3	30725.4	64% (21 of 33 reads)	42nd
AGPAT6_1	SFEIGA**I**VYPV	11	186.1	309.2	100% (388 of 388 reads)	92nd
KDM6B	GLATS**S**PFQL	10	202.8	237.6	100% (17 of 17 reads)	67th
KLHL13_4	I**M**SDTTHLVTL	11	395.7	23672.4	64% (21 of 33 reads)	43rd
BARD1	KMWFSP**Q**SKKV	11	399.0	1560.2	33% (15 of 46 reads)	67th
CEP44	KIS**T**EAVGV	9	410.8	260.9	52% (38 of 73 reads)	57th
AGPAT6_4	EIGA**I**VYPV	9	426.3	809.0	100% (388 of 388 reads)	95th
KLHL13_5	TAI**M**SDTTHLV	11	467.7	7036.3	64% (21 of 33 reads)	44th
KRAS_G12D	KLVVVGA**D**GV	10	498.0	506.9	68% (315 of 461 reads)	89th
PIK3CA_2	**F**MSELLFQN	9	572.3	3329.9	55% (54 of 98 reads)	93rd
AGPAT6_2	FEIGA**I**VYPVA	11	626.6	1033.6	100% (388 of 388 reads)	93rd
DDX5	MLDMGFEPQI**S**	11	828.9	826.3	20% (679 of 3456 reads)	99th
PPM1D	VMNKSGV**S**RV	10	888.9	842.3	27% (23 of 86 reads)	68th
AUTS2	HLDERE**C**LHML	11	958.3	3064.3	43% (32 of 75 reads)	60th
ANKRD32	LLD**R**YAGNI	9	988.5	680.1	100% (47 of 47 reads)	41st

Table S13 – HLA-A02:01 epitope prediction for expressed mutations of patient TIPC236. Mutated positions are highlited in bold & underlined. Peptides sorted by predicted binding affinity of the mutated epitope to HLA-A02:01. The respective peptide name is derived from the mutated gene followed by an arbitrary running number. The peptides for this patient were not ordered in the end, due to the negative results from the mutation validation (see table S17).

Peptide name	Sequence	Length	Predicted affinity [nM]		RNASeq MAF & Read Count	Expression percentile (GDS4336)
			mutated	wild type		
SLC43A1_1	F**M**LSATTLPL	10	6.14	13.3	46% (11 of 24 reads)	71st
SLC43A1_2	**M**LSATTLPL	9	6.87	17.6	46% (11 of 24 reads)	71st
CDKN2A_1	VMMM**V**SARV	9	8.35	8.1	99% (886 of 889 reads)	51st
RBL2_1	LLACCLE**A**V	9	9.25	17.9	52% (134 of 259 reads)	95th
TGFBRAP1_1	A**M**FALNENPV	10	19.5	623.7	20% (14 of 71 reads)	73rd
RBL2_2	SLLACCLE**A**V	10	19.6	22.1	52% (134 of 259 reads)	95th
RBL2_3	SLLACCLE**A**	9	21.4	6.4	52% (134 of 259 reads)	95th
SLC43A1_3	SF**M**LSATTLPL	11	31.9	114.7	46% (11 of 24 reads)	71st
CDKN2A_2	QVMMM**V**SARV	10	57.6	80.6	99% (886 of 889 reads)	51st
CDKN2A_3	MMM**V**SARV	8	91.7	146.4	99% (886 of 889 reads)	51st
CDKN2A_4	MM**V**SARVAEL	10	96.4	151.7	99% (886 of 889 reads)	51st
SLC43A1_4	**M**LSATTLPLG	10	96.5	461.5	46% (11 of 24 reads)	71st
SLC43A1_5	F**M**LSATTLPLG	11	97.1	360.6	46% (11 of 24 reads)	71st
RBL2_4	RSLLACCLE**A**	10	104.6	23.8	52% (134 of 259 reads)	95th
RBL2_5	LLACCLE**A**VT	10	113.1	239.9	52% (134 of 259 reads)	95th
CDKN2A_5	MMM**V**SARVAEL	11	118.9	73.8	99% (886 of 889 reads)	51st
RBL2_6	RSLLACCLE**A**V	11	134.9	138.0	52% (134 of 259 reads)	95th
SLC43A1_6	F**M**LSATTL	8	151.8	4365.4	46% (11 of 24 reads)	71st
CDKN2A_6	VMMM**V**SARVA	10	161.7	286.7	99% (886 of 889 reads)	51st
SLC43A1_7	FTIGSF**M**LSA	10	162.6	173.8	46% (11 of 24 reads)	71st
TGFBRAP1_2	AA**M**FALNENPV	11	178.1	6405.7	20% (14 of 71 reads)	73rd
CDKN2A_7	IQVMMM**V**SARV	11	220.9	395.6	99% (886 of 889 reads)	51st
CDKN2A_8	M**V**SARVAEL	9	242.3	10574.7	99% (886 of 889 reads)	51st
RBL2_7	LACCLE**A**V	8	331.7	747.2	52% (134 of 259 reads)	95th
SLC43A1_8	**M**LSATTLPLGI	11	341.1	1585.3	46% (11 of 24 reads)	71st
RBL2_8	SLLACCLE**A**VT	11	364.1	371.5	52% (134 of 259 reads)	95th
PRKACB	**S**TLCGTPEYL	10	398.9	298.8	46% (391 of 853 reads)	81st
SLC43A1_9	F**M**LSATTLP	9	440.5	8695.1	46% (11 of 24 reads)	71st
KRAS_G12D	KLVVVGA**D**GV	10	498.0	506.9	42% (121 of 287 reads)	89th
N4BP1	**T**DLLILPTSL	10	621.0	120.7	48% (171 of 360 reads)	85th
CDKN2A_9	MMM**V**SARVA	9	624.7	248.2	99% (886 of 889 reads)	51st
TGFBRAP1_3	A**M**FALNENPVS	11	646.8	12777.9	20% (14 of 71 reads)	73rd
RBL2_9	LLACCLE**A**	8	657.8	80.6	52% (134 of 259 reads)	95th
RBL2_10	HRSLLACCLE**A**	11	767.6	767.6	52% (134 of 259 reads)	95th
CCDC88C	VTWVKTFGP**L**	10	823.9	9648.2	39% (21 of 54 reads)	73rd
COPS7A	KTIKVT**M**AA	9	886.5	2395.5	46% (240 of 517 reads)	80th
SLC43A1_10	TIGSF**M**LSA	9	907.7	932.2	46% (11 of 24 reads)	71st

6.3.2 Cell line mutation validation

Mutations yielding potentially HLA-A02:01 binding epitopes (table S14-S17) were validated in each respective cell line to avoid unnecessary screening of mutations lost during xenograft and cell line propagation. Due to a loss of HLA-A02:01 during xenograft outgrowth, as mentioned in section 4.4.2, the mutation validation of the PDX-derived cell line from patient TIPC102 was performed on the respective, HLA-A02:01 transduced cell line (TIPC102_A2; figure 47).

Table S14 – TIPC102_A2 cell line mutation validation. *Pyrosequencing primers were readily available for a part of the mutations and kindly provided by Dr. M. Volkmar.

Gene	Mutation	Exome MAF		PDX RNASeq MAF (read count)	Cell line	
		Primary	PDX		Pyro Sequencing*	Sanger Sequencing
ATAD2	R913C	0.190	0.422	42% (39 of 92 reads)	49% mutated	heterozygous
CDC16	L447V	0.416	0.996	100% (99 mutant reads)	—	homozygous mutated
DTNBP1	A123V	—	0.979	90% (9 of 10 reads)	98% mutated	—
FILIP1L	F109V	0.159	0.646	71% (5 of 7 reads)	70% mutated	—
FOXJ2	D4G	0.217	0.538	47% (9 of 19 reads)	—	heterozygous
GBAS	G203D	—	0.289	26% (14 of 54 reads)	—	wild type
KRAS	G12D	0.228	0.495	40% (22 of 55 reads)	33% mutated	—
LRP12	R330H	—	0.300	75% (3 of 4 reads)	—	heterozygous
MAP2K4	G294R	0.369	1.0	100% (23 mutant reads)	—	homozygous mutated
RASSF6	A238V	0.235	0.635	60% (76 of 126 reads)	69% mutated	—

Table S15 – TIPC113 cell line mutation validation.

Gene	Mutation	Exome MAF		PDX RNASeq MAF (read count)	Cell line
		Primary	PDX		Sanger Sequencing
CDH1	R90W	—	0.034	12% (134 of 1097 reads)	wild type
CDKN2A	P114R	0.120	1.0	100% (7 of 7 reads)	homozygous mutated
DCAF6	A242V	0.100	0.268	38% (106 of 280 reads)	heterozygous
FAM193B	I530V	0.144	0.181	20% (8 of 41 reads)	heterozygous
KIFC1	P435L	0.110	0.404	42% (14 of 33 reads)	homozygous mutated
KRAS	G12V	0.122	0.411	49% (69 of 142 reads)	heterozygous
PGM3	L156F	—	0.357	39% (35 of 90 reads)	wild type
SARM1	F591L	—	0.476	52% (17 of 33 reads)	subclonal mutated
TLE4	S48G	—	0.989	92% (12 of 13 reads)	wild type
UGT1A6	H54N	0.100	0.437	59% (48 of 82 reads)	heterozygous

Table S16 – TIPC222 cell line mutation validation. *Sanger sequencing did not reveal a conclusive result and the mutation was assumed to be present in the cell line.

Gene	Mutation	Exome MAF		PDX RNASeq MAF (read count)	Cell line
		Primary	PDX		Sanger Sequencing
AGPAT6	T344I	0.133	0.962	100% (388 of 388 reads)	homozygous mutated
ANKRD32	L1010R	0.139	0.983	100% (47 of 47 reads)	homozygous mutated
AUTS2	R1154C	0,19	0.437	43% (32 of 75 reads)	heterozygous
BARD1	R150Q	0.163	0.359	33% (15 of 46 reads)	heterozygous
CEP44	A153T	0.204	0.404	52% (38 of 73 reads)	heterozygous
CSNK1A1	E60D	—	0.494	52% (371 of 708 reads)	wild type
DDX5	R263S	0.158	0.242	20% (679 of 3456 reads)	heterozygous
KDM6B	P272S	0.203	1.0	100% (17 of 17 reads)	—*
KLHL13	R336M	—	0.385	64% (21 of 33 reads)	homozygous mutated
KPNA7	P371S	—	0.052	8% (7 of 88 reads)	wild type

Table S17 – TIPC236 cell line mutation validation.

Gene	Mutation	Exome MAF		PDX RNASeq MAF (read count)	Cell line Sanger Sequencing
		Primary	PDX		
CCDC88C	F27L	0.205	0.450	39% (21 of 54 reads)	wild type
CDKN2A	G55V	0.341	0.994	99% (886 of 889 reads)	wild type
COPS7A	T224M	0.22	0.519	46% (240 of 517 reads)	wild type
KRAS	G12D	0.255	0.488	42% (121 of 287 reads)	heterozygous
N4BP1	M173T	0.218	0.493	48% (171 of 360 reads)	wild type
PRKACB	W185S	0.237	0.508	46% (391 of 853 reads)	wild type
RBL2	V539A	0.238	0.440	52% (134 of 259 reads)	wild type
SLC43A1	V86M	0.276	0.441	46% (11 of 24 reads)	wild type
TGFBRAP1	T121M	—	0.090	20% (14 of 71 reads)	wild type

6.4 Purification of PDX derived cell lines

Since there was high chance of contaminating xenograft derived cell lines with mouse fibroblasts during setup of the cultures, we designed a protocol to test each line for mouse cell contamination. During the initial setup of the protocol we microscopically monitored each PDX derived line for the appearance of multiple phenotypes in combination with human EpCAM expression (figure S7A and B). We tried to separate these phenotypes by differential trypsinisation. However, this approach led to the outgrowth of mouse cells after several passages. In order to overcome this issue, we later treated each cell line with IFNγ for 48h, followed by flow cytometry sorting of the top 5% pan-MHC-I$^+$ (human) population (figure S7C). To get a better insight into the species origin of each cellular phenotype monitored, we designed a fast sequencing approach focused on three interspecies (human and mouse) SNPs (figure S7D). The final combination of sequencing and flow cytometry sorting allowed for a robust and fast depletion of mouse cell contaminations in PDX derived cell lines.

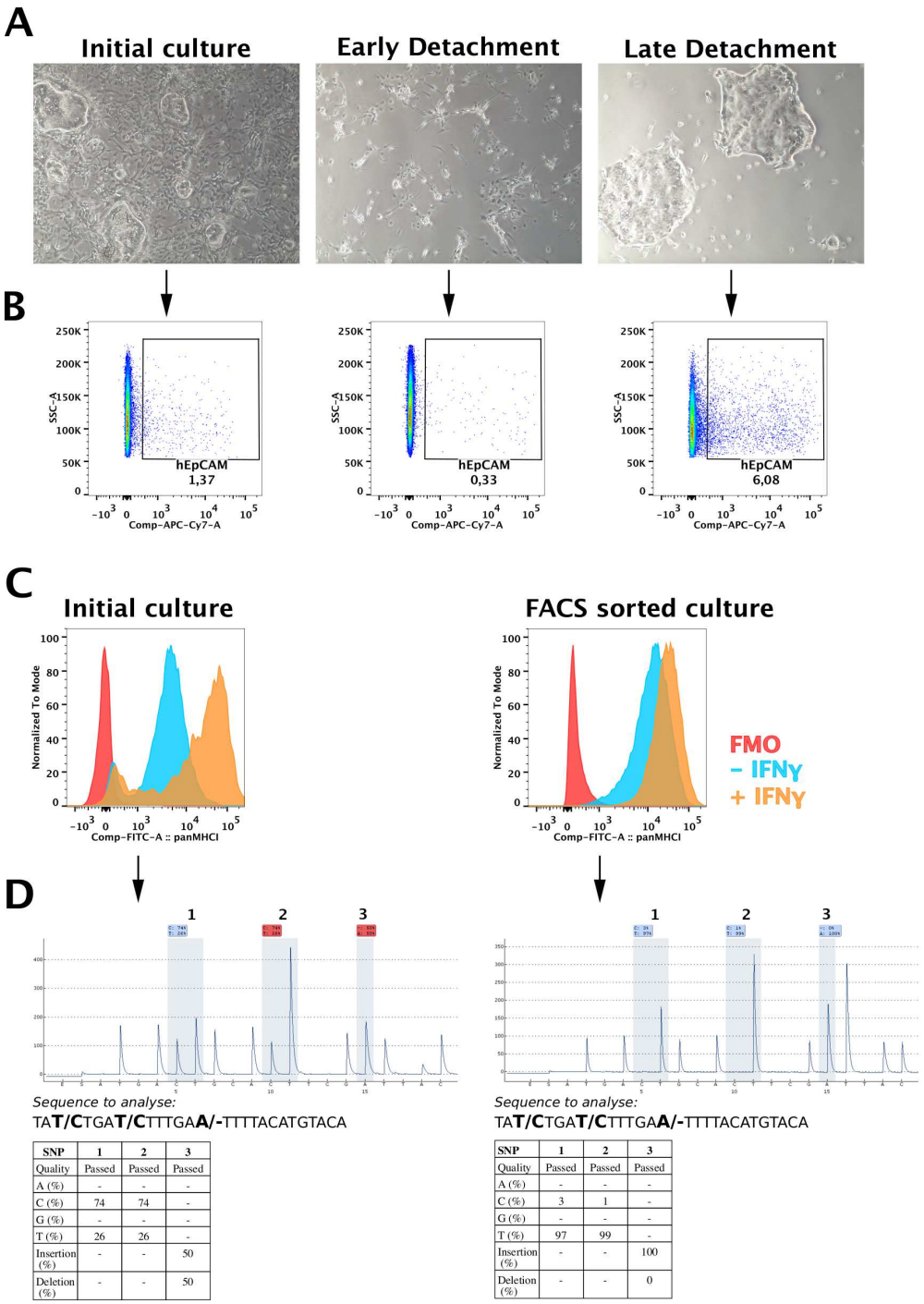

SNP	1	2	3
Quality	Passed	Passed	Passed
A (%)	-	-	-
C (%)	74	74	-
G (%)	-	-	-
T (%)	26	26	-
Insertion (%)	-	-	50
Deletion (%)	-	-	50

SNP	1	2	3
Quality	Passed	Passed	Passed
A (%)	-	-	-
C (%)	3	1	-
G (%)	-	-	-
T (%)	97	99	-
Insertion (%)	-	-	100
Deletion (%)	-	-	0

Figure S7 – Example for the purification of mouse cell contaminated cell lines. (A) Cellular phenotype of the initial PDX cell line and the two resulting populations after differential trypsinisation. Early = fast detachment after addition of trypsin (≈3 min). Late = slow detachment after addition of trypsin (≈20 min). (B) Surface staining for human EpCAM on the three cell line cultures following differential trypsinisation. Staining performed using the cell line contamination panel. (C) Illustration of human MHC-I upregulation after 48 h treatment with IFNγ on the initial and panMHC-I$^+$ (human) sorted culture. Stainings performed using the MHC expression panel. (D) Species PCR on the initial PDX derived cell line (left) and its panMHC-I$^+$ (human) sorted cell line (right). Species specific SNP positions are highlighted in blue. For a pure human cell line SNP_1 = T, SNP_2 = T and SNP_3 = A (insertion).

6.5 Stable cell line selection using G418

To ensure proper selection of stably transduced cell lines, the respective parental cell lines were first titrated against increasing amounts of G418. For all cell lines stably transduced during this work a concentration of 500 µg/ mL G418 in the culture medium was sufficient for selection (see figure S8).

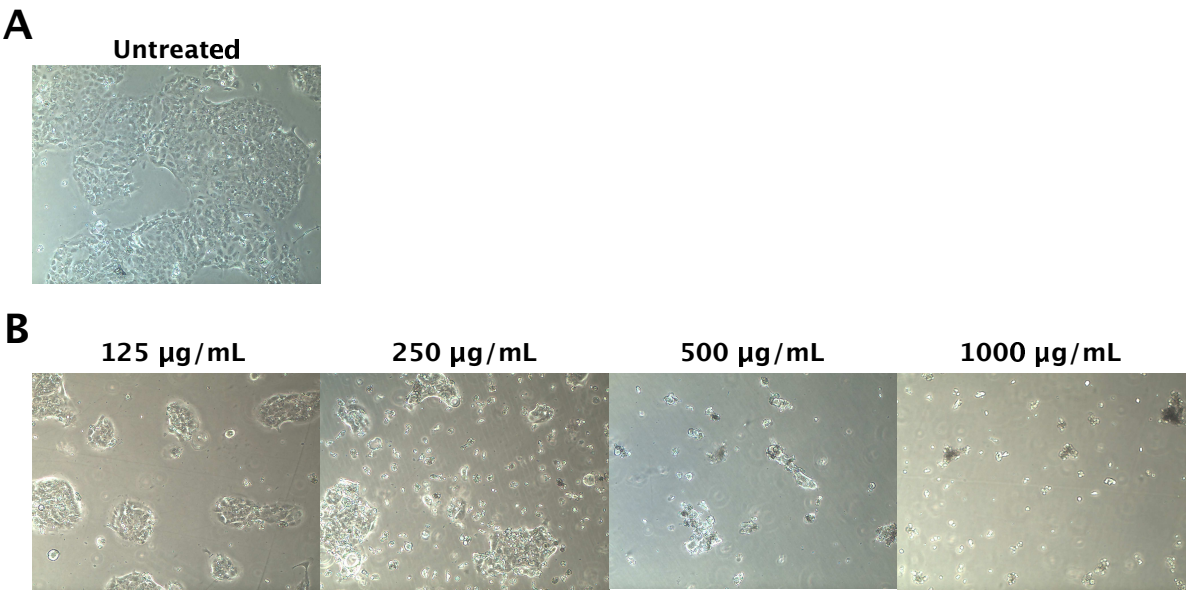

Figure S8 – G418 titration example for the generation of stably transduced cell lines. Shown here the untransduced TIPC102 cell line. (A) Regular culture without G418. (B) Culture with an increased concentration of G418 to determine the neccessary selection concentration .

6.6 Vector used in this study

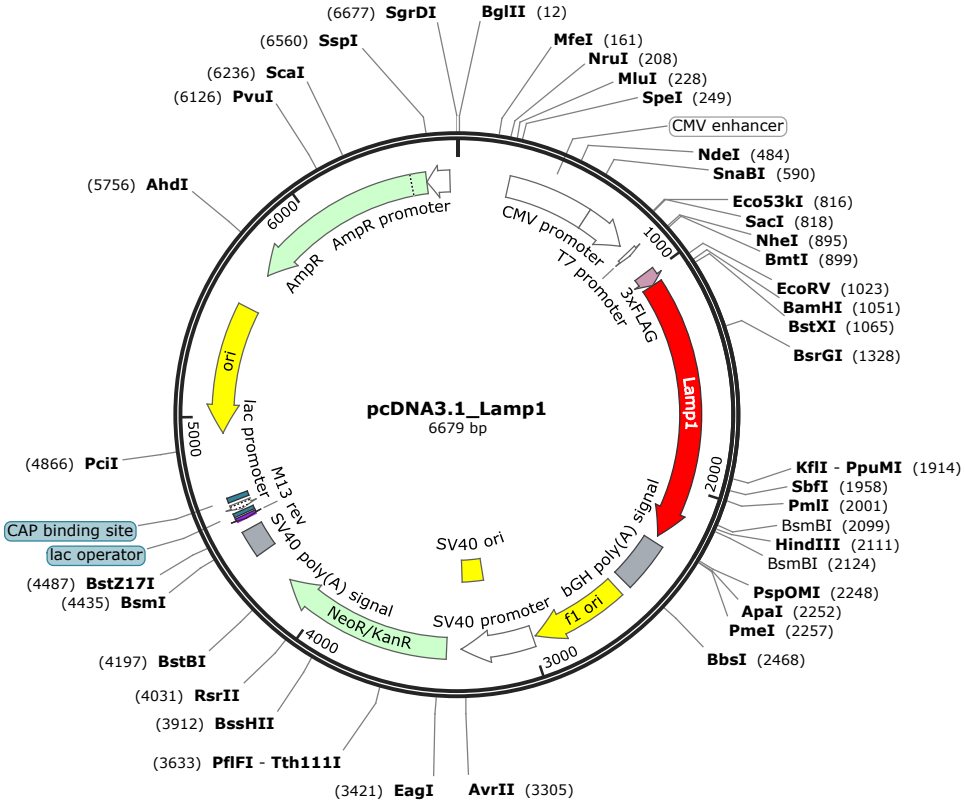

Figure S9 – pcDNA3.1(+)_Lamp1 vector map

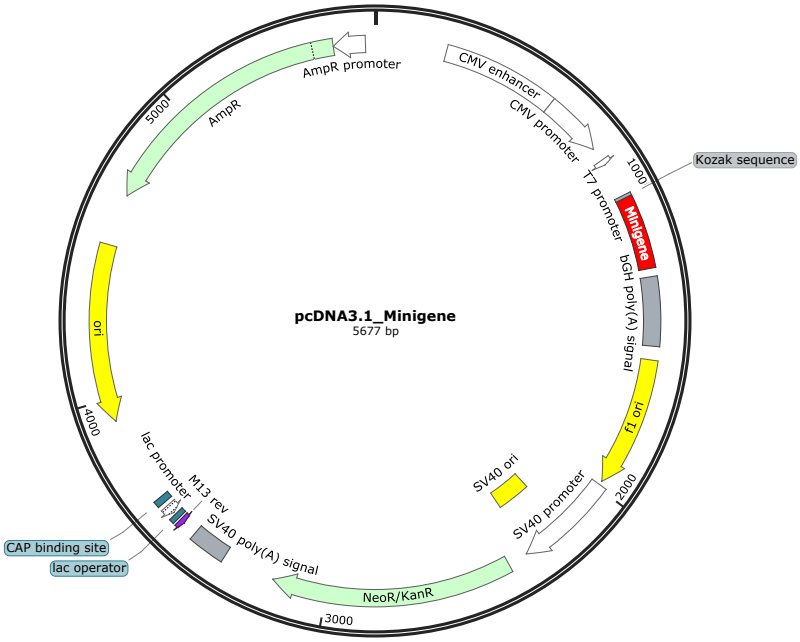

Figure S10 – pcDNA3.1(+)_Minigene vector map

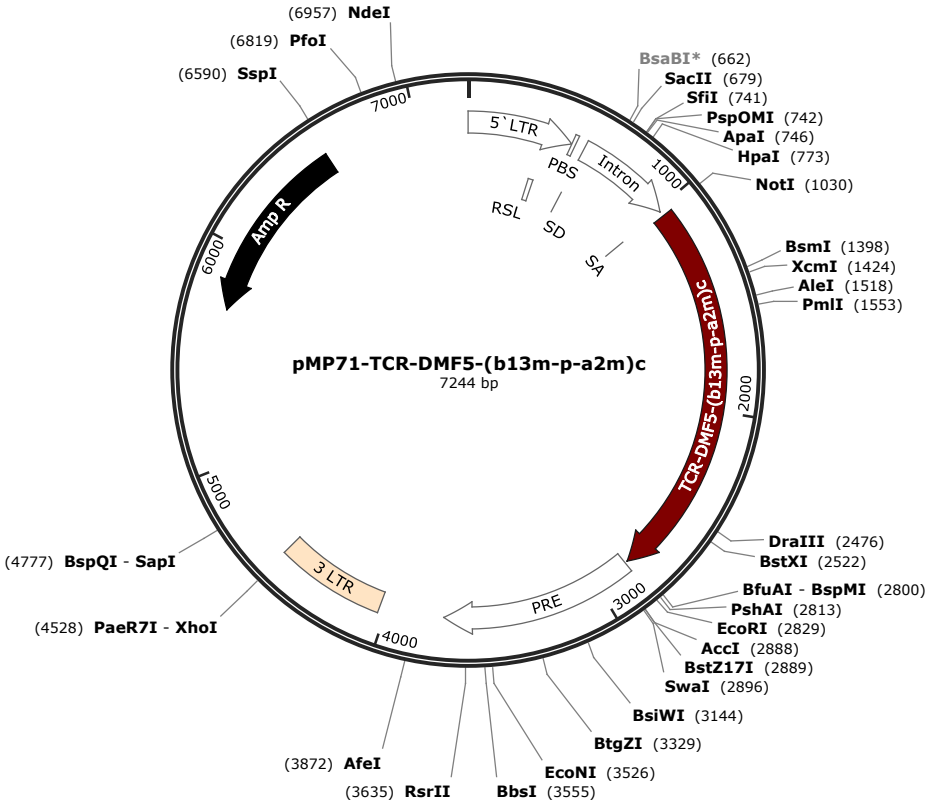

Figure S11 – DMF5/ Mart1 TCR vector map (as described in [372, 389])

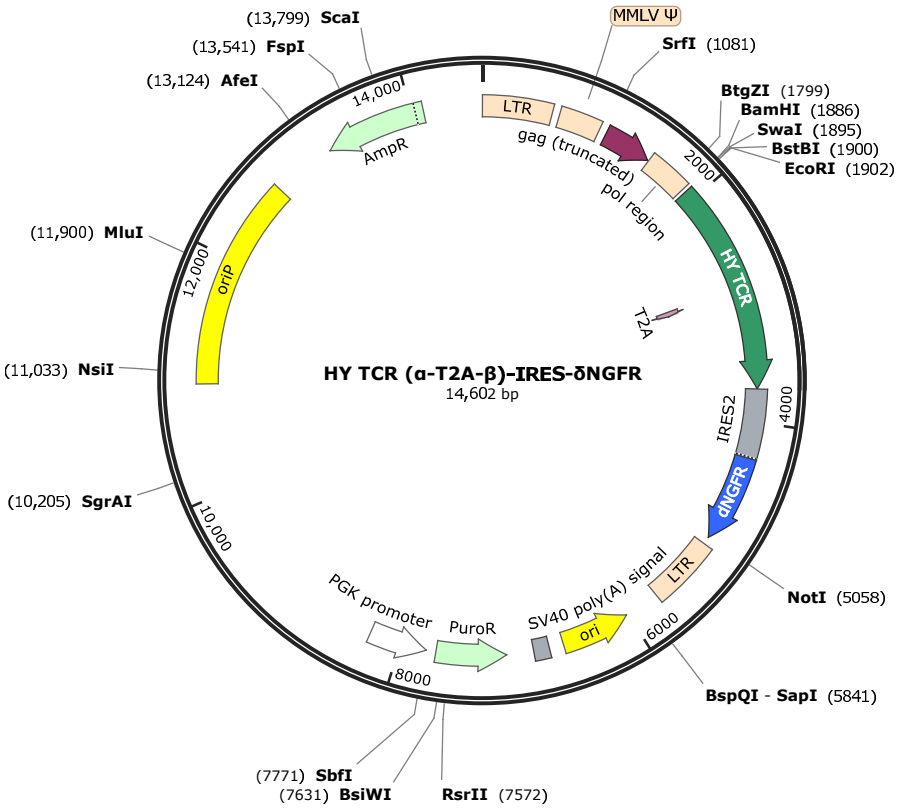

Figure S12 – pLZRS_HY-TCR(α-T2A-β)_IRES_δNGFR vector map (as described in [316])

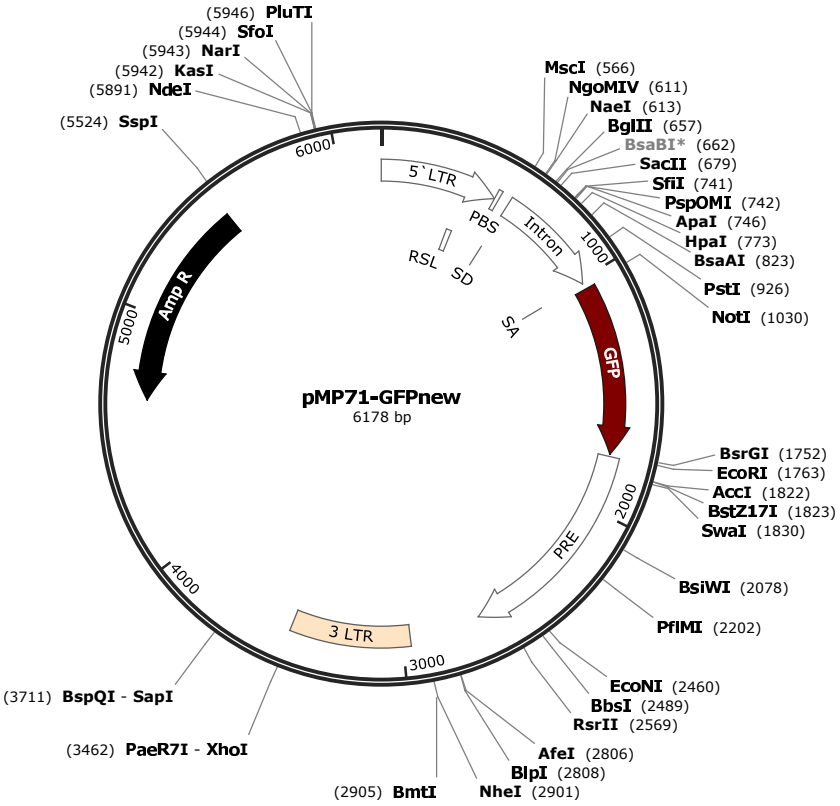

Figure S13 – pMP71_GFP vector map

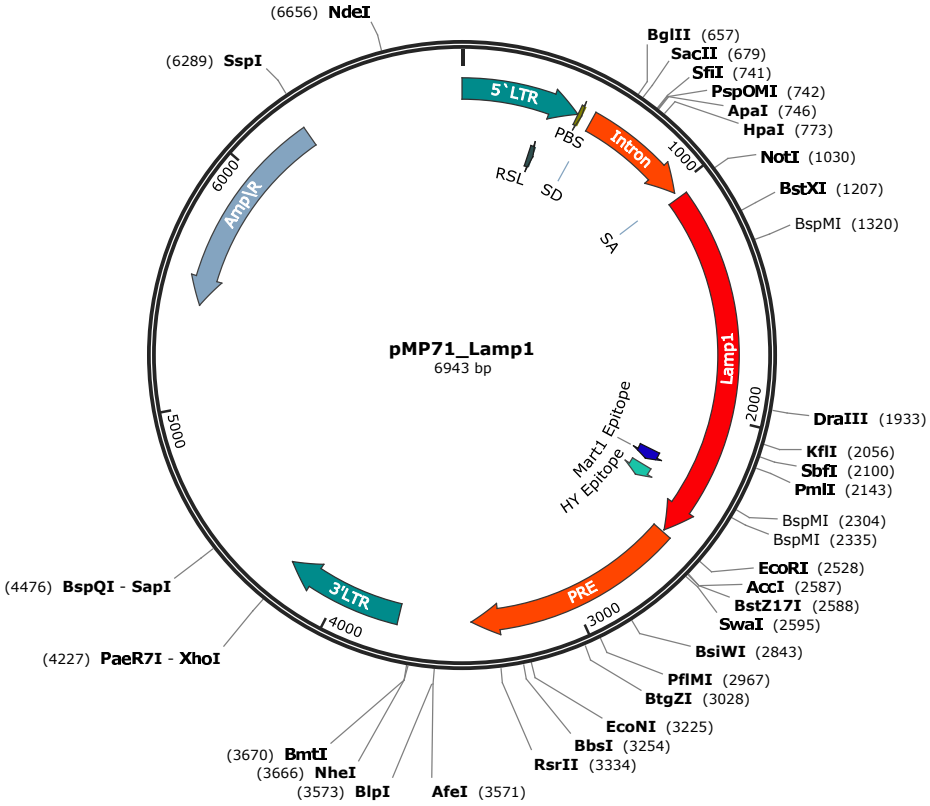

Figure S14 – pMP71_Lamp1 vector map

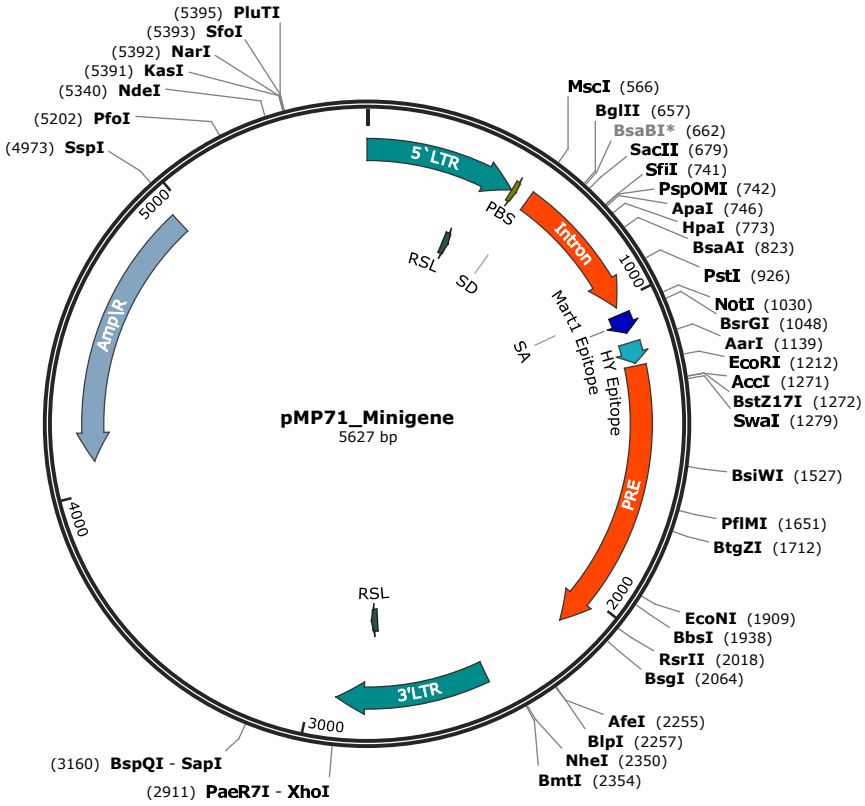

Figure S15 – pMP71_Minigene vector map. The minigenes Mart1 and HY are represented by their core sequence: Mart1 = ELAGIGILTV; HY = HIENFSDIDMGE.

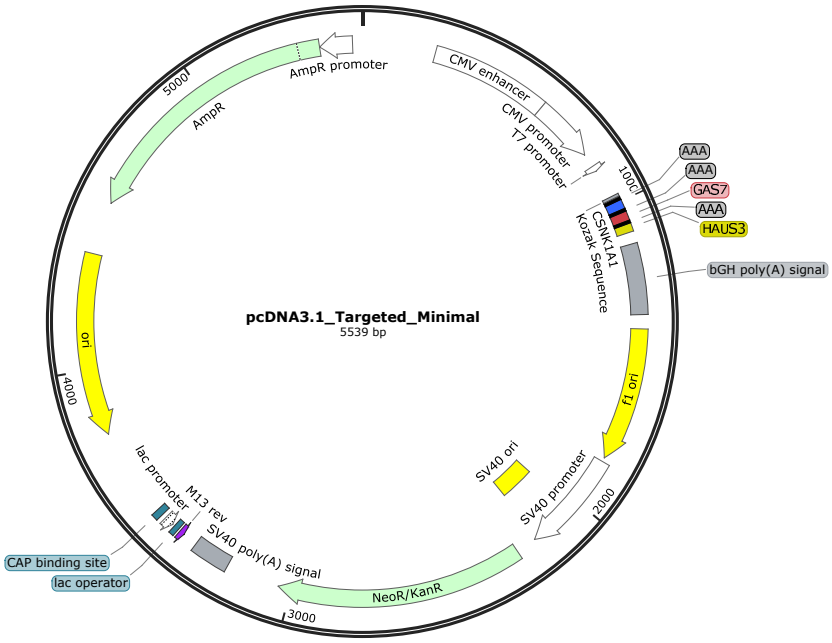

Figure S16 – pcDNA3.1_Minimal vector for targeted proteomics. The sequences of CSNK1A1, GAS7 and HAUS3 are represented by their core sequence separated by triple alanine linkers: CSNK1A1 = GLFGDIYLAI; GAS7 = SLADEAEVYL; HAUS3 = ILNAMIAKI.

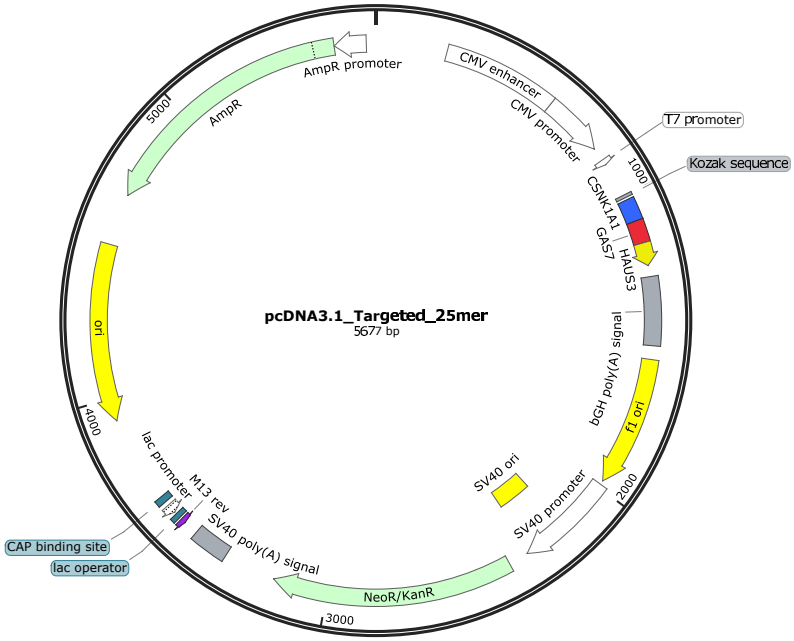

Figure S17 – pcDNA3.1_25mer vector for targeted proteomics

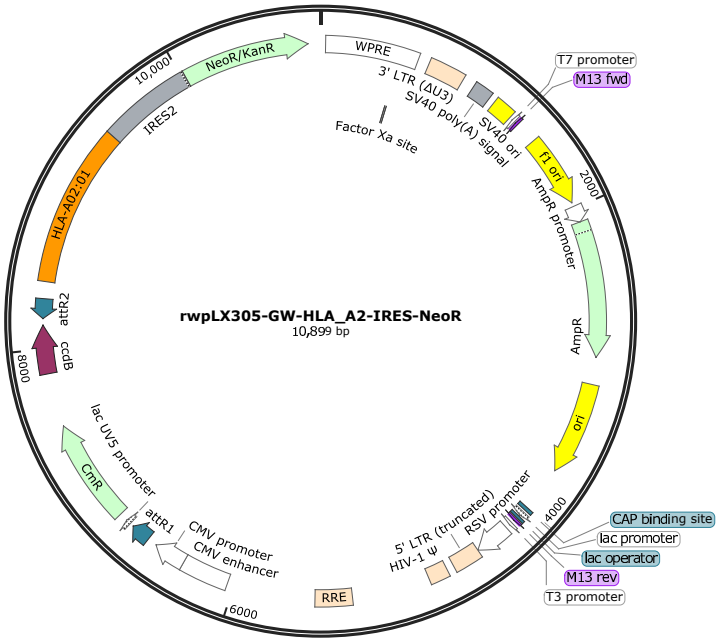

Figure S18 – rwpLX305-GW-HLA_A2-IRES-NeoR gateway vector for stable cell line generation. The vector was kindly provided by Dr. R. Will from the Genomics and Proteomics core facility at the DKFZ.

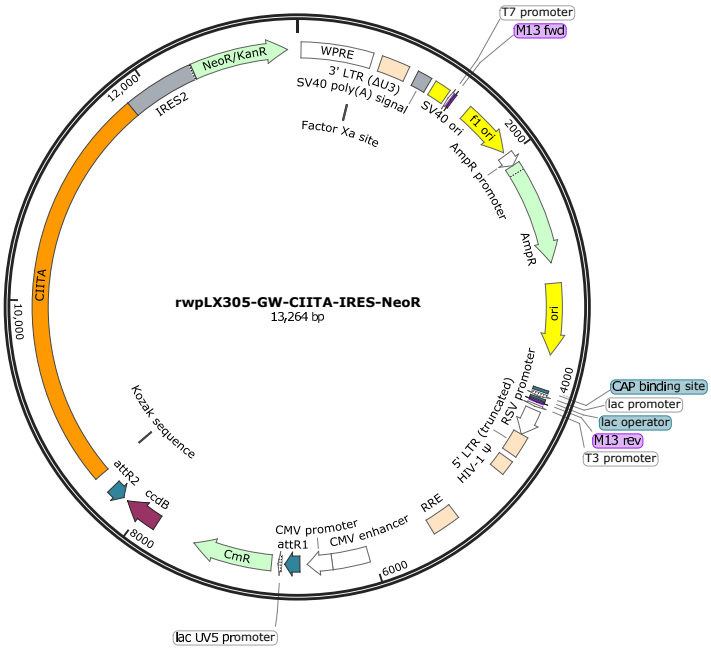

Figure S19 – rwpLX305-GW-CIITA-IRES-NeoR gateway vector for stable cell line generation. The vector was kindly provided by Dr. R. Will from the Genomics and Proteomics core facility at the DKFZ.

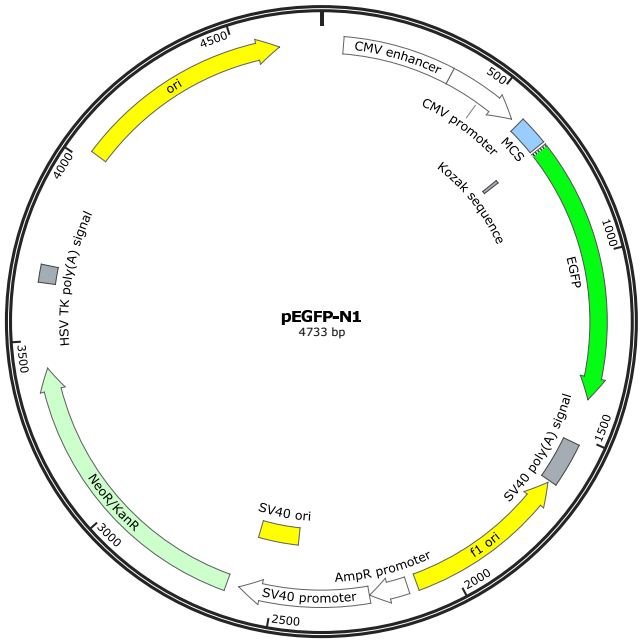

Figure S20 – pEGFP-N1 vector map

6.7 Sequences

>Lamp1 (Nucleotide Sequence)

(including 3x FLAG-Tag; [] = indication of TMD mutation variants; () = multi epitope insertion site)

ATGGCTGCCCCTGGCAGCGCCAGAAGGCCCCTGCTTCTGCTCCTTTTGCTCCTGCTGCTGGGCCTGATGCACTGCGCC
AGCGCCGACTACAAGGACCACGACGGCGATTACAAGGATCACGATATCGACTATAAGGACGACGATGACAAGGGATCC
GCCATGTTCATGGTGAAAAACGGCAACGGCACCGCCTGCATCATGGCCAACTTCAGCGCCGCCTTCAGCGTGAACTAC
GACACCAAGAGCGGCCCCAAGAACATGACCTTCGACCTGCCCAGCGACGCCACCGTGGTGCTGAACAGAAGCAGCTGC
GGCAAAGAGAACACCAGCGACCCCAGCCTGGTGATCGCCTTCGGCAGAGGCCACACCCTGACCCTGAACTTCACCCGG
AACGCCACCCGGTACAGCGTGCAGCTGATGAGCTTCGTGTACAACCTGAGCGACACCCACCTGTTCCCCAACGCCAGC
AGCAAAGAAATCAAGACCGTGGAATCCATCACCGACATCCGGGCCGACATCGACAAAAAGTACAGATGCGTGTCCGGC
ACCCAGGTGCACATGAACAACGTGACCGTGACCCTGCACGACGCCACCATCCAGGCCTACCTGAGCAACAGCAGCTTC
AGCAGAGGCGAGACAAGATGCGAGCAGGACCGGCCCAGCCCTACCACAGCTCCTCCAGCCCCTCCAAGCCCCAGCCCT
AGCCCTGTGCCTAAGAGCCCCAGCGTGGACAAGTACAACGTGTCCGGGACCAACGGCACCTGTCTGCTGGCCTCCATG
GGCCTGCAGCTGAACCTGACCTACGAGCGGAAGGACAACACCACCGTGACCCGGCTGCTGAACATCAACCCCAACAAG
ACCAGCGCCAGCGGCAGCTGTGGCGCCCACCTGGTGACACTGGAACTGCACAGCGAGGGCACCACCGTGCTGCTGTTC
CAGTTCGGCATGAACGCCAGCTCCAGCCGGTTCTTTCTGCAAGGCATCCAGCTGAACACCATCCTGCCCGACGCCCGG
GACCCTGCCTTTAAGGCCGCCAATGGCTCCCTGAGAGCCCTGCAGGCCACCGTGGGCAACAGCTACAAGTGCAACGCC
GAGGAACACGTGCGCGTGACCAAGGCCTTCTCCGTGAACATCTTCAAAGTGTGGGTGCAGGCCTTCAAGGTGGAAGGC
GGCCAGTTCGGCTCCGTGGAAGAGTGCCTGCTG(GGAGACGAAGCTTCCGTCTCG)GACGAGAACAGCATGCTGATCC
CTATCGCCGTGGGC[GGA/AGA]GCCCTGGCTGGA[CTG/AAG]GTGCTGATCGTGCTGATTGCCTACCTGGTCGGAC
GGAAGCGGAGCCACGCCGGCTACCAGACCATCTGA

>Lamp1 (Amino acid Sequence)

(including 3x FLAG-Tag; [] = indication of TMD mutation variants; () = multi epitope insertion site)

MAAPGSARRPLLLLLLLLLLGLMHCASADYKDHDGDYKDHDIDYKDDDDKGSAMFMVKNGNGTACIMANFSAAFSVNY
DTKSGPKNMTFDLPSDATVVLNRSSCGKENTSDPSLVIAFGRGHTLTLNFTRNATRYSVQLMSFVYNLSDTHLFPNAS
SKEIKTVESITDIRADIDKKYRCVSGTQVHMNNVTVTLHDATIQAYLSNSSFSRGETRCEQDRPSPTTAPPAPPSPSP
SPVPKSPSVDKYNVSGTNGTCLLASMGLQLNLTYERKDNTTVTRLLNINPNKTSASGSCGAHLVTLELHSEGTTVLLF
QFGMNASSSRFFLQGIQLNTILPDARDPAFKAANGSLRALQATVGNSYKCNAEEHVRVTKAFSVNIFKVWVQAFKVEG
GQFGSVEECLL(GDEASVS)DENSMLIPIAVG[G/R]ALAG[L/K]VLIVLIAYLVGRKRSHAGYQTI

Lamp1 multi epitope construct inserts:

>TIPC102_TC1 Insert

ACCCTGCAGTACCTGAACGGCGACTACGAGGTGGAGCCCGGCAGAGTGGGCGAGAGAAACGCCTACCTGAAGGAGCAG
CACATCGAGACCCCCGACGGCCTGTACGAGTACCTGAGACCCAGCGGCACCCCCGCCCAGCTGAGCTGCCTGAGCAAG
AACCTGAACTACGACACCTTCGGCAAGCCCCACAGCGCCCTGCCCGAGGAGGTGCAGGAGCTGTTCATCTGCGACTAC
GGCGAGATCTTCAACGTGCAGCTGCCCGACAAGGAGCACCAGAGCAAGACCAACAGAGCCACCGGCAGCCCCAGCGTG
AGACAGATGAAGGGCGGCAGCGCCCTGGGCACCAAGACCGCCCAGGCCATCAAGGCCATCGGCAACGAGGTGACCGTG
GACAAGTGGGAGCCCGTGCTGAACAACCTGGGCCACGTGTGCAGAAAGCTGAAGAAGTACCTGGAGCTGAGCGGCGGC
GCCAAGATCAACAGAATCTTCCACGAGCACTTCCCCTTCGAGATCGTGAAGATGGAGTTCAACGAGAAGGAG

>TIPC102_TC2 Insert

ATGGCCAGCGGCCTGGAGAGCAGCCTGACCAGCATCGACTGGCTGCCCCAGCTGGCCGAGCAGTACGAGAACGAGATG
TTCGACTACGAGCAGCTGAGCAAGCTGCTGAAGAAGCAGGCCCAGTTCTACGAGAACATCGTGAAGATCGCCGACCTG
GAGAGCATGACCGCCAACCTGACCCACCTGGAGGTGAGCTTCGAGGAGGTGGAGAACAATCTGCTGCACCTGGAGGAC
AAGGCCGAGAAGATGGACCTGGCCCTGCTGGAGGCCCAGTACGGCGTGGTGACCCCCAAGAAGGTGCTGGAGGCCCTG
CAGAGAGACGCCGAGCTGAGAAGCTACCAGCTCAGACCCGGCACCATGATCGAGTGGGACAACTACTGGGCCAGAGCC
ATCAGATTCAGACAGGACGGCAACGCCAAGGAGGACCCCCTGCTGACCCCCGTGCCCGCCAGCGAGAACCTGTTCAGA
GAGAAGAAGTTCTTCTGCGCCATCCTG

>TIPC102_TC3 Insert

ATGACCGAGTACAAGCTGGTGGTGGTGGGCGCCGACGGCGTGGGCAAGAGCGCCCTGACCATCCAGCTGATCCAGAAC
CACTTCGTGGACAACAGCCAGGTGGACAGCCCCAGCAGCGAGAAGAGCCCCGTGATGAAGCCCCAGTTCAAGTTCTGG
GCCTGGGACCCCGAGGAGGAGAGAAAGGTGGTGGACATCGAGATCAACGGCGAGAGCGTGGATCTGCACATCAAGCTG
GGCGACAACGGCGAGGCCTTCTTCGTGCAGGAAACCGTGAAGATCTACGACGGCCTGGAGGAGAACCCCCACAAGCTG
CTGCACGTGCTGACCGCCTTCGACAGCCACGCCCCCCTGACCGTGGTGGCCAGCAGACAGGGCTACGACGTGAGAAGC
GACGTGTGGAGCCTGAGAATCACCCTGTACGAGCTGGCCACCGGCAGATTCCCCTACCCCATGGCCAGCGACAGCAGC
AACACCAGCCTGCCCTTCAGCAACATGGAGAACCCCATGAACACCACCCAGCTGGGCAAGAGCCTGTTCCAG

>TIPC102_TC4 Insert

GAGAGCGTGCCCGGCAAGCCCAGCGTGAACGCCGACGAGGAGGTGAGAGGCCCCCAGATCTGCAGAGTGTGCGGCGAC
AAGGCCACCGGCATCAAGGCCGGCACCGAGCTGACCTTCAACTACAACCTGGAGTGCTTCGGCAACGGCAAGACCGTG
TGCAAGTGCGGCGCCCCCAACTGCAAGATCGAGAACAGCCCCCAGGACTTCGCCCTGCACATCATCTTCGTGACCGGC
GAGCAGAGAAGACTGAAGAAGACCGACATCCCCCTGAGACAGGCCAAGTACACCGAGAACAAGCTGAAGGCCATCAAG
GCCAGAAACGAGTATCTGCTGGCCCTGGAGGCCACCAACGCCAGCGTG

>TIPC222_TC1 Insert

ACCAGCGTGATGATGTTCAAGAAGGGCAGCTTCGAGATCGGCGCCATCGTGTACCCCGTGGCCATCAAGTACGACCCC
CAGTTCGGCGACAAGGAGGAGCTGTTCGCCATCACCAAGATCGAGGACACCGTGGAGGACTTCCACGCCCAGGCCGAG
AAGCACTTCCACTACCAGCAGCTGAGCCACAAGGAGACCACCAGCGTGCACACCGACTGGCTGCTGGACAGATACGCC
GGCAACATCAAGACCCTGCAGAAGCTGCCCCACATCCCCAGAAGAGAGCACGAGAGAGGCGGCCACCTGGACGAGAGA
GAGTGCCTGCACATGCTGAGAGAGGACTACGAGCACACCAGACTGCACGACGCCGGCAACAAGAAGAACAGCATCAAG
ATGTGGTTCAGCCCCCAGAGCAAGAAGGTGAGATACGTGGTGAGCAAGGCCAGCGTGCAGAGCACCGAGAAGACCCAG
CCCGGCGAGGGCCTGGAGGAGAGCGGCCTGCCCCAGCCCGGCGGCAAGGAGGACGCCCCCGCCGCCGAGGGC

>TIPC222_TC2 Insert

ACCCCCCCCGCCACCCCCGGCAGCAGAGGCTGGCCCCCCCAGCCCATCCCCACCCTGAGACTGGAGGGCGTGGAGAGC
AGCGAGAAGCTGAGCAGCGGCAAGAGCGAGCCCCCCCTGGGCAACGAGAAGATCAGCACCGAGGCCGTGGGCGTGGAC
ATCAGCGGCAGATTCATGACCAGCGGCGAGGGCGAGAGCGTGGACCACGTGGAGACCGTGGGCAACGTGGTGATGCAG
AAGAAGGCCCCCATCACCGAGGACGTGAGAGTGGCCTTCATGGTGGACAACGCCCAGCTGGGCTTCCTGGTGAGCGAC
AGAAACAGAAACCTGATGGTGTACATGTACCTGCCCGAGGCCAAGCCCACCAAGTGCATCAGCACCACCGAGAGCATC
GAGATCAAGGCCAGATTCACCTACATCGACTACGAGGGCAGAAGCGACGGCGACAGCATCGTGAAGCTGGAGAGCCAG
AAGGCCAGACACCCCCAGCTGCTGTACGACAGCAAGCTGTACAAGATCCTGCAGGGCGGCGTGGGCATCCCC

>TIPC222_TC3 Insert

GACGAGGCCGACAGAATGCTGGACATGGGCTTCGAGCCCCAGATCAGCAAGATCGTGGACCAGATCAGACCCGACAGA
CAGACCCTGATGCAGGACCTGGCCAAGGACACCGACCCCCTGAAGCTGAAGCTGCTGGTGTGGATCGAGGGCAAGGAG
AGAAACATCAGAGCCCTGCTGAGCGCCCTGCTGACCCTGCTGGGCGTGGTGCTGGCCCTGACCTGCAGATGCCCCCAG

AGCGGCCCCGGCCCCGCCAGACCCGTGCTGCTGCTGCTGGAGTTCGGCGTGATCTACCACTGCACCGAGGAGAGACTG
TACATGGGCAGAAGAGGCAGAGGCGCCTTCTGCAACGGCCAGAGACTGATGCCCTACATGCAGCCCGTGATGCAGAGC
GACAGAACCGCCATCATGAGCGACACCACCCACCTGGTGACCCTGGGCGGCGTGCTGAGAGGCTACCTGGCCCTGTGC
AGCTACAACTGCAAGGAGGCCATCAACCCCCTGAGCCACCTGCCCAGCCACCACTACAACACCGGCTGGGTG

>TIPC222_TC4 Insert

ATGACCGAGTACAAGCTGGTGGTGGTGGGCGCCGACGGCGTGGGCAAGAGCGCCCTGACCATCCAGCTGATCCAGAAC
CACTTCGTGGACCCCCCCCCCCCCCCCCCCCCCCCCCTGCCCGGCCTGGCCACCAGCAGCCCCTTCCAGCTGACCAAG
CCCGGCCTGTGGAGCACCCTGCACCTGATGACCCCCCAGGAGCTGATCAACTACGTGCAGACCGTGGACAGCATGAGA
ACCGACAACACCTGCGTGAACCTGCTGCTGGAGGCCCCCTGCCACCACATCCAGCAGCTGCTGGCCTACGACGTGCTG
CCCAGCCTGGTGGCCCTGCTGAAGAACGGCGAGTTCAAGGTGCAGAAGGAGTTCGTGTTCGCCACCAGCCTGGACACC
AAGGACATCGAGCAGAACGCCGAGTTCCTGGAGCAGAGCGTGAAGGACAGCTGCGAGGGC

>TIPC222_TC5 Insert

AGCAGACCCAGCAGCGCCAAGAGAGCCAGCAGCAGCGGCAGCGCCTACAAGAGCGACAAGGACCTGGAGACCCAGGTG
ATCCAGCTGAACAAGCTGCTGAAGACCCTGACCGCCAGCGAGATGCTGCCCCTGCTGAACCACTGGAACACCCAGACC
AAGAAGGTGAGCCTGAGAGAGATCAAGTACCAGCTGAGCCCCAACGAGTACTTCAGCCTGGTGGAGAAGAACAACCCC
GACGGCGGCAAGTACCCCGAGCTGGTGCTGCAGAAGATCACCGACGCCCCCAAGAGCCAGCCCACCACCCCCCAGGAG
ACCATGACCGGCAAGCTGTTCGGCTTCGGCGCCAGCATCTTCAGCCAGATCGGCGACGTGATCACCGCCATCGACGGC
GAGAACACCAGCAACGTGACCCACCTGGAGGCCCAGAACAGAATCAAGGGCTGCACCGAC

>TIPC222_TC6 Insert

AGCAGCGCCAAGAGACCCCTGTGGCTGAACTGGGAGAACCCCGACTTCATGAGCGAGCTGCTGTTCCAGAACAACGAG
ATCATCTTCAAGAGAATCGAGGGCCTGGGCGGCAGCGTGATGAACAAGAGCGGCGTGAGCAGAGTGGTGTGGAAGAGA
CCCAGACTGACCCACAACGGCCCCTGGAGAGGCGGCGCCGTGCAGCCCCCCAGAGACGGCGTGCTGGAGAGAAAGGCC
GCCAAGGAGCAGCCCAAGGCCGGCAAGGAGCCCGCCAGCGTGAAGGTGAAGATCAAGCTGAACAAGAAGGACGACAAG
GGCCAGGACAAGGGCAAGGGCAAGAAGAGACCCAACAGAGGCAAGGCCACCGCCCACGCCGACGAGTTCGACTGCCCC
AGCGAGCTGCAGCACAGCCAGGAGCTGTTCCCCCAGTGGCACCTGCCCATCAAGATCGCC

>TIPC222_TC7 Insert

CAGAGCCAGCACATGACCGAGGTGGTGAGAAGATGCCCCCACGACGAGAGATGCAGCGACAGCGACGGCCTGGCCCCC
CCCCAGCACCTGGTGGGCGGCCAGTGCGTGCCCCTGAACGGCGGCAGCAGCCTGGACCTGGTGGAGCTGCAGCCCCTG
CTGACCGAGATCAGCAGAACCCTGAGACTGAGATACCTGGAGAGCCTGGACCTGAGCCACAACGGCCTGCCCGCCCTG
CCCGCCGAGAGCTTCACCAGCAGCCCCCTGAGCGACCAGGCCACCGCCGCCGGCGACGTGATCAAGGCCGCCTACAAC
CAGCTGAAGACCATCGCCCAGGGCAACCTGAGCAACACCGACGTGCAGCTGAGCGGCGCCGTGCACGACAGACTGCTG
AACGTGTGGCAGGTGCAGAGCGAGAACAAGGAGAAGAGCGCCGTGATGAGCTTCACCGTG

>TIPC236_TC1 Insert

ATGACCGAGTACAAGCTGGTGGTGGTGGGCGCCGGCGACGTGGGCAAGAGCGCCCTGACCATCCAGCTGATCCAGAAC
CACTTCGTGGACTTCCTGCAGAGCCCCCTGGTGACCTGGGTGAAGACCTTCGGCCCCCTGGGCAGCGGCAGCCAGGAC
AACCTGACCATGTACATGGACCTGGCCCCCAACAGCTACGGCAGAAGACCCATCCAGGTGATGATGATGGTGAGCGCC
AGAGTGGCCGAGCTGCTGCTGCTGCACGGCGCCGAGAGCGCCCTGCCCAAGGAGAGAGACAGCAGCAGCGAGAAGGAC
GGCCACAGCCCCAACAAGAGAGAGAAGGACCACATCAGAAGACCCATGATCGAGAGCGAGGTGGCCAACCTGAAGAAG
ACCATCAAGGTGACCATGGCCGCCGCCGCCGCCGCCACCAGCCAGGACCCCGAGCAGCACGAGTTCCTGTGCGTGGTG
AGCAAGGAGCTGCACAACACCCCCTACAGCACCGCCAGCGAGCCCAGCGAGAAGGCCAAGATCCTGCAGGAG

>TIPC236_TC2 Insert

AGAAACAGCATGGAGAAGCTGAGCAAGGACGGCGTGGACCTGATCGCCAGAAAGGAGAAGAAGGCCAACCTGATGGAG

CAGCTGTTCGGCAGAGAGTTCAAGCAGTTCGTGGAGGCCCACGCCGACAACTACACCACCGATCTGCTGATCCTGCCC
ACCAGCCTGAAGAAGGAGCTGCTGCTGTACCCCGCCCTGCCCACCGACGGCAGCACCGGCGTGGAGCTGGTGCCCAGA
AGCGCCGAGCCCGGCTACCTGGTGACCAAGGTGGTGAGCAAGCTGCACGTGACCCTGTACAACTGCAGCTTCGGCAGA
AGCAACTGCAGCCTGTGCAGAGCCGCCAACCCCGACTACAGATGCGCCCAGGTGACCGACTTCGGCTTCGCCAAGAGA
GTGAAGGGCAGAACCAGCACCCTGTGCGGCACCCCCGAGTACCTGGCCCCCGAGATCATCGAGCAGGACGCCTTCCAC
AGAAGCCTGCTGGCCTGCTGCCTGGAGGCCGTGACCTTCAGCTACAAGCCCCCCGGCAACTTCCCCTTCATC

>TIPC236_TC3 Insert

CACTACGGCGTGATCACATGCGAGGGCTGCAAGGGCTTCTTCAGACAGAGCCAGAGATGCAACGCCGCCTACAGCTGC
ACCAGACAGCAGCAGCAGGACGAGATGCTGAACCTGGGCTTCACCATCGGCAGCTTCATGCTGAGCGCCACCACCCTG
CCCCTGGGCATCCTGATGGACAGATACAACAACAACCTGAACGGCATCCTGGCCGACGAGATGGGCCTGAGAAAGACC
ATCCAGACCATCGCCCTGATCACCTACCTGATGGAGTTCAAGAACCAGATCACCACCCTGCAGGGCCAGGCCAAGAAC
AGAACCAACCCCAACAGAAGCGAGGTGCAGGCCAACCTGAGCCTGTTCGACACCATGGCCGACGGCCTGAGCCTGGAG
GAGCAAGTGACCGGCAAGGGCGCCGACAGAGAGCTGCTGGTGGGCGACAGCATCGCCAACCTGACCGAGGCCACCAAC
CACAGACAGAACATCGAGAAGATGGCCGTGGAGCAGAAGGAGAAGTACCTGGGCCTGTACACCATCCTGCCC

>TIPC236_TC4 Insert

AACCTGGAGCCCGTGCCCAGCGGCGCCAGAATCAAGGGCGCCGCCATGTTCGCCCTGAACGAGAACCCCGTGAGCGGC
GACCCCTTCTGCGTGAGCGGCCTGGACCCCGCCAGAAAGTACAAGTTCCTGCTGTTCAGACTGCAGAACGGCAAGAGA
CACGGCCCCGTGCCCGTGGAGGCCAAGCAGAGCCAGCACATGACCGAGGTGGTGAGAAGATGCCCCCACAGAGAGAGA
TGCAGCGACAGCGACGGCCTGGCCCCCCCCCAGCACGGCGGCAAGAAGCCCAAGTACCCCCCCAACAAGGTGATGATC
TGGGGCGACCTGAAGAAGAAGACCGTGATCGAGATCGAGTTCAGCACCTATCTGCCCAGCAGCCCCGAGAGAGAGGTG
CAGATCGTGAGCACCACCGACAGCAGCTTCCCCTACGCCATCTACACCCAGAGAGTGAGA

> MITD Construct

(including Mart1 and HY epitope; () = indication of multi epitope insertion site)

ATGAGAGTGACCGCCCCCAGAACCCTGATCCTGCTGCTGAGCGGCGCCCTGGCCCTGACCGAGACCTGGGCCGGCAGC
TACACCACCGCCGAGGAGCTGGCCGGCATCGGCATCCTGACCGTGATCCTGGGCGTGCTGCTG(GAGAGCAGGTACGC
TTCACCTGCGAGAGAC)GAGTGCCCCCCCCCACATCGAGAACTTCAGCGACATCGACATGGGCGAGATCATCATGGGCA
ACATCGTGGGCATCGTGGCCGGCCTGGCCGTGCTGGCCGTGGTGGTGATCGGCGCCGTGGTGGCCACCGTGATGTGCA
GAAGAAAGAGCAGCGGCGGCAAGGGCGGCAGCTACAGCCAGGCCGCCAGCAGCGACAGCGCCCAGGGCAGCGACGTGA
GCCTGACCGCCTGATAA

References

[1] Fitzgerald PJ (1980). Medical anecdotes concerning some diseases of the pancreas. *Monographs in Pathology*, **21**, 1–29

[2] Howard JM and Hess W (November 2002). *History of the Pancreas: Mysteries of a Hidden Organ*. Springer

[3] Gray H and Harmon LW (1918). *Anatomy of the human body*. Philadelphia: Lea and Febiger

[4] Bockman DE (1993). *The Pancreas: Biology, Pathobiology and Disease*. Raven Press Limited, second edition

[5] Ionescu-Tirgoviste C et al. (September 2015). A 3D map of the islet routes throughout the healthy human pancreas. *Scientific Reports*, **5**(14634)

[6] Langerhans P (1869). *Über Beiträge zur pathologischen Anatomie der Bauchspeicheldrüse*. Ph.D. thesis, Berlin Pathological Institute

[7] Cabrera O et al. (February 2006). The unique cytoarchitecture of human pancreatic islets has implications for islet cell function. *PNAS*, **103**(7), 2334–2339

[8] Brissova M et al. (September 2005). Assessment of human pancreatic islet architecture and composition by laser scanning confocal microscopy. *Journal of Histochemistry and Cytochemistry*, **53**(9), 1087–1097

[9] Williams JA (March 2001). Intracellular signaling mechanisms activated by cholecystokinin-regulating synthesis and secretion of digestive enzymes in pancreatic acinar cells. *Annual Reviews of Physiology*, **63**, 77–97

[10] Githens S (July 1988). The pancreatic duct cell: proliferative capabilities, specific characteristics, metaplasia, isolation, and culture. *Journal of Pediatric Gastroenterology and Nutrition*, **7**(4), 486–506

[11] Grapin-Botton A (March 2005). Ductal cells of the pancreas. *International Journal of Biochemical Cell Biology*, **37**(3), 504–510

[12] Shih HP, Wang A and Sander M (October 2013). Pancreas Organogenesis: From Lineage Determination to Morphogenesis. *Annual Review of Cell and Developmental Biology*, **29**, 81–105

[13] Ryan DP, Hong TS and Nabeel B (September 2014). Pancreatic Adenocarcinoma. *New England Journal of Medicine*, **317**(11), 1039–1049

[14] Kleeff J et al. (April 2016). Pancreatic Cancer. *Nature Reviews Disease Primers*, **2**(16022), 1–22

[15] Yachida S et al. (October 2010). Distant metastasis occurs late during the genetic evolution of pancreatic cancer. *Nature*, **467**(7319), 1114–1117

[16] Haeno H et al. (January 2012). Computational modeling of pancreatic cancer reveals kinetics of metastasis suggesting optimum treatment strategies. *Cell*, **148**(1-2), 362–375

[17] Rhim AD et al. (January 2012). EMT and dissemination precede pancreatic tumor formation. *Cell*, **148**(1-2), 349–361

[18] for-Research-on Cancer IA (May 2018). World Cancer Report 2014
URL `http://www.iarc.fr/en/publications/pdfs-online/pat-gen/bb2/`

[19] Mayo, Foundation, for Medical Education and Research (March 2018). Pancreatic Cancer
URL `https://www.mayoclinic.org/diseases-conditions/pancreatic-cancer/symptoms-causes/syc-20355421?p=1`

[20] Bakkevold KE, Arnesjo B and Kambestad B (April 1992). Carcinoma of the pancreas and papilla of Vater: presenting symptoms, signs, and diagnosis related to stage and tumour site. A prospective multicentre trial in 472 patients. Norwegian Pancreatic Cancer Trial. *Scandinavian Journal of Gastroenterology*, **27**(4), 317–325

[21] Wolfgang CL et al. (September 2013). Recent progress in pancreatic cancer. *CA: A Cancer Journal for Clinicians*, **63**(5), 318–348

[22] Klimstra DS, Modlin IR, Coppola D, Lloyd RV and Suster S (August 2010). The pathologic classification of neuroendocrine tumors: a review of nomenclature, grading, and staging systems. *Pancreas*, **39**(6), 707–712

[23] Asa SL (April 2011). Pancreatic endocrine tumors. *Modern Pathology*, **24 Suppl 2**, S66–77

[24] Zhou C, Zhang J, Zheng Y and Zhu Z (September 2012). Pancreatic neuroendocrine tumors: a comprehensive review. *International Journal of Cancer*, **131**(5), 1013–1022

[25] Fesinmeyer MD, Austin MA, Li CI, De Roos AJ and Bowen DJ (July 2005). Differences in survival by histologic type of pancreatic cancer. *Cancer Epidemiology, Biomarkers and Prevention*, **14**(7), 1766–1773

[26] Turaga KK and Kvols LK (March 2011). Recent progress in the understanding, diagnosis, and treatment of gastroenteropancreatic neuroendocrine tumors. *CA: A Cancer Journal for Clinicians Cancer J Clin*, **61**(2), 113–132

[27] Mews P et al. (April 2002). Pancreatic stellate cells respond to inflammatory cytokines: potential role in chronic pancreatitis. *Gut*, **50**(4), 535–541

[28] Li J, Wientjes MG and Au JLS (June 2010). Pancreatic cancer: pathobiology, treatment options, and drug delivery. *AAPS Journal*, **12**(2), 223–232

[29] Erkan M et al. (May 2009). Cancer-stellate cell interactions perpetuate the hypoxia-fibrosis cycle in pancreatic ductal adenocarcinoma. *Neoplasia*, **11**(5), 497–508

[30] Lunardi S, Muschel RJ and Brunner TB (February 2014). The stromal compartments in pancreatic cancer: are there any therapeutic targets? *Cancer Letter*, **343**(2), 147–155

[31] Reichert M, Blume K, Kleger A, Hartmann D and von Figura G (November 2016). Developmental Pathways Direct Pancreatic Cancer Initiation from Its Cellular Origin. *Stem Cells International*, **2016**

[32] Ferreira RMM et al. (October 2017). Duct- and Acinar-Derived Pancreatic Ductal Adenocarcinomas Show Distinct Tumor Progression and Marker Expression. *Cell Reports*, **21**(4), 966–978

[33] Yamaguchi J, Yokoyama Y, Kokuryo T, Ebata T and Nagino M (January 2018). Cells of origin of pancreatic neoplasms. *Surgery Today*, **48**(1), 9–17

[34] Ferlay J et al. (2013). GLOBOCON 2012: Cancer Incidence and Mortality Worldwide: IARC CancerBase No. 11 [Internet]. *International Agency for Research on Cancer* URL `http://globocan.iarc.fr`

[35] Siegel RL, Miller KD and Jemal A (January 2018). Cancer statistics, 2018. *CA: A Cancer Journal for Clinicians*, **68**(1), 7–30

[36] Gillen S, Schuster T, Meyer Zum Buschenfelde C, Friess H and Kleeff J (April 2010). Preoperative/neoadjuvant therapy in pancreatic cancer: a systematic review and meta-analysis of response and resection percentages. *PLoS Medicine*, **7**(4), e1000267

[37] Hackert T and Büchler MW (June 2013). Pancreatic Cancer: Advances in Treatment, Results and Limitations. *Digestive Diseases*, **31**, 51–56

[38] Oettle H et al. (October 2013). Adjuvant chemotherapy with gemcitabine and long-term outcomes among patients with resected pancreatic cancer: the CONKO-001 randomized trial. *JAMA*, **310**(14), 1473–1481

[39] Conroy T et al. (May 2011). FOLFIRINOX versus gemcitabine for metastatic pancreatic cancer. *New England Journal of Medicine*, **364**(19), 1817–1825

[40] Van den Broeck A et al. (June 2009). Patterns of recurrence after curative resection of pancreatic ductal adenocarcinoma. *Eurpean Journal of Surgical Oncology*, **35**(6), 600–604

[41] Hruban RH, Maitra A, Kern SE and Goggins M (December 2007). Precursors to pancreatic cancer. *Gastroenterology Clinics of North America*, **36**(4), 831–849

[42] Basturk O et al. (December 2015). A Revised Classification System and Recommendations From the Baltimore Consensus Meeting for Neoplastic Precursor Lesions in the Pancreas. *American Journal of Surgical Pathology*, **39**(12), 1730–1741

[43] Kozuka S et al. (April 1979). Relation of pancreatic duct hyperplasia to carcinoma. *Cancer*, **43**(4), 1418–1428

[44] Cubilla AL and Fitzgerald PJ (July 1976). Morphological lesions associated with human primary invasive nonendocrine pancreas cancer. *Cancer Research*, **36**(7 PT 2), 2690–2698

[45] Andea A, Sarkar F and Adsay VN (October 2003). Clinicopathological correlates of pancreatic intraepithelial neoplasia: a comparative analysis of 82 cases with and 152 cases without pancreatic ductal adenocarcinoma. *Modern Pathology Pathol*, **16**(10), 996–1006

[46] Allen PJ et al. (October 2006). A selective approach to the resection of cystic lesions of the pancreas: results from 539 consecutive patients. *Annuals of Surgery*, **244**(4), 572–582

[47] Kanda M et al. (April 2012). Presence of somatic mutations in most early-stage pancreatic intraepithelial neoplasia. *Gastroenterology*, **142**(4), 730–733

[48] Perera RM and Bardeesy N (December 2015). Pancreatic Cancer Metabolism: Breaking It Down to Build It Back Up. *Cancer Discovery*, **5**(12), 1247–1261

[49] Castellano-Megias VM, Andres CId, Lopez-Alonso G and Colina-Ruizdelgado F (September 2014). Pathological features and diagnosis of intraductal papillary mucinous neoplasm of the pancreas. *World Journal of Gastroenterology*, **6**(9), 311–324

[50] Salvia R et al. (May 2004). Main-duct intraductal papillary mucinous neoplasms of the pancreas: clinical predictors of malignancy and long-term survival following resection. *Annals of Surgery*, **239**(5), 678–685

[51] Machado NO, Al Qadhi H and Al Wahibi K (May 2015). Intraductal Papillary Mucinous Neoplasm of Pancreas. *North American Journal of Medical Sciences*, **7**(5), 160–175

[52] Yamaguchi K et al. (May 2011). Pancreatic ductal adenocarcinoma derived from IPMN and pancreatic ductal adenocarcinoma concomitant with IPMN. *Pancreas*, **40**(4), 571–580

[53] Takano S et al. (June 2014). Deep sequencing of cancer-related genes revealed GNAS mutations to be associated with intraductal papillary mucinous neoplasms and its main pancreatic duct dilation. *PLoS One*, **9**(6), e98718

[54] Yoshizawa K et al. (November 2002). Clonality and K-ras mutation analyses of epithelia in intraductal papillary mucinous tumor and mucinous cystic tumor of the pancreas. *Virchows Archiv*, **441**(5), 437–443

[55] Adsay NV et al. (January 2001). Colloid (mucinous noncystic) carcinoma of the pancreas. *American Journal of Surgical Pathology*, **25**(1), 26–42

[56] Luttges J et al. (June 2003). Pancreatic mucinous noncystic (colloid) carcinomas and intraductal papillary mucinous carcinomas are usually microsatellite stable. *Modern Pathology*, **16**(6), 537–542

[57] Jimenez RE et al. (October 1999). Sequential accumulation of K-ras mutations and p53 overexpression in the progression of pancreatic mucinous cystic neoplasms to malignancy. *Annals of Surgery*, **230**(4), 501–509

[58] Iacobuzio-Donahue CA et al. (November 2000). Dpc4 protein in mucinous cystic neoplasms of the pancreas: frequent loss of expression in invasive carcinomas suggests a role in genetic progression. *American Journal of Surgical Pathology*, **24**(11), 1544–1548

[59] Kim SG et al. (November 2003). Comparison of epigenetic and genetic alterations in mucinous cystic neoplasm and serous microcystic adenoma of pancreas. *Modern Patholog*, **16**(11), 1086–1094

[60] Hezel AF, Kimmelman AC, Stanger BZ, Bardeesy N and Depinho RA (May 2006). Genetics and biology of pancreatic ductal adenocarcinoma. *Genes and Development*, **20**(10), 1218–1249

[61] Jones S et al. (September 2008). Core signaling pathways in human pancreatic cancers revealed by global genomic analyses. *Science*, **321**(5897), 1801–1806

[62] Biankin AV et al. (November 2012). Pancreatic cancer genomes reveal aberrations in axon guidance pathway genes. *Nature*, **491**(7424), 399–405

[63] Waddell N et al. (February 2015). Whole genomes redefine the mutational landscape of pancreatic cancer. *Nature*, **518**(7540), 495–501

[64] Bailey P et al. (March 2016). Genomic analyses identify molecular subtypes of pancreatic cancer. *Nature*, **531**(7592), 47–52

[65] Cancer-Genome-Atlas-Research-Network (August 2017). Integrated Genomic Characterization of Pancreatic Ductal Adenocarcinoma. *Cancer Cell*, **32**(2), 185–203

[66] Collisson EA et al. (April 2011). Subtypes of pancreatic ductal adenocarcinoma and their differing responses to therapy. *Nature Medicine*, **17**(4), 500–503

[67] Moffitt RA et al. (October 2015). Virtual microdissection identifies distinct tumor- and stroma-specific subtypes of pancreatic ductal adenocarcinoma. *Nature Genetics*, **47**(10), 1168–1178

[68] Lemoine NR et al. (January 1992). Ki-ras oncogene activation in preinvasive pancreatic cancer. *Gastroenterology*, **102**(1), 230–236

[69] Knickelbein K and Zhang L (March 2015). Mutant KRAS as a critical determinant of the therapeutic response of colorectal cancer. *Genes and Diseases*, **2**(1), 4–12

[70] Grant RC et al. (March 2015). Prevalence of germline mutations in cancer predisposition genes in patients with pancreatic cancer. *Gastroenterology*, **148**(3), 556–564

[71] Roberts NJ et al. (February 2016). Whole Genome Sequencing Defines the Genetic Heterogeneity of Familial Pancreatic Cancer. *Cancer Discovery*, **6**(2), 166–175

[72] Schumacher TN and Schreiber RD (April 2015). Neoantigens in cancer immunotherapy. *Science*, **348**(6230), 69–74

[73] Biankin AV et al. (November 2012). Pancreatic cancer genomes reveal aberrations in axon guidance pathway genes. *Nature*, **491**(7424), 399–405

[74] Ying H et al. (February 2016). Genetics and biology of pancreatic ductal adenocarcinoma. *Genes and Development*, **30**(4), 355–385

[75] Lowenfels AB et al. (March 1997). Hereditary pancreatitis and the risk of pancreatic cancer. International Hereditary Pancreatitis Study Group. *Journal of the National Cancer InstituteNational*, **89**(6), 442–446

[76] Lowenfels AB, Maisonneuve P, Whitcomb DC, Lerch MM and DiMagno EP (July 2001). Cigarette smoking as a risk factor for pancreatic cancer in patients with hereditary pancreatitis. *JAMA*, **286**(2), 169–170

[77] Tersmette AC et al. (March 2001). Increased risk of incident pancreatic cancer among first-degree relatives of patients with familial pancreatic cancer. *Clinical Cancer Research*, **7**(3), 738–744

[78] Klein AP et al. (April 2004). Prospective risk of pancreatic cancer in familial pancreatic cancer kindreds. *Cancer Research*, **64**(7), 2634–2638

[79] Rebours V et al. (January 2008). Risk of pancreatic adenocarcinoma in patients with hereditary pancreatitis: a national exhaustive series. *American Journal of Gastroenterology*, **103**(1), 111–119

[80] Aune D et al. (April 2012). Body mass index, abdominal fatness and pancreatic cancer risk: a systematic review and non-linear dose-response meta-analysis of prospective studies. *Annals of Oncology*, **23**(4), 843–852

[81] Duell EJ et al. (November 2012). Pancreatitis and pancreatic cancer risk: a pooled analysis in the International Pancreatic Cancer Case-Control Consortium (PanC4). *Annals of Oncology*, **23**(11), 2964–2970

[82] Goldstein AM et al. (October 1995). Increased risk of pancreatic cancer in melanoma-prone kindreds with p16INK4 mutations. *New England Journal of Medicine*, **333**(15), 970–974

[83] Giardiello FM et al. (December 2000). Very high risk of cancer in familial Peutz-Jeghers syndrome. *Gastroenterology*, **119**(6), 1447–1453

[84] Borg A et al. (August 2000). High frequency of multiple melanomas and breast and pancreas carcinomas in CDKN2A mutation-positive melanoma families. *Journal of the National Cancer Institute*, **92**(15), 1260–1266

[85] Vasen HF et al. (September 2000). Risk of developing pancreatic cancer in families with familial atypical multiple mole melanoma associated with a specific 19 deletion of p16 (p16-Leiden). *International Journal of Cancer*, **87**(6), 809–811

[86] Kastrinos F et al. (October 2009). Risk of pancreatic cancer in families with Lynch syndrome. *JAMA*, **302**(16), 1790–1795

[87] Bosetti C et al. (July 2012). Cigarette smoking and pancreatic cancer: an analysis from the International Pancreatic Cancer Case-Control Consortium (Panc4). *Annals of OncologyOncol*, **23**(7), 1880–1888

[88] Ben Q et al. (September 2011). Diabetes mellitus and risk of pancreatic cancer: A meta-analysis of cohort studies. *European Journal of Cancer*, **47**(13), 1928–1937

[89] Maisonneuve P, Marshall BC and Lowenfels AB (September 2007). Risk of pancreatic cancer in patients with cystic fibrosis. *Gut*, **56**(9), 1327–1328

[90] Iqbal J et al. (December 2012). The incidence of pancreatic cancer in BRCA1 and BRCA2 mutation carriers. *British Journal of Cancer*, **107**(12), 2005–2009

[91] Jones S et al. (April 2009). Exomic sequencing identifies PALB2 as a pancreatic cancer susceptibility gene. *Science*, **324**(5924), 217

[92] Yeh R, Steinman J, Luk L, Kluger MD and Hecht EM (March 2017). Imaging of pancreatic cancer: what the surgeon wants to know. *Clinical Imaging*, **42**, 203–217

[93] Amin MB et al. (March 2017). The Eighth Edition AJCC Cancer Staging Manual: Continuing to build a bridge from a population-based to a more "personalized" approach to cancer staging. *CA: A Cancer Journal for Clinicians*, **67**(2), 93–99

[94] Scialpi M et al. (April 2016). Pancreatic tumors imaging: An update. *International Journal of Surgery*, **28 Suppl 1**, S142–55

[95] Loizou L et al. (November 2016). Multidetector CT of pancreatic ductal adenocarcinoma: Effect of tube voltage and iodine load on tumour conspicuity and image quality. *European Radiology*, **26**(11), 4021–4029

[96] Shin EJ et al. (November 2015). Linear-array EUS improves detection of pancreatic lesions in high-risk individuals: a randomized tandem study. *Gastrointestinal Endoscopy*, **82**(5), 812–818

[97] Harinck F et al. (September 2016). A multicentre comparative prospective blinded analysis of EUS and MRI for screening of pancreatic cancer in high-risk individuals. *Gut*, **65**(9), 1505–1513

[98] Kiriyama S et al. (April 1990). Usefulness of a new tumor marker, Span-1, for the diagnosis of pancreatic cancer. *Cancer*, **65**(7), 1557–1561

[99] Fabris C et al. (March 1991). Serum DU-PAN-2 in the differential diagnosis of pancreatic cancer: influence of jaundice and liver dysfunction. *British Journal of Cancer*, **63**(3), 451–453

[100] Poruk KE et al. (March 2013). The clinical utility of CA 19-9 in pancreatic adenocarcinoma: diagnostic and prognostic updates. *Current Molecular Medicine*, **13**(3), 340–351

[101] Reitz D et al. (June 2015). Combination of tumour markers CEA and CA19-9 improves the prognostic prediction in patients with pancreatic cancer. *Journal of Clinical Pathology*, **68**(6), 427–433

[102] Bergquist JR et al. (July 2016). Carbohydrate Antigen 19-9 Elevation in Anatomically Resectable, Early Stage Pancreatic Cancer Is Independently Associated with Decreased

Overall Survival and an Indication for Neoadjuvant Therapy: A National Cancer Database Study. *Journal of the American College of Surgeons*, **223**(1), 52–65

[103] Kausch W (1912). Das Carcinom der Papilla duodeni und seine radikale Entfernung. *Beiträge zur klinischen Chirurgie*, **78**, 439–486

[104] Whipple AO (July 1963). A reminiscence: pancreaticduodenectomy. *Review of Surgery*, **20**, 221–225

[105] Bockhorn M et al. (June 2014). Borderline resectable pancreatic cancer: a consensus statement by the International Study Group of Pancreatic Surgery (ISGPS). *Surgery*, **155**(6), 977–988

[106] Hartwig W et al. (July 2014). Extended pancreatectomy in pancreatic ductal adenocarcinoma: definition and consensus of the International Study Group for Pancreatic Surgery (ISGPS). *Surgery*, **156**(1), 1–14

[107] Hartwig W et al. (March 2015). Total pancreatectomy for primary pancreatic neoplasms: renaissance of an unpopular operation. *Annals of Surgery*, **261**(3), 537–546

[108] Büchler MW et al. (December 2003). Changes in Morbidity After Pancreatic Resection: Toward the End of Completion Pancreatectomy. *Archives of Surgery*, **138**(12), 1310–1314

[109] Bramhall SR et al. (January 1995). Treatment and survival in 13,560 patients with pancreatic cancer, and incidence of the disease, in the West Midlands: an epidemiological study. *British Journal of Surgery*, **82**(1), 111–115

[110] Baumel H et al. (January 1994). Results of resection for cancer of the exocrine pancreas: a study from the French Association of Surgery. *British Journal of Surgery*, **81**(1), 102–107

[111] He J et al. (January 2014). 2564 resected periampullary adenocarcinomas at a single institution: trends over three decades. *HPB (Oxford)*, **16**(1), 83–90

[112] Mayo SC et al. (January 2012). Management of patients with pancreatic adenocarcinoma: national trends in patient selection, operative management, and use of adjuvant therapy. *Journal of the American College of Surgeons*, **214**(1), 33–45

[113] Heidelberger C et al. (March 1957). Fluorinated pyrimidines, a new class of tumour-inhibitory compounds. *Nature*, **179**(4561), 663–666

[114] Mallinson GN et al. (December 1980). Chemotherapy in pancreatic cancer: results of a controlled, prospective, randomised, multicentre trial. *British Medical Journal*, **281**, 1589–1591

[115] Glimelius B et al. (August 1996). Chemotherapy improves survival and quality of life in advanced pancreatic and biliary cancer. *Annals of Oncology*, **7**(6), 593–600

[116] Bakkevold KE, Arnesjo B, Dahl O and Kambestad B (June 1993). Adjuvant combination chemotherapy (AMF) following radical resection of carcinoma of the pancreas and papilla of Vater–results of a controlled, prospective, randomised multicentre study. *European Journal of Cancer*, **29A**(5), 698–703

[117] Cullinan SA et al. (April 1985). A comparison of three chemotherapeutic regimens in the treatment of advanced pancreatic and gastric carcinoma. Fluorouracil vs fluorouracil and doxorubicin vs fluorouracil, doxorubicin, and mitomycin. *JAMA*, **253**(14), 2061–2067

[118] Cullinan S et al. (May 1990). A phase III trial on the therapy of advanced pancreatic carcinoma. Evaluations of the Mallinson regimen and combined 5-fluorouracil, doxorubicin, and cisplatin. *Cancer*, **65**(10), 2207–2212

[119] DeCaprio JA, Mayer RJ, Gonin R and Arbuck SG (December 1991). Fluorouracil and high-dose leucovorin in previously untreated patients with advanced adenocarcinoma of the pancreas: results of a phase II trial. *Journal of Clinical Oncology*, **9**(12), 2128–2133

[120] Van Rijswijk REN et al. (September 2004). Weekly high-dose 5-fluorouracil and folinic acid in metastatic pancreatic carcinoma: a phase II study of the EORTC GastroIntestinal Tract Cancer Cooperative Group. *European Journal of Cancer*, **40**(14), 2077–2081

[121] Burris HAr et al. (June 1997). Improvements in survival and clinical benefit with gemcitabine as first-line therapy for patients with advanced pancreas cancer: a randomized trial. *Journal of Clinical Oncology*, **15**(6), 2403–2413

[122] Moore MJ et al. (May 2007). Erlotinib plus gemcitabine compared with gemcitabine alone in patients with advanced pancreatic cancer: a phase III trial of the National Cancer Institute of Canada Clinical Trials Group. *Journal of Clinical Oncology*, **25**(15), 1960–1966

[123] Herreros-Villanueva M, Hijona E, Cosme A and Bujanda L (April 2012). Adjuvant and neoadjuvant treatment in pancreatic cancer. *World Journal of Gastroenterology*, **18**(14), 1565–1572

[124] Adamska A, Domenichini A and Falasca M (June 2017). Pancreatic Ductal Adenocarcinoma: Current and Evolving Therapies. *International Journal of Molecular Sciences*, **18**(7)

[125] See F (August 2018). FDA approves Novartis drug Afinitor to treat pancreatic neuroendrocrine tumors
URL `https://www.pancan.org/about-us/news-press-center/2011-press-releases/fda-approves-novartis-drug-afinitor-to-treat-pancreatic-neuroendocrine-tumors-2/`

[126] of Health NI (August 2018). Targeted Therapies Sunitinib and Everolimus Improve Survival for Patients with Rare Type of Pancreatic Cancer
URL `https://www.cancer.gov/types/pancreatic/research/neuroendocrine-sunitinib-everolimus`

[127] Gourgou-Bourgade S et al. (January 2013). Impact of FOLFIRINOX compared with gemcitabine on quality of life in patients with metastatic pancreatic cancer: results from the PRODIGE 4/ACCORD 11 randomized trial. *Journal of Clinical Oncology*, **31**(1), 23–29

[128] Von Hoff DD et al. (October 2013). Increased survival in pancreatic cancer with nab-paclitaxel plus gemcitabine. *New England Journal of Medicine*, **369**(18), 1691–1703

[129] Neoptolemos JP et al. (March 2017). Comparison of adjuvant gemcitabine and capecitabine with gemcitabine monotherapy in patients with resected pancreatic cancer (ESPAC-4): a multicentre, open-label, randomised, phase 3 trial. *Lancet*, **389**(10073), 1011–1024

[130] Giordano G et al. (August 2017). Nano albumin bound-paclitaxel in pancreatic cancer: Current evidences and future directions. *World Journal of Gastroenterology*, **23**(32), 5875–5886

[131] Ehrlich P (1909). Ueber den jetzigen stand der Karzinomforschung. *Nederlandsch Tijdschrift voor Geneeskunde*, **1**(5)

[132] Dvorak HF (December 1986). Tumors: wounds that do not heal. Similarities between tumor stroma generation and wound healing. *New England Journal of Medicine*, **315**(26), 1650–1659

[133] Foley EJ (December 1953). Antigenic properties of methylcholanthrene-induced tumors in mice of the strain of origin. *Cancer Research*, **13**(12), 835–837

[134] PREHN RT and MAIN JM (June 1957). Immunity to methylcholanthrene-induced sarcomas. *Journal of the National Cancer Institute*, **18**(6), 769–778

[135] Shinkai Y et al. (March 1992). RAG-2-deficient mice lack mature lymphocytes owing to inability to initiate V(D)J rearrangement. *Cell*, **68**(5), 855–867

[136] Flanagan SP (December 1966). 'Nude', a new hairless gene with pleiotropic effects in the mouse. *Genetical Research*, **8**(3), 295–309

[137] Shankaran V et al. (April 2001). IFNgamma and lymphocytes prevent primary tumour development and shape tumour immunogenicity. *Nature*, **410**(6832), 1107–1111

[138] Rosenberg SA et al. (December 1985). Observations on the systemic administration of autologous lymphokine-activated killer cells and recombinant interleukin-2 to patients with metastatic cancer. *New England Journal of Medicine*, **313**(23), 1485–1492

[139] Rosenberg SA, Spiess P and Lafreniere R (September 1986). A new approach to the adoptive immunotherapy of cancer with tumor-infiltrating lymphocytes. *Science*, **233**(4770), 1318–1321

[140] Dudley ME et al. (October 2002). Cancer regression and autoimmunity in patients after clonal repopulation with antitumor lymphocytes. *Science*, **298**(5594), 850–854

[141] Morgan RA et al. (October 2006). Cancer regression in patients after transfer of genetically engineered lymphocytes. *Science*, **314**(5796), 126–129

[142] Tran E et al. (May 2014). Cancer immunotherapy based on mutation-specific CD4+ T cells in a patient with epithelial cancer. *Science*, **344**(6184), 641–645

[143] Tran E et al. (December 2015). Immunogenicity of somatic mutations in human gastrointestinal cancers. *Science*, **350**(6266), 1387–1390

[144] Tran E et al. (December 2016). T-Cell Transfer Therapy Targeting Mutant KRAS in Cancer. *New England Journal of Medicine*, **375**(23), 2255–226

[145] Zacharakis N et al. (June 2018). Immune recognition of somatic mutations leading to complete durable regression in metastatic breast cancer. *Nature Medicine*, **24**, 724–730

[146] Lu YC et al. (July 2014). Efficient identification of mutated cancer antigens recognized by T cells associated with durable tumor regressions. *Clinical Cancer Research*, **20**(13), 3401–3410

[147] Boveri T (1914). *Zur Frage der Entstehung maligner Tumoren*. Gustav Fischer

[148] Cairns J (May 1975). Mutation selection and the natural history of cancer. *Nature*, **255**(5505), 197–200

[149] Nowell PC (October 1976). The clonal evolution of tumor cell populations. *Science*, **194**(4260), 23–28

[150] Martincorena I et al. (November 2017). Universal Patterns of Selection in Cancer and Somatic Tissues. *Cell*, **171**(5), 1029–1041

[151] Venter JC et al. (February 2001). The sequence of the human genome. *Science*, **291**(5507), 1304–1351

[152] Margulies M et al. (September 2005). Genome sequencing in microfabricated high-density picolitre reactors. *Nature*, **437**(7057), 376–380

[153] Matsushita H et al. (February 2012). Cancer exome analysis reveals a T-cell-dependent mechanism of cancer immunoediting. *Nature*, **482**(7385), 400–404

[154] Castle JC et al. (March 2012). Exploiting the mutanome for tumor vaccination. *Cancer Research*, **72**(5), 1081–1091

[155] Heemskerk B, Kvistborg P and Schumacher TNM (January 2013). The cancer antigenome. *EMBO Journal*, **32**(2), 194–203

[156] Vogelstein B et al. (March 2013). Cancer genome landscapes. *Science*, **339**(6127), 1546–1558

[157] McGranahan N et al. (April 2015). Clonal status of actionable driver events and the timing of mutational processes in cancer evolution. *Science Translational Medicine*, **7**(283), 283ra54

[158] Dagogo-Jack I and Shaw AT (February 2018). Tumour heterogeneity and resistance to cancer therapies. *Nature Reviews Clinical Oncology*, **15**(2), 81–94

[159] Ye CJ, Liu G, Bremer SW and Heng HHQ (November 2007). The dynamics of cancer chromosomes and genomes. *Cytogenetic and Genome Research*, **118**(2-4), 237–246

[160] Bhang HeC et al. (May 2015). Studying clonal dynamics in response to cancer therapy using high-complexity barcoding. *Nature Medicine*, **21**(5), 440–448

[161] Russo M et al. (February 2016). Tumor Heterogeneity and Lesion-Specific Response to Targeted Therapy in Colorectal Cancer. *Cancer Discovery*, **6**(2), 147–153

[162] Jamal-Hanjani M et al. (June 2017). Tracking the Evolution of Non-Small-Cell Lung Cancer. *New England Journal of Medicine*, **376**(22), 2109–2121

[163] McGranahan N et al. (March 2016). Clonal neoantigens elicit T cell immunoreactivity and sensitivity to immune checkpoint blockade. *Science*, **351**(6280), 1463–1469

[164] Rooney MS, Shukla SA, Wu CJ, Getz G and Hacohen N (January 2015). Molecular and genetic properties of tumors associated with local immune cytolytic activity. *Cell*, **160**(1-2), 48–61

[165] Gilboa E (September 1999). The makings of a tumor rejection antigen. *Immunity*, **11**(3), 263–270

[166] Hewitt HB, Blake ER and Walder AS (March 1976). A critique of the evidence for active host defence against cancer, based on personal studies of 27 murine tumours of spontaneous origin. *British Journal of Cancer*, **33**(3), 241–259

[167] Van Pel A and Boon T (August 1982). Protection against a nonimmunogenic mouse leukemia by an immunogenic variant obtained by mutagenesis. *PNAS*, **79**(15), 4718–4722

[168] Knuth A, Wolfel T, Klehmann E, Boon T and Meyer zum Buschenfelde KH (April 1989). Cytolytic T-cell clones against an autologous human melanoma: specificity study and definition of three antigens by immunoselection. *PNAS*, **86**(8), 2804–2808

[169] van der Bruggen P et al. (December 1991). A gene encoding an antigen recognized by cytolytic T lymphocytes on a human melanoma. *Science*, **254**(5038), 1643–1647

[170] Brichard V et al. (August 1993). The tyrosinase gene codes for an antigen recognized by autologous cytolytic T lymphocytes on HLA-A2 melanomas. *Journal of Experimental Medicine*, **178**(2), 489–495

[171] Kawakami Y et al. (July 1994). Identification of the immunodominant peptides of the MART-1 human melanoma antigen recognized by the majority of HLA-A2-restricted tumor infiltrating lymphocytes. *Journal of Experimental Medicine*, **180**(1), 347–352

[172] Kawakami Y et al. (July 1994). Identification of a human melanoma antigen recognized by tumor-infiltrating lymphocytes associated with in vivo tumor rejection. *PNAS*, **91**(14), 6458–6462

[173] Coulie PG et al. (August 1995). A mutated intron sequence codes for an antigenic peptide recognized by cytolytic T lymphocytes on a human melanoma. *PNAS*, **92**(17), 7976–7980

[174] Wolfel T et al. (September 1995). A p16INK4a-insensitive CDK4 mutant targeted by cytolytic T lymphocytes in a human melanoma. *Science*, **269**(5228), 1281–1284

[175] Linnemann C et al. (January 2015). High-throughput epitope discovery reveals frequent recognition of neo-antigens by CD4+ T cells in human melanoma. *Nature Medicine*, **21**(1), 81–85

[176] Sahin U et al. (July 2017). Personalized RNA mutanome vaccines mobilize poly-specific therapeutic immunity against cancer. *Nature*, **547**(7662), 222–226

[177] Bailey P et al. (October 2016). Exploiting the neoantigen landscape for immunotherapy of pancreatic ductal adenocarcinoma. *Scientific Reports*, **6**, 35848

[178] Balachandran VP et al. (November 2017). Identification of unique neoantigen qualities in long-term survivors of pancreatic cancer. *Nature*, **551**(7681), 512–516

[179] Yadav M et al. (November 2014). Predicting immunogenic tumour mutations by combining mass spectrometry and exome sequencing. *Nature*, **515**(7528), 572–576

[180] Kalaora S et al. (February 2016). Use of HLA peptidomics and whole exome sequencing to identify human immunogenic neo-antigens. *Oncotarget*, **7**(5), 5110–5117

[181] Bassani-Sternberg M et al. (November 2016). Direct identification of clinically relevant neoepitopes presented on native human melanoma tissue by mass spectrometry. *Nature Communications*, **7**, 13404

[182] Backert L and Kohlbacher O (November 2015). Immunoinformatics and epitope prediction in the age of genomic medicine. *Genome Medicine*, **7**(20), 119

[183] Editorial (February 2017). The problem with neoantigen prediction. *Nature Biotechnology*, **35**(2), 97

[184] Thomas L and Lawrence H (1959). Cellular and humoral aspects of the hypersensitive states. *Hoeber-Harper*, pp. 529–532

[185] Burnet M (April 1957). Cancer; a biological approach. I. The processes of control. *British Journal of Medicine*, **1**(5022), 779–786

[186] Dunn GP, Bruce AT, Ikeda H, Old LJ and Schreiber RD (November 2002). Cancer immunoediting: from immunosurveillance to tumor escape. *Nature Immunology*, **3**(11), 991–998

[187] Schreiber RD, Old LJ and Smyth MJ (March 2011). Cancer immunoediting: integrating immunity's roles in cancer suppression and promotion. *Science*, **331**(6024), 1565–1570

[188] Nicholaou T et al. (November 2011). Immunoediting and persistence of antigen-specific immunity in patients who have previously been vaccinated with NY-ESO-1 protein formulated in ISCOMATRIX. *Cancer Immunology Immunotherapy Immunother*, **60**(11), 1625–1637

[189] von Boehmer L et al. (July 2013). NY-ESO-1-specific immunological pressure and escape in a patient with metastatic melanoma. *Cancer Immununity*, **13**(15), 12

[190] Diamond MS et al. (September 2011). Type I interferon is selectively required by dendritic cells for immune rejection of tumors. *Journal of Experimental Medicine*, **208**(10), 1989–2003

[191] Mittal D, Gubin MM, Schreiber RD and Smyth MJ (April 2014). New insights into cancer immunoediting and its three component phases–elimination, equilibrium and escape. *Current Opinion in Immunology*, **27**, 16–25

[192] Koebel CM et al. (December 2007). Adaptive immunity maintains occult cancer in an equilibrium state. *Nature*, **450**(7171), 903–907

[193] Eyles J et al. (June 2010). Tumor cells disseminate early, but immunosurveillance limits metastatic outgrowth, in a mouse model of melanoma. *Journal of Clinical Investigation*, **120**(6), 2030–2039

[194] Muller-Hermelink N et al. (June 2008). TNFR1 signaling and IFN-gamma signaling determine whether T cells induce tumor dormancy or promote multistage carcinogenesis. *Cancer Cell*, **13**(6), 507–518

[195] Terness P et al. (August 2002). Inhibition of allogeneic T cell proliferation by indoleamine 2,3-dioxygenase-expressing dendritic cells: mediation of suppression by tryptophan metabolites. *Journal of Experimental Medicine*, **196**(4), 447–457

[196] Atkins D et al. (March 2004). MHC class I antigen processing pathway defects, ras mutations and disease stage in colorectal carcinoma. *International Journal of Cancer*, **109**(2), 265–273

[197] Huang Y, Obholzer N, Fayad R and Qiao L (September 2005). Turning on/off tumor-specific CTL response during progressive tumor growth. *Journal of Immunology*, **175**(5), 3110–3116

[198] Guiducci C, Vicari AP, Sangaletti S, Trinchieri G and Colombo MP (April 2005). Redirecting in vivo elicited tumor infiltrating macrophages and dendritic cells towards tumor rejection. *Cancer Research*, **65**(8), 3437–3446

[199] Stockwin LH, McGonagle D, Martin IG and Blair GE (April 2000). Dendritic cells: immunological sentinels with a central role in health and disease. *Immunology and Cell Biology*, **78**(2), 91–102

[200] Mann ER and Li X (August 2014). Intestinal antigen-presenting cells in mucosal immune homeostasis: crosstalk between dendritic cells, macrophages and B-cells. *World Journal of Gastroenterology*, **20**(29), 9653–9664

[201] O'Keeffe M, Mok WH and Radford KJ (November 2015). Human dendritic cell subsets and function in health and disease. *Cellular and Molecular Life Sciences*, **72**(22), 4309–4325

[202] Dalod M, Chelbi R, Malissen B and Lawrence T (May 2014). Dendritic cell maturation: functional specialization through signaling specificity and transcriptional programming. *EMBO Journal*, **33**(10), 1104–1116

[203] Neefjes J, Jongsma MLM, Paul P and Bakke O (November 2011). Towards a systems understanding of MHC class I and MHC class II antigen presentation. *Nature Reviews Immunology*, **11**(12), 823–836

[204] den Haan JMM, Arens R and van Zelm MC (December 2014). The activation of the adaptive immune system: cross-talk between antigen-presenting cells, T cells and B cells. *Immunology Letters*, **162**(2 Pt B), 103–112

[205] Dembic Z, Schenck K and Bogen B (March 2000). Dendritic cells purified from myeloma are primed with tumor-specific antigen (idiotype) and activate CD4+ T cells. *PNAS*, **97**(6), 2697–2702

[206] Corthay A et al. (March 2005). Primary antitumor immune response mediated by CD4+ T cells. *Immunity*, **22**(3), 371–383

[207] Joffre OP, Segura E, Savina A and Amigorena S (July 2012). Cross-presentation by dendritic cells. *Nature Reviews Immunology*, **12**(8), 557–569

[208] Schwarz BA and Bhandoola A (February 2006). Trafficking from the bone marrow to the thymus: a prerequisite for thymopoiesis. *Immunology Reviews*, **209**, 47–57

[209] Klein L, Hinterberger M, Wirnsberger G and Kyewski B (December 2009). Antigen presentation in the thymus for positive selection and central tolerance induction. *Nature Reviews Immunology*, **9**(12), 833–844

[210] Ma D, Wei Y and Liu F (January 2013). Regulatory mechanisms of thymus and T cell development. *Developmental and comparative immunology*, **39**(1-2), 91–102

[211] Klein L, Kyewski B, Allen PM and Hogquist KA (June 2014). Positive and negative selection of the T cell repertoire: what thymocytes see (and don't see). *Nature Reviews Immunology*, **14**(6), 377–391

[212] Zhu J, Yamane H and Paul WE (2010). Differentiation of effector CD4 T cell populations (*). *Annual Review of Immunology*, **28**, 445–489

[213] DuPage M and Bluestone JA (March 2016). Harnessing the plasticity of CD4(+) T cells to treat immune-mediated disease. *Nature Reviews Immunology*, **16**(3), 149–163

[214] Sallusto F, Lenig D, Förster R, Lipp M and Lanzavecchia A (October 1999). Two subsets of memory T lymphocytes with distinct homing potentials and effector functions. *Nature*, **401**, 708–712

[215] Dong C and Martinez GJ (2015). T cells: the usual subsets. *Nature Reviews Immunology*

[216] Mempel TR, Henrickson SE and Von Andrian UH (January 2004). T-cell priming by dendritic cells in lymph nodes occurs in three distinct phases. *Nature*, **427**(6970), 154–159

[217] Obst R (November 2015). The Timing of T Cell Priming and Cycling. *Frontiers in Immunology*, **6**, 563

[218] Wherry EJ (June 2011). T cell exhaustion. *Nature Immunology*, **12**(6), 492–499

[219] Wherry EJ and Kurachi M (August 2015). Molecular and cellular insights into T cell exhaustion. *Nature Reviews Immunology*, **15**(8), 486–499

[220] Antony PA et al. (March 2005). CD8+ T cell immunity against a tumor/self-antigen is augmented by CD4+ T helper cells and hindered by naturally occurring T regulatory cells. *Journal of Immunology*, **174**(5), 2591–2601

[221] Quezada SA et al. (March 2010). Tumor-reactive CD4(+) T cells develop cytotoxic activity and eradicate large established melanoma after transfer into lymphopenic hosts. *Journal of Experimental Medicine*, **207**(3), 637–650

[222] Haabeth OAW et al. (April 2014). How Do CD4(+) T Cells Detect and Eliminate Tumor Cells That Either Lack or Express MHC Class II Molecules? *Frontiers in Immunology*, **5**(15), 174

[223] Martinez-Lostao L, Anel A and Pardo J (November 2015). How Do Cytotoxic Lymphocytes Kill Cancer Cells? *Clinical Cancer Research*, **21**(22), 5047–5056

[224] Peter ME et al. (April 2015). The role of CD95 and CD95 ligand in cancer. *Cell Death and Differentiation*, **22**(4), 549–559

[225] Kohler G and Milstein C (August 1975). Continuous cultures of fused cells secreting antibody of predefined specificity. *Nature*, **256**(5517), 495–497

[226] Nadler LM et al. (September 1980). Serotherapy of a patient with a monoclonal antibody directed against a human lymphoma-associated antigen. *Cancer Research*, **40**(9), 3147–3154

[227] Ritz J and Schlossman SF (January 1982). Utilization of monoclonal antibodies in the treatment of leukemia and lymphoma. *Blood*, **59**(1), 1–11

[228] Maloney DG et al. (September 1997). IDEC-C2B8 (Rituximab) anti-CD20 monoclonal antibody therapy in patients with relapsed low-grade non-Hodgkin's lymphoma. *Blood*, **90**(6), 2188–2195

[229] James JS and Dubs G (December 1997). FDA approves new kind of lymphoma treatment. Food and Drug Administration. *AIDS Treatment News*, (284), 2–3

[230] Brunet JF et al. (July 1987). A new member of the immunoglobulin superfamily–CTLA-4. *Nature*, **328**(6127), 267–270

[231] Tivol EA et al. (November 1995). Loss of CTLA-4 leads to massive lymphoproliferation and fatal multiorgan tissue destruction, revealing a critical negative regulatory role of CTLA-4. *Immunity*, **3**(5), 541–547

[232] Butte MJ, Keir ME, Phamduy TB, Sharpe AH and Freeman GJ (July 2007). Programmed death-1 ligand 1 interacts specifically with the B7-1 costimulatory molecule to inhibit T cell responses. *Immunity*, **27**(1), 111–122

[233] Karwacz K et al. (October 2011). PD-L1 co-stimulation contributes to ligand-induced T cell receptor down-modulation on CD8+ T cells. *EMBO Molecular Medicine*, **3**(10), 581–592

[234] Pardoll DM (March 2012). The blockade of immune checkpoints in cancer immunotherapy. *Nature Reviews Cancer*, **12**(4), 252–264

[235] Zou W, Wolchok JD and Chen L (March 2016). PD-L1 (B7-H1) and PD-1 pathway blockade for cancer therapy: Mechanisms, response biomarkers, and combinations. *Science Translational Medicine*, **8**(328), 328rv4

[236] Hodi FS et al. (April 2003). Biologic activity of cytotoxic T lymphocyte-associated antigen 4 antibody blockade in previously vaccinated metastatic melanoma and ovarian carcinoma patients. *PNAS*, **100**(8), 4712–4717

[237] Phan GQ et al. (July 2003). Cancer regression and autoimmunity induced by cytotoxic T lymphocyte-associated antigen 4 blockade in patients with metastatic melanoma. *PNAS*, **100**(14), 8372–8377

[238] Hodi FS et al. (August 2010). Improved survival with ipilimumab in patients with metastatic melanoma. *New England Journal of Medicine*, **363**(8), 711–723

[239] Beatty GL et al. (November 2013). A phase I study of an agonist CD40 monoclonal antibody (CP-870,893) in combination with gemcitabine in patients with advanced pancreatic ductal adenocarcinoma. *Clinical Cancer Research*, **19**(22), 6286–6295

[240] Morales-Kastresana A et al. (November 2013). Combined immunostimulatory monoclonal antibodies extend survival in an aggressive transgenic hepatocellular carcinoma mouse model. *Clinical Cancer Research*, **19**(22), 6151–6162

[241] Weigelin B et al. (June 2015). Focusing and sustaining the antitumor CTL effector killer response by agonist anti-CD137 mAb. *PNAS*, **112**(24), 7551–7556

[242] Kantarjian H et al. (March 2017). Blinatumomab versus Chemotherapy for Advanced Acute Lymphoblastic Leukemia. *New England Journal of Medicine*, **376**(9), 836–847

[243] Platform ACTI (May 2018). Monoclonal Antibodies Approved by the EMA and FDA for Therapeutic Use (Status 2017)
URL `http://www.actip.org/products/monoclonal-antibodies-approved-by-the-ema-and-fda-for-therapeutic-use/`

[244] Cancer-Research-Institute (May 2018). Timeline of Progress
URL https://www.cancerresearch.org/immunotherapy/timeline-of-progress

[245] Melero I et al. (September 2014). Therapeutic vaccines for cancer: an overview of clinical trials. *Nature Reviews Clinical Oncology*, **11**(9), 509–524

[246] Melief CJM, van Hall T, Arens R, Ossendorp F and van der Burg SH (September 2015). Therapeutic cancer vaccines. *Journal of Clinical Investigation*, **125**(9), 3401–3412

[247] Beatty PL and Finn OJ (May 2013). Preventing cancer by targeting abnormally expressed self-antigens: MUC1 vaccines for prevention of epithelial adenocarcinomas. *Annals of the New York Academy of Science*, **1284**, 52–56

[248] Ott PA et al. (July 2017). An immunogenic personal neoantigen vaccine for patients with melanoma. *Nature*, **547**(7662), 217–221

[249] Ogi C and Aruga A (May 2013). Clinical evaluation of therapeutic cancer vaccines. *Human Vaccines and Immunotherapeutics*, **9**(5), 1049–1057

[250] Pedersen SR, Sorensen MR, Buus S, Christensen JP and Thomsen AR (October 2013). Comparison of vaccine-induced effector CD8 T cell responses directed against self- and non-self-tumor antigens: implications for cancer immunotherapy. *Journal of Immunology*, **191**(7), 3955–3967

[251] Kantoff PW et al. (July 2010). Sipuleucel-T immunotherapy for castration-resistant prostate cancer. *New England Journal of Medicine*, **363**(5), 411–422

[252] Kreiter S et al. (January 2008). Increased antigen presentation efficiency by coupling antigens to MHC class I trafficking signals. *Journal of Immunology*, **180**(1), 309–318

[253] Kreiter S et al. (April 2015). Mutant MHC class II epitopes drive therapeutic immune responses to cancer. *Nature*, **520**(7549), 692–696

[254] Rosenberg SA and Restifo NP (April 2015). Adoptive cell transfer as personalized immunotherapy for human cancer. *Science*, **348**(6230), 62–68

[255] Morgan DA, Ruscetti FW and Gallo R (September 1976). Selective in vitro growth of T lymphocytes from normal human bone marrows. *Science*, **193**(4257), 1007–1008

[256] Welte K et al. (August 1982). Purification of human interleukin 2 to apparent homogeneity and its molecular heterogeneity. *Journal of Experimental Medicine*, **156**(2), 454–464

[257] Eberlein TJ, Rosenstein M and Rosenberg SA (August 1982). Regression of a disseminated syngeneic solid tumor by systemic transfer of lymphoid cells expanded in interleukin 2. *Journal of Experimental Medicine*, **156**(2), 385–397

[258] Donohue JH et al. (April 1984). The systemic administration of purified interleukin 2 enhances the ability of sensitized murine lymphocytes to cure a disseminated syngeneic lymphoma. *Journal of Immunology*, **132**(4), 2123–2128

[259] Muul LM, Spiess PJ, Director EP and Rosenberg SA (February 1987). Identification of specific cytolytic immune responses against autologous tumor in humans bearing malignant melanoma. *Journal of Immunology*, **138**(3), 989–995

[260] Rosenberg SA et al. (December 1988). Use of tumor-infiltrating lymphocytes and interleukin-2 in the immunotherapy of patients with metastatic melanoma. A preliminary report. *New England Journal of Medicine*, **319**(25), 1676–1680

[261] Rosenberg SA et al. (August 1994). Treatment of patients with metastatic melanoma with autologous tumor-infiltrating lymphocytes and interleukin 2. *Journal of the National Cancer Institute*, **86**(15), 1159–1166

[262] Rosenberg SA et al. (July 2011). Durable complete responses in heavily pretreated patients with metastatic melanoma using T-cell transfer immunotherapy. *Clinical Cancer Research*, **17**(13), 4550–4557

[263] Pilon-Thomas S et al. (October 2012). Efficacy of adoptive cell transfer of tumor-infiltrating lymphocytes after lymphopenia induction for metastatic melanoma. *Journal of Immunotherapy*, **35**(8), 615–620

[264] Parkhurst MR et al. (March 2011). T cells targeting carcinoembryonic antigen can mediate regression of metastatic colorectal cancer but induce severe transient colitis. *Molecular Therapy*, **19**(3), 620–626

[265] Nishimura T et al. (September 1999). Distinct role of antigen-specific T helper type 1 (Th1) and Th2 cells in tumor eradication in vivo. *Journal of Experimental Medicine*, **190**(5), 617–627

[266] Zhang L et al. (January 2003). Intratumoral T cells, recurrence, and survival in epithelial ovarian cancer. *New England Journal of Medicine*, **348**(3), 203–213

[267] Galon J et al. (September 2006). Type, density, and location of immune cells within human colorectal tumors predict clinical outcome. *Science*, **313**(5795), 1960–1964

[268] Fridman WH, Pages F, Sautes-Fridman C and Galon J (March 2012). The immune contexture in human tumours: impact on clinical outcome. *Nature Reviews Cancer*, **12**(4), 298–306

[269] Carstens JL et al. (April 2017). Spatial computation of intratumoral T cells correlates with survival of patients with pancreatic cancer. *Nature Communications*, **8**, 15095

[270] Kochenderfer JN et al. (November 2010). Eradication of B-lineage cells and regression of lymphoma in a patient treated with autologous T cells genetically engineered to recognize CD19. *Blood*, **116**(20), 4099–4102

[271] van der Stegen SJC, Hamieh M and Sadelain M (July 2015). The pharmacology of second-generation chimeric antigen receptors. *Nature Reviews Drug Discovery*, **14**(7), 499–509

[272] Novartis-Pharma-AG (August 2017). Novartis receives first ever FDA approval for a CAR-T cell therapy, Kymriah(TM) (CTL019), for children and young adults with B-cell ALL that is refractory or has relapsed at least twice
URL https://www.novartis.com/news/media-releases/novartis-receives-first-ever-fda-approval-car-t-cell-therapy-kymriahtm-ctl019

[273] and Drug-Administration F (October 2017). FDA approves CAR-T cell therapy to treat adults with certain types of large B-cell lymphoma
URL https://www.fda.gov/NewsEvents/Newsroom/PressAnnouncements/ucm581216.htm

[274] Ademmer K et al. (April 1998). Effector T lymphocyte subsets in human pancreatic cancer: detection of CD8+CD18+ cells and CD8+CD103+ cells by multi-epitope imaging. *Clinical and Experimental Immunology*, **112**(1), 21–26

[275] von Bernstorff W et al. (March 2001). Systemic and local immunosuppression in pancreatic cancer patients. *Clinical Cancer Research*, **7**(3 Suppl), 925s–932s

[276] Ryschich E et al. (January 2005). Control of T-cell-mediated immune response by HLA class I in human pancreatic carcinoma. *Clinical Cancer Research*, **11**(2 Pt 1), 498–504

[277] Hartmann N et al. (July 2014). Prevailing role of contact guidance in intrastromal T-cell trapping in human pancreatic cancer. *Clinical Cancer Research*, **20**(13), 3422–3433

[278] Winograd R et al. (April 2015). Induction of T-cell Immunity Overcomes Complete Resistance to PD-1 and CTLA-4 Blockade and Improves Survival in Pancreatic Carcinoma. *Cancer Immunology Research*, **3**(4), 399–411

[279] Poschke I et al. (October 2016). Identification of a tumor-reactive T-cell repertoire in the immune infiltrate of patients with resectable pancreatic ductal adenocarcinoma. *Oncoimmunology*, **5**(12), e1240859

[280] Hall M et al. (October 2016). Expansion of tumor-infiltrating lymphocytes (TIL) from human pancreatic tumors. *Journal for Immunotherapy of Cancer*, **4**(61)

[281] Meng Q et al. (February 2016). Expansion of Tumor-reactive T Cells From Patients With Pancreatic Cancer. *Journal of Immunotherapy*, **39**(2), 81–89

[282] Shibuya KC et al. (May 2014). Pancreatic ductal adenocarcinoma contains an effector and regulatory immune cell infiltrate that is altered by multimodal neoadjuvant treatment. *PLoS One*, **9**(5), e96565

[283] Fukunaga A et al. (January 2004). CD8+ tumor-infiltrating lymphocytes together with CD4+ tumor-infiltrating lymphocytes and dendritic cells improve the prognosis of patients with pancreatic adenocarcinoma. *Pancreas*, **28**(1), e26–31

[284] Karakhanova S et al. (March 2015). Prognostic and predictive value of immunological parameters for chemoradioimmunotherapy in patients with pancreatic adenocarcinoma. *British Journal of Cancer*, **112**(6), 1027–1036

[285] Dieu-Nosjean MC, Goc J, Giraldo NA, Sautes-Fridman C and Fridman WH (November 2014). Tertiary lymphoid structures in cancer and beyond. *Trends in Immunology*, **35**(11), 571–580

[286] Hiraoka N et al. (May 2015). Intratumoral tertiary lymphoid organ is a favourable prognosticator in patients with pancreatic cancer. *British Journal of Cancer*, **112**(11), 1782–1790

[287] Castino GF et al. (April 2016). Spatial distribution of B cells predicts prognosis in human pancreatic adenocarcinoma. *Oncoimmunology*, **5**(4), e1085147

[288] Clark CE et al. (October 2007). Dynamics of the immune reaction to pancreatic cancer from inception to invasion. *Cancer Research*, **67**(19), 9518–9527

[289] Vonderheide RH and Bayne LJ (April 2013). Inflammatory networks and immune surveillance of pancreatic carcinoma. *Current Opinion in Immunology*, **25**(2), 200–205

[290] Hodi FS et al. (August 2010). Improved survival with ipilimumab in patients with metastatic melanoma. *New England Journal of Medicine*, **363**(8), 711–723

[291] Topalian SL et al. (June 2012). Safety, activity, and immune correlates of anti-PD-1 antibody in cancer. *New England Journal of Medicine*, **366**(26), 2443–2454

[292] Topalian SL et al. (April 2014). Survival, durable tumor remission, and long-term safety in patients with advanced melanoma receiving nivolumab. *Journal of Clinical Oncology*, **32**(10), 1020–1030

[293] Royal RE et al. (October 2010). Phase 2 trial of single agent Ipilimumab (anti-CTLA-4) for locally advanced or metastatic pancreatic adenocarcinoma. *Journal of Immunotherapy*, **33**(8), 828–833

[294] Brahmer JR et al. (June 2012). Safety and activity of anti-PD-L1 antibody in patients with advanced cancer. *New England Journal of Medicine*, **366**(26), 2455–2465

[295] Aglietta M et al. (September 2014). A phase I dose escalation trial of tremelimumab (CP-675,206) in combination with gemcitabine in chemotherapy-naive patients with metastatic pancreatic cancer. *Annals of Oncology*, **25**(9), 1750–1755

[296] Grewal IS and Flavell RA (April 1998). CD40 and CD154 in cell-mediated immunity. *Annual Review of Immunology*, **16**, 111–135

[297] van Kooten C and Banchereau J (January 2000). CD40-CD40 ligand. *Journal of Leukocyte Biology*, **67**(1), 2–17

[298] Beatty GL et al. (March 2011). CD40 agonists alter tumor stroma and show efficacy against pancreatic carcinoma in mice and humans. *Science*, **331**(6024), 1612–1616

[299] Jaffee EM et al. (January 2001). Novel allogeneic granulocyte-macrophage colony-stimulating factor-secreting tumor vaccine for pancreatic cancer: a phase I trial of safety and immune activation. *Journal of Clinical Oncology*, **19**(1), 145–156

[300] Kaufman HL et al. (November 2007). Poxvirus-based vaccine therapy for patients with advanced pancreatic cancer. *Journal of Translational Medicine*, **5**, 60

[301] Hardacre JM et al. (January 2013). Addition of algenpantucel-L immunotherapy to standard adjuvant therapy for pancreatic cancer: a phase 2 study. *Journal of Gastrointestinal Surgery*, **17**(1), 94–100

[302] Nishida S et al. (February 2014). Wilms tumor gene (WT1) peptide-based cancer vaccine combined with gemcitabine for patients with advanced pancreatic cancer. *Journal of Immunotherapy*, **37**(2), 105–114

[303] Laheru D et al. (March 2008). Allogeneic granulocyte macrophage colony-stimulating factor-secreting tumor immunotherapy alone or in sequence with cyclophosphamide for metastatic pancreatic cancer: a pilot study of safety, feasibility, and immune activation. *Clinical Cancer Research*, **14**(5), 1455–1463

[304] Le DT et al. (April 2015). Safety and survival with GVAX pancreas prime and Listeria Monocytogenes-expressing mesothelin (CRS-207) boost vaccines for metastatic pancreatic cancer. *Journal of Clinical Oncology*, **33**(12), 1325–1333

[305] Kawaoka T et al. (July 2008). Adoptive immunotherapy for pancreatic cancer: cytotoxic T lymphocytes stimulated by the MUC1-expressing human pancreatic cancer cell line YPK-1. *Oncology Reports*, **20**(1), 155–163

[306] Kondo H et al. (January 2008). Adoptive immunotherapy for pancreatic cancer using MUC1 peptide-pulsed dendritic cells and activated T lymphocytes. *Anticancer Research*, **28**(1B), 379–387

[307] Beatty GL et al. (February 2014). Mesothelin-specific chimeric antigen receptor mRNA-engineered T cells induce anti-tumor activity in solid malignancies. *Cancer Immunology Research*, **2**(2), 112–120

[308] Pear WS, Nolan GP, Scott ML and Baltimore D (September 1993). Production of high-titer helper-free retroviruses by transient transfection. *PNAS*, **90**(18), 8392–8396

[309] Swift S, Lorens J, Achacoso P and Nolan GP (May 2001). Rapid production of retroviruses for efficient gene delivery to mammalian cells using 293T cell-based systems. *Current Protocols Immunology*, **Chapter 10**, Unit 10.17C

[310] Nolan-Lab (May 2018). Retroviral Systems
URL `https://web.stanford.edu/group/nolan/_OldWebsite/retroviral_systems/phx.html`

[311] Sijts AJ, Ossendorp F, Mengede EA, van den Elsen PJ and Melief CJ (January 1994). Immunodominant mink cell focus-inducing murine leukemia virus (MuLV)-encoded CTL epitope, identified by its MHC class I-binding motif, explains MuLV-type specificity of MCF-directed cytotoxic T lymphocytes. *Journal of Immunology*, **152**(1), 106–116

[312] Ossendorp F, Mengede E, Camps M, Filius R and Melief CJ (March 1998). Specific T helper cell requirement for optimal induction of cytotoxic T lymphocytes against major

histocompatibility complex class II negative tumors. *Journal of Experimental Medicine*, **187**(5), 693–702

[313] Schoenberger SP et al. (July 1998). Efficient direct priming of tumor-specific cytotoxic T lymphocyte in vivo by an engineered APC. *Cancer Research*, **58**(14), 3094–3100

[314] van Stipdonk MJ, Lemmens EE and Schoenberger SP (May 2001). Naive CTLs require a single brief period of antigenic stimulation for clonal expansion and differentiation. *Nature Immunology*, **2**(5), 423–429

[315] DuBridge RB et al. (January 1987). Analysis of mutation in human cells by using an Epstein-Barr virus shuttle system. *Molecular Cell Biology*, **7**(1), 379–387

[316] van der Veken LT et al. (December 2005). HLA class II restricted T-cell receptor gene transfer generates CD4+ T cells with helper activity as well as cytotoxic capacity. *Gene Therapy*, **12**(23), 1686–1695

[317] Salter RD, Howell DN and Cresswell P (March 1985). Genes regulating HLA class I antigen expression in T-B lymphoblast hybrids. *Immunogenetics*, **21**(3), 235–246

[318] Kwakkenbos MJ, van Helden PM, Beaumont T and Spits H (March 2016). Stable long-term cultures of self-renewing B cells and their applications. *Immunology Reviews*, **270**(1), 65–77

[319] Noll EM et al. (March 2016). CYP3A5 mediates basal and acquired therapy resistance in different subtypes of pancreatic ductal adenocarcinoma. *Nature Methods*, **22**(3), 278–287

[320] Chakraborty S, Rahman T and Chakravorty R (March 2014). Characterization of the Protective HIV-1 CTL Epitopes and the Corresponding HLA Class I Alleles: A Step towards Designing CTL Based HIV-1 Vaccine. *Advances in virology*, **2014**, 321974

[321] Herr W et al. (October 1999). Identification of naturally processed and HLA-presented Epstein-Barr virus peptides recognized by CD4(+) or CD8(+) T lymphocytes from human blood. *PNAS*, **96**(21), 12033–12038

[322] Laurin D et al. (November 2006). Minor histocompatibility antigen DDX3Y induces HLA-DQ5-restricted T cell responses with limited TCR-Vbeta usage both in vivo and in vitro. *Biology of Blood and Marrow Transplantation*, **12**(11), 1114–1124

[323] Rotzschke O et al. (November 1991). Exact prediction of a natural T cell epitope. *European Journal of Immunology*, **21**(11), 2891–2894

[324] Johnsen G and Elsayed S (September 1990). Antigenic and allergenic determinants of ovalbumin–III. MHC Ia-binding peptide (OA 323-339) interacts with human and rabbit specific antibodies. *Molecular Immunology*, **27**(9), 821–827

[325] Robbins PF et al. (June 2013). Mining exomic sequencing data to identify mutated antigens recognized by adoptively transferred tumor-reactive T cells. *Nature Medicine*, **19**(6), 747–752

[326] Medical Association W (November 2013). World Medical Association Declaration of Helsinki: ethical principles for medical research involving human subjects. *JAMA*, **310**(20), 2191–2194

[327] Dudley ME, Wunderlich JR, Shelton TE, Even J and Rosenberg SA (July 2003). Generation of tumor-infiltrating lymphocyte cultures for use in adoptive transfer therapy for melanoma patients. *Journal of Immunotherapy*, **26**(4), 332–342

[328] Komuro K, Itakura K, Boyse E and John M (December 1975). Ly-5: A new lymphocyte antigen system. *Immunogenetics*, **1**, 452–456

[329] Hogquist K et al. (January 1994). T cell receptor antagonist peptides induce positive selection. *Cell*, **76**(1), 17–27

[330] Barnden M, Allison J, Heath W and Carbone F (February 1998). Defective TCR expression in transgenic mice constructed using cDNA-based alpha- and beta-chain genes under the control of heterologous regulatory elements. *Immunology and Cell Biology*, **76**(1), 34–40

[331] Shultz L et al. (May 2005). Human lymphoid and myeloid cell development in NOD/LtSz-scid IL2Rg(null) mice engrafted with mobilized human hemopoietic stem cells. *Journal of Immunology*, **174**(10), 6477–6489

[332] Lyons AB and Parish CR (May 1994). Determination of lymphocyte division by flow cytometry. *Journal of Immunological Methods*, **171**(1), 131–137

[333] Schneider CA, Rasband WS and Eliceiri KW (July 2012). NIH Image to ImageJ: 25 years of image analysis. *Nature Methods*, **9**(7), 671–675

[334] Consortium TU (January 2017). UniProt: the universal protein knowledgebase. *Nucleic Acids Research*, **45**(D1), D158–D169

[335] O'Leary NA et al. (January 2016). Reference sequence (RefSeq) database at NCBI: current status, taxonomic expansion, and functional annotation. *Nucleic Acids Research*, **44**(D1), D733–45

[336] Kent W et al. (June 2002). The human genome browser at UCSC. *Genome Research*, **12**(6), 996–1006

[337] Reference Consortium G (February 2001). Initial sequencing and analysis of the human genome. *Nature*, **409**(6822), 860–921

[338] Ye J et al. (June 2012). Primer-BLAST: A tool to design target-specific primers for polymerase chain reaction. *BMC Bioinformatics*, **13**(134)

[339] IDT (February 2018). PrimerQuest® program
URL `http://www.idtdna.com/SciTools`

[340] Cormack B, Valdivia R and Falkow S (1996). FACS-optimized mutants of the green fluorescent protein (GFP). *Gene*, **173**(1), 33–38

[341] Li H and Durbin R (March 2010). Fast and accurate long-read alignment with Burrows-Wheeler Transform. *Bioinformatics*, **26**(5), 589–595

[342] Li H and Durbin R (July 2009). Fast and accurate short read alignment with Burrows-Wheeler Transform. *Bioinformatics*, **25**(14), 1754–1760

[343] Broadinstitute (February 2018). Picard Tools
URL `https://broadinstitute.github.io/picard/`

[344] McKenna A et al. (September 2010). The Genome Analysis Toolkit: a MapReduce framework for analyzing next-generation DNA sequencing data. *Genome Research*, **20**(9), 1297–1303

[345] DePristo M et al. (May 2011). A framework for variation discovery and genotyping using next-generation DNA sequencing data. *Nature Genetics*, **43**(5), 491–498

[346] der Auwera GV et al. (October 2013). From FastQ data to high confidence variant calls: the Genome Analysis Toolkit best practices pipeline. *Current Protocols Bioinformatics*, **11**(1110), 1–33

[347] Cibulskis K et al. (February 2013). Sensitive detection of somatic point mutations in impure and heterogeneous cancer samples. *Nature Biotechnology*, **31**, 213–219

[348] Robinson J et al. (January 2011). Integrative Genomics Viewer. *Nature Biotechnology*, **29**(1), 24–26

[349] Thorvaldsdóttir H, Robinson J and Mesirov J (March 2013). Integrative Genomics Viewer (IGV): high-performance genomics data visualization and exploration. *Briefings in Bioinformatics*, **14**(2), 178–192

[350] Edgar R, Domrachev M and Lash A (January 2002). Gene Expression Omnibus: NCBI gene expression and hybridization array data repository. *Nucleic Acids Research*, **30**(1), 207–210

[351] Barrett T et al. (January 2013). NCBI GEO: archive for functional genomics data sets–update. *Nucleic Acids Research*, **41**, 991–995

[352] Zhang G et al. (February 2012). DPEP1 inhibits tumor cell invasiveness, enhances chemosensitivity and predicts clinical outcome in pancreatic ductal adenocarcinoma. *PLoS ONE*, **7**(2)

[353] Zhang G et al. (September 2013). Integration of metabolomics and transcriptomics revealed a fatty acid network exerting growth inhibitory effects in human pancreatic cancer. *Clinical Cancer Research*, **19**(18), 4983–4993

[354] Boegel S et al. (December 2012). HLA typing from RNA-Seq sequence reads. *Genome Medicine*, **4**(102)

[355] Andreatta M and Nielsen M (February 2016). Gapped sequence alignment using artificial neural networks: application to the MHC class I system. *Bioinformatics*, **32**(4), 511–517

[356] Nielson M et al. (May 2003). Reliable prediction of T-cell epitopes using neural networks with novel sequence representations. *Protein Science*, **12**(5), 1007–1017

[357] Blatnik R et al. (March 2018). A targeted LC-MS strategy for low-abundant HLA class I-presented peptide detection identifies novel human papillomavirus T-cell epitopes. *Proteomics*, p. e1700390

[358] Dudley ME et al. (November 2008). Adoptive cell therapy for patients with metastatic melanoma: evaluation of intensive myeloablative chemoradiation preparative regimens. *Journal of Clinical Oncology*, **26**(32), 5233–5239

[359] Fukuda M, Viitala J, Matteson J and Carlsson SR (December 1988). Cloning of cDNAs encoding human lysosomal membrane glycoproteins, h-lamp-1 and h-lamp-2. Comparison of their deduced amino acid sequences. *Journal of Biological Chemistry*, **263**(35), 18920–18928

[360] Carlsson SR and Fukuda M (December 1989). Structure of human lysosomal membrane glycoprotein 1. Assignment of disulfide bonds and visualization of its domain arrangement. *Journal of Biological Chemistry*, **264**(34), 20526–20531

[361] Guarnieri FG, Arterburn LM, Penno MB, Cha Y and August JT (January 1993). The motif Tyr-X-X-hydrophobic residue mediates lysosomal membrane targeting of lysosome-associated membrane protein 1. *Journal of Biological Chemistry*, **268**(3), 1941–1946

[362] Marques ETAJ et al. (September 2003). HIV-1 p55Gag encoded in the lysosome-associated membrane protein-1 as a DNA plasmid vaccine chimera is highly expressed, traffics to the major histocompatibility class II compartment, and elicits enhanced immune responses. *Journal of Biological Chemistry*, **278**(39), 37926–37936

[363] de Arruda LB, Chikhlikar PR, August JT and Marques ETA (May 2004). DNA vaccine encoding human immunodeficiency virus-1 Gag, targeted to the major histocompatibility complex II compartment by lysosomal-associated membrane protein, elicits enhanced long-term memory response. *Immunology*, **112**(1), 126–133

[364] Fernandes DM, Vidard L and Rock KL (August 2000). Characterization of MHC class II-presented peptides generated from an antigen targeted to different endocytic compartments. *European Journal of Immunology*, **30**(8), 2333–2343

[365] De Keersmaecker B et al. (April 2010). Lumenal part of the DC-LAMP protein is not required for induction of antigen-specific T cell responses by means of antigen-DC-LAMP messenger RNA-electroporated dendritic cells. *Human Gene Therapy*, **21**(4), 479–485

[366] Fleig L et al. (August 2012). Ubiquitin-dependent intramembrane rhomboid protease promotes ERAD of membrane proteins. *Molecular Cell*, **47**(4), 558–569

[367] Yewdell JW, Antón LC and Bennink JR (September 1996). Defective ribosomal products (DRiPs): a major source of antigenic peptides for MHC class I molecules? *The Journal of Immunology*, **157**(5), 1823–1826

[368] Bourdetsky D, Schmelzer CEH and Admon A (April 2014). The nature and extent of contributions by defective ribosome products to the HLA peptidome. *PNAS*, **111**(16), E1591–E1599

[369] Barnaba V, Watts C, de Boer M, Lane P and Lanzavecchia A (January 1994). Professional presentation of antigen by activated human T cells. *European Journal of Immunology*, **24**(1), 71–75

[370] Holling TM, van der Stoep N, Quinten E and van den Elsen PJ (January 2002). Activated human T cells accomplish MHC class II expression through T cell-specific occupation of class II transactivator promoter III. *Journal of Immunology*, **168**(2), 763–770

[371] Holling TM, Schooten E and van Den Elsen PJ (April 2004). Function and regulation of MHC class II molecules in T-lymphocytes: of mice and men. *Human Immunology*, **65**(4), 282–290

[372] Johnson LA et al. (November 2006). Gene transfer of tumor-reactive TCR confers both high avidity and tumor reactivity to nonreactive peripheral blood mononuclear cells and tumor-infiltrating lymphocytes. *Journal of Immunology*, **177**(9), 6548–6559

[373] Cruz FM, Colbert JD, Merino E, Kriegsman BA and Rock KL (April 2017). The Biology and Underlying Mechanisms of Cross-Presentation of Exogenous Antigens on MHC-I Molecules. *Annual Review of Immunology*, **35**, 149–176

[374] Ljunggren HG et al. (August 1990). Empty MHC class I molecules come out in the cold. *Nature*, **346**(6283), 476–480

[375] Schumacher TN et al. (August 1990). Direct binding of peptide to empty MHC class I molecules on intact cells and in vitro. *Cell*, **62**(3), 563–567

[376] Poschke I and Offringa R (2018). Unpublished. Internal communication

[377] Yang H, Zhong Y, Peng C, Chen JQ and Tian D (September 2010). Important role of indels in somatic mutations of human cancer genes. *BMC Medical Genetics*, **11**, 128

[378] Turajlic S et al. (August 2017). Insertion-and-deletion-derived tumour-specific neoantigens and the immunogenic phenotype: a pan-cancer analysis. *Lancet Oncology*, **18**(8), 1009–1021

[379] Brennicke A, Marchfelder A and Binder S (June 1999). RNA editing. *FEMS Microbiology Reviews*, **23**(3), 297–316

[380] Paz-Yaacov N et al. (October 2015). Elevated RNA Editing Activity Is a Major Contributor to Transcriptomic Diversity in Tumors. *Cell Reports*, **13**(2), 267–276

[381] Han L et al. (October 2015). The Genomic Landscape and Clinical Relevance of A-to-I RNA Editing in Human Cancers. *Cancer Cell*, **28**(4), 515–528

[382] Eisenberg E and Levanon EY (April 2018). A-to-I RNA editing - immune protector and transcriptome diversifier. *Nature Reviews Genetics*

[383] Roth SH et al. (April 2018). Increased RNA Editing May Provide a Source for Autoantigens in Systemic Lupus Erythematosus. *Cell Reports*, **23**(1), 50–57

[384] Hanada KI, Yewdell JW and Yang JC (January 2004). Immune recognition of a human renal cancer antigen through post-translational protein splicing. *Nature*, **427**(6971), 252–256

[385] Vigneron N et al. (April 2004). An antigenic peptide produced by peptide splicing in the proteasome. *Science*, **304**(5670), 587–590

[386] Warren EH et al. (September 2006). An antigen produced by splicing of noncontiguous peptides in the reverse order. *Science*, **313**(5792), 1444–1447

[387] Dalet A et al. (July 2011). An antigenic peptide produced by reverse splicing and double asparagine deamidation. *PNAS*, **108**(29), E323–31

[388] Gillette MA and Carr SA (January 2013). Quantitative analysis of peptides and proteins in biomedicine by targeted mass spectrometry. *Nature Methods*, **10**(1), 28–34

[389] Engels B et al. (August 2003). Retroviral vectors for high-level transgene expression in T lymphocytes. *Human Gene Therapy*, **14**(12), 1155–1168